Programma Operativo Fondo Sociale Europeo 2014/2020 - Asse 5 Ob. 5.4 – Azione 5.4.3
Programma Operativo Complementare Sicilia 2014/2020 - Asse 5 Ob.10.5 – Azione 10.5.6
Avviso 01/2021 per il finanziamento di borse regionali di dottorato di ricerca in Sicilia - A.A 2021/2022
CIP BORSE.SICILIA.REG.NAZ/3.10.5/AVVISO1.2021/9.2.10/0008 - CUP G79J21012770001

Università degli Studi di Palermo
PhD Course in Chemical, Environmental, Biomedical, Hydraulic and Materials Engineering
Dipartimento di Ingegneria
Settore Scientifico Disciplinare (ING-IND/26)

Green Hydrogen Production with Ion Exchange Membranes

PhD Candidate:
Giovanni Campisi

Phd Course Coordinator:
Prof. Giorgio Domenico Maria Micale

Supervisor:
Prof. Giorgio Domenico Maria Micale

Co-Supervisors:
Prof. Alessandro Tamburini
Dr. Simone Dussi

XXXVII CYCLE
GRADUATION YEAR 2025

"I don't want your hope.

I don't want you to be hopeful.

I want you to panic.

I want you to feel the fear I feel every day.

I want you to act.

I want you to act as you would in a crisis.

I want you to act as if the house is on fire, because it is."

Greta Thunberg, Activist

Acknowledgements

I began this PhD after three incredible years within the same research group, starting as a thesis student, then continuing through my internship, and eventually as a PhD student. At the beginning, fresh out of university, I was excited to jump into the world of work and start shaping my path. But along the way, my time in the group made me see research in a whole new light. It slowly sparked a genuine passion in me and a curiosity that keeps pushing me to ask why things happen, always leaving space for creativity and the freedom to explore new ideas, like hydrogen.

The research group was like a close-knit family. Just like in any family, we went through highs and lows, moments of quiet perseverance and others filled with laughter. I owe so much to all of them, starting with my incredible colleagues: those who welcomed me at the beginning and those who stood by my side until the very end of this amazing journey. There are too many names to write down, but they are all important; They've given me memories I'll carry with me for a lifetime, moments that will always bring a smile whenever I look back on this chapter of my life. I owe a huge amount of gratitude to Giorgio, Alessandro and Andrea, my professors and mentors. They constantly challenged me and gave me a thousand new things to do, well beyond the original hundred! But through it all, for better or worse, they were always a source of inspiration, helping me grow both professionally and personally.

I owe the incredible DC2P group the most amazing memories of these six years of my life, and I can't thank you enough!

I'm extremely grateful to Simone and all the HTFD group of TNO-Delft, and to Nicola and Stefania from CNR-ITAE for the time they've given me and for the incredible new experiences that have helped me mature. I would also like to thank Federica and Prof. Scialdone for the invaluable help they gave us in taking our first steps. Lastly, I would like to thank Alessandra, my amazing companion on this incredible journey called PhD. We shared so much of the journey together, and she wasn't just a great friend but also a key part of the hydrogen team. Her presence really made a difference.

To my family, my parents and my sister, who have always supported me in my choices, even when they didn't fully agree with them. Their support has given me the strength to stay true to myself and keep moving forward. And for that, I'm truly grateful (though let's be honest, stubbornness definitely runs in the family!).

To my friends, my "relief valve" and distraction.

To my new colleagues of Enapter, who have patiently endured all my ups and downs, and my moments of madness, throughout these past few months.

To my amazing life partner, best friend and biggest supporter, Marco, for always being there for me and giving me all the energy I need in this world!

To my beloved Nonna Pina, who I'm sure is still watching over me. She was always proud of everything I did, even if she never quite understood what this PhD was really about.

To this earth, which still has so much to offer us, and which we have the duty to protect.

And to myself, for always believing in it.

Ad Maiora!

Preface

The world news of the last 20 years shows how (i) climate change is a serious problem and how (ii) humanity must do as much as possible to avoid reaching the critical point beyond which there is no chance of remedying the mistakes made. Hydrogen, through water electrolysis, has been identified as an energy carrier to replace fossil fuels. Indeed, H_2 can be used not only as a reactant to produce chemicals, but as a vector for storing energy and as a possible solution for heating and producing electrical energy. Many companies, also promoted by governments, are investing in research and ways to reduce the production costs of green hydrogen.

The present thesis is part of this economic-geopolitical framework to propose using electro-membrane technologies to produce hydrogen in addition to their traditional aim. As a matter of fact, red-ox reactions occur within the electrodic compartments to close the electric circuit in electro-membrane processes. The idea is that of producing hydrogen there. As far as the development of this idea is concerned, the first step is to define the technical feasibility of coupling the technologies and the effectiveness of the production of the species. And then the implementation of a technical model associated with it, capable of describing and predicting the main results of the process. The models, once calibrated and validated, are then linked to an economic model to determine the cost-effectiveness of the process by identifying economic indices such as the levelized cost and net present value.

A visual representation of this thesis work is reported in Figure A. In particular, Chapter 1 and Chapter 2 are proposed as an overview and review of the literature of hydrogen production and electro-membrane processes, among which (i) (Assisted-)Reverse Electrodialysis, (ii) Electrodialysis and (ii) Electrodialysis with bipolar membranes.

The following chapters are committed to analysing each technology from both an experimental and techno-economic point of view, highlighting critical issues, possibilities for improvement and performance parameters of the process.

In detail, chapter 3 focuses on the study of the reverse electrodialysis process and assisted reverse electrodialysis, while chapters 4 and 5 analyse the electrodialysis technology for the two cases of

low and high salinity of the feed solution. The case of low salinity, i.e., brackish water, is dealt with in chapter 4, while the case of high salinity, such as seawater, is discussed in chapter 5. Finally, the electrodialysis technology with bipolar membranes is described and analysed in chapter 6, where, in addition to the desalination of an incoming salt solution, there is also the production of chemicals such as acid and base aqueous solutions.

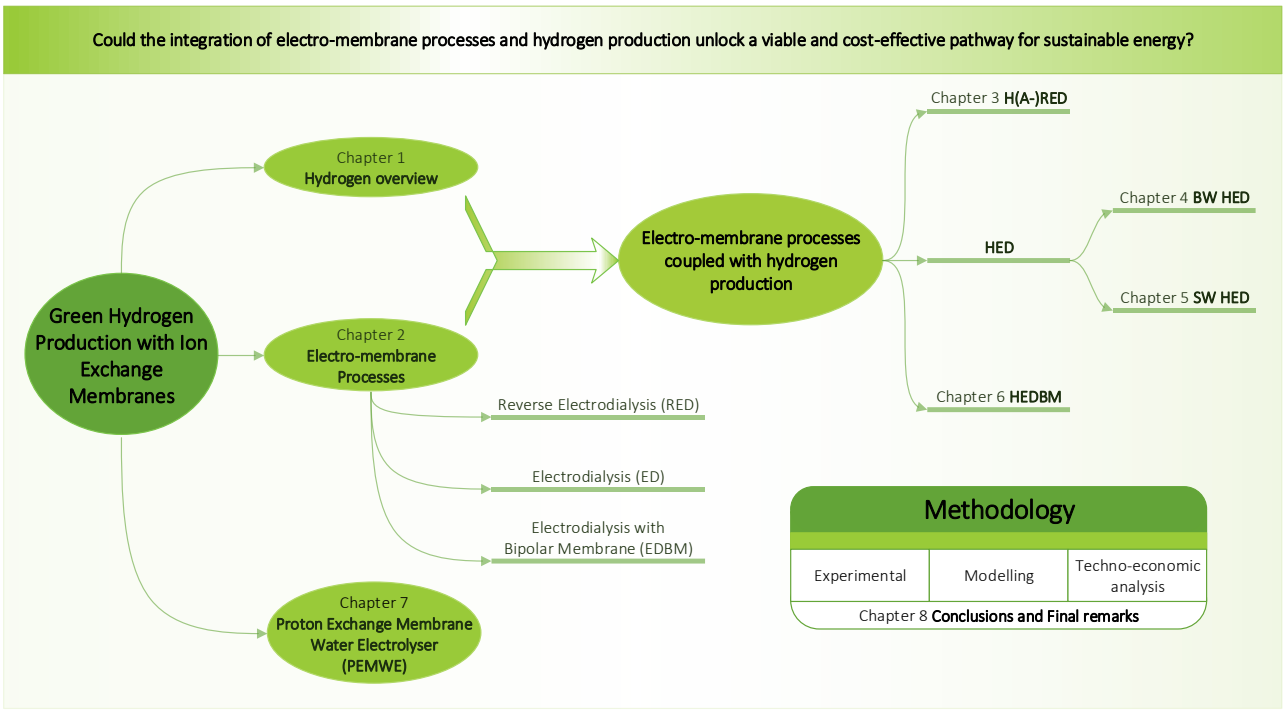

Figure A: Visual representation of the thesis structure.

Last but not least, chapter 7 deals with the modelling and the study of a proton exchange membrane water electrolyser. The electrolyser was studied from various aspects using the Fluent software, applying the basics of the computational fluid dynamics. This last chapter constitutes a significant part of the PhD research undertaken abroad at the Dutch research centre TNO.

A concluding section for all the technologies considered is also present, to summarise in part what has been done and the main takeaways of this work.

Table of contents

Acknowledgements ..... **iii**

Preface ..... **v**

Table of contents ..... **vii**

1 Hydrogen overview **1**

1.1 Why hydrogen? *2*

1.1.1 Different hydrogen colours 3

1.1.1.1 "Dark" hydrogen 3

1.1.1.2 Green Hydrogen 4

1.2 Electrochemistry principles *8*

1.2.1 Thermodynamics 8

1.2.2 Kinetics 12

1.2.2.1 Activation overvoltage 13

1.2.2.2 Ohmic overpotential 17

1.2.2.3 Diffusion overpotential 17

1.2.2.4 Chemical reaction 18

1.2.3 Water Electrolysis 19

2 Electro membrane processes **21**

2.1 Electrodialysis (ED), Reverse Electrodialysis (RED) and Assisted Reverse Electrodialysis (A-RED) *22*

2.2 Electrodialysis with Bipolar Membrane (EDBM) *25*

2.3 Aim of this work *27*

3 Hydrogen (Assisted-)Reverse Electrodialysis H(A-)RED **29**

3.1 Experimental *31*

3.1.1 Set-up 31

3.1.2 Experimental investigation 33

3.1.3 Results 34

3.2 Model and validation *39*

3.3 Economic analysis *41*

3.4 Final remarks and future perspectives for H(A-)RED *44*

4 Hydrogen Electrodialysis HED: Brackish water **46**

4.1 HED technology *46*

4.2 Technical model *48*

4.2.1 Model equations 48

4.2.2 Model validation 52

4.2.3 Economic model 53

4.3 Techno-Economical analysis *55*

4.3.1 Investigated scenario 55

4.3.2 Technical analysis 58

4.3.3 Economic analysis 61

4.4 Final remarks and future perspectives for HED *68*

5 Hydrogen Electrodialysis HED: Sea water **70**

5.1 Experimental *72*

5.1.1 Experimental Set-up 72

5.1.2 Multi-stage open loop test 73

5.1.3 Polarization curves A/B vs B/B 78

5.1.4 Closed-Loop tests 79

5.1.4.1 A/B closed loop test 79

5.1.4.2 Comparison closed loop tests: A/B vs B/B 82

5.2 Technical model *85*

5.2.1 Model equations 85

5.2.2 Model validation 86

5.3 Economical aspects and future perspectives *88*

5.3.1 Case studies 88

5.3.2 Techno-economic analysis 89

5.3.3 A/B and B/B comparison 96

5.4 Final remarks and future perspectives for SWHED *97*

6 Hydrogen Electrodialysis with bipolar membrane HEDBM **100**

6.1 Experimental *100*

4.2.2 Experimental Set-up 100
4.2.3 Results 102
6.2 Techno-economic HEDBM model 104
6.2.1 Model validation 105
6.2.2 Economic model 108
6.3 Techno-economic analysis 110
6.3.1 Case study 110
6.3.2 Technical analysis 112
6.3.3 Economic analysis 114
6.4 Final remarks and future perspectives for HEDBM 122
7 On the modelling of PEM water electrolysers 124
7.1 PEMWE system description 124
7.2 Technical model 127
7.3 Simulated scenario 131
7.4 Polarization curves and results 132
7.5 Final remarks 136
8 Conclusion and Final remarks 138
Appendix 145
Appendix I: Model equations 145
Appendix II: Solution properties 146
Appendix III: Electrodes polarization 147
Appendix IV: Limit current estimation methods 148
Appendix V: Linear sweep voltammetry 149
List of ISI publications 153
Abstracts at international conferences 155
Submitted abstract for oral presentations 158
Bibliography 159

1 *Hydrogen overview*

History is full of environmental events and disasters, yet in recent decades, nations are witnessing more and more frequent and catastrophic phenomena. The floods in Pakistan in the 2022 summer, the dramatic fires in Australia and California, Hurricane Helene that hit Florida, the devastating flood in Valencia, and the terrible drought that is hitting southern European countries, are just some of these examples.

By the end of the last century, the scientific community had warned nations about the possible consequences of uncontrolled greenhouse gas (GHG) emissions and their effects on the population. However, only a few countries have taken the first steps towards green policies aimed at protecting the environment. The first historic event is dated December 1997, when the Kyoto Protocol was agreed. The agreement called for a reduction of at least 5 % from 1990 values of the most impactful greenhouse gases (such as CO_2, methane, N_2O, etc). Though, for the agreement to be valid, it had to be ratified by no less than 55 countries contributing at least 55 % of global emissions. However, the Kyoto agreement only came into force in 2005, following ratification by Russia, which alone contributed about 17 % of global emissions. However, neither the USA nor China participated in this agreement. The COP21 therefore becomes significant, which takes on historical significance in this narrative as 197 countries belonging to the UNFCCC signed the Paris agreement on 12 December 2015, in which they committed to keeping the increase in the average global temperature below 2°C compared to pre-industrial levels and in any case not to exceed the threshold of 1.5°C. The agreement had a certain significance as it was the first legally binding agreement on combating global warming. However, history teaches us that the will to change must first and foremost come from the people and consequently the representatives they choose. If in fact, the Paris agreement included the participation of the USA, with the Trump presidency, the USA withdrew from the agreement (with an effective date) in 2020, then re-entered with the Biden administration, and it retired a few days after Trump's inauguration in 2025.

The COP21 targets were updated and strengthened by the EU as part of the European Green Deal [1], in which the European community aimed to cut emissions by 55 % compared to 1990 levels by 2030. It also aimed to become a climate-neutral society, both as a challenge and an opportunity for building a better future by 2050. As a part of this ecological transition, and in an effort to move away

from highly polluting energy sources such as carbon-fossil fuels, the challenge of hydrogen as a future energy carrier has been opened [2,3]. The scientific and the European community are very interested in obtaining hydrogen from clean energies, both (i) as an improvement of existing technologies, and (ii) as research in identifying new methods for its production. Above all, the aim is to reduce the cost of hydrogen produced from renewable sources down to values lower than 2 € kg^{-1}_{H2}, thereby ensuring its production at a cost comparable to that from fossil fuels (grey hydrogen).

1.1 Why hydrogen?

The idea of using hydrogen as an energy source dates back two centuries [4], but it was only after the energy crisis of 1970 that this possibility began to be seriously considered. Hydrogen is the first element in the periodic table, the lightest, the simplest from a chemical point of view and is also the most abundant element in the universe. Although it is among the most widespread elements on our planet, it is difficult to find it in molecular form (H_2, white hydrogen), and it is found in stable compounds such as water (H_2O) or bound to carbon as in hydrocarbon compounds. It is therefore necessary to produce it starting from these resources, and among the main production methods are steam reforming and water electrolysis.

The first process leads to the production of syngas, i.e. a mixture of carbon monoxide (CO) and hydrogen from methane; the second, on the other hand, promotes the splitting of water by applying an external potential.

A generic electrolysis unit consists of two electrodes in which oxygen oxidation occurs at the anode, while hydrogen is reduced at the cathode. More generally, the global redox reaction leads to the formation of 1 mole of hydrogen and half a mole of oxygen, and being a non-spontaneous reaction, it is necessary to apply a potential equal to 1.23 V.

The energy density of hydrogen is equal to 120 MJ kg^{-1}, about three times that of diesel and gasoline, which are respectively 45.5 and 45.8 MJ kg^{-1}. Considering that, the combustion reaction of hydrogen [$H_2 + \frac{1}{2}O_2 \rightarrow H_2O$] does not lead to the formation of CO_2 or unburnt matter, its advantages are not debated.

However, in the case of reforming, there is the release of large quantities of co-products such as CO_2, since the process starts from a carbon-based raw material, i.e., hydrocarbons. While in the case of water electrolysis, high energy consumption would be required, making the process economically disadvantageous, moreover, this electricity is obtained from steam plants that involve the use of fuel sources for the phase transition of the carrier. As an alternative, electrolysis could be driven by the use of renewable energies (e.g. photovoltaic, wind, etc.). Thus, the hydrogen produced would be zero-emission, and would be the only one that can be defined as 100 % sustainable (green hydrogen).

1.1.1 Different hydrogen colours

Depending on the type of hydrogen production process and/or origin, it is matched with an identifying colour [5–7] to define the level of pollutants produced with that hydrogen. Among the most famous are the grey, black (or brown) and turquoise hydrogen, which are related respectively to Steam Methane Reforming SMR, coal gasification and methane pyrolysis processes. And today, these processes are the most common in hydrogen production.

These processes are all associated with large amounts of CO_2 emissions, and the idea is to replace them with more eco-friendly and sustainable processes. The high-polluting processes could be combined with CO_2 sequestration systems, such as for the steam reforming, to obtain blue hydrogen [8] and reduce the release of greenhouse gases. Another possibility is to produce hydrogen by electrolysis of water using energy from nuclear power (pink hydrogen) or renewable sources in the case of green hydrogen. Today, SMR is responsible for supplying 50 % of the world's hydrogen, while the remaining percentages are distributed as follows: 30 % from petroleum fraction supply, 18 % from coal gasification, 3.9 % from water electrolysis, and 0.1 % from other sources [9].

1.1.1.1 “Dark” hydrogen

Grey hydrogen is produced from natural gas, specifically methane, mainly through two processes: Steam Methane Reforming (SMR) and Autothermal Reforming (ATR) [10,11]. This endothermic process requires significant heat input (up to 1000 °C) and water vapour. Hydrogen is produced as a result of the syngas (mixture of hydrogen and carbon monoxide in a ratio of 3:1), extensively used as a building block for most chemical processes, it is also the main source of hydrogen after undergoing several purification steps.

Before starting the process, the methane must be purified to remove traces of sulphur, which could compromise the efficiency of the catalyst (poisoning). Today, SMR is the most widely used method for hydrogen production, thanks to its easy handling and low plant costs. The global production capacity through SMR is around 300 GW, with each plant ranging between 50 and 1000 MW. Compared to SMR, ATR operates at higher temperatures (up to 1150 °C) and involves an oxidation reaction that takes place with the supply of oxygen: $4CH_4 + O_2 + 2H_2O \rightarrow 4CO + 10H_2$. ATR is more efficient than SMR as the exothermic oxidation reaction generates the heat needed for reforming, thus reducing external energy consumption.

These processes produce hydrogen at a really low cost, around 1.5 € kg^{-1}, however, the purity achieved with these processes is about 94 %, and additional purification treatment is required to meet the hydrogen combustion specification (minimum purity of 98 % for common fuel cells).

Brown hydrogen is produced through coal gasification [7]. In this process, coal is partially oxidised, gasifying itself into mainly hydrogen and carbon monoxide and other light hydrocarbons. Although coal gasification produces hydrogen, this is the most polluting solution currently available.

"Turquoise" hydrogen is extracted from methane through a process that differs greatly from other methods, such as grey and blue hydrogen. In this case, the process used is methane pyrolysis, which involves heating the gas in the absence of oxygen, causing the chemical bonds of the molecules to break and leading to the formation of hydrogen and carbon.

1.1.1.2 Green Hydrogen

One of the Green Deal objectives is to reduce the current cost of hydrogen obtained from renewable sources (i.e., green hydrogen) under 2 € kg^{-1}_{H2} and to minimise emissions for its production. Today, green hydrogen production costs are strongly affected by multiple variables, such as electricity cost and consumption, working hours per year (or full load hours), plant size, electrolyser costs, etc. The perspectives consider the green hydrogen production cost through water electrolysis about 4– 8 € kg^{-1}_{H2} [12–14]. A generic electrolysis unit can produce H_2 by applying an external electrical potential sufficiently high to allow water electrolysis. The redox reactions involved occur at the electrodes, in which hydrogen and oxygen are produced at the cathode and anode, respectively. Renewable energies can be used (e.g., photovoltaics PV, wind power, etc.) to supply the energy drawn by the electrolyser, thus guaranteeing carbon-free hydrogen production. When the same pH is used at both electrodes, the thermodynamic standard redox potential of the electrolysis reaction

is equal to 1.229 V, according to the Pourbaix water diagram. The water electrolysis reactions are schematised in *Table 1*, with the corresponding standard reduction potentials. However, this ideal potential is not sufficient for Hydrogen and Oxygen Evolution Reactions (HER and OER) to take place, and an additional energy supply (i.e., higher voltage) has to be given to the cell due to kinetic reasons and overvoltage. A more in-depth discussion on water electrolysis and the potential involved can be found in the next paragraph: Electrochemistry principles.

Table 1 Water electrolysis reactions in acid or neutral/alkaline medium.

	Acid Medium		***Neutral or Alkaline medium***	
	Semi-Reaction	***Potential [V/SHE]***	***Semi-Reaction***	***Potential [V/SHE]***
Reduction	$4H^+ + 4\,e^- \leftrightarrow 2H_2$	0	$4H_2O + 4\,e^- \leftrightarrow 2H_2 + 4OH^-$	-0.828
Oxidation	$2H_2O \leftrightarrow O_2 + 4H^+ + 4\,e^-$	1.229	$4OH^- \leftrightarrow O_2 + 2H_2O + 4\,e^-$	0.401
Global	$2H_2O \leftrightarrow 2H_2 + O_2$			*1.229 V*

There are several electrolysers proposed in literature, but only two are used at industrial scale: (i) Alkaline Water Electrolysers (AWEs) [15–17] and (ii) Proton Exchange Membrane Water Electrolysers (PEMWEs) [15,18,19]. AWEs (Fig. 1a) are the most commonly used and consist of two electrodes separated by a diaphragm, and high concentrated KOH (~30% wt.) is used as electrolyte. The OH^- produced by the water reduction at the cathode go through the separator and are oxidised in the anode, producing oxygen. The separator is used to better separate the products to avoid the undesired mixing of the two gases (furtherly avoided by a no-zero gap configuration), although its presence causes an increase in the ohmic losses. Typical current densities for these systems range between 0.2–0.8 A cm^{-2} and require an average energy consumption of 56.5 kWh kg^{-1}_{H2}. Conversely, PEMWEs (Fig. 1b) involve lower volume, higher purity of products and allow higher current densities (typically more than 1 A cm^{-2}, up to 10 A cm^{-2}). The PEMWE is a zero-gap electrolyser composed by a proton exchange membrane, a Catalyst Coated Membrane (CCM), which means that the membrane is coated on both sides with the cathode and the anode catalyst layer, Gas Diffusion Layers (GDL) and the bipolar plates of the cell. The cell uses high-purity water (>18.2 MΩ·cm) as feed, due to the platinum group metals (PGM) used as catalysts. It works with a wet anode and a dry or wet cathode, depending on the configuration chosen. The dry cathode configuration is the most preferred one, because this minimises the separation steps of the gas with the liquid phase.

Concerning the electrolyte solution, water first goes through the GDL, and once it reaches the anode catalyst layer, it reacts according to the acid medium redox reaction, producing oxygen and protons. H^+ ions pass across the membrane (typically a Nafion®), reach the catalyst layer, and react, thereby producing hydrogen. The operative conditions of the cell are typically 70–80 °C temperature and pressurised (up to 30 bar) [12]. PEMWEs have been recently proposed at industrial scale (MW plant) in many projects (HOPE project 5MW [20], Gibson Island project PLUG 550 [21], GALP Sines refinery of a PLUG 100 MW [22], etc.) and their use is growing steadily. Their advantages include: (i) high current and hydrogen productivity, (ii) high hydrogen purity, (iii) low electrolysers volume and (iv) possibility to compress the products, with a reduction of pressurization and storage costs. Electrochemical pressurisation is one of the greatest advantages of PEMWEs, however, working under pressure at the cathode increases the phenomenon of hydrogen crossover to the anode, creating potentially explosive mixtures and compromising O_2 purity.

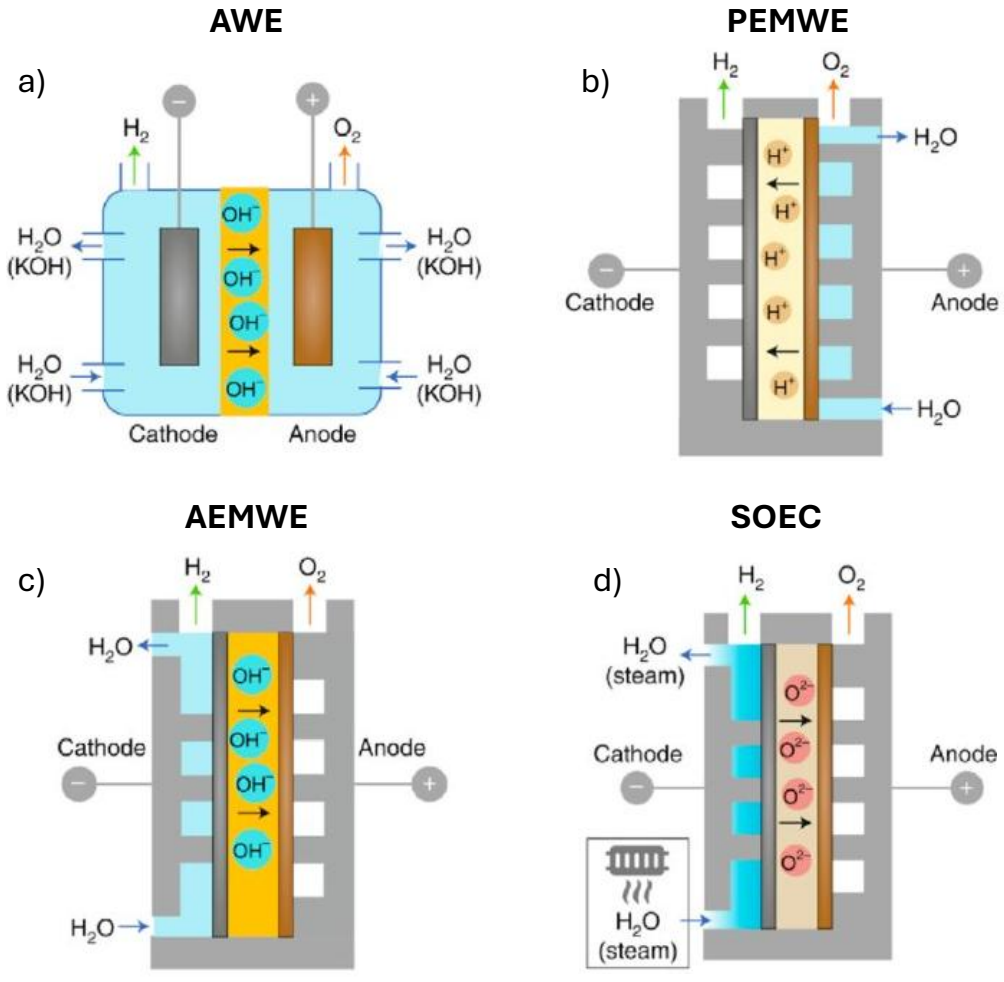

Fig. 1 Schematic representation of the traditional and most studied electrolysers [23].

Water quality plays a decisive role in electrolysers: for instance, PEMWE requires ultrapure water (UPW) [24]. UPW is a water that has a resistivity of 18.2 MΩ cm at 25°C [25] according to the American Society for Testing and Materials International (ASTM International), and it represents a water that has been purified to uncommonly specifications depending on their final use. The reason for such a purity in PEMWE is because water impurities (i.e., cations, anions, and organic compounds) can significantly affect the electrolyser operation, degrading its performances [26]. The main effect of the ion presence is the poisoning of membrane, catalyst, and ionomer. In addition, the water-impurities can give: (i) co-ion substitution in the membrane and the ionomer, (ii) undesired reactions (e.g., reactions of chlorine compound evolution) and (iii) inorganic precipitation or adsorption on the catalysts. In addition, the presence of organic compounds can lead to their preferential oxidation at the anode, as against the OER [26]. All these phenomena worsen the operation of electrolysers and accelerate their degradation. For this reason, complex desalination chains are devised. These desalination chains mostly use seawater [27–29] and include the following steps: (i) pretreatment and ultrafiltration of the water; (ii) the desalination step, usually consisting of two steps in series of Reverse Osmosis (RO) [30,31]; (iii) post-treatments devoted to purifying the water produced, such as degasification, UV treatments and Electro-DeIonisation (EDI) [32]; (iv) a possible final polishing, taking advantage of mixed bed Ion eXchanger (IX). The higher the water quality required, the higher the complexity and the cost of the chain. Among the existing desalination technologies, Reverse Osmosis, Multi-Effect Distillation (MED) [33] and ElectroDialysis (ED) [34–36] are the most studied and present in desalination plants. Nowadays, studies and research focus on the integration of desalination systems with renewable energy sources [37–39]. RO currently dominates the desalination field, but its use can be replaced by other desalination technologies depending on several factors. For instance, MED can be considered wherever a large employment of PV or a solar concentrator is present [40], for which a high availability of radiation can reduce the costs associated with the required heat energy.

Another interesting electrolyser is the Solid Oxide Electrolyser Cell (SOEC, Fig. 1d) [41,42]. This electrolyser significantly reduces electricity requirements thanks to the high temperature involved (700-850°C). A solid electrolyte made of stabilised zirconia is placed between the electrodes, and the high temperature promotes the diffusion of oxygen from the cathode to the anode for oxygen production. However, this technology has a low Technology Readiness Level (TRL). Excessive costs and the elevated temperature requirement are currently holding back its spread. Among the

emerging low-temperature electrolysers, the Anionic Exchange Membrane Water Electrolyser (AEMWE, Fig. 1c) is spreading as one of the most promising [43,44]. It boasts features similar to PEMWE and AWE, with a cell composed of two Catalyst Coated Substrates (CCS), an anion exchange membrane separator that is thinner and outperforms a diaphragm, and a less than 1 M KOH (5– 6% wt.) solution as feed.

AEMWEs and AWEs are similar in operation, but AEMWEs outperform AWEs in several key areas. They deliver higher currents, ensure the electrochemical pressurisation of products, and significantly reduce the risk of explosive mixtures. Unlike PEMWEs, AEMWEs do not require PGM electrodes, relying on nickel-based catalysts instead, making them more environmentally friendly. While AEMWE is a recent technology, it is promising and is still in the research phase.

1.2 Electrochemistry principles

1.2.1 Thermodynamics

A generic galvanic cell consists of two electrodes, a cathode and an anode, immersed in an electrolyte solution (or any medium that can promote electrical continuity) and connected via a conductor through which electrons pass. The driving force in the process is a potential difference at the ends of the terminals E_{MN}, which defines the direction of the current. A galvanic cell can be understood either as a battery, which is a system that converts chemical energy into electrical energy, or as an electrolyser, which does the opposite. Electrodes are the site of reduction and oxidation (redox) reactions according to the following equation:

$$O^{n^+} + ne^- = R \qquad 1$$

The direction of the reaction is defined by the ΔG (Gibbs free energy), which is a function of temperature, pressure and the degree of progress of the reaction. In a system with constant temperature and pressure, dG would only be a function of ζ_i, and it can be written:

$$\frac{dG}{d\zeta_i}_{T,P=cost} = \Delta G \qquad 2$$

For a closed system at constant pressure and temperature, thermodynamics states that the Gibbs free energy is defined as $G = U + pV - TS$ from which $dG = dU + pdV - TdS$, but for the 1st principle of thermodynamics the internal energy is defined as $dU = đQ + đW$, where Q is the

energy that enters the system as heat, while W is the work done in the system that can be the sum of the mechanical work of compression $-pdV$ and other forms of work W_x (such as electrical one). Note that $đQ - TdS = 0$ if it describes a reversible process, but $đQ - TdS = Td_iS$ in the case of irreversibility, for which:

$$dW_u = dG + Td_iS \quad (3)$$

Considering that the work (incoming or outgoing) exchanged with a galvanic cell is an isochoric work, the useful work can be written as:

$$dW_u = E_{MN}Idt = E_{MN}dq = E_{MN}\, nF\, d\zeta_i \quad (4)$$

$d\zeta_i$ is the variation of the extent of reaction, defined as the ratio between the amount of product that has been formed dn_y and the respective stoichiometric coefficient ν_y. Since in an electrochemical reaction, a molar variation corresponds to a variation of the charge, it can be written:

$$d\zeta_i = \frac{dn_y}{\nu_y} = \frac{dq}{nF} \quad (5)$$

where *n* is the number of electrons exchanged in the reaction and *F* is Faraday's constant, 96485 C mol^{-1}, corresponding to the charge associated with and carried by a mole of electrons.

From 4, it is possible to calculate E_{MN}, and substituting with equations 2 and 3, the following expression can be obtained:

$$E_{MN} = \frac{dW_u}{nFd\zeta_i} = \frac{\Delta G}{nF} + \frac{T}{nF}\frac{d_iS}{d\zeta_i} \rightarrow E_{MN} + fem = e^* \quad (6)$$

If the reaction is in equilibrium then the dissipation $e^* = 0$ and the voltage at the terminals is equal and opposite to the electromotive force. Thus $E_{MN} = -fem = \frac{\Delta G}{nF} = E_{an} - E_{cat}$.

It follows that if $\Delta G < 0$ then the chemical reaction will be spontaneous and the galvanic cell will act as a generator; otherwise, if $\Delta G > 0$, the reaction is not spontaneous, and to make it happen it is necessary to give energy to the system, corresponding to the case of the electrolyser. The reference ΔG is however an electrochemical ΔG, and the equilibrium condition refers to it.

This equilibrium condition refers to the open circuit, for which a balance is created between the electrode and the electrolyte solution in which it is immersed. Assuming a Daniel pile (Copper-Zinc) as an example, the chemical equilibrium involves the dissolution of zinc ions Zn^{2+} in the electrolyte, as a consequence, an excess of electrons (2 for each ion) is left on the electrode that becomes negatively charged. As the chemical equilibrium proceeds, the increasingly negatively polarised

electrode will act as a counterforce to bring the Zn^{2+} ions back onto the electrode. Electrochemical equilibrium is established when the forces involving the ions that pass into solution and the ions that are re-attracted to the electrode are equal. This separation identifies a potential difference for the semi-element. This will clearly also apply to copper, but with opposite dynamics, i.e. the ions present in solution will want to group on the electrode. Since the two contributions of the equilibria of the semi-elements cannot be separated, it is necessary to compare them against a fixed reference, such as the standard hydrogen electrode SHE, obtained as platinum immersed in aqueous solution at pH=0 and atmospheric pressure.

Each element is compared to the potential of hydrogen, assumed to be zero. Thereby, the standard reduction potential of the other elements is defined. A larger potential outlines a greater tendency of the species to reduce, a smaller potential expresses a tendency of the semi-element to oxidise.

When moving away from standard conditions, it is necessary to use the Nernst equation:

$$\mathrm{E}_{\mathrm{O/R}} = \mathrm{E}° - \frac{\mathrm{RT}}{\mathrm{nF}} \ln\left(\frac{[R]}{[O]}\right) = \mathrm{E}° + \frac{\mathrm{RT}}{\mathrm{nF}} \ln\left(\frac{[O]}{[R]}\right) \qquad 7$$

where $E°$ is the standard reduction potential of the reaction, n is the number of electrons exchanged, R is the universal constant of gases, T is the temperature, and [O] and [R] are the concentrations of the oxidising and the reducing species.

Table 2 shows some of the most interesting potentials for the narrative of this work, which concern the possible redox pairs at the electrodes, each with its own reduction standard potential.

Taking into account the reactions involving oxidation and reduction of water, it can be said that these are dependent on the media involved, which directly influences the potentials. For instance, the oxygen reduction equations (6, 9 in Table 2) identify different potentials depending on whether the reaction takes place: in an acidic environment the potential is + 1.229 V, in a neutral-alkaline media it is + 0.401 V. The Pourbaix diagrams (Fig. 2) allow linking the pH of the solution with the potentials involved.

Table 2 Standard reduction potential of water, chlorine and sodium.

Reaction	E° SHE [V]	
$HClO_2 + 3H^+ + 4e^- \leftrightarrow Cl^- + 2H_2O$	+ 1.570	1
$HClO + H^+ + 2e^- \leftrightarrow Cl^- + H_2O$	+ 1.142	2
$ClO_3^- + 6H^+ + 6e^- \leftrightarrow Cl^- + 3H_2O$	+ 1.451	3
$ClO_4^- + 8H^+ + 8e^- \leftrightarrow Cl^- + 4H_2O$	+ 1.389	4
$Cl_2 + 2e^- \leftrightarrow 2Cl^-$	+ 1.358	5
$O_2 + 4H^+ + 4e^- \leftrightarrow 2H_2O$	+ 1.229	6
$ClO^- + H_2O + 2e^- \leftrightarrow Cl^- + 2OH^-$	+ 0.890	7
$ClO_2^- + 2H_2O + 4e^- \leftrightarrow Cl^- + 4OH^-$	+ 0.760	8
$O_2 + 2H_2O + 4e^- \leftrightarrow 4OH^-$	+ 0.401	9
$2H^+ + 2e^- \leftrightarrow H_2$	**0.000**	10
$2H_2O + 2e^- \leftrightarrow H_2 + 2OH^-$	- 0.827	11
$Na^+ + e^- \leftrightarrow Na$	- 2.710	12

Regarding equation 10 in Table 2, the (a) line in Fig. 2a relative to the stability of hydrogen can be easily obtained, starting from the Nernst equation (8).

$$\mathrm{E}_{\mathrm{H^+/H_2}} = \mathrm{E}^\circ + \frac{\mathrm{RT}}{\mathrm{nF}} \ln\left(\frac{[O]}{[R]}\right) = \mathrm{E}^\circ{}_{\mathrm{H^+/H_2}} + \frac{\mathrm{RT}}{\mathrm{nF}} \ln\left(\frac{[H^+]}{P_{H_2}}\right) \qquad 8$$

In conditions of atmospheric pressure ($P_{H_2} = 1$) and temperature of 25°C, by making the necessary substitutions and multiplying by 2.3 to change to the logarithm in base 10, the expression of the potential as a function of the pH is obtained as reported in the following equation:

$$\mathrm{E}_{\mathrm{H^+/H_2}} = \mathrm{E}^\circ{}_{\mathrm{H^+/H_2}} + \frac{\mathrm{RT}}{\mathrm{nF}} \ln\left(\frac{[H^+]^2}{P_{H_2}}\right) = 0 + \frac{0.059}{2} \ln([H^+]^2) = -0.059pH \qquad 9$$

Similarly, the same steps can be carried out to obtain the oxygen equilibrium curve, as a result, the (b) line in Fig. 2a is: $\mathrm{E}_{\mathrm{O_2/H_2}O} = 1.23 - 0.059pH$. By diagramming the results as the pH varies, the graph in Fig. 2a is obtained.

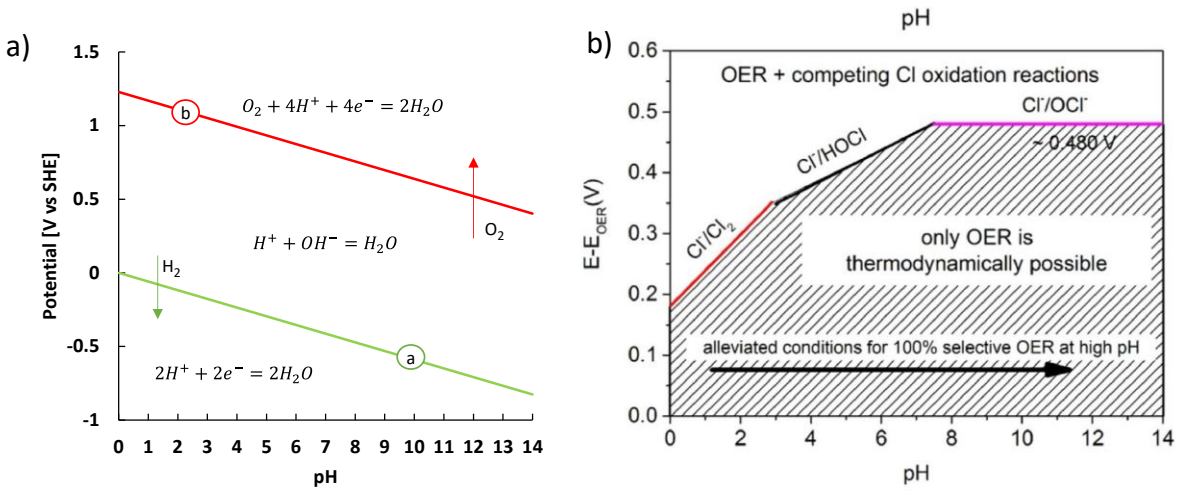

Fig. 2 Pourbaix diagram of (a) water and (b) chlorine [45].

Lines identify the region of stability of one or the other product. The line (a) defines the stability of hydrogen with respect to water, the line (b) that of oxygen. Between the two lines, water is the more stable compound, and corresponds to a situation in which the potential is less than 1.23 V, e.g., fuel cell. If this potential is increased, exceeding 1.23 V promotes the formation of hydrogen and oxygen, i.e. the electrolysis reaction. Interesting, for the chosen conditions (P=1 atm and 25°C), regardless of the pH, the thermodynamic potential of the electrolysis reaction of water is always 1.23 V. Fig. 2b shows the Pourbaix diagram of chlorine. In this case, the diagram becomes quite complicated due to the multiple reactions of chlorine related to its different oxidation numbers. The diagram compares the stability line of the O_2/H_2O pair with those of the Cl^- and its possible compounds. Interestingly, for pH values above 4, the gaseous form of chlorine is never thermodynamically favoured, but rather forms of oxygenated chlorine compounds are more stable. If the goal becomes to produce gaseous chlorine at the anode, it becomes essential to work at extremely acidic pH values.

1.2.2 Kinetics

In a system without irreversibility, the voltage read at the ends of the terminal is equal and opposite to the electromotive force of the system. However, irreversibility is almost always present and the e* term of eq. 6 is understood to be a dissipative term that collects all electrode overvoltage within it. On the other hand, if the electrolysis of water at a fixed pH must be promoted, thermodynamics suggests that it is necessary to supply the system with 1.23 V, yet if it is tried experimentally, nothing happens. This is because the system needs an additional boost, which defines its reaction kinetics.

$$E_{MN} = E° + \eta_{act} + \eta_{ohm} + \eta_{diff} \quad (10)$$

More generally, electrode overvoltage increases the electrode potential that must be given to the system for the desired reaction to take place (in the case of an electrolyser), or conversely, it decreases the potential that can be generated in the case of a battery (fuel cell). Of course, these surges are undesirable dissipative phenomena, which is why academic and non-academic research is striving to identify new materials or solutions to minimise these contributions. Among them are (i) activation losses η_{act}, (ii) ohmic losses η_{ohm} and (iii) mass transport losses η_{diff}.

Each contribution identifies specific dynamics of electrochemical kinetics. For instance, the reactant species must reach the surface of the electrode from the bulk of its solution, then it must be absorbed or otherwise interact with it, exchange electrons and finally move away from it. Each step determines an additional potential for the reaction to occur.

1.2.2.1 Activation overvoltage

Many steps are involved for a typical reaction phenomena before reactions can take place. The real peculiarity of redox reactions is that the reactive step includes a charge transfer step, in which the reactive species exchanges electrons with the metal (electrode). The first approaches to the world of electrochemical kinetics were made by Julius Tafel [46]. Tafel's intuition was to plot the variation of the electrode overvoltage against the current density i rather than the absolute potential of the reaction. The electrode overvoltage trend for hydrogen reduction reactions for various metals was thus reported and it was noted that these presented a linear trend when plotted against a $\log(i)$ diagram. These lines, are expressed as 11:

$$\eta = a + b \log(i) \quad (11)$$

known as the Tafel line [47]. In which η is the overvoltage of the electrode, a and b are coefficients, and i is the current density. The trend of this line is the one shown in Fig. 3d:

The Tafel line, despite being a purely empirical correlation, gave fundamental indications on the electrode overvoltage linked to charge transfer, and is still widely used today to characterize the electrodes of the different reactions, however the logical principles of the process were still unclear. Several years later, two scientists who were involved in studying electrochemical kinetics, namely Max Volmer and John Butler, came to the same conclusion in two different studies.

A generic equilibrium reaction can be written as $A \leftrightarrow B$ for which there will be a velocity constant k_f and k_b for the reaction that goes forward and backward. At equilibrium, the reaction rate will be given by:

$$v_{net} = v_f - v_b = k_f C_A - k_b C_B \quad (12)$$

where a first-order kinetics was assumed for both reactions. Kinetic constants can be described by Arrhenius' law: $k = A' e^{-\frac{\Delta G^*}{R_g T}}$ where A' is a pre-exponential factor, and ΔG^* is the Standard Free Energy of Activation, which represents an energy barrier that must be overcome by the activated complex for the reaction to take place.

In the case of an electrochemical reaction (1), it can be written that the reaction rates would be proportional, also in this case to a kinetic constant and to the concentration of the reactant, which however is located at the interface with the electrode at position x=0 and at the generic time instant t, with the notation $C_i(x = 0, t)$. Since the forward reaction is a reduction reaction, then this will be proportional to the cathode current density and similarly the backward reaction will be proportional to the anodic reaction. So the net reaction rate can be written as:

$$v_{net} = v_f - v_b = k_f C_O(0,t) - k_b C_R(0,t) = \frac{i}{nFA} \quad (13)$$

where i is the net total current density and A is the surface of the electrode. By rearranging equation (13), eq. 14 is given, which represents the total current density of the system.

$$i = i_c - i_a = nFA[k_f C_O(0,t) - k_b C_R(0,t)] \quad (14)$$

Depending on the prevalence of cathodic and anodic (i_c and i_a) current density over the other, the behaviour of the electrode is decided, which will act as a cathode or anode, thus favouring the reduction or oxidation of the species.

According to Arrhenius' law, it is shown that the electrode acts as a catalyst of the redox reaction for which the standard free energy of activation can be linked to the overvoltage for charge transfer η. The details of the logical-mathematical steps can be read in [47,48], but for the sake of brevity, the final expression of these passages is reported in eq. 15, known today as Butler-Volmer (BV) equation:

$$i = i_0 [\frac{C_O(0,t)}{C_O^*} e^{(1-\alpha)nf\eta} - \frac{C_R(0,t)}{C_R^*} e^{-\alpha nf\eta}] \quad (15)$$

where i_0 is defined as the exchange current density, C_i^* represents the concentration of the species in the bulk of the solution, α is the transfer coefficient and represents a measure of the symmetry

of the energy barrier of the activated complex, n is the number of electrons involved in the reaction, and f is defined as F/RT.

Expression 15 is used to calculate the overvoltage of the electrode for charge transfer (or activation), it is indicative of how much the system moves from the equilibrium conditions (and not from the potential in an absolute sense). It defines the current circulating through the electrode, or even the speed of the half-reaction. The term i_0 takes into account the Arrhenius, the temperature and the chemical-physical properties of the species-electrolyte-electrode interactions. The equation, in its most general form, also takes into account possible concentration variations between the bulk of the solution and the electrode interface.

Equation 15 can be further simplified if a condition of pure kinetic control by charge transfer is assumed, in this case the expression is rewritten in 16:

$$i = i_0[e^{(1-\alpha)nf\eta} - e^{-\alpha nf\eta}] \qquad 16$$

The equation if represented on a $i\ vs\ \eta$ diagram presents the trend shown in Fig. 3a. In fact, since the total current is the resultant of the anode and cathodic current (dotted lines), the trend of eq. 15 is represented by the curve in black.

The exchange current density defines how good an electrode is, in fact, the larger this value, the lower the associated overvoltage and consequently the greater the efficiency of the process. A schematic representation of how i_0 influences the kinetics of the system is shown in Fig. 3b. The meaning of the term alpha is shown in Fig. 3c. As can be seen, as α varies, the magnitude of the overvoltage contribution for the same electrode varies depending on whether it operates as an anode or cathode. For example, the grey curve, which corresponds to an $\alpha = 0.75$, is synonymous with an excellent cathode trend, for which η is low, but on the contrary shows a worsening of the anodic behaviour. This translates into the fact that, compared to the activated complex, the cathodic forward reaction is more favoured than the anodic backwards reaction, which finds a greater energy barrier.

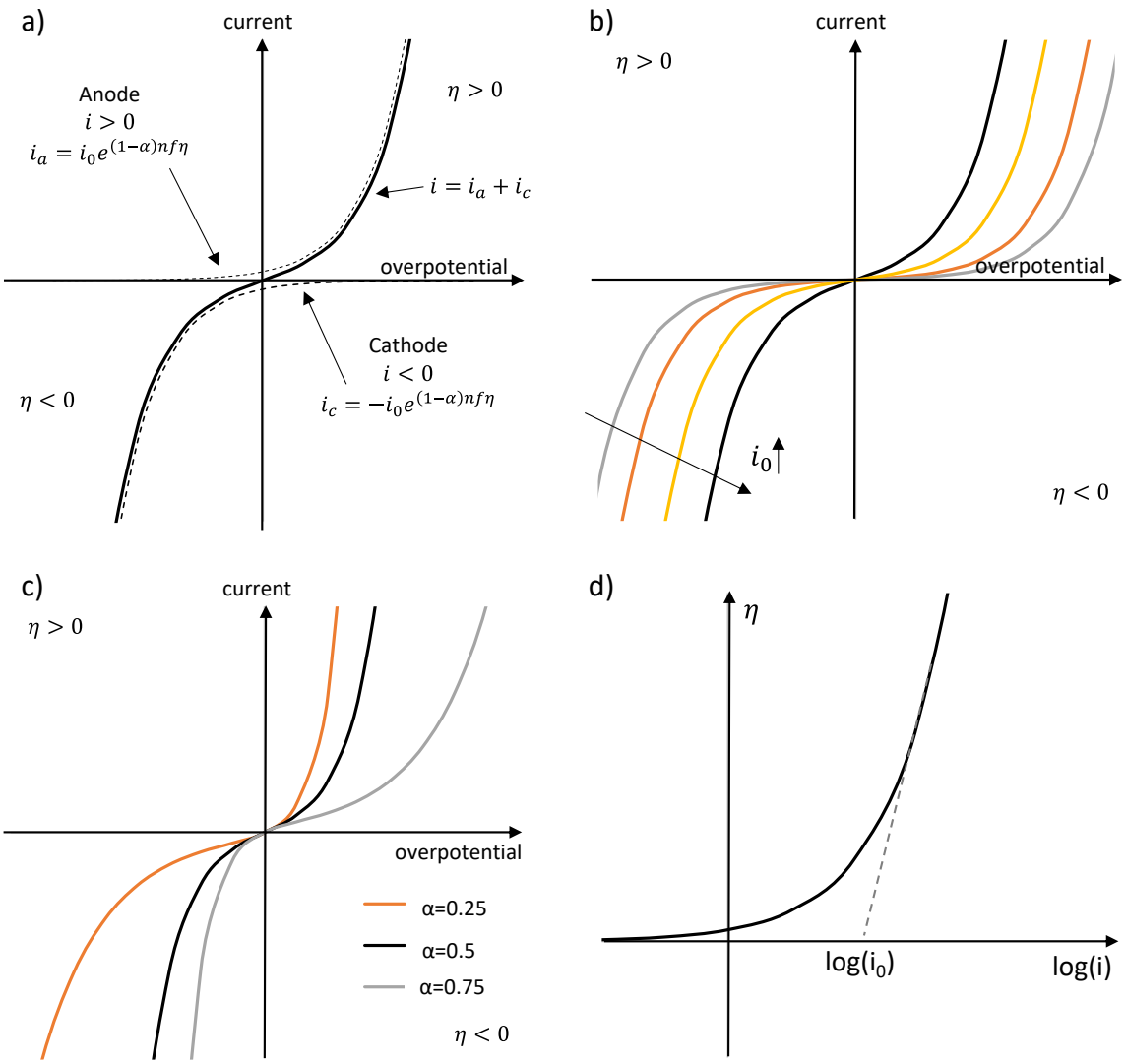

Fig. 3 (a) Butler Volmer trend, (b) effect of the exchange current density in BV equation, (c) effect of the transfer coefficient in BV equation and (d) Tafel plot.

At high fields, i.e. for high currents, the behaviour of the electrode as an anode or as a cathode is prevalent, this means that one of the two exponential terms of equation 16 can be neglected. In fact, assuming a cathode behaviour, expression 16 can be rearranged in expression 17:

$$\eta = -\frac{1}{\alpha nf}\ln\left(\frac{i}{i_0}\right) = -\frac{2.3\,RT}{\alpha nF}\log(i) + \frac{2.3\,RT}{\alpha nF}\log(i_0) \qquad 17$$

Which is actually eq. 11, identified by Tafel years earlier, where $a = -\frac{2.3\,RT}{\alpha nF}$ and $b = \frac{2.3\,RT}{\alpha nF}\log(i_0)$. Therefore, the Tafel equation is a specific case of the Butler-Volmer's, which refers to high-field reactions and is also a very useful tool for the experimental determination of BV parameters, i.e. i_0 and α.

1.2.2.2 Ohmic overpotential

Ohmic overvoltage is mainly caused by all possible ohmic drops in the system. These certainly include the losses of the electrolyte solution, the ohmic drops related to any separators/membranes, the resistance to the transport of charges of the materials of the system and of the electrodes themselves. More generally, these surges are referred to as follows:

$$\eta = Ri \qquad 18$$

They are directly proportional to the current that passes through the system, unless a constant R that defines the resistance of the medium in which the charge is transported (Ohm's first law). The resistance can be calculated according to Ohm's second law, as shown in expression 19:

$$R = \frac{\rho l}{A} = \frac{l}{\sigma A} \qquad 19$$

where ρ is the resistivity of the material in Ω m while l and A are the length and cross-sectional area of the conductor, respectively. The inverse of resistivity is conductivity σ expressed in S m^{-1}. Expression 19 can be used both to estimate the ohmic drops of a solid material and a liquid, such as the electrolyte itself.

1.2.2.3 Diffusion overpotential

If the speed of the process, i.e. the current, is increased, a higher and faster reactant consumption will occur in the system due to the reaction. Between the step from eq. 15 to eq. 16 it was assumed that the concentration of the reactive species was always guaranteed and that at the interface of the electrode there was the same concentration as the bulk of the solution. Depending on the type of reaction promoted, this flat concentration profile is not always ensured and could fall back into the case of a reaction kinetically controlled by mass transport.

The flux of matter is due to a concentration gradient at the interface of the electrode, defined by Fick's law, which can be transformed into current density by multiplying it by zF:

$$i = zF\left(-D\frac{\partial C}{\partial x}\right)_{x=0} \qquad 20$$

where D is the diffusion coefficient of the species. More generally, there will be a boundary layer δ where the species will be consumed due to the reaction rate very close to the electrode, identifying a concentration profile. Equation 20 can be simplified into 21, assuming a linear profile.

$$i = -zFD\frac{\partial C}{\partial x} \approx -zFD\frac{C^* - C(0,t)}{\delta} \qquad 21$$

The faster the charge transfer phase, the closer a limit condition is achieved, for which the concentration at the interface tends to 0. Therefore, everything that reaches the electrode interface reacts, identifying a current to not exceed, representing a real technical limit of the process. If the extreme limit current condition occurs in the system, then:

$$i_L = -zFD\frac{C^*}{\delta} \qquad 22$$

where i_L is the limit current density for which $C(0,t) = 0$. The ratio between the eq. 21 and 22 allows linking the ratio between the concentration at the interface and the bulk concentration with the limit current of the system, for which, making the necessary substitutions, expression 24 is obtained:

$$\frac{i}{i_L} = \frac{C^* - C(0,t)}{C^*} = 1 - \frac{C(0,t)}{C^*} \qquad 23$$

$$i = i_0\left[\left(1 - \frac{i}{i_{cat,L}}\right)e^{-\alpha nf\eta} - \left(1 - \frac{i}{i_{cat,L}}\right)e^{(1-\alpha)nf\eta}\right] \qquad 24$$

In general, the problem of limiting current for mass transport can occur both for systems operating at high electric fields, for which it is possible to neglect the double behaviour of the electrode, and at low electric fields. This means that mathematically different expressions are obtained depending on the case. In literature, the most refers to mass transfer or diffusion overpotential as:

$$\eta_{diff} = \frac{RT}{nF}ln\left(1 - \frac{i}{i_L}\right) = \frac{RT}{nF}\ln\left(\frac{C(0,t)}{C^*}\right) \qquad 25$$

All these equations are related to the chemical species that must react and reach the surface of the electrodes. However, it must be borne in mind that a problem of mass transport is also related to the removal of the product from the electrode, to leave room for new reactant to react. Very often, an overpotential diffusion is calculated in relation to the species produced compared to their concentration/pressure in the bulk. In the case of water electrolysis reactions, where gases are formed, a bubble overvoltage is considered, often estimated with empirical correlations.

1.2.2.4 Chemical reaction

With regard to the electrolysis reaction of water, attention has to be paid to the step that precedes (or follows) the transfer of charge. In this case, a real chemical reaction could take place, which does not directly affect the overall potential and which could be the kinetic control stage of the process. Chemical steps, such as species absorption or desorption, need the electrode not only to exchange

electrons but precisely to make the reaction take place, although the metal does not participate in the overall reaction balance.

Depending on the electrode used, the hydrogen development reaction can be easy or particularly demanding. Two possible reactive steps can affect the H^+ ion. The first step is called "first proton discharge", which involves a reactive intermediate M-H_{ads} where the H^+ has been reduced and adsorbed on the surface of the metal. The next stage presents two reactive possibilities. The first is a stage of chemical desorption, known as the Tafel-Volmer mechanism, where there are no electron exchanges. The second possibility, on the other hand, is the Heyrovsky-Volmer mechanism, which is an electrochemical desorption involving an electron. In both mechanisms, the Volmer step represents the initial step for the adsorption and reduction of the proton, while the Tafel and Heyrovsky steps are the concluding steps for the formation of the hydrogen gas molecule. The discussed mechanisms are shown in Table 3.

Table 3 Electrolysis mechanisms for HER reactions [15,49]

Reactions:	**Hydrogen**	
	Acid	Alkaline
Electrode reaction	$2H^+ + 2e = H_2$	$2H_2O + 2e = H_2$+OH^-
Tafel-Volmer	$H^+ + M + e = MH_{ads}$ $2MH_{ads} = 2M + H_2$	$H_2O + M + e = MH_{ads}$+OH^- $2MH_{ads} = 2M + H_2$
Heyrovsky-Volmer	$H^+ + M + e = MH_{ads}$ $MH_{ads} + H^+ + e = M + H_2$	$H_2O + M + e = MH_{ads}$+OH^- $MH_{ads} + H_2O + e = M + H_2$+$OH^-$

These mechanisms are among the most accredited, but their mathematical treatment is particularly complex, since to characterise these reactive steps it is necessary to pass through the concept of surface coverage, which expresses a measure of the H_{ads} on the active sites of the catalyst depending on the kinetic constants of the reactions.

1.2.3 Water Electrolysis

In the electrolysis of water, the kinetically limiting step is that of charge transfer, especially for oxygen reactions. Regardless of the media, this involves the exchange of 4 electrons, for which the process inherently requires more time. Typical activation overvoltages for water oxidation are between 0.2 - 0.4 V [50], presenting for ruthenium and iridium oxide electrodes, i_0 in the range of 10^{-7}-10^{-12} A cm^{-2} depending on the conditions. Hydrogen, on the other hand, is more kinetically

favoured and its peaks are typically lower, around 0.05 V, with exchange current densities of about 10^{-3} A cm^{-2} [51]. However, the chemical reaction step associated with the adsorption and desorption steps shown in Table 3 is the controlling process for the HER. The electrode material determines the rate at which these ad/desorption reactions take place. On one hand, if the affinity of the material has to be increased to promote the adsorption of H^+, on the other hand, the desorption energy cannot be taken too high to become the kinetic control step. For this reason, different metals have been studied to find the material that best favours these two steps, making them as simple and fast as possible. The volcano plot [52] in Fig. 4 shows this tendency. It plots the logarithm of the exchange current density against the energy of the M-H_{ads} bond. If the energy is too high, the desorption step is disadvantaged due to excessive affinity, whereas if the energy is too low, the adsorption step is disadvantaged.

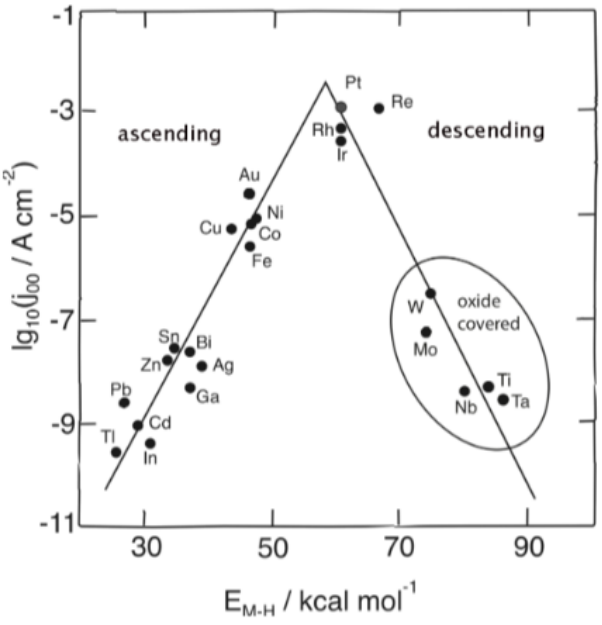

Fig. 4 Volcano plot for hydrogen evolution reaction [52].

The family of metals at the top of the volcano is the perfect middle ground, favouring both processes. However, these metals are platinum, ruthenium and iridium, all of which are particularly rare and expensive. An excellent alternative is the nickel, cobalt and iron group of metals, for which there is a good affinity and fairly high exchange current densities.

2 *Electro membrane processes*

Osmotic processes have been well known and studied since the early 1800s. Specifically, in the case of osmosis, for example, if two solutions of different salinity are separated by a porous diaphragm impermeable to salts, spontaneously the water (or solvent) will tend to move from the more diluted solution to the more concentrated one, to restore equilibrium and cancel the chemical potential gradient that has been generated. At equilibrium, a certain volume of solvent has shifted, which results in an osmotic pressure. Concerning the osmotic processes, the porous septum is ideally impermeable to salt, regardless of whether it is dissolved in cations or anions. Therefore, it can be imagined using special membranes that selectively retain only anions or only cations. These special separators are known with the name of ion exchange membranes (IEMs).

Electro-membrane technologies exploit the presence of IEMs to selectively move ions, for different purposes: desalination, energy production and storage and production of chemicals. The best-known and widely used electro-membrane process is the ElectroDialysis (ED), used for the desalination of water or the selective removal of ions present in solution. The addition of bipolar membranes to the system (Electrodialysis with Bipolar Membrane, EDBM) makes it possible to exploit an external electric field to promote the dissociation of water with the consequent formation of HCl and NaOH, thus of chemicals, starting from a saline and freshwater solution.

The processes can also be used to do exactly the opposite, for example, the Reverse ElectroDialysis (RED) has been proposed in literature for obtaining electrical energy from solutions with different salinity, i.e. when a salt gradient is available. The latter process, which is relatively less efficient, can be improved if a pH gradient is used instead of exploiting a salinity gradient. This is precisely the case of Reverse ElectroDialysis with Bipolar Membrane (REDBM), i.e. the opposite process to EDBM. If the latter is associated with charging (EDBM) and discharge (REDBM) phases, it is also possible to use these systems for energy detachment; this system is known as Acid Base Flow Battery (ABFB).

2.1 Electrodialysis (ED), Reverse Electrodialysis (RED) and Assisted Reverse Electrodialysis (A-RED)

When low salinity feeds are to be desalinated, ED become competitive compared to RO. Generosus et al. stated that ED can be more profitable when a salty feed lower than 10 g L^{-1} is treated. For a feed concentration ranging 2–10 g L^{-1}, water costs are about 0.25–0.5 \$ m^{-3}_{w} [53]. The ED unit is a stack constituted by two electrode plates that enclose a repetition of cationic and anionic exchange membranes (CEMs and AEMs) separated by spacer-filled channels. A schematic representation of an ED unit is reported in Fig. 5. The repetitive unit of the system is called cell pair, and it is composed of two Ionic Exchange Membranes (a CEM and an AEM) and two channels. An electric voltage is applied at the electrodes through a power supply, while the feed to be desalinated is flowing in the spacer-filled channels of the stack. As a consequence, red-ox reactions occur at the electrodic compartments and ions start moving across the IEMs according to their electrical charge (ideally, cations pass through the CEMs, while they are blocked by the AEMs). As a result, the feed solution is split into a low salinity one (i.e., freshwater, hereafter indicated with the subscript L) and a high salinity solution (i.e., brine, hereafter indicated with the subscript H).

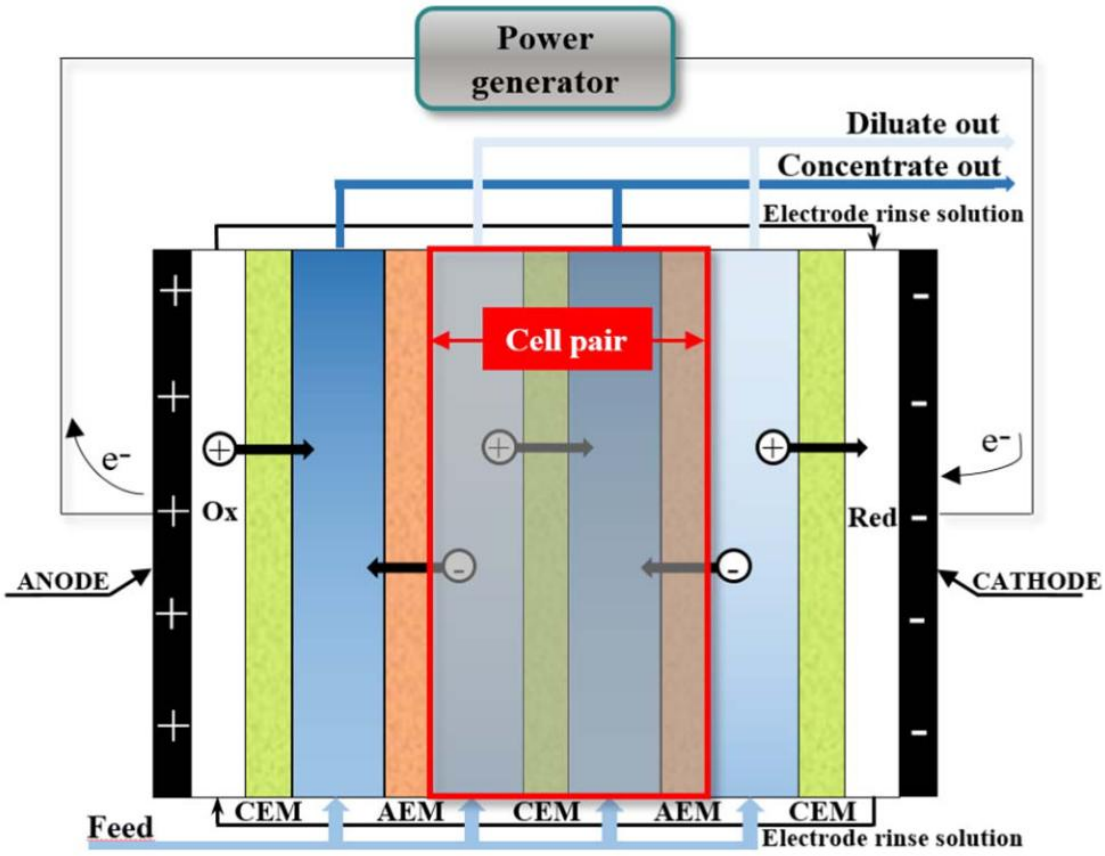

Fig. 5 Schematic representation of an electrodialysis unit [34]

In conventional ED plants [35], as electrode rinse solution (ERS) in the electrodic compartments, demineralised water with a chosen electrolyte is employed. Typically, hydrogen at the cathode and oxygen at the anode are produced because of the redox reactions needed to close the circuit. These two gases (especially the hydrogen) are considered a waste for ED plants, and attention is paid to their handling and release. The electrodic compartments-related power drawn is negligible in industrial plants where several (up to 1000) cell-pairs are assembled. This power consumption is due to (i) the thermodynamic potential, (ii) the overpotential needed for the redox reactions, and (iii) the corresponding ohmic losses in the compartments.

The majority of industrial plants of electrodialysis (ED), electrodialysis reversal (EDR) and electro-deionisation (EDI) deals with brackish water, with a capacity ranging between a few tens of $m^3 \cdot day^{-1}$, to 10,000 $m^3 \cdot day^{-1}$ [34]. ED is a well-known technology applied in various industrial fields such as in the food sector [54], ultrapure water production [55], heavy metals removal [56] and studied in several innovative application, such as the tertiary treatment of municipal wastewaters [57] and as a pre-treatment step for RO seawater desalination [58].

RED is the opposite process of the ED, it exploits a salinity gradient to convert it into electrical energy. Reverse electrodialysis has mainly been proposed and designed so far for the production of electricity using seawater and river water. During the last years, many improvements have been achieved in laboratories using artificial seawater (~30 gL^{-1} NaCl) and river water (~1 gL^{-1} NaCl) [59– 61]. The RED technology was also tested with non-conventional solutions, such as human urine [62], artificial solutions of ammonium bicarbonate [63,64], or real solutions of Produced Waters [65,66]. The latter are waters that originate during the oil and gas extraction, are characterised by high salinity (up to 300 gL^{-1}) and the presence of dissolved hydrocarbon compounds. The authors proposed the use of RED technology as an intermediate step to reduce the salinity of produced waters and make them more compliant with a possible next bioremediation step. In the context of controlled dilution of salty streams, Assisted Reverse Electrodialysis (ARED) has been suggested as a method to deal with produced waters [67]. ARED is a novel technique which is attracting a growing interest in the desalination community. As a difference from standard RED, in ARED the spontaneous ion passage from the concentrate stream to the dilute stream is assisted (i.e. enhanced) by applying an external voltage. As a consequence, in ARED, no energy is generated; rather, it is consumed to assist the controlled dilution [68,69]. On the other hand, a lower membrane area is required for desalination, thus resulting in lower capital costs. RED and ARED have been

proposed in different schemes to pre-desalinate streams before further treatment [58,70–72]. Gurreri et al. [58] tested ED-ED-RO, ED-RO and RED (in short circuit conditions)-ARED-RO configurations, finding that the energy consumption was about 5.6–8.4 kWh·m^{-3} in the firstly mentioned configuration, while it reduced to about 4.1 kWh·m^{-3} with the simpler ED-RO system. The lowest energy consumption (about 3.5 kWh·m^{-3}) was found for the case of ARED, demonstrating that this process represents an interesting alternative in the fields of desalination and wastewater treatment. La Cerva et al. [70] used a model to evaluate the performances and costs of ARED-RO and ED-RO and compare them with a stand-alone RO system. ARED-RO was found to require a lower energy consumption for a wide range of applied external voltage, with a maximum cost saving of about 7.5 %. Conversely, in the ED-RO system, the energy consumption in the ED pre-treatment exceeded the energy saving of the following RO step.

The operation of the system in ED, RED and ARED conditions is represented in Fig. 6.

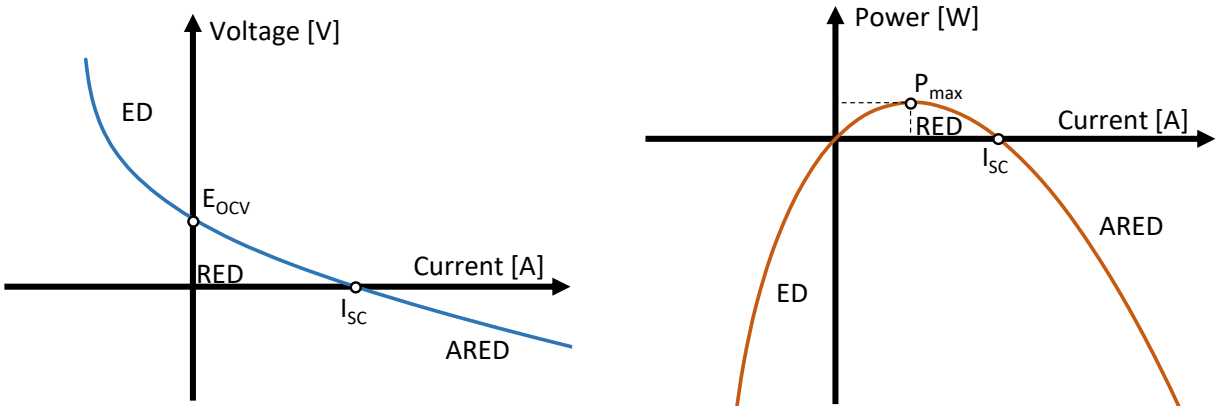

Fig. 6 Schematic representation of a typical polarisation curve (on the left) and Power curve (on the right) for the electro-membrane processes [65].

When the system is fed by the solutions and the external circuit is open, the open-circuit voltage (E_{OCV}) is measured between the electrodes, and no current circulates in the system. By closing the electric circuit, i.e. by connecting the electrodes to an external load, and progressively reducing the external load value, the voltage is progressively reduced, and a progressively higher ionic current spontaneously occurs in the system. The unit is working in RED condition with the ions transferred from the high solution to the low solution. At the electrodes, the ionic current is converted into an electric current circulating in the external circuit. Note that in RED, the cathode and anode of the system are defined by the direction in which the ions move, migration, which is defined by the order in which the solutions enter the system, i.e. by which solution is adjacent to the electrode

compartments. This means that in RED the cathode is polarised positively and the anode negatively, remaining respectively the site of reduction and oxidation. The product of the electric current and the stack voltage is the power generated by the unit. The maximum current spontaneously produced by the system is the short circuit current (I_{SC}), corresponding to an electric voltage and a power generated equal to 0. A higher ionic current can be induced in the system by applying an external electric field in the same direction as the natural flux of ions (power supply connected in series). In this condition, the system operates in ARED mode with a certain consumption of electric power given by the product of the applied voltage and the electric current.

Reversing the polarity of the electrodes would make the system work in ED mode, i.e. change the flow of ions from the dilute solution to the concentrated solution, polarising the cathode negatively and the anode positively (as in typical electrolysers). Note, however, that the ED condition in Fig. 6 is specific to the case in which the feed had two different concentrations, and therefore to work in ED, it is necessary to apply a potential higher than the OCV. However, classical ED employs a single feed at the same concentration, so a classic polarisation curve for ED would have an OCV equal to zero, and the two branches of the ED and ARED curve would start from the same point, where the only difference is the direction of migration of the ions. In addition, the ED curve has an exponential growth as the potential increases, as also shown in the graph, for which, despite applying a gradually larger potential, the current does not grow. This specific condition is called limit current, i.e. a condition for which the concentration of ions in the diluted compartment becomes zero close to the membrane. This is a situation similar to what is described in 1.2.2.3, with the only difference that in this case the reduction of the concentration, and therefore the concentration profile close to the boundary layer of the membrane, is due to the migrative flux for which these ions are transported to the other side of the membrane.

2.2 Electrodialysis with Bipolar Membrane (EDBM)

EDBM is an interesting electro-membrane process, which enables chemical production, such as HCl and NaOH. The system is fed with fresh and salty water, identifying 3 different compartments, one for the acid, one for the base and the last for the salty solution. By the application of an external electrical field, the separation of ions is promoted, so does the dissociation of water as well. The latter occurs in the BPM, where a special catalytic layer, inserted among a cationic and an anionic

layer, promotes the formation of the H^+ and of the OH^- starting from water. The hydroxyl ions go through the AEM side and are recombined in NaOH thanks to the migration of the Na^+ coming from the adjacent saline compartment, and identifying the base channel. On the other side, the protons go through the cationic layer of the BPM, where they form HCl, i.e., the acid compartment. During the process, the salty channel continuously provides the Na^+ and Cl^- to the adjacent fresh water compartments, and as a consequence, is desalinated. Conversely, the freshwater streams go out of the system as acid and base solutions. The single repetition of the three channels (acid, base and salty) and the 3 membranes (AEM, BPM and CEM) is called a triplet. A schematic representation of the EDBM unit is reported in Fig. 7.

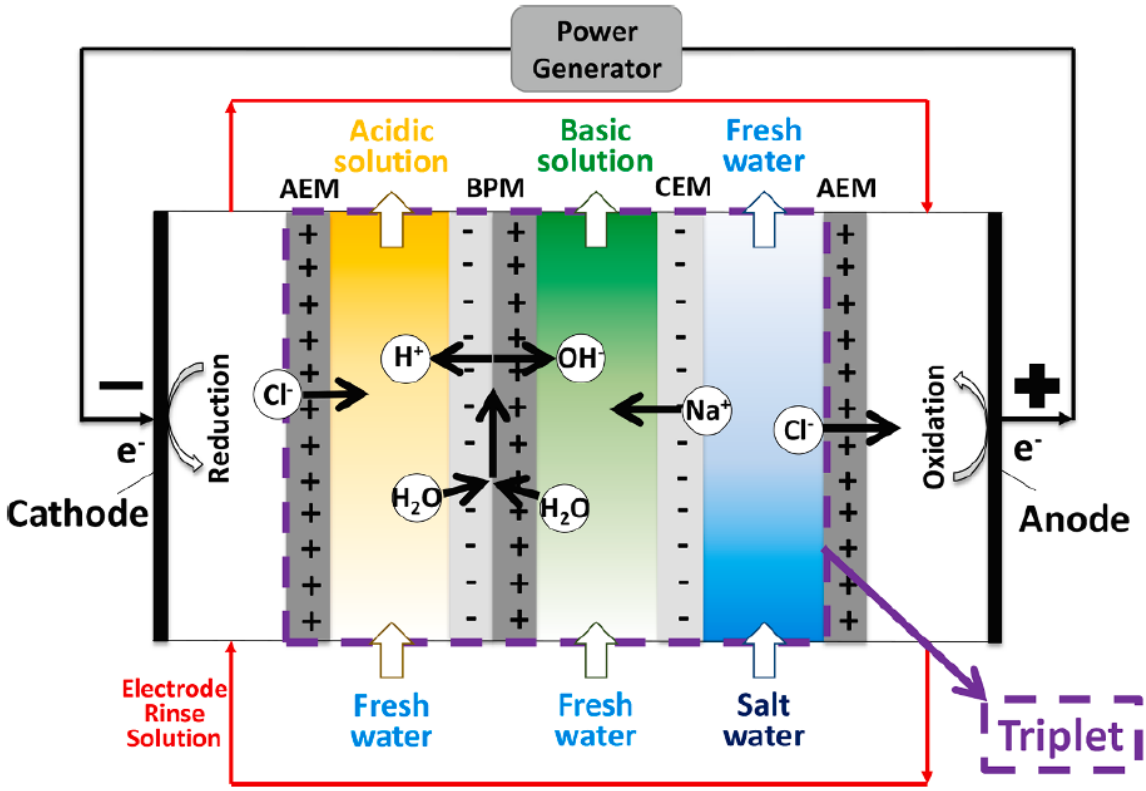

Fig. 7 Scheme of an EDBM unit, with reference to the single triplet in the dashed block in purple [73].

EDBM is today emerging as a new and promising technology for the desalination of salty streams and the production of chemicals. Furthermore, it has also been proposed for several applications such as the inorganic [74] and organic [75] acids and bases production, CO_2 capture [76] and wastewater valorisation [77] (even on a pilot scale [78]).

2.3 Aim of this work

The electro-membrane processes seen so far are systems consisting of two electrodes, for which it would be possible to produce hydrogen at the cathode and oxygen at the anode, clearly, after a careful selection of the materials of the electrodes and of the electrolyte solutions to be used. The objective of this research is to identify new opportunities for the production of green hydrogen. It explores technologies that, although not specifically designed for this purpose, could generate it as a by-product. The experiments conducted for each technology analysed and reported in this document are mainly intended to certify the technical feasibility of the processes and collect data useful for the calibration/validation of the models. Indeed, the results obtained are then integrated into a technical model capable of predicting the behaviour of the unit, even in the case of scale-up from laboratory to industrial scale. Utilising economic correlations has facilitated the execution of techno-economic analyses, enabling the evaluation of each proposed technology in various operating scenarios. This has enabled the determination of the cost associated with hydrogen production. This aspect is the focus of the work, which was conceived with a multidisciplinary approach to promote dialogue between academia and industrial applications. Consequently, the question that will guide the reader through each chapter is, and is intended to be: "*Could the integration of electro-membrane processes and hydrogen production unlock a viable and cost-effective pathway for sustainable energy?*".

To answer to this question, the methodology adopted for each technology is always the same, and hereafter explained as follows: firstly, the feasibility of such technologies is established through laboratory experiments; secondly, reliable models are set up to describe the behaviour of the units; and thirdly, the economic profitability of the processes is assessed.

Specifically, the results of the coupling of hydrogen with the RED process are described in chapter 3; the hydrogen-ED is reported in chapters 4 and 5 with an investigation for the desalination of both low and high salinity feed; and finally, in chapter 6, hydrogen-EDBM is discussed. Each technology is studied both from a technical-experimental and a modelling-economic point of view, with the aim of both characterising these systems and evaluating their cost-effectiveness and profitability. The main takeaway of this work are summarised in the final remarks of chapter 8.

During the period abroad, there was also the opportunity to model PEM water electrolyser using numerical calculation software for solving the process equations. The model used is described and reported in a separate chapter (Chapter 7), where some results of the investigation are also shown.

3 Hydrogen (Assisted-)Reverse Electrodialysis H(A-)RED

From the perspective of clean energy, therefore without pollution, the energy that can be obtained from salt gradients (SGP, Salinity Gradient Power) is included. Among the most promising SGP technologies there is the Reverse ElectroDialysis (RED), which allows to recover the normal mixing energy that two solutions with different salinity have, and to convert it into electrical energy, through the use of IEMs. For example, from the controlled mixing of 1 m^3 of seawater and river water, a theoretical energy potential of 1.7 MJ [79] would be obtainable, value that could increase if a larger amount of seawater or a higher salinity gradient were used. In recent years, the combination of salinity gradient energy and green hydrogen production has been proposed and the technology is suggested as a unit to provide energy to electrolyser or to be itself the electrolyser.

Among the first to couple RED (or its variants) to hydrogen production is Zhu et al. [80] which experimented the MRECC (Microbial Reverse-electrodialysis Electrolysis and Chemical production Cell). This technology consists of a mixed system between Microbial Electrolysis Cell (MEC) and RED, i.e. an electrolysis cell in which at the anode bacteria consume acetic acid releasing protons, electrons and CO_2, while at the cathode there is a reduction of H^+ forming gaseous hydrogen. However, an external potential must be applied to the system, and this is where RED comes into play, which transforms the flow of ions between ion exchange membranes into electron flow. In 2015, Watson et al. [81] improved the MEC system, making it continuous and achieving hydrogen productions of 0.9 ± 0.1 L_{H2} $L^{-1}_{reactor}$ d^{-1} (or yields of 1.1 ± 0.1 L_{H2} g^{-1}_{COD}). Yields improved as the number of cell pairs of the RED increased, and with this increase in cells, there was a greater removal of COD. The research also showed that hydrogen production improved if the anolyte had a sufficient COD concentration to maintain a stable potential at the anode.

This research had significant results and has a very wide industrial application, as the technology is offered as a method of waste treatment, and from this it is possible to obtain a useful and desired product such as biohydrogen. Biomass processes can help diversify Europe's energy supply and are considered renewable energy despite the inevitable production of carbon dioxide during the fermentation of organic material. However the CO_2 could be removed, for example, by using a fixed bed of magnesium and calcium silicates (carbon capture) making the process sustainable.

In 2014, Hatzell et al. [82] developed a new way to treat acid waste stream and make the Ammonium Bicarbonate (AmB) RED system, by using waste heat energy. In their work, H_2 was

produced in the system using the acid that was to be disposed of and they achieved a maximum cathodic recovery of 70.5 % ± 4 % of H_2. In 2017, Nazemi et al. [83] developed a thermodynamic model for the RED and hydrogen system in order to evaluate the electricity and hydrogen produced by the system. Natural mixing process of NaCl solutions were used, resulting in a current of 11.5 mA cm^{-2} and a productivity of 1.72 mol m^{-2} h^{-1}. In 2020, Raka et al. [84] conducted thermally driven H_2 production via RED using AmB solutions. The research team implemented a model to predict the behaviour of the RED-AmB unit, producing 1.19 mol m^{-2} h^{-1} of hydrogen at the cathode with low waste heat as thermal source. Moreover, they found some minimum costs of the equipment for being the technology competitive in the market, like very low cost of membranes (less than 2.86 € m^{-2}_{IEMs}) and identified the critical key performance of the unit: (i) membrane cost, (ii) hydrogen production rate and (iii) membrane area.

Chen et al. [85] experimentally investigated the REED (Reverse Electro-Electrodialysis), i.e., a classical RED unit with hydrogen production. They studied the system for different concentrations of NaCl diluted and concentrated solutions and exploited the part of the same energy generated by the RED for producing both hydrogen and electricity. Results showed a strong dependence in hydrogen production to the current density and the electrode solution concentration. The same author, 2 years later [86] inserted a bipolar end-membrane in the cathode-side in order to produce directly the proton necessary for the HER in situ. For this new configuration, they obtained a H_2 productivity of 5.6 L m^{-2} h^{-1} (0.25 mol m^{-2} h^{-1}) with a Faradic Efficiency (FE) of 91 % ± 6 %.

The first two pilot-scale applications of RED for hydrogen production were performed in 2018 and 2019 by Tufa et al. [87] and Higa et al. [88]. Tufa et al. used a RED unit of 200 cell pair (31.5 x 63.5 cm^2) to directly supply energy to an alkaline electrolyser (6 cells, 5 x 5 cm^2) which required a Specific Energy Consumption (SEC) of 56 kWh kg_{H2}^{-1}. The electrolyser worked at current densities of 88–110 mA cm^{-2} and an average H_2 productivity of 18 mol m^{-2} h^{-1} was obtained. Conversely, Higa et al. tested a single RED-H_2 pilot unit for which the H_2 is produced at the cathode of the RED unit and partially generate electrical energy. The unit was a 200 cell pair 20 x 50 cm^2 and used as feed seawater (SW) and sewage treated water (STW). They obtained a H_2 production rate of 0.9 L h^{-1} (H_2 productivity of 0.4 mol m^{-2} h^{-1}) and a faradic efficiency of almost 100 %.

In this chapter, RED is studied as a method for producing hydrogen at the cathode an oxygen at the anode for different configurations. In particular, the short-circuit current was investigated to performing the experiment in order to work with the maximum current density the unit can provide.

A schematic representation of the process is shown in Fig. 8. Note that hereafter the letter H, anticipating the name of the membrane technology, indicates the same revised membrane process for the production of hydrogen at the cathode, e.g., H(A-)RED Hydrogen (Assisted-)Reverse Electrodialysis.

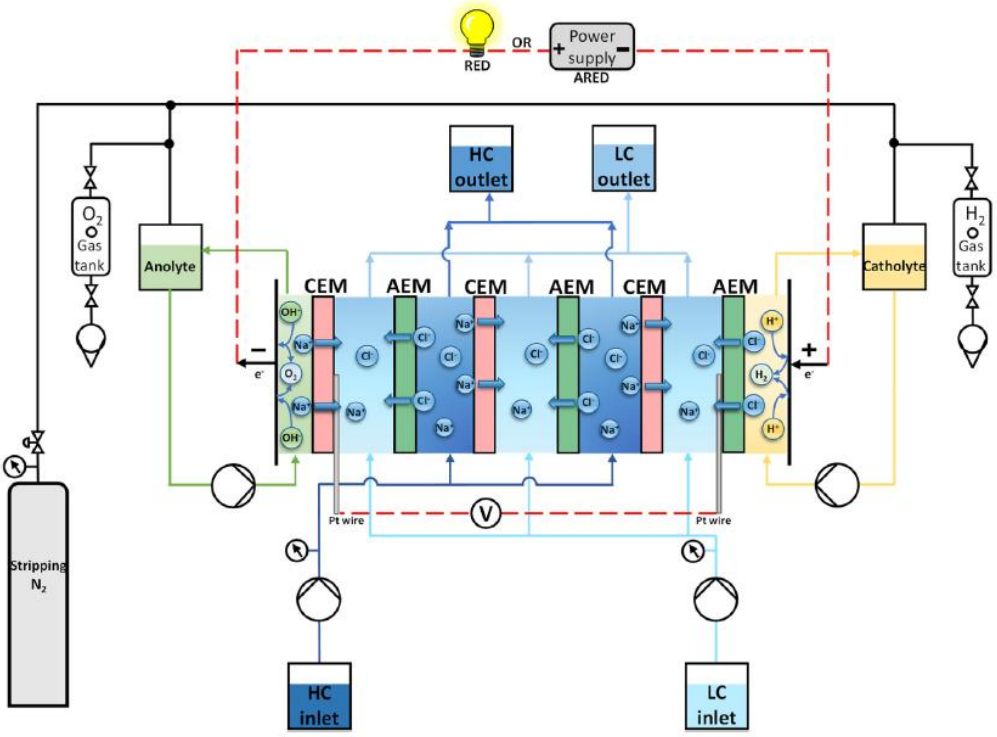

Fig. 8 Schematic representation of the H(A-)RED unit and of the set-up

Furthermore, the system was also tested in Assisted configuration, for reaching higher current density, and consequently, higher hydrogen productivity. A simplified model able to predict the experimental data was also implemented and coupled with economic correlation to establish the economic feasibility of the process.

The following chapter contain some scientific results published in [89]. A more thorough discussion of these results may be found in the paragraphs below.

3.1 Experimental

3.1.1 Set-up

A co-current lab-scale unit, 10 x 10 cm^2 was used for the experimental investigation. The unit was equipped with 20 cell pairs, constituted by commercial IEMs Fujifilm Type 10 AEM and CEM (Tilburg, The Netherlands) and by woven spacers (Redstack, Sneek, The Netherlands) of 300 µm thick for

create the channels. At the electrodes, Ti mesh grid substrate with Pt/Ir ox (MMO – Mixed Metal Oxide) electrodes were used for both the cathode and anode, based on the Sabatier volcano plot and the excellent material properties for the HER and OER [50,52]. An aqueous solution of HCl (0.5 M) was employed as catholyte, whilst an aqueous solution of NaOH (0.5 M) was used as anolyte, prepared by diluting HCl (37 %, Merck) and NaOH pellets (98–100 %, Honeywell Fluka), respectively. The two solutions are stored in two separated chambers with volumes of 150 mL for the anolyte and 200 mL for the catholyte. The different volumes were due to the availability of the glassworks, nevertheless, the solutions are recirculated by two Leadfluid YT15 peristaltic pumps (BT601S, Lead Fluid Technology, CO LTD, China) ensuring the same flow rate of 525 mL min^{-1}. Such high flow rate is wanted to increase the velocity in the electrode channels and quickly remove the bubbles.

Two different IEMs were chosen as end-membranes. A Nafion® CEM membrane was used for the anode, for its fast Na^+ exchange capacity and its better stability at alkaline pH [90], since it is in contact with a basic solution. It is also functional that it is a CEM as it must retain OH^- and ensure the salt bridge. On the contrary, the same AEM Fujifilm Type 10 (Tilburg, The Netherlands) used to assemble the stack was used as end-membrane at the cathode, to retain the H^+ and allow the exchange of the Cl^-. Closing the cell package with an AEM instead of a CEM means that there is one less salt channel, which is why the system worked with 20 channels of the diluted and 19 of the concentrated solutions. The choice to have the outermost diluted compartments is dictated by the fact that the diffusion of the Cl^- anion towards the anode compartment is disadvantaged, since the latter is found at a lower concentration.

During the assembly, two platinum wires were inserted between the channels, immediately after the first end-membrane and before the last one. The reason of this addition is to measure and isolate the voltage of the cell pairs, thus without the electrodes. However, the platinum excluded from the measure the end-membranes, reducing the effective value of the cell pairs voltage. This is due to the fact that the platinum (if inserted in the electrodic channel) would be site of electrode reactions. Concerning the feed solution, NaCl (99.7% ChemSolute) was used to prepare the saline solutions that flowed at a velocity of 0.5 cm s^{-1} (180 mL min-1) and two Cole-Parmer Masterflex I/P (77601-00, Illinois, USA) pumps were used to do so. In addition, two pressure gauges (Cewal, 2.5 bar) were installed in the hydraulic circuit to monitor the pressure drops.

To supply energy to the system, a power supply PS (EA PS2042-10B, Elektro-Automatik GmbH & Co.KG) was used, to work both in potentiostatic and galvanostatic mode. Moreover, Fluke 175

multimeters were used to measure the voltage, and a Fluke 8808A 5-1/2 Digit Multimeter was used to measure the current. Also conductivities and pH measures were taken during the test, using a WTW conductivity and pH meter (WTW™ ProfiLine™ pH/Cond 3320 Universal Multi-parameter Portable) was used.

As for the part of the gas circuit, the outlets from the stack were positioned at the top of the catholyte and anolyte solution tanks to promote the gas separation. Nitrogen (purity 99.999 %; supplied by Air Liquide) was also insufflated in the tanks and used as stripping gas. The outlet gas flow rates (measured using two KROHNE DK800/R (KROHNE Messtechnik GmbH, Duisburg, Germany) 0.01-0.1 LPM AIR 0.04-0.5) were sent to a second gas tank from which gas samples were collected. A 250 µL gastight syringe (Hamilton Company Gastight 1725 TLL, Graubünden, Switzerland) was adopted to collect the sample, later analysed by gas chromatography, (Agilent 7890B GC) with helium of 99.999 % purity at constant pressure of 1 bar as carrier gas. In addition, a few millilitres of anolyte and catholyte and solutions were taken during the tests for monitoring the concentration during the test with acid-base titration. Furthermore, samples were also used for performing UV-Vis (Agilent cary 60 UV spectrophotometer) analysis in order to detect the presence of hypochlorite in solution.

3.1.2 Experimental investigation

The experimental campaign investigated both polarization curves and long-run test to establish the performance and stability of the system. For both the polarisation curves and the RED/ARED tests, the diluted and concentrated solutions were fed in open-loop, hence without recirculating the outlets. In this way it is possible to have always the same electromotive force during the tests.

Table 4. Overview of the test sets performed and their operating conditions.

Set 1	***RED$_{SC}$***	***ARED 1***	***ARED 2***	***ARED 3***
External Voltage set ($\Delta \boldsymbol{V_{ext}}$ / V)	0.00	0.65	1.20	1.40
Current	I_{SC}	$I_{cell,SC}$	I_{SC} x 2	I_{SC} x 2.5

Each test was performed at a different current as summarized in Table 4. ARED tests were performed under different potentiostatic conditions by setting the voltage in order to obtain the desired current. Tests were repeated three times and for each point the standard deviation was calculated.

Based on the result of the polarization curves, the unit short-circuit current (RED_{SC}) was identified and used as starting point for the next investigation. Indeed, the other tests were performed at a current of 2 (ARED2) and 2.5 (ARED3) times the I_{SC}. Another interesting point investigated is the equivalent short-circuit current of the cell pairs, identified as $I_{cell,SC}$ and also estimated by the polarization curves. For the latter, the external voltage was set in order to have a zero voltage at platinum wires. The tests described in 3.1.3 refers to a concentration of the salty solution equal to 35 g L^{-1} (typical concentration of the SeaWater SW), meanwhile the diluted solution was chosen equal to a concentration of 1 g L^{-1}. Tests were also performed at different concentrations: 70 and 300 g L^{-1}, corresponding to the typical concentration of a reverse osmosis retentate and a saltworks water. The latter are fully described in [89] and not reported in the next section. However, the data of such experiments were used to validate the associated H(A-)RED technical model (see 3.2).

3.1.3 Results

The polarization curve and the voltage to the platinum wires is shown in Fig. 9. The curves take into account both the RED part and the assisted mode (negative voltages). The RED system acts as a generator itself, and the voltage produced depends on the energy that the salt gradient holds. The greater the difference in concentration, the greater this electromotive force that can be generated. Since this is proportional to the number of cell pairs, the greater the number of repeating units, the greater the potential generated. The orange curve represents the platinum wire measurement, this has an almost perfectly linear trend and shows a value in the open circuit voltage OCV condition of about 2.74 V. The measurement of the platinum wire excludes the two outermost end-membranes due to technical limit, consequently it exhibits a slightly lower value than the real one. In addition, compared to the theoretical value, the membranes show a permselectivity of about 85 %. Permselectivity averages around 95% [91] and represents the ratio between the measured OCV and the theoretical one. It represents the membranes ability to block the passage of the co-ions. Low permselectivity results in lower electromotive force, and clearly the best way to improve it is using higher-performance membranes. IEMs were originally designed for ED processes. Therefore, they inevitably demonstrate lower yields due to the different operating conditions. If RED technology will be used as an alternative source of electricity in the future, it is plausible that researching and developing new membranes could significantly improve the process's performance.

The stack voltage, on the other hand, is represented in blue, its value at the OCV is 3.24 V and due to very low current density it drops dramatically to the value of 2.8 V as a result of the energy demand of the electrode due to the electrode reaction. The typical logarithmic trend is precisely due to the activation energy for charge transfer η_{act}, a trend that becomes linear for higher current densities where the ohmic aspect of the system prevails, and for which, excluding the first part of the graph (low current densities) there is a stack resistance of 5.44 Ω.

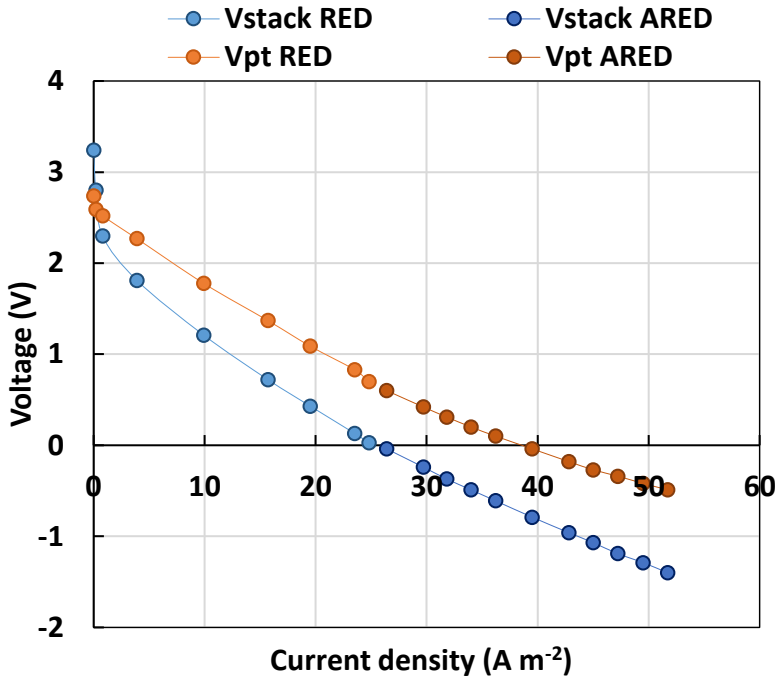

Fig. 9 Polarization curve and platinum wires voltage for the H(A-)RED unit

Interestingly, if the first section of the curve is not considered, the voltage at the platinum wires is always greater than that at the stack, precisely because the stack voltage also includes the voltage drops related to the electrodes. The difference between the two curves, therefore, represents precisely the potential of the electrodes which after an initial transient remains constant at a value of about 0.83 V, and then returns to increase for the high current of the ARED up to 1.05 V at 52 A m^{-2}. It might be surprising how opposite the trend between the potential of the stack and that of platinum at lower current densities, for which there is a reversal of the trend just described. However, it should be remembered that the system uses two electrode solutions different from the salt water of the feed, and the multimeter reading is offset by this additional potential, which cannot be measured by platinum, but which increases the total electromotive force of the system.

The short-circuit current identified by the test corresponds to approximately 25 A m^{-2} and at a current of 40 A m^{-2} also the voltage of the platinum wires becomes zero, corresponding to the $I_{cells,SC}$.

Based on the polarization curves, for which have been taken average values, the point of short-circuit has been used as a reference for the performance tests of the unit.

Fig. 10 and Fig. 11a show the current and the stack voltage, respectively. The experiments were carried out in potentiostatic mode and as a consequence both current and platinum voltage could change. In RED_{SC} the system worked at the lowest current density among the ones studied, showing a constant 0.22 A during the test, as shown in Fig. 10. When an external voltage was applied to the stack (ARED tests) setting the power supply in series with the polarization of the system (negative of PS link to the anode, i.e., the positive of the RED stack), higher current densities were observed. These currents are not constant and slightly decrease during the tests due to the potentiostatic configuration. Note, the difference between the initial and the final current registered was higher as the potential applied increases, respectively of 8, 13 and 19 % in the ARED 1, ARED 2 and ARED 3 tests.

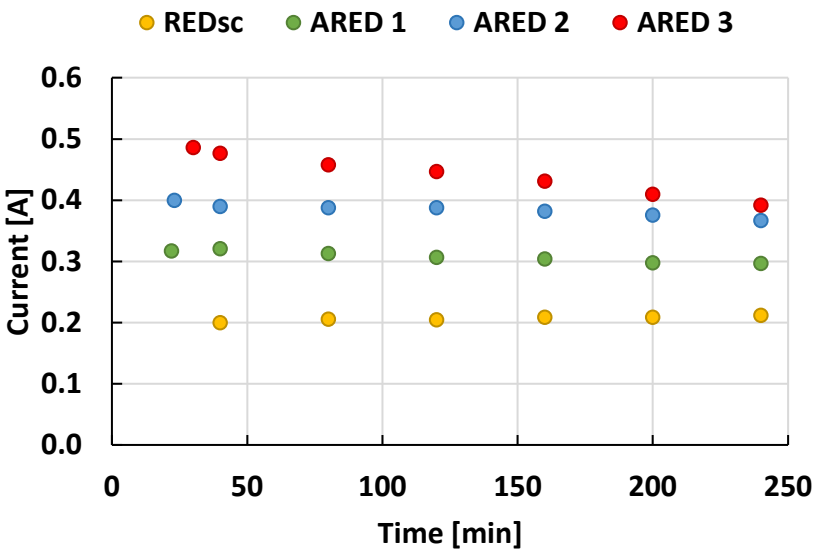

Fig. 10 Current as a function of time for the tests performed with NaCl concentrations of 1 g L^{-1} for the dilute and 35 g L^{-1} for the concentrate solutions.

Interestingly, the decrease observed reflected the cell pairs voltage (platinum) variation with time, reported in Fig. 11b. Over time, in fact, the difference between the external fixed voltage and that of the platinum wire for the ARED tests increases, while this difference remains more or less constant for the entire duration of the test at a value of about 0.67 V for the RED_{SC} test.

To better understand what actually happens for higher current densities (and therefore for the cases in ARED) samples of both liquid and gaseous solutions were analysed.

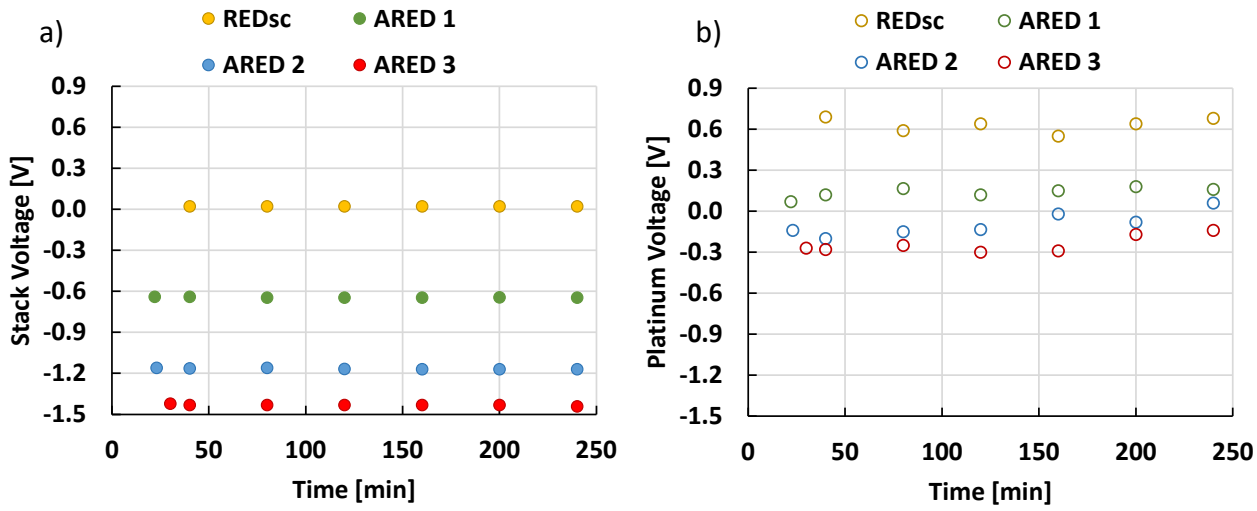

Fig. 11 (a) Stack and (b) platinum voltage measured in RED_{SC}; ARED 1, ARED 2 and ARED 3 tests.

At the cathode compartment, there was a decrease in the concentration of HCl from a value at the beginning of the test of 0.5 M to that of about 0.2 and 0.1 M for the tests in RED_{SC} and ARED, respectively. Despite the use of an anionic membrane as a separator of the saline solution and the cathode compartment, part of the H^+ dissolved in solution diffuses towards the adjacent compartments (about 15 %) for which there has been a slight acidification of the solutions (pH about 4.5). The faradic efficiencies for the 4 tests conducted and the respective productivity found at the gas chromatograph are shown in Fig. 12. As can be seen, the efficiencies are almost always 100 % and the productivity values ranges from a minimum of almost 0.4±0.066 mol m^{-2} h^{-1} in the 35 RED_{SC} test to a maximum of 0.9±0.13 mol m^{-2} h^{-1} in the ARED 3, values perfectly in line with the theoretical ones. This actually confirms what was expected, thus, there are no other competitive reactions to the cathode and, unless measurement errors, all the electric current circulating in the system produces hydrogen.

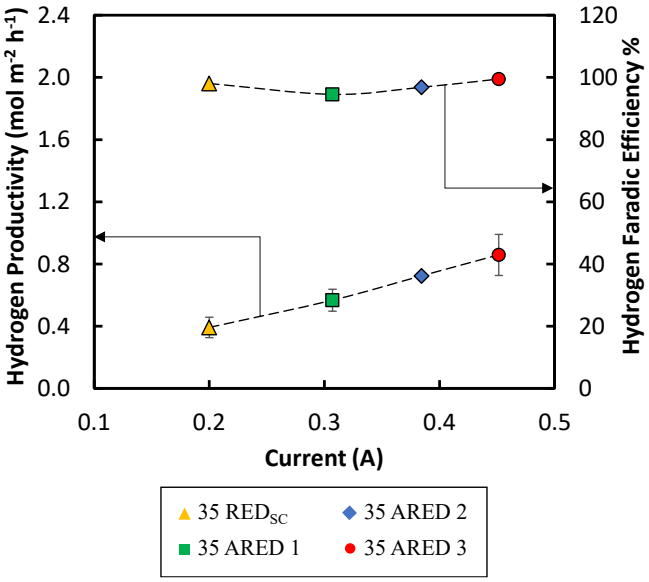

Fig. 12 Average faradic efficiencies and productivities of hydrogen versus the average current for each test performed. The error bars are based on the standard deviation.

Conversely, the anolyte NaOH concentration varied from an initial value of 0.5 M to a final value of 0.23 M in the 35 RED_{SC} test and to 0.1 M in the ARED tests. At the anode compartment, OER was expected to be the main anodic process. A FE of approximately 99 % was observed for the RED_{SC} and ARED 1 tests. Instead, when higher external voltages were used, the oxygen FE was of 88 % for the ARED 2 and about the 76 % for the ARED 3.

To clarify what happened under relatively high potential, anolyte solutions were analysed using UV- Vis spectroscopy. The instrument revealed the presence of hypochlorite (ClO^-) with concentrations of 17 mM in ARED 2 and 42 mM in ARED 3 but nothing for the RED_{SC} and ARED. Furthermore, a concentration in Cl^- of about 0.05 M and of 0.08 M in ARED 2 and ARED 3 was found in the anolyte and detected by using the ion chromatography.

These results could be explained by considering the reaction of Cl^- in an alkaline media [23]. In particular, active chlorines can be formed at the anode due to the oxidation of chloride according to reaction 7 of Table 2 and to the Pourbaix diagram of the oxygen evolution reaction and chloride chemistry Fig. 2b. Hence, at the anode, the OER competed with hypochlorite formation reaction which was favoured under alkaline conditions. The Faradic efficiency of hypochlorite was found to be 9 % in the ARED 2 tests and 20 % in the ARED 3 tests, which are the complement values to the overall faradic efficiency of the anodic compartment.

Table 5. Oxygen and hypochlorite productivities for the tests performed.

	RED$_{SC}$	***ARED 1***	***ARED 2***	***ARED 3***
Oxygen productivity (mol m^{-2} h^{-1})	0.210	0.280	0.320	0.290
Hypochlorite productivity (mol m^{-2} h^{-1})	-	-	0.066	0.160

In Table 5 is reported the relative productivity of the hypochlorite and of the oxygen, which increased with the ARED tests due to the increase of the external potential. According to the potential of the hypochlorite formation reaction (+0.89 V), this phenomenon only occurs in ARED tests 2 and 3, for which the difference between the stack voltage and the platinum wire voltage is greater. Moreover, this phenomenon is further amplified by the higher diffusion of the chlorine ions from the adjacent dilute channel, which increases its concentration in salt at large currents (Fig. 10).

3.2 Model and validation

A semi-empirical mathematical model was implemented to assess the main outputs of the H(A)RED unit, such as the hydrogen productivity and the energy (produced in RED or consumed in ARED). To establish if the unit could be economical advantageous, a simplified model was implemented. The model was not discretised, and the main properties of the unit (such as permselectivity, membrane resistance, densities, etc.) were assumed equal to a constant value or averaged between the inlet and outlet streams (lumped parameter model). The model was inspired by already existent and validated models in the literature [92,93]. However, the main changes with the literature regards the electrodes modelling. Usually, these models consider a fixed resistance, called blank resistance, that englobes the electrodes voltage drops in one term, which also takes into account the additional end-membrane and the resistance of the electrodic compartments. This is possible because reversible redox couples at the electrodes (such as iron potassium hexocyanides) are usually used to minimize the dissipation of the energy produced at the electrodes, therefore the potential drops. This choice means that the contribution of the electrodes is very small, and the blank resistance is more influenced by the ERS and the end-membrane than by the electrodes. Furthermore, since the energy production from the RED is directly proportional to the number of cell pairs, when hundreds of cell-pairs are assembled, the contribution of the blank resistance becomes negligible. Conversely, the presence of a none reversible redox reaction at the electrodes like the water electrolysis,

required the implementation of an appropriate voltage drop estimation based on the thermodynamic potentials (0.401 V), and the activation overvoltage, assumed with a conservatory constant value of 0.6 V (inferred by the experiments).

As shown in Fig. 13, the model is capable of predicting with a very good agreement the experimental data, even the simplification. And the errors among the experimental data and the model do not exceed 5 %.

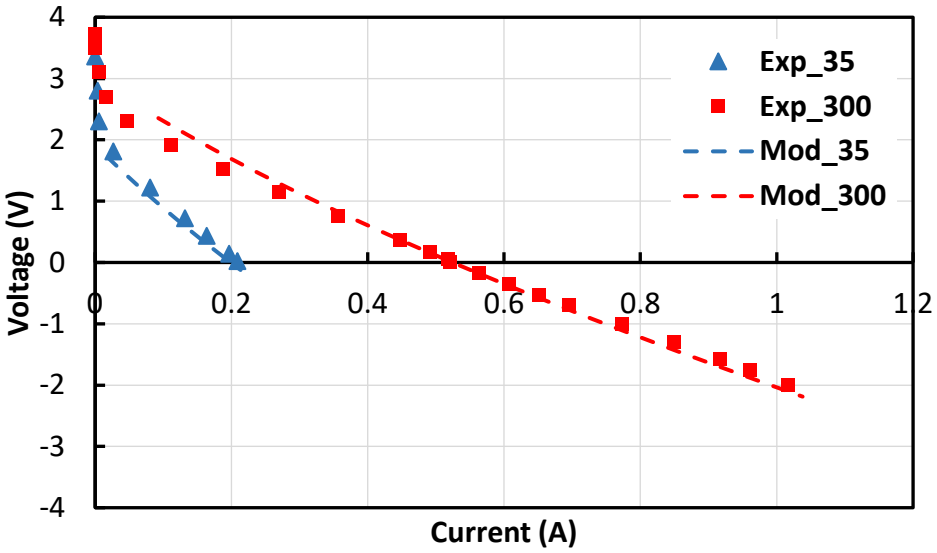

Fig. 13 Validation of the model based on the experimental data of tests at 35 and 300 g L^{-1} (see also [89]).

The model was calibrated with the results obtained during the experimental campaign, and given the good match with the experimental data, it is considered validated. The two main parameters that significantly affect the semi-empirical model are the membrane resistance and the permselectivity.

The membrane resistance was inferred from the cell package resistance (i.e., r_{cell}) assuming an averaged value between the AEM and CEM resistance (i.e., r_{AEM} and r_{CEM}), for which the following expression is valid:

$$r_{cell} = N_{cp}(r_{AEM} + r_L + r_{CEM} + r_H) \quad (26)$$

where r_L and r_H are the diluted and concentrated compartment resistances calculated as described in eq. 19. Instead, the value of r_{cell} can easily be estimated by experiments, because it corresponds to the slope of the platinum wires in the polarisation curves. The use of the platinum voltage instead of the stack one is justified because in this way the electrode influence is directly excluded. Conversely, the permselectivity can be estimated by the definition, i.e., the ratio between the

measured open circuit voltage (i.e., the electromotive force) and the theoretical Nerst potential (see eq. 28). These parameters are widely described in [94] and similar procedure/definition can also be found in [65].

The unit operated at the same conditions of the experimental campaign, e.g., flow rates, anolyte and catholyte solutions, feed concentrations, etc. Moreover, the main properties of the stack and the geometry features of the simulated unit used for the economic analysis are reported in Table 6.

Table 6. Scenario features and main economic parameters adopted in the techno-economic analysis of the H(A-)RED unit.

Membrane resistance	7	Ω cm^2
Membrane thickness	155*	µm
Permselectivity	0.8	-
Salt diffusivity	4.52 x10^{-12}	m^2 s^{-1}
Electrode voltage drops	1**	V
Number of cell pairs	20	-
Length	1	m
Width	1	m
Spacers thickness	300*	µm
Residence time per channel	20	s

*considered from technical datasheets

**average value based on the experimental test results.

3.3 Economic analysis

The main output of the technical model were used as input for the preliminary economic analysis. The time over which the investment is to be recovered, and thus the years of useful lifetime of the plant, was 20 years. A discount rate of 3 % was considered and a total amount of 5 % on the profit was destined to taxes; in addition, a straight-line depreciation method was used. The main economic parameters costs (concerning both capital investment and operating expenditure) and prices are summarised in Table 7. While a more detailed economic model description can be found in 4.3.3. The latter is specifically for the chapter 4 and 5, but the more general equation can be applied also to this chapter. The choice of not reporting the economic model here as well is to avoid repetition, as the two are very similar.

Table 7. Main economic parameters, costs and prices.

Plant lifetime	20	year
Discount rate	3	%
Working hour	8000	h $year^{-1}$
Tax	5	%
Membrane cost [29,70]	4	€ m^{-2}_{IEMS}
Membrane Lifetime [68]	10	Year
Electrode cost	100*	€ m^{-2}
Spacers cost [29,68]	2	€ m^{-2}_{IEMS}
Casing cost [29,68]	2	€ m^{-2}_{IEMS}
Labour cost [42]	10 % of equipment costs**	
Other costs [29]	3 % of FCI***	
Electricity cost [71]	0.1	€ kWh^{-1}
Oxygen price	0.1	€ kg^{-1}
Hydrogen price	variable	€ kg^{-1}

* Estimated according to IRENA [12] and corresponding to an electrode cost of 30 € kW^{-1}
** The sum of the cost of the equipment costs (i.e., membranes, electrodes etc.)
*** Fixed capital investment (i.e., equipment cost and labour cost)

By the sum of the revenues and all the expenditures, Net Present Value (NPV) can be calculated by the incoming and outgoing cash flows, and it represents the cumulative amount of money obtained at the end of the plant lifetime. The recovery of electrical energy from the RED is out of scope, and the unit is assumed to work in short-circuit or directly in Assisted mode, and as a consequence, hydrogen is the only outcome of the plant. NPV is defined by its selling price: a too low price of hydrogen involves a negative NPV (i.e., no remuneration at the end of the plant lifetime), whereas a higher price made the plant profitable. The particular case in which the NPV is equal to zero, identifying a specific price of hydrogen, that represents its production cost, known as Levelized Cost of Hydrogen (LCOH). The power density and the LCOH are shown in Fig. 14a and Fig. 14b as a function of the electric current flowing into the system. The power curves are shown for three different concentrated feed solutions: (i) the short-circuit current I_{SC} (triangle), (ii) the double of the I_{SC} (diamond) and (iii) the 2.5 times the I_{SC} (circle), according to the experimental campaign. These points were associated with the corresponding LCOH, in Fig. 14b.

As it can be seen, the LCOH varied with current, but with different trends depending on the type of feed used. When using a feed similar to the SW (35 g L^{-1}), the LCOH was among the highest, approaching 12 € kg^{-1}_{H2} in the case of the short-circuit, due to a too low current produced. In this case, the capital cost weighs heavily on the system, increasing the production cost of hydrogen. In short-circuit mode as the feed concentration increased, the corresponding current increased as

well. For instance, the LCOH decreased to a very competitive value of 3.2 € kg^{-1}_{H2} at 300 g L^{-1} thanks to the higher productivity. This optimistic value is relevant to a future membrane cost of 4 € m^{-2}_{IEMs} (see Table 7). Interestingly, with a membrane cost of 10 € m^{-2}_{IEMs} this value would increase to the still competitive value of 5.5 € kg^{-1}_{H2}. As the current increased (ARED), different trends were observed depending on the feed concentration. In the 35 g L^{-1} case, a minimum was reached at a current equal to twice the I_{SC}, a value that increases again for higher current values, due to the ohmic voltage losses that became consistent. On the contrary, the LCOH rises almost linearly with the increase in the current flowing through the system in the 300 g L^{-1} case, reaching an LCOH of more than 10 € kg^{-1}_{H2} for the 2.5x I_{SC} case.

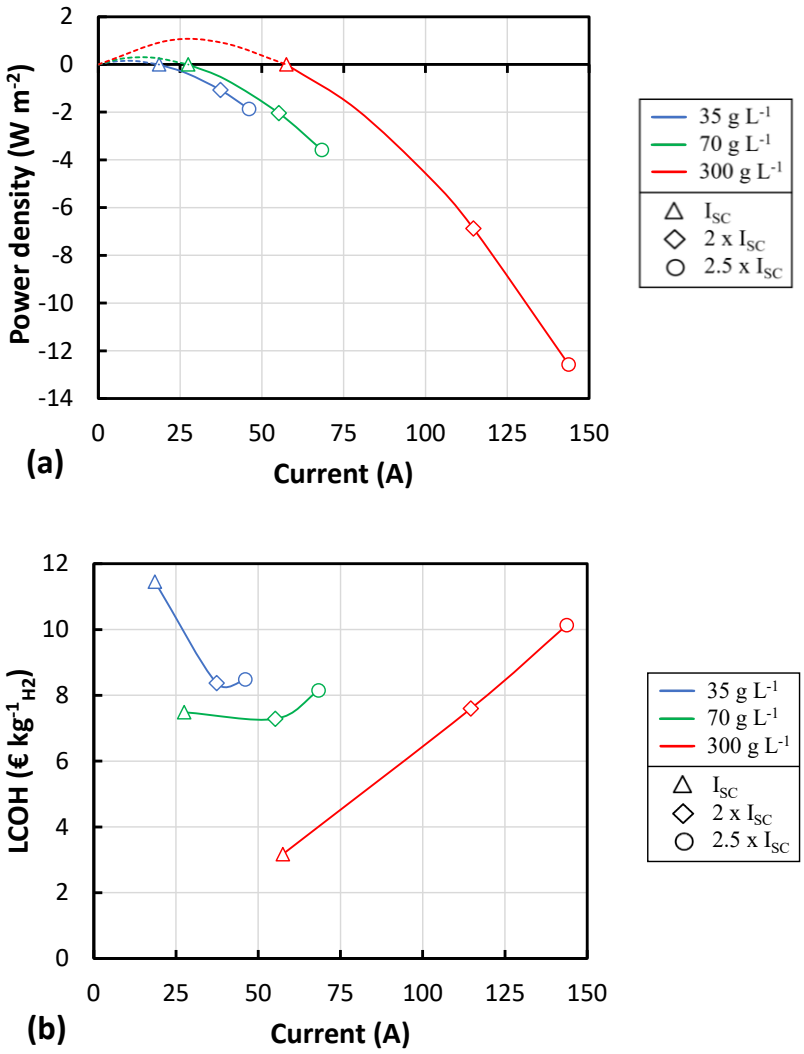

Fig. 14 (a) Power curves and (b) LCOH trend versus the current for the three different concentrated feed solutions studied (35, 70 and 300 g L^{-1}). The dashed curves in (a) refer to the power curve obtained in RED mode, conversely, the bold curves refer to ARED operations.

The techno-economic model and the results obtained are based on the results of the lab-scale experimental campaign. The scaling up of the process certainly affects the actual consumption of the unit compared to that assumed based on the experiments. However, the purpose of this preliminary economic analysis is to determine whether there is a profit margin for the future spread of the technology in the hydrogen industry. Even a non-in-depth analysis using a simplified technical model provides crucial information for recognising the potential of the process. This makes it possible to understand whether the technology can be improved and whether it can be proposed as an innovative alternative.

3.4 Final remarks and future perspectives for H(A-)RED

This preliminary economic analysis shows that, surprisingly, the cost of hydrogen production using an (A-)RED unit is not prohibitive. However, it must be taken into account that this analysis was carried out under optimistic conditions for (A-)RED technology: just think about the 4 € m^{-2}_{IEM} used in the analysis. The latter cost, according to recent quotations, has a retail cost between 25 and 100 € m^{-2}_{IEM}, value well over the one considered. However, a value of 4 € m^{-2}_{IEM} is often adopted as a future membrane cost [95,96], for which is expected to benefit from both technological developments and the spreading of RED and ED technologies at world level, whose have recently been inserted as renewable energy in the European directive [97].

The current membrane cost (assumed of 25 € m^{-2}_{IEM}) would bring the most positive LCOH (i.e. the one obtained under the conditions of 300 g L^{-1} in I_{SC}) to increase from 3.2 to almost 13 € kg^{-1}_{H2}. A very high value, which would negatively affect the proposed technology and its use in the market.

Ranade et al. [98] suggested a techno-economic study for the combining of RED process with hydrogen. They investigated the system, for the production of hydrogen at the cathode, chlorine gas at the anode and in the maximum power condition in RED, therefore at even lower current densities. As a result of the analysis, a LCOH of 117 € kg^{-1}_{H2} and a levelized cost of electricity (LCOE) of 1.5 € kWh^{-1} were found, presenting values that were definitely out of range for any future possibility. However they also showed that these costs were clearly very susceptible to the price of the membrane and its properties (thickness, permselectivity, resistance, etc.). However, under specific parameters, the LCOH could be brought to values below 4 € kg^{-1}_{H2}. Although the results have been disappointing, the idea to reduce costs with more products, remains a good idea.

Notwithstanding this, the findings of the Ranade study indicated that remuneration from three products was unable to produce positive figures for the success of this technology.

In any case, it is necessary to keep in mind what the limits of technology are in order to overcome the problems. In fact, RED has inherently low current densities that inevitably result in low hydrogen productivity, and in the case of Ranade et al. [98], also in lower energy and chlorine production. Furthermore, the point corresponding to the maximum power generated by the RED is not the point that maximizes the production of hydrogen and chlorine, making the process disadvantageous. In the case of H(A-)RED, the application of technology is completely finalised to the production of hydrogen, indeed, all the power that can be generated by the salinity gradient is converted entirely into hydrogen (short-circuit). For this reason the prices have been more advantageous, and in any case much lower than the 117 € kg^{-1}_{H2} of hydrogen.

For example, the co-production of water and H_2 are both facilitated in ED. An increase in the desalination degree corresponds to an increase in the current, which means into an increase in hydrogen productivity. The two productions are no longer as competitive with each other as in Ranade's work, and in this case, the simultaneous production of hydrogen and freshwater could further reduce costs. This last proposal is extensively developed and argued in the following chapters (4 and 5).

4 Hydrogen Electrodialysis HED: Brackish water

As a difference from the coupling of RED with green H_2 production, there are only barely references that use ED for this purpose in the literature. In 2023, Alshebli et al. [99] experimented with the possibility to employ an ED stack for producing H_2 at the cathode while desalinating a 0.14 M Na_2SO_4 solution. A specific energy consumption (SEC) of 9.9 kWh per m^3 of desalinated Na_2SO_4 solution was found, together with a hydrogen productivity of 16 mmol h^{-1} with an electrode surface of 64 cm^2 (the equivalent of 2.5 mol h^{-1} m^{-2}). Recently, Fonseca et al. [100] evaluated the feasibility of the desalination with different feed concentration in the range 10–30 g L^{-1} of NaCl, different electrolyte solution concentration of Na_2SO_4 and two different brands of membranes. A 5 cell pairs unit with an active surface of 56.3 cm^2 was tested, and they obtaining a H_2 production up to 21.6 mL h^{-1} cm^2 (corresponding to almost 9.67 mol h^{-1} m^{-2}) at a current density of 469 A m^{-2}. The latter works by Alshebli [99] and Fonseca [100] define the possibility to produce hydrogen and desalinate a salty solution with an ED unit. However, the two cited papers assess only the technical feasibility of the technology without evaluating whether producing hydrogen via ED might be remunerative or not.
The ED technology is studied here for the production of hydrogen at the cathode and the simultaneous desalination of salt water to produce water with a lower salt content. In this chapter, the technology is studied for the desalination of brackish water (BW), while in the following chapter (Chapter 5), the same technology is proposed for the seawater (SW) desalination.
The following chapter contain some scientific results published in [101]. A thorough examination of these findings is provided in the next paragraphs.

4.1 HED technology

A novel ED configuration is proposed to simultaneously (i) desalinate brackish water (BW) and (ii) produce green H_2 and O_2 (if a renewable energy source RES is adopted) with higher productivities than the previous H(A-)RED case. A schematic representation of the proposed idea, hereafter named Hydrogen Electro-Dialysis (HED) or Brackish Water Hydrogen Electro-Dialysis (BWHED) is reported in *Fig. 15*. Energy is supplied to the unit by a power supply: the current is converted into ionic current within the stack thanks to the red-ox reactions occurring at the electrode channels.

Precisely, H_2 is generated at the cathode while O_2 is produced at the anode in alkaline conditions, according to the related reactions reported in *Table 1*. As a result of the transport of ions through the IEMs, freshwater and a more concentrated stream are produced. At the electrodes, part of the water is consumed due to the electrode reaction, so it is possible to think about re-using the stochiometric quantity to make up the alkaline solution used as electrodic rinse solution, as it occurs in AWEs. Overall, when electric energy is supplied, the system is able to produce freshwater, H_2 and O_2 from brackish water.

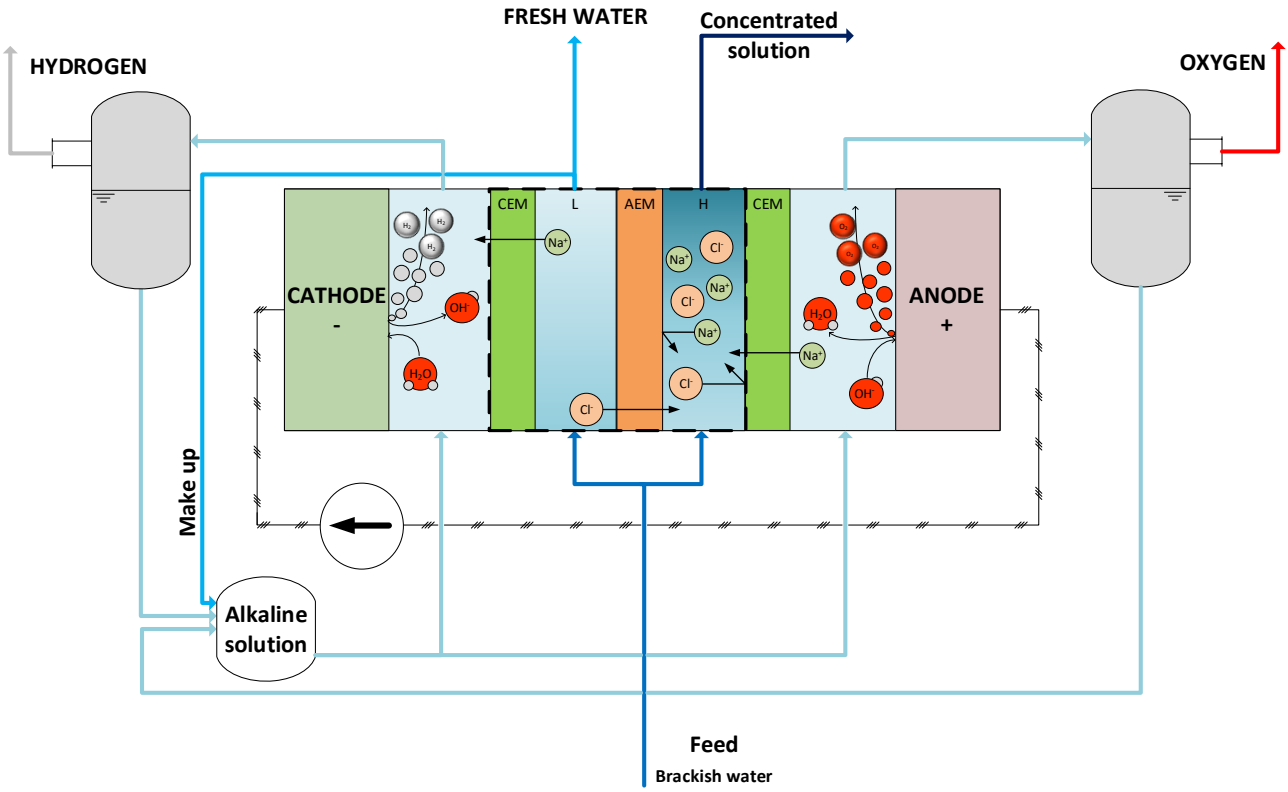

Fig. 15 Schematic representation of the HED technology, in which the repeating unit (cell pair) is evidenced in the dashed rectangle.

A mathematical model previously developed by our group [102] was properly modified to predict the performance and the behaviour of the HED stack, and to estimate the H_2 production rate. Traditional ED only uses two electrodes. This severely limits hydrogen production, which is mostly seen as an unwanted by-product. The novelty of the proposed system (see 4.3.1) is to increase the number of electrodes in order to increase the hydrogen productivity and make it a valuable co-product. Economic equations were also implemented to assess the economic feasibility of such technology.

4.2 Technical model

4.2.1 Model equations

The mathematical ED models are widely discussed in literature and further details can be found in [102–105]. Due to the preliminary nature of the investigation, the multi-scale, semi-empirical mathematical model (implemented on Excel VBA) here adopted [105] is based on the following assumptions:

1. The model is only discretised along the main flow direction;
2. The feed saline stream is assumed as constituted by sodium chloride and water only;
3. Parasitic currents through the manifolds are neglected;
4. Faradaic efficiencies of 100 % are assumed for HER and OER.

The model considers the physics of the system with a multi-scale approach ranging from the low channel level to the whole stack. The channel model is the low-scale level, where Computational Fluid Dynamics is used to provide appropriate correlations for the Sherwood number. The cell-pair model is the intermediate-scale model: it accounts for the balance and mass transport equations including convective, diffusive and migrative fluxes. The high scale model is related to the whole unit which is modelled as a number of cell pairs (N_{CP}) placed in parallel.

As stated above, the model is discretised along the main flow direction by partitioning the length into N_k elements. The flow rates, the concentrations, the physical properties, and the electrical variables are calculated for each k element. The system can be compared to an equivalent electrical circuit, schematically represented in *Fig. 16*, for which each component of the cell pair is associated to an item of the electrical circuit. The ohmic resistance of the spacer-filled channels can be calculated as follows:

$$r_{sol}(k) = f_x \frac{\delta_{sp,sol}}{\sigma_{sol}} \qquad 27$$

where f_x is the spacer shadow factor, $\delta_{sp,sol}$ is the spacer width and σ_{sol} is the solution conductivity (estimated via Islam's modified equation [106], see Appendix II). The subscript "sol" is referred to the generic solution that flows in the channel (i.e., either the dilute L or the concentrate H). IEMs can be compared and modelled as generators and ohmic resistances: the resistance term (r_{AEM}, r_{CEM}) is often provided by producers and can be taken from the technical datasheet. The whole cell resistance can be calculated as the sum of the ohmic losses through the membranes and

the compartments: $r_{cell} = r_{AEM} + r_{CEM} + r_H + r_L$. Conversely, the electromotive force (the generator-like term) can be calculated as follows:

$$E_{cell}(k) = 2\,PS_{av}(k)\,\frac{R_g T}{zF} ln\left(\theta_H(k)\theta_L(k)\frac{\gamma_H(k)c_H^b(k)}{\gamma_L(k)c_L^b(k)}\right) \qquad 28$$

where PS_{av} [103] is the average permselectivity of the membranes (i.e., the averaged value between *CEM* and *AEM*), R_g is the gas constant, *T* is the absolute temperature, *F* is Faraday constant, *z* is the ion valence (equal to 1 for NaCl), θ is the polarization factor [102], γ and *c* are the activity coefficients of the solution and the bulk molar concentrations, respectively.

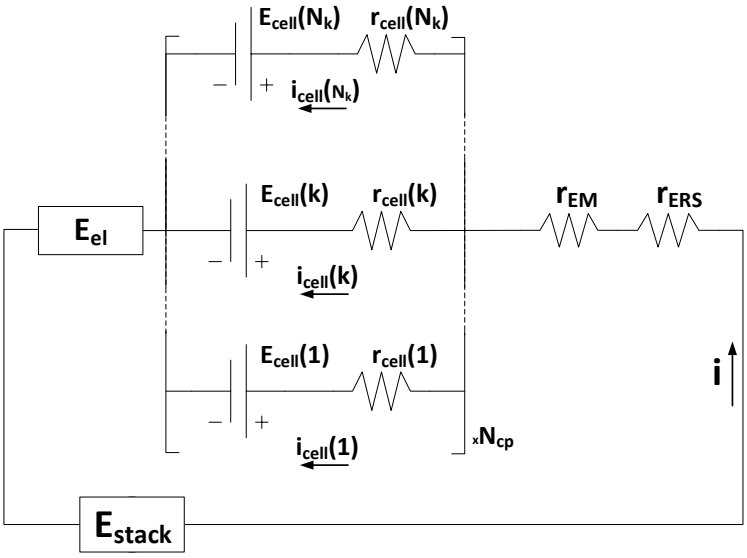

Fig. 16 Equivalent electrical circuit of the electrodialysis unit.

By resolving Kirchhoff's voltage law for the circuit in *Fig. 16*, it is possible to calculate the current density as follow:

$$i_{cell}(k) = \frac{{E_{stack}}/{N_{cp}} - E_{cell}(k) - {(E_{el} + r_{EM} i + r_{ERS} i)}/{N_{cp}}}{r_{cell}(k)} \qquad 29$$

where E_{stack} is the stack electric potential difference (i.e., the voltage applied by the power supply), r_{EM} and r_{ERS} are the resistance of the end-membrane and the electrode-compartment solution, respectively. E_{el} is the electrodes voltage drop, that comprises of the thermodynamic (standard red-ox electrode potentials, 1.2.1) and the kinetic contribution (i.e., overpotentials due to electrode activation, transport, etc., 1.2.2). For the preliminary nature of the present investigation, E_{el} was considered constant and equal to 1.7 V, plausible value also suggested by IRENA [107]. The current density i flowing in the external circuit is defined as the sum, over the stack length *L*, of all the current densities $i_{cell}(k)$ calculated in each k-element, in formula: $i = \sum_1^{N_k} i_{cell}(k)$. Remember

that, in RED and ED literature, the sum $E_{el}/_{i} + r_{EM} + r_{ERS}$ is typically indicated as blank resistance [102,103,108]. Resuming, all the voltage losses which are not related to the resistance of the cell package (r_{cell}) are collected in the blank resistance, which corresponds to the sum of the end-membrane resistance, the ERS solution resistance and the electrode potential losses. The blank resistance is normally low compared to the resistance of the stack, thus providing a negligible contribution to the energy consumption of the system, especially when a larger number of cell pairs is assembled, as it occurs in industrially relevant stacks. For the HED technology, these contributions (especially the electrodes one) might be significant, in particular when several electrodes are added in the stack to increase H_2 and O_2 productivity (see 4.3.1).

The flow rate and the concentration of the outlet streams, once coupled with the electrical equations, can be calculated by solving the mass balance equations (the main equations are summarize in Appendix I and full details on the model can be also found in [103]). Once the current density *i* has been calculated, the hydrogen and oxygen molar fluxes at the electrodes can be easily calculated as follows:

$$J = \frac{i}{n_e F} \tag{30}$$

where n_e is the number of electrons that participate to the semi-redox reaction (2 for hydrogen and 4 for oxygen). Multiplying the molar flux *J* by the molecular weight of the gas and by the membrane area A_m, it is possible to calculate the hydrogen $\dot{Q}_{H_2}$ and oxygen $\dot{Q}_{O_2}$ mass flow rate.

As main performance indicators, the Specific Energy Consumption (SEC) is calculated as the amount of power required by the unit (defined as the product by the external potential E_{stack} and the current $I = i \cdot A_m$) divided by the flow rate of obtained product. Thus, the water SEC (WSEC) and hydrogen SEC (HSEC) can be calculated as follows:

$$WSEC = \frac{P[kW]}{\dot{V}_w[m_w^3\ h^{-1}]} \tag{31}$$

$$HSEC = \frac{P[kW]}{\dot{Q}_{H2}[kg\ h^{-1}]} \tag{32}$$

Since HED unit can be seen as the coupling of two different processes (ED and water electrolyser), a thermodynamic efficiency can be assessed for both processes.

For the electrodialysis, the efficiency η_{ED} (33) is defined as the ratio between the minimum power supplied to an ideal ED unit operating as a thermodynamically reversible process (B_{ED}^{id}, see 34) and the power P actually consumed by the HED unit [103]:

$$\eta_{ED} = \frac{B_{ED}^{id}}{P} \quad (33)$$

$$B_{ED}^{id} = (B_{L,out} - B_{L,in}) + (B_{H,out} - B_{H,in}) = \Delta B_L + \Delta B_H \quad (34)$$

In other words, B_{ED}^{id} represents the minimum power requested by an ED unit that works reversibly, i.e., without any irreversible loss. Conversely, all the irreversibility are taken into account by the real power P consumed. The exergy of the streams (ΔB_L and ΔB_H) are evaluated with respect to the pressure, composition and temperature, of the thermodynamic equilibrium condition (i.e., T_0, P_0 and x_0, see below). The latter can be calculated as follows:

$$\begin{aligned}\Delta B_L &= (B_{L,out} - B_{L,in}) \\ &= R_g T_0 \left[V_{L,out} \left(c_{s,L}^{out} \nu \ln \frac{a_{s,L}^{out}}{a_{s,0}} - c_{w,L}^{out} \ln \frac{a_{w,L}^{out}}{a_{w,0}} \right) \right. \\ &\left. - V_{L,in} \left(c_{s,L}^{in} \nu \ln \frac{a_{s,L}^{in}}{a_{s,0}} - c_{w,L}^{in} \ln \frac{a_{w,L}^{in}}{a_{w,0}} \right) \right]\end{aligned} \quad (35)$$

$$\begin{aligned}\Delta B_H &= (B_{H,out} - B_{H,in}) \\ &= R_g T_0 \left[V_{H,out} \left(c_{s,H}^{out} \nu \ln \frac{a_{s,H}^{out}}{a_{s,0}} - c_{w,H}^{out} \ln \frac{a_{w,H}^{out}}{a_{w,0}} \right) \right. \\ &\left. - V_{H,in} \left(c_{s,H}^{in} \nu \ln \frac{a_{s,H}^{in}}{a_{s,0}} - c_{w,H}^{in} \ln \frac{a_{w,H}^{in}}{a_{w,0}} \right) \right]\end{aligned} \quad (36)$$

where V is the volumetric flow rate of solutions ($m^3\ s^{-1}$), c is the molal concentration ($mol\ kg^{-1}$), ν is the sum of ions of the solute molecule, and a is the activity (activities are taken from [109]). “in” and “out” subscripts reference to the inlet (x=0) and outlet (x=L) spatial coordinates, “s” and “w” refer to salt and water. The subscript “0” refers to the equilibrium condition, for which it was assumed a pressure of 1 bar, a composition of 5 g L^{-1} and a temperature of 25 °C. Furthermore, no pressure variations are taken into account between inlet and outlet streams. Note that the concentrate exergy was also considered (ΔB_H) under the hypothesis of giving a value to the brine produced by the ED unit. Otherwise, only the diluted term ΔB_L should be considered in 34.

As far as the electrolyser is concerned, the efficiency is defined as the thermo-neutral potential of 1.48 V (including the red-ox couple thermodynamic potential and the heat of reaction) divided by the actual stack voltage [110]:

$$\eta_{H2-El.} = \frac{E_{thermo-neutral}}{E_{stack}} \quad (37)$$

4.2.2 Model validation

To calibrate and validate the technical model, an ad-hoc experimental campaign was carried out with an ED unit 10 x 40 cm^2 of active area and equipped with 10 cell pairs. Fujifilm Type 10 (Tilburg, The Netherlands) membranes were used to perform the experiment, separated by woven spacers 155 µm thick (Redstack, Sneek, The Netherlands). A Nafion® membrane was used as end membranes. In order to separate the voltage loss of the electrodic compartments from that of the cell package, two platinum wires were inserted between the end membranes and the cell-package side. The cell package voltage (i.e., $N_{cp}E_{cell}$) is reported in *Fig. 17a* as a function of the current density. While the corresponding values of the streams concentration at the outlet of the ED unit versus the current density are shown in *Fig. 17b*.

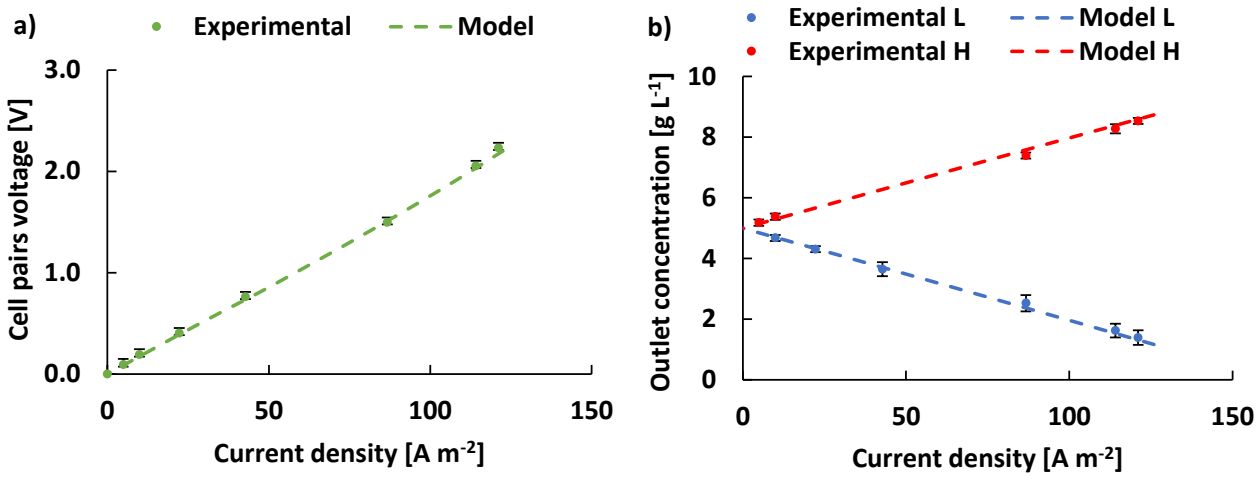

Fig. 17 Model validation: (a) Polarization curve and (b) concentration of the solutions at the unit outlet versus current density. Stack 10x40 cm^2 with 10 cell pairs. An artificial solution of 5 g L^{-1} of NaCl (i.e., 0.086 M) was used as feed solution. Solution velocity equal to 5 cm s^{-1} in both channels. These were filled with woven spacers 155 µm thick. The error bars represent the standard deviation.

As shown, there is a very good agreement between the experimental data and the model predictions. Specifically, a maximum discrepancy of about 3% was found and, as a result, the technical model can be considered validated. Additional details on the validation of the multi-scale semi-empirical model can be also found in [105].

Note that an experimental validation of the electrodes is not possible, since the model does not describe the electrode compartments in detail, and a fixed voltage drop of 1.7 V has been used. As a validation of the technical feasibility of producing H_2 and freshwater at the same time, some

experiments were performed on a 20 cell pairs 10x10 cm^2 ED stack and further details can be found in 5.1.2.

4.2.3 Economic model

To assess the HED technology cost, an economic model was implemented using, as input, the output values of the technical model. For instance, (i) the stack potential (E_{stack}) defines how much energy has to be taken by the grid (or by standalone RES); (ii) the H_2 and O_2 flowrates produced are used to calculate the technology revenues. Both capital and operating costs were estimated, and a cumulative cash flow diagram was used to estimate the plant profitability. The Fixed Capital Investment (FCI) is calculated as the sum of all the equipment and indirect costs as follows:

$$FCI = C_m + C_{electrode} + C_{casing} + C_{spacer} + C_{pump} + C_{piping} + C_{labour} = \\ = C_{equipment} + C_{labour} \quad (38)$$

Each term is defined in *Table 8*, where the costs are referred to specific stack geometrical features: e.g., for evaluating the overall spacers cost it is necessary to multiply the specific cost $\bar{C}_{\text{spacer}}$ reported in *Table 8* by the total active membrane area (i.e., $m^2_{IEMs} = 2\ N_{cp} \cdot A_m$). For 1 electrode, being the active area $m^2_{electrode}$ equal to A_m, the electrode cost is equal to $A_m \cdot \bar{C}_{electrode}$, etc.

Table 8 Main cost items for the economic analysis.

Membranes cost $\overline{\boldsymbol{C}}_{\boldsymbol{m}}$ [65,92,95]	25	$€ \cdot m^{-2*}_{IEMs}$
Electrodes cost $\overline{\boldsymbol{C}}_{\textbf{electrode}}$ [65,92,95]	100	$€ \cdot m^{-2**}_{electrode}$
Casing cost $\overline{\boldsymbol{C}}_{\textbf{casing}}$ [65,92,95]	5	$€ \cdot m^{-2}_{IEMs}$
Spacers cost $\overline{\boldsymbol{C}}_{\textbf{spacer}}$ [65,92,95]	4	$€ \cdot m^{-2}_{IEMs}$
Pump cost $\mathbf{C}_{\textbf{pump}}$ [111]	$900\left({\mathrm{P_{pump}[W]}}/{300}\right)^{0.25}$	€
Piping cost $\mathbf{C}_{\textbf{piping}}$ [111]	$\left(0.087 + 0.21\mathrm{D_{pipe}[mm]}\right)\mathrm{L_{pipe}[m]}$	€
Labour cost $\mathbf{C}_{\textbf{labour}}$ [84,95]	10% of $C_{equipment}$	€
Other costs $\widetilde{\boldsymbol{C}}_{\boldsymbol{other}}$ [65,92,95]	4% of FCI	$€ \cdot year^{-1}$

*$m^{-2}_{IEMs} = 2\ N_{cp} \cdot A_m$

**$m^{-2}_{electrodes} = 2\ N_{cp} \cdot A_{electrode}$

Some costs are not the actual real costs, such as the membrane and spacer ones, rather, these should be viewed as possible costs which could be reasonably expected as a consequence of a worldwide employment of this technology on the market (as suggested by [92,95]).

The OPerative EXpenditures (Opex), i.e., the manufacturing and operative costs, are the sum of day-by-day operation costs and of the maintenance of the plant, and are calculated according to 39:

$$Opex = \tilde{C}_{power} + \tilde{C}_{other} + d^{SL} \quad 39$$

where $\tilde{C}_{power}$ is the electricity costs required by the unit, while $\tilde{C}_{other}$ (see *Table 8*) includes all the other manufacturing expenditures such as indirect costs, maintenance, etc. Depreciation d^{SL} is estimated with a straight line method as equal to $(FCI - S)/n$, according to Turton [112], where S is the salvage value and n is the project lifetime.

Completely, the product between the total amount of fresh water produced $\dot{V}_w$ and the price of water $\bar{C}_w$ provides the revenue obtainable from the selling of water. In the case of HED technology, the co-production of H_2 and O_2 represents a further plant revenue. Thus, the total revenue $\mathcal{R}$ is calculated as follows:

$$\mathcal{R} = \mathcal{R}_W + \mathcal{R}_{H_2} + \mathcal{R}_{O_2} = \bar{C}_w \cdot \dot{V}_w + \bar{C}_{H_2} \cdot \dot{Q}_{H_2} + \bar{C}_{O_2} \cdot \dot{Q}_{O_2} \quad 40$$

where $\bar{C}_{H_2}$ and $\bar{C}_{O_2}$ are the hydrogen and oxygen specific prices, respectively. Net Present Value (NPV) is calculated at the end of the project lifetime according to its definition [112]:

$$NPV = -FCI + \sum_{p=1}^{n} \frac{\left[\mathcal{R}_p - Opex_p - Tax_p + d_p^{SL}\right]}{(1+d)^p} \quad 41$$

where d is the discount rate. Clearly, being expenditures, the capital and operative costs are negative cash flows. Tax is also a negative cash flow and is estimated as a percentage *t* of the yearly net profit (i.e., $\mathcal{R} - Opex$).

Levelized Cost Of Hydrogen (LCOH) (42) and Levelized Cost Of Water (LCOW) (43) were adopted as profitability indexes in order to compare HED with conventional ED and electrolysers units:

$$LCOH\ [€\ kg_{H2}^{-1}] = \frac{FCI + \sum_{p=1}^{n}\left(\frac{Opex_p + Tax_p - d_p^{SL} - \mathcal{R}_{W,p} - \mathcal{R}_{O_2,p}}{(1+d)^p}\right)}{\sum_{p=1}^{n}\left(\frac{\dot{Q}_{H_2}[kg_{H2}\ year^{-1}]}{(1+d)^p}\right)} \quad 42$$

$$LCOW\ [€\ m_w^{-3}] = \frac{FCI + \sum_{p=1}^{n}\left(\frac{Opex_p + Tax_p - d_p^{SL} - \mathcal{R}_{H_2,p} - \mathcal{R}_{O_2,p}}{(1+d)^p}\right)}{\sum_{p=1}^{n}\left(\frac{\dot{V}_w[m_w^3\ year^{-1}]}{(1+d)^p}\right)} \quad 43$$

Levelized cost corresponds to the selling price at which a product (i.e., either H_2 or H_2O) has to be sold in order to get a NPV equal to zero at the end of the project lifetime *n*. In other words, the Levelized cost is the minimum selling price of hydrogen (or water) to recover all the expenditures faced during the entire plant lifetime. Notably, in order to calculate the levelized cost of a product (i.e., either H_2 or H_2O), the revenue relevant to the other product has to be fixed: more precisely, it is necessary to set the water selling price to assess LCOH, and to set the hydrogen one for the LCOW calculation.

4.3 Techno-Economical analysis

4.3.1 Investigated scenario

In general, ED processes work with BWs, i.e. waters with a low salinity. BWs are defined as waters with a salinity greater than that of freshwater (less than 0.5 g L^{-1}) and not greater than that of seawater (more than 30 g L^{-1}). It was therefore decided to operate the HED technology at an intermediate concentration of 5 g L^{-1}, which is chosen to be desalinated down to a target concentration of 0.5 g L^{-1}. The feed velocity is of 5 cm s^{-1} and 1000 cell pairs are overall assembled in the system, thus corresponding to a total flowrate of 89.1 m^3 h^{-1} per stack. The aim of this analysis is to evaluate the profitability of the HED technology. To this purpose, in *Table 9* are reported the adopted scenario variables.

Table 9 Technical and economic scenario variables

Plant lifetime $\boldsymbol{n}$ [65,89]	20	year
Discount rate $\boldsymbol{d}$ [65,89]	3	%
Taxation rate $\boldsymbol{t}$	10	%
Salvage Value $\boldsymbol{S}$ (% of FCI) [112]	10	%
Working hours	8000	$\mathrm{h} \cdot year^{-1}$
Membrane lifetime $\boldsymbol{t_m}$ [65,92,113]	7	year
Electricity cost $\boldsymbol{C_{electricity}}$ [65]	0.1	$€ \cdot kWh^{-1}$
Oxygen price $\boldsymbol{C_{oxygen}}$ [89,114]	0.2	$€ \cdot kg_{O_2}^{-1}$
Stack length $\mathbf{L}$	1	m
Stack width $\mathbf{b}$	1	m
Spacers thickness (concentrate channel) $\boldsymbol{\delta_{sp,H}}$	150	µm
Spacers thickness (dilute channel) $\boldsymbol{\delta_{sp,L}}$	450	µm
Shadow factor $\mathbf{f_x}$ [65]	1.5625	-
Number of cell pairs $\boldsymbol{N_{CP}}$	1000	-
Inlet velocity of the feed $\boldsymbol{v}$ [34]	5	$cm \cdot s^{-1}$
Permselectivity $\boldsymbol{PS_{av}}$ [1]	0.95	-
Membrane resistance $\boldsymbol{r_{CEM}, r_{AEM}}$ [1]	1.85	$\Omega \cdot cm^2$
Membrane width $\boldsymbol{\delta_m}$ [1]	135	µm

[1] Averaged from technical datasheet - Fujifilm IEM Type 10

In order to guarantee the dilution target, a current density of 146.82 A m^{-2} has to be reached. This current would allow a H_2 production of 44 kg_{H2} $year^{-1}$ in a conventional ED unit, where only one cathode is present. For the analysis, an ED stack of 1000 cell pairs has been taken as reference for traditional electrodialysis. The productivity of the 1000 cell ED stack is quite low and makes this standard ED unit unsuitable for a significant production of H_2. The limited productivity is due to (i) the low current density and (ii) the available active surface of the electrode. The former is not an input variable of the process, since it is defined by the feed inlet concentration and the desalination target. The latter is a stack geometric variable considered as suitable for industrial stacks and it is not recommended to be changed.

Industrial electrolyser stacks are constituted by a several repetition of cathodes and anodes to increase the hydrogen productivity. By taking electrolysers as guide, the idea is to insert multiple

electrodes in the ED stack of 1000 cell-pairs as shown in *Fig. 18*. In this way, the number of total cell-pairs (i.e., 1000) and the treated feed flowrate is always the same, without any kind of variation. Also the desalination target is kept constant. On the contrary, the addition of the cathodes generates a proportional increase in the hydrogen production rate. The cathodes are inserted within the cell package and shared by the two adjacent sub-cell-packages formed (see *Fig. 18*). Moreover, for each extra electrode a further end-membrane has to be inserted. An illustrative example is given in *Fig. 18* for the sake of clarity. A HED stack composed of 16 cell-pairs is shown in *Fig. 18a*, and as a consequence of the addition of a new electrode, the cell package is split up into 2 sub-cell-packages (*Fig. 18b*). With two cathodes, the new stack is now able to produce a double quantity of H_2. By adding 2 more electrodes (*Fig. 18c*), the hydrogen productivity became 4 times higher (compared to case a). Electrode addition can be further performed up to an upper limit corresponding to a couple of electrodes per cell-pair.

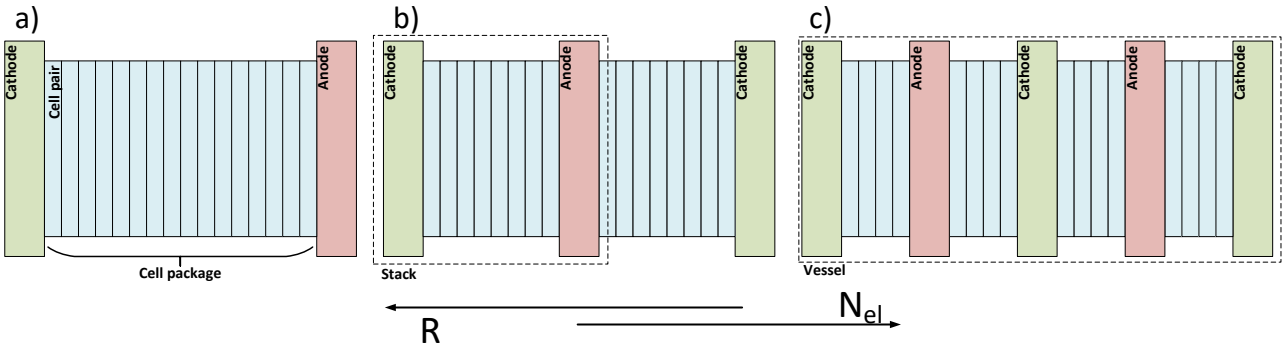

Fig. 18 Schematic representation of the HED technology for different R-values

The number of electrodes added is indicated by N_{el} and by the corresponding *R*-factor purposely defined as follows:

$$R = \frac{N_{CP}}{N_{el} - 1} = \frac{1000}{N_{el} - 1} \qquad 44$$

where N_{CP} is the number of cell-pairs (set as reference to 1000), and N_{el} is the total number of electrodes. According to the definition, when R increases, the number of electrodes of the system decreases: for R=1, HED is constituted by the repetition of 1001 electrodes (500 anodes and 501 cathodes) spaced by 1 cell-pair; when R=1000, all the cell-pairs are assembled between one single couple of cathode and anode (representing the standard ED configuration). Additionally, the denominator ($N_{el} - 1$) numerically corresponds to the number of sub-cell-packages in parallel, and *R* also corresponds to the number of cell pairs assembled per each sub-cell-package.

Moreover, being the unit a hybrid technology between an ED unit and an electrolyser, two different Energy Repartition Efficiencies (ERE%) can be defined:

$$HERE\% = \frac{HSEC_{H2-El}}{HSEC} = \frac{(E_{el} \cdot I_{stack})/\dot{Q}_{H_2}}{(E_{stack} - E_{el})/\dot{Q}_{H_2}} = \frac{E_{el}}{E_{stack}} \quad 45$$

$$WERE\% = \frac{WSEC_{ED}}{WSEC} = \frac{[(E_{stack} - E_{el})\, I_{stack}]/\dot{V}_w}{(E_{stack} - E_{el})/\dot{V}_w} = \frac{E_{stack} - E_{el}}{E_{stack}} \quad 46$$

where $HSEC_{H2-El}$ is the SEC of an equivalent electrolyser and $WSEC_{ED}$ is the SEC of an equivalent ED unit (see eqs. 31 and 32 for the definition of $WSEC$ and $HSEC$). Clearly, as it can be easily inferred from 45 and 46, being HERE and WERE energy repartition efficiencies, their sum is equal to 1.

4.3.2 Technical analysis

HED technology can be compared to 2 opposite limit cases: (i) the classical ED process (corresponding to R=1000), where freshwater is the main product and H_2 is a by-product with a negligible economic value; (ii) the alkaline electrolyser AWE, composed of 1000 units in parallel (referred as H_2-El.), producing H_2 and O_2 and operating at the same current of the ED stack. HED is a fusion of these 2 limit cases, and its main characteristic is the co-production of freshwater and H_2. This is why HED main performs are compared to an equivalent electrolyser in terms of produced H_2 and to an equivalent ED unit for water production. Note that O_2 is also a product of HED, but its worth was assumed constant, and no analysis was performed on it given its low market value (about 0.05 € kg^{-1}_{O2} [115]).

Fig. 19 shows the energetic analysis of the HED unit in terms of hydrogen and water specific energy consumption (HSEC and WSEC) compared to the energy demand of the equivalent Electrolyser H2- El. and ED unit (dashed lines). For the case of low R-values, hydrogen production becomes crucial and a higher power has to be provided to the HED system respect the standard ED, thus resulting into higher WSEC as well (*Fig. 19a*). For instance, at R=1000, ED WSEC is about 0.97 kWh m^{-3}_{w}, which is almost 5 times lower than the WSEC at R=1. This is due to a constant flowrate of freshwater produced that does not vary with R. In other words, the higher R, the lower the gross power required due to the minor number of cathodes. Notably, when R values more than 100, the curves asymptotically approach the dashed lines of ED, since the electrodes voltage losses

are almost negligible compared to the total power supplied for the desalination of the brackish water.

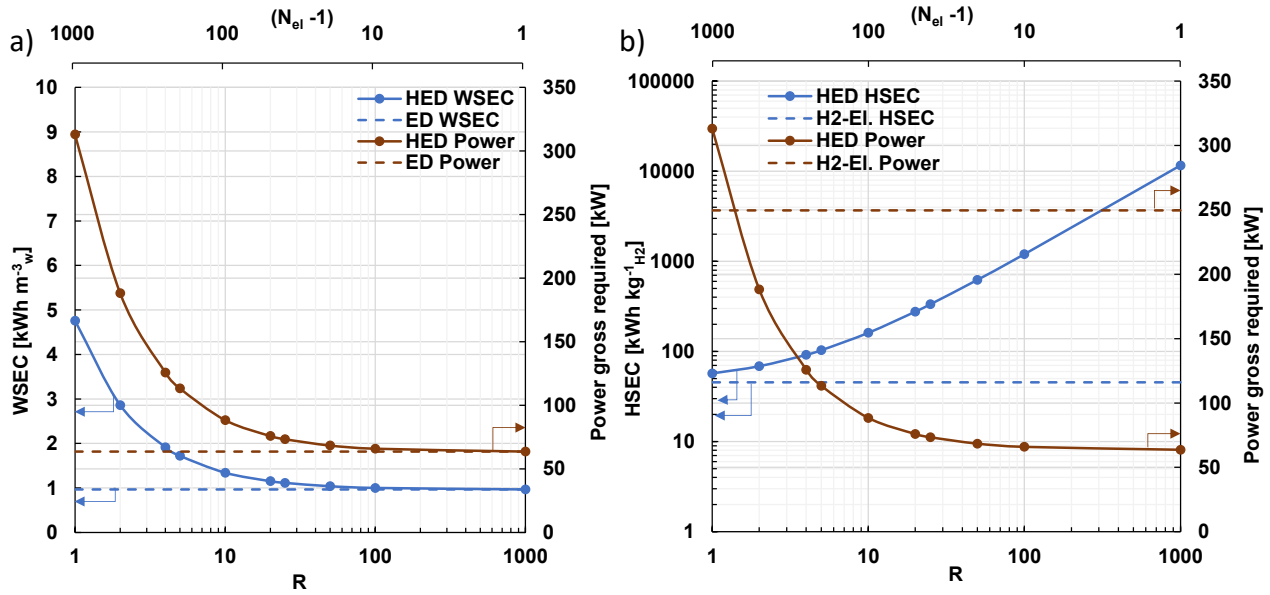

Fig. 19 Energetic analysis of HED technology and comparison with equivalent Electrodialysis (ED) unit and with equivalent electrolyser (H2-El.): gross power drawn and the specific energy consumption SEC as a function of the R-value and of the number of electrodes. a) focus to water, b) focus to hydrogen.

The power drawn and the HSEC respect the H_2 production are shown in *Fig. 19b*. Also in this case, when R=1 (the scenario closest to the 1000-units electrolyser), the HED power required is higher than that of the equivalent AWE, due to the extra energy consumption required by the desalination (almost 64 kW as observable in the figure for R=1000). Compared to *Fig. 19a*, the SEC trend versus R is the opposite, in fact HSEC increases with R. As a matter of fact, the higher the R value, the lower the H_2 production and the number of electrodes, while the desalted water (and the energy to do it) is the same. Therefore, the entire energy consumed is normalized by a decreasing amount of H_2 produced, reaching the unrealistic value of more than 10 MWh $kg^{-1}_{H_2}$ for R=1000.

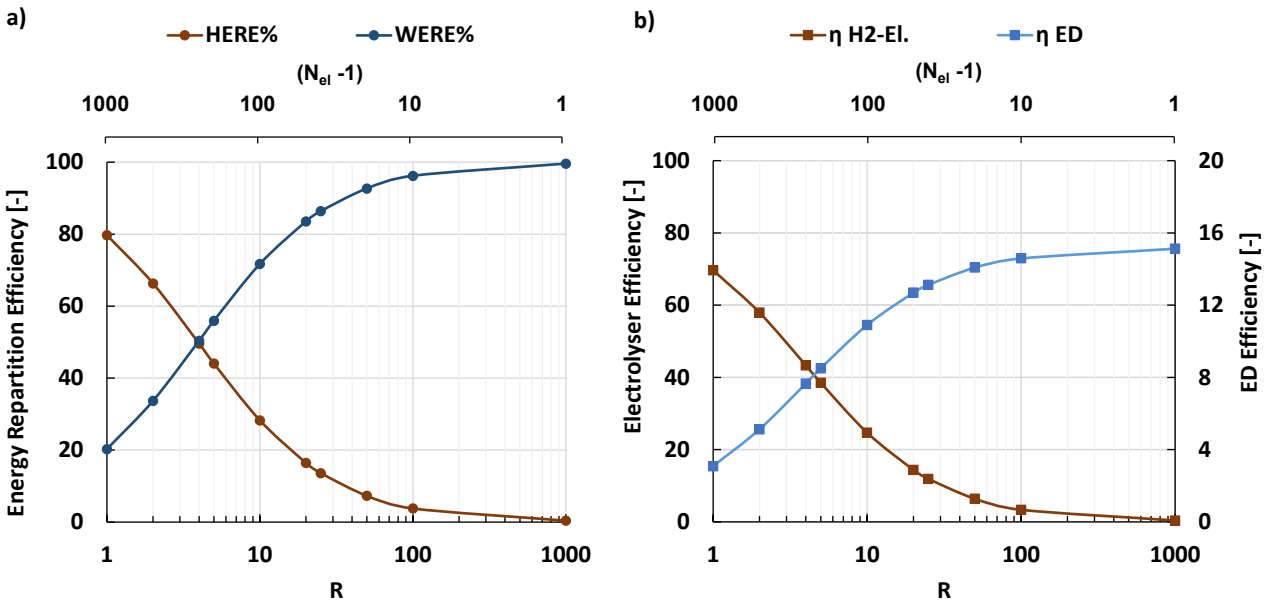

Fig. 20 a) Hydrogen and water energy repartition efficiencies and b) Electrolyser and ED thermodynamic efficiencies trend versus R-value and the number of electrodes.

The trend of the efficiencies as a function of R are shown in *Fig. 20a*. An increasing R-value significantly decreases the hydrogen efficiency. On the contrary, the hydrogen efficiency increases for low R-values, becoming almost 50 % for R=4, and reaching the 80 % for R=1. The curves asymmetry is because the power required for the desalination of the feed is comparable with the one required by the electrodes when R=1. Conversely, the electrodes contribution becomes negligible compared to the energy required by the desalination for high R-values. A similar trend can be also observed in *Fig. 20b*. The electrolyser efficiency of the HED technology (i.e., $\eta_{H_2-El.}$) shows a maximum value of 70 % for R=1 and decreases as R increases, achieving a very low value when the amount of H_2 produced is unworthy. Conversely, the ED exergy efficiency (i.e., η_{ED}) is almost 3 % when R=1 for the high energy demand of the electrodes and increases with R, reaching a maximum of about 15 % when R = 1000. This low efficiency is due to all the process irreversibilities, such as non-ideal permselectivity, ohmic losses, concentration polarisation, diffusion phenomena, electrodic compartments losses, etc.. Although this value is small, it is worth observing that it is comparable with the values shown in the literature, thus further confirming the relevance of the modelling approach here adopted [103,116].

4.3.3 Economic analysis

In *Fig. 21* the Fixed Capital Investment (FCI) normalized with both the water and hydrogen production is shown as a function of R: the trends reported somehow recall the behaviour of the corresponding WSEC and HSEC trends shown in *Fig. 19*. FCI variation with R mainly depends on the addition of electrodes. When R is low and the hydrogen production is the highest, the specific hydrogen FCI reduces with a minimum value of 0.45 € kg^{-1}_{H2} for the case of R=1. When R is high and hydrogen productivity is low, the hydrogen specific FCI increases because the capital costs for the water production (i.e., membranes, spacers, etc.) count more, reaching a value of 21.71 € kg^{-1}_{H2} when R=100 (almost 48 times higher than the value obtained for the R=1 case). Conversely, when FCI is normalized with the water production, it decreases with R as expected, but the variation range is lower (it only about halves with R) due to the constant freshwater production.

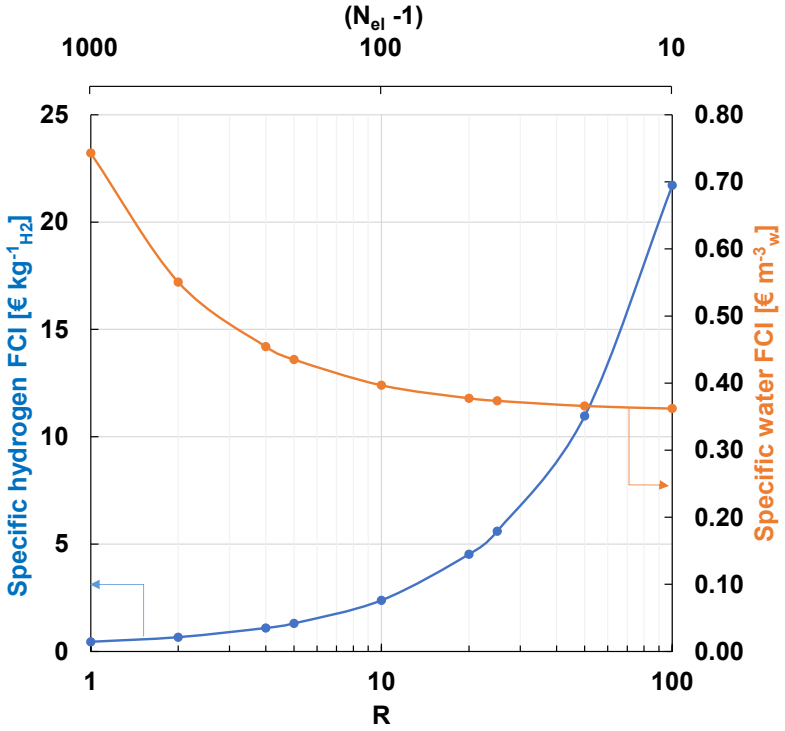

Fig. 21 Specific fixed capital investment FCI, normalized with respect to hydrogen (in blue) and water (in orange).

The FCIs are limited to the initial investment for the plant production, conversely, levelized costs allow the profitability of the investment to be assessed. *Fig. 22a* and *Fig. 22b* show the trend of the levelized costs of freshwater and hydrogen for the HED technology *versus* the R-value for the input values reported in *Table 9*. The figures also provide a comparison with standard equivalent ED unit

(R=1000) and 1000-cells electrolyser. Those trends are calculated assuming, respectively, the price of hydrogen, for the LCOW calculation, and the price of water, for the LCOH calculation, equal to zero. In *Fig. 22a*, when R is low, the HED LCOW is the highest with a value of 0.43 € m^{-3}_{w}, due to the additional electrodes and the corresponding increase in power requirement for hydrogen production. As R increases, the two curves approach each other up to match a common value of almost 0.14 € m^{-3}_{w}, that is the LCOW found for the case R=1000 (ED) where hydrogen production is irrelevant.

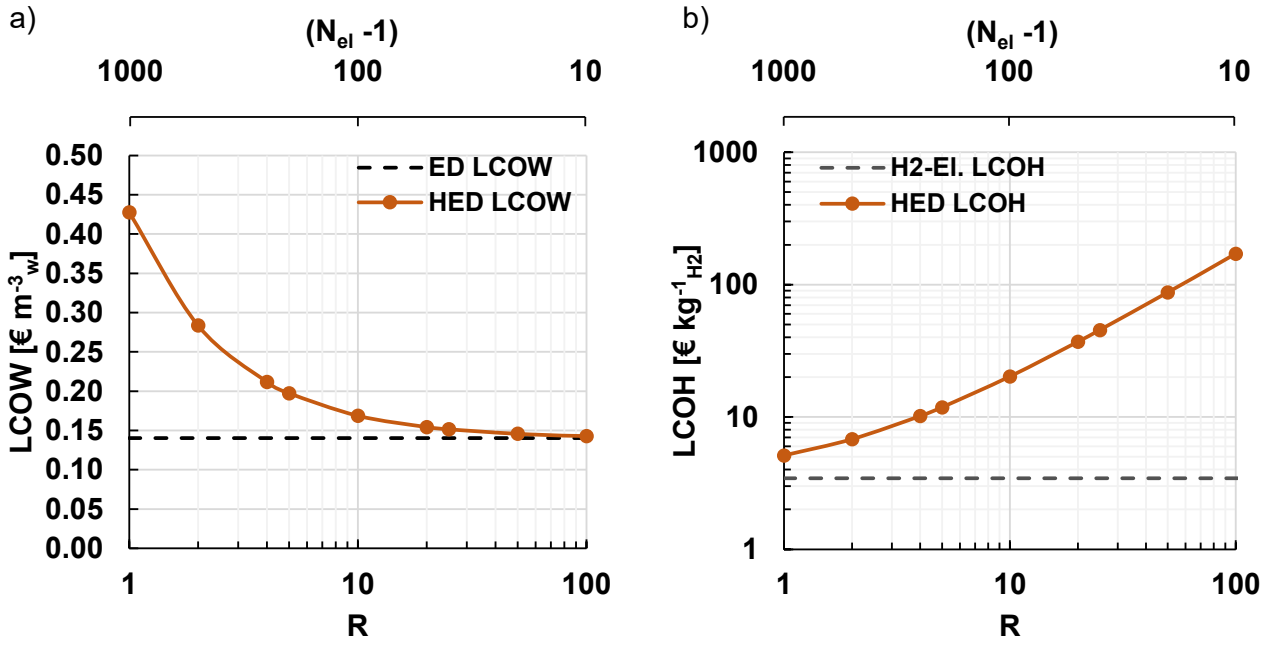

Fig. 22 Levelized costs versus R and the number of electrodes: a) LCOW of ED and HED technologies assuming a selling price for hydrogen equal to 0 € kg^{-1}_{H2}; b) LCOH of HED and of the equivalent electrolyser H2-El. assuming a selling price for water equal to 0 € m^{-3}_{w}.

Conversely, *Fig. 22b* shows the levelized cost of hydrogen. LCOH of the corresponding electrolyser is found equal to 3.43 € kg^{-1}_{H2}, while the HED technology always exhibits higher values due to the additional costs relevant to water production. Due to the decreasing number of cathodes (and according to the HSEC trend), the higher R, the higher LCOH.

Notably, the trends shown in *Fig. 22* are calculated without giving a worth to the other product but, clearly, a couple of possible prices for hydrogen and freshwater can always be given. This is why LCOH is plotted in *Fig. 23* as a function of R and of the selling price of water. Each line shown represents the locus of points where NPV is equal to zero for a specific R value. The higher the R-factor, the higher the line slope, i.e., small variation on water price corresponds to large difference in the LCOH. All the lines intercept in one single point, corresponding to the couple of values

0.14 € m^{-3}_{w} and 3.43 € kg^{-1}_{H2}, seen in *Fig. 22* for the standard ED and electrolyser, respectively. As R increases, the lines exhibit a clockwise rotation around this last point, reaching the ED limit of the plot corresponding to the vertical dashed blue line (for R=1000). The two dashed lines (limit LCOH of the ED and electrolyser cases) also identify 3 different regions identified by: (i) lower selling prices of water and hydrogen (pink colour region in *Fig. 23*), in which NPV is always negative and there is no revenue by the plant; (ii) higher selling prices (green colour region in *Fig. 23*), where NPV is always positive and there is room for economic profitability; (iii) the grey colour regions indicate the possible couple of selling prices for which NPV=0.

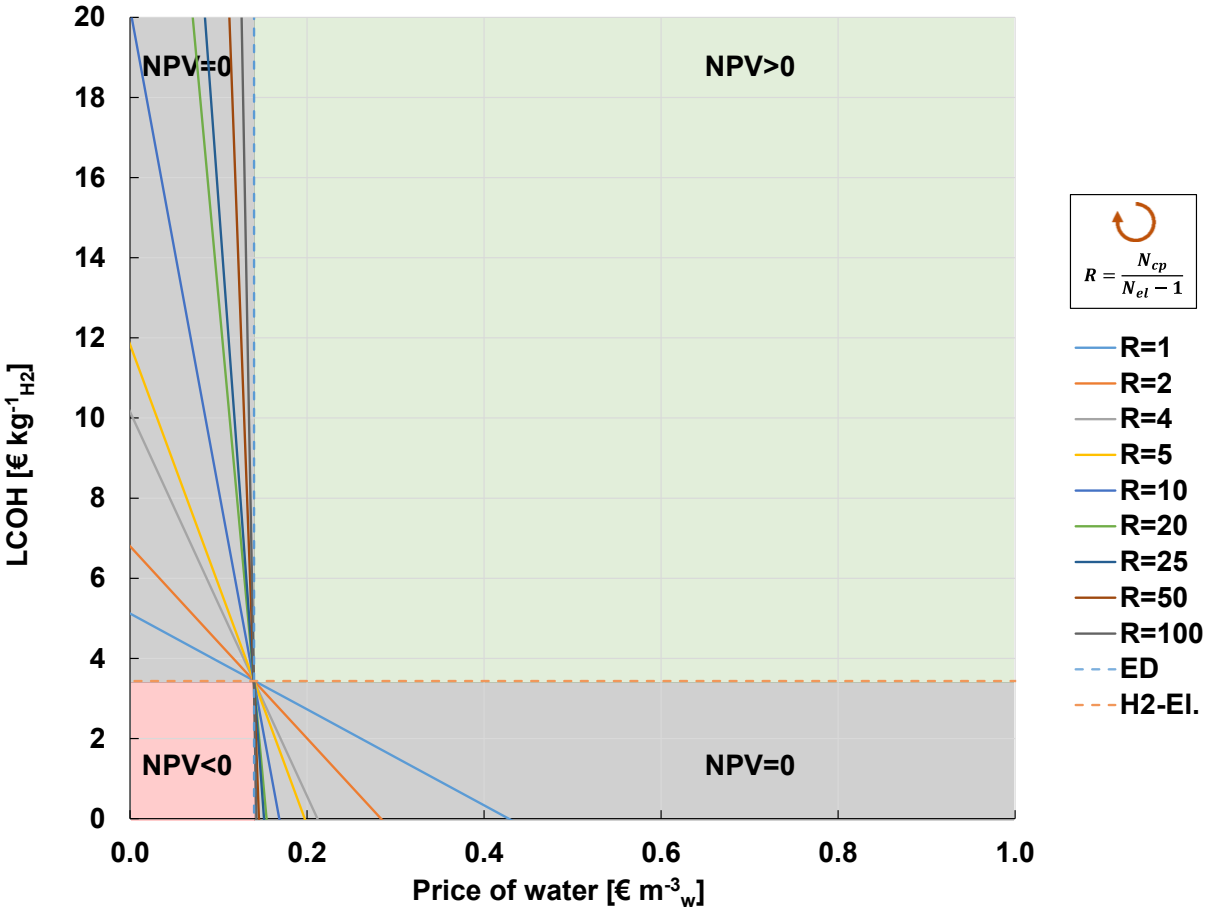

Fig. 23 LCOH versus the price of water. The curves are parameterized with R-value.

Similar considerations can be inferred from *Fig. 24* where LCOW *vs* R is reported as a function of the hydrogen selling price. Increasing H_2 selling price allows water to be sold at a lower price to breakeven after *n* years (i.e., lower LCOW). Clearly, LCOW is equal to 0.14 € m^{-3}_{w} when H_2 selling price is 3.43 € kg^{-1}_{H2}. Thus, LCOW is found lower than 0.14 € m^{-3}_{w} when H_2 selling price is higher than 3.43 € kg^{-1}_{H2}. In particular, for values higher than 5 € kg^{-1}_{H2} and low R, a negative LCOW occurs, meaning the freshwater should be sold at a negative value to breakeven after n years: being this

unrealistic, a positive NPV is expected even if water would be given for free. Note that, the chosen hydrogen prices reported in the figure refer to the price of grey hydrogen (2 € kg^{-1}_{H2}, [13]), the lower green hydrogen (5 € kg^{-1}_{H2}, [12,13]), the upper green hydrogen (8 € kg^{-1}_{H2}, [12,13]), and the today price in refuelling station (12 € kg^{-1}_{H2}, [117]).

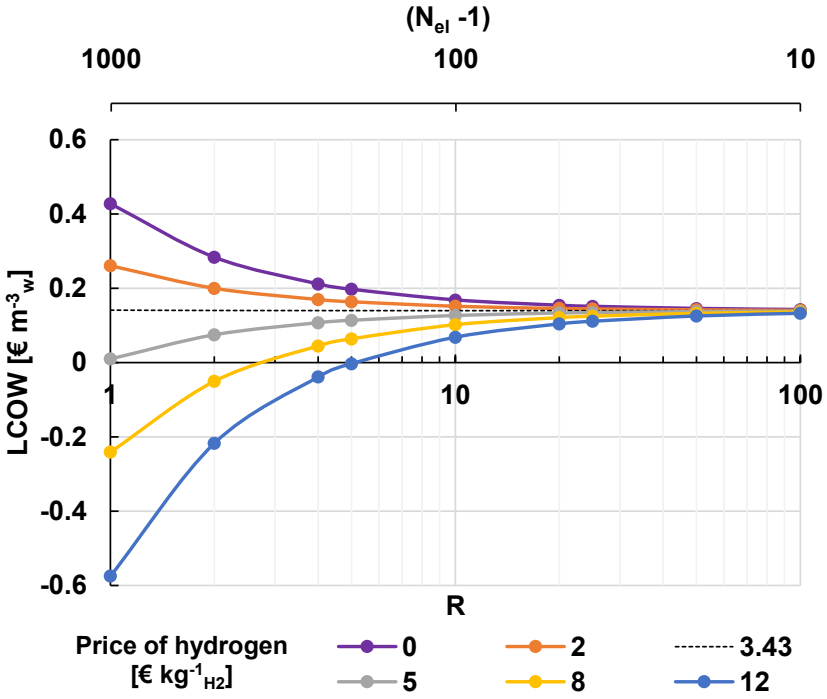

Fig. 24 LCOW versus R and number of electrodes as a function of the hydrogen selling price.

An interesting point of view could be the one of a water producer, who already holds an ED plant and needs only to add the electrodes and the end-membranes to the stacks (i.e., ED plant revamping). In this case the FCI takes into account the addition of the new equipment only (i.e., electrodes and end membranes), and the operative costs account for the increment in power required for the water electrolysis (i.e., overall voltage drop at the electrodes, E_{el}). The contour plot in *Fig. 25a* shows the NPV provided by the revamped plant (hereafter named $NPV^{revamping}$) when the price of water is fixed to the LCOW of the equivalent ED unit (R=1000), i.e., 0.14 € m^{-3}_{w}. As shown and as expected, positive NPV can be achieved for hydrogen selling prices higher than 3.43 € kg^{-1}_{H2} and low R-values. Interestingly, a $NPV^{revamping}$ of 2.7 M€ can be reached when H_2 is sold at 8 € kg^{-1}_{H2} and R=1. It is worth noting that this value is relevant to a single stand-alone HED unit, while in industrial ED plants several stacks are installed. In that case, $NPV^{revamping}$ would increase proportionally. As an example, if the described HED configuration is applied to the Electrodialysis Reversal EDR plant in Abrera (Spain) [118] that is able to produce 220,000 m^3 per day of drinking

water, the corresponding $NPV^{revamping}$ would be equal to 376 M€. When H_2 selling prices is reduced and R is increased, the plant profitability reduces. Just to give an example, $NPV^{revamping}$ decreases from almost 950 k€ for R=1 to 11 k€ for R=100 when a price of 5 € kg^{-1}_{H2} is considered.

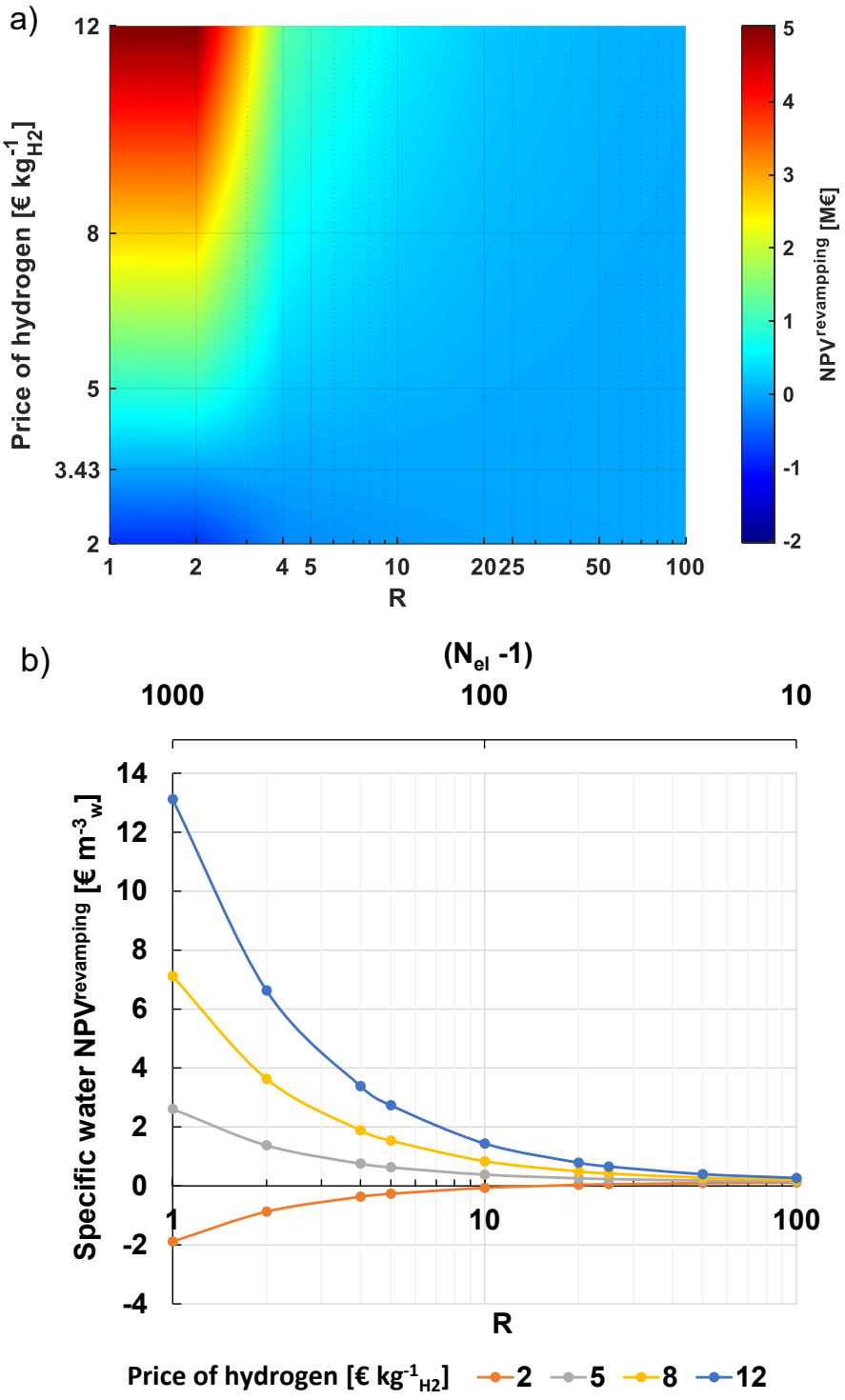

Fig. 25 Economic features of an ED plant revamped to HED as a function of R and hydrogen selling price: a) $NPV^{revamping}$, b) Specific water $NPV^{revamping}$. The corresponding water selling price is fixed to the one required by an equivalent ED unit of 1000 cell pair (i.e., 0.14 € m^{-3}_{w}).

The specific water NPV reported in *Fig. 25b* represents how much money can be earned for each cubic meter of freshwater produced by the revamped ED plant (now HED). As expected, there is room for profit especially for a hydrogen price higher than 3.43 € kg^{-1}_{H2} (corresponding to a specific water NPV of 0 k€, *x*-axis). Its influence becomes negligible for high values of R, while a significant profit is possible for low values of R: e.g., a maximum of 13.1 € m^{-3}_{w} would be earned if hydrogen were sold at the value of 12 € kg^{-1}_{H2}.

A sensitivity analysis was performed only for case of the ED plant revamping. In *Table 10*, the economic data are reported for the worse, the base and the better scenario. The base case corresponds to the values adopted above in the previous sections. Trivially, the "better" scenario represents all those values that lead to an increase in the plant revenue, and the "worse" scenario is related to the values that cause a worsening of the plant remunerability.

Table 10 Economical data input for the scenario analysis

	Input Scenario		***Worse***	***Base case***	***Better***
Discount rate	**[%]**	[65,92,95]	6	3	0
Membrane cost	**[€ m^{-2}_{IEMs}]**	[65,95,98,105]	100	25	4
Electrode cost	**[€ m^{-2}_{el}]**	[12,89]	500	100	-
Electrode lifetime	**[y]**	[12]	-	17(60000 h)	20
H_2 selling price	**[€ kg^{-1}_{H2}]**	[13,117]	2.00	3.43	12.00
Tax rate	**[%]**	[65]	40	10	0
Electricity cost	**[€ kWh^{-1}]**	[65,105]	0.12	0.10	0.05
Labour cost	**[%]**	[65,84,95,98]	20	10	0
Other costs	**[%]**	[89,95,98]	6	4	3
Working hours	**[$h\ y^{-1}$]**	[65,119]	2500	8000	-

The tornado diagrams of *Fig. 26* assess the effect of the economic data input for the case of R=1, on the $NPV^{revamping}$ and the specific water $NPV^{revamping}$ (*Fig. 26a*) and the LCOH (*Fig. 26b*). In the case of *Fig. 26a*, H_2 selling price is set equal to the LCOH of 3.43 € kg^{-1}_{H2}, which, coupled with the freshwater selling price of 0.14 € m^{-3}_{w} (i.e., the ED LCOW), makes the $NPV^{revamping}$ for the base case equal to zero. The main variation in $NPV^{revamping}$ is due to H_2 selling price and it ranges between -800 k€ to +5000 k€, respectively, for variation between 2 and 12 € kg^{-1}_{H2}. The second most affecting parameter is electricity cost as it represents the main cost associated with the operative expenditure. Both ED and electrolyser are energy-intensive processes, and an increase in the electricity cost can be dramatically disadvantageous for the economy of the process. The increase of only 2 euro cent causes an LCOH increase of 34% (*Fig. 26b*). On the other hand, if the cost of energy becomes 50 € MWh (according to the today price of renewable energy [120]) the

corresponding LCOH becomes incredibly low and equal to a value lower than 1 € kg^{-1}_{H2}.

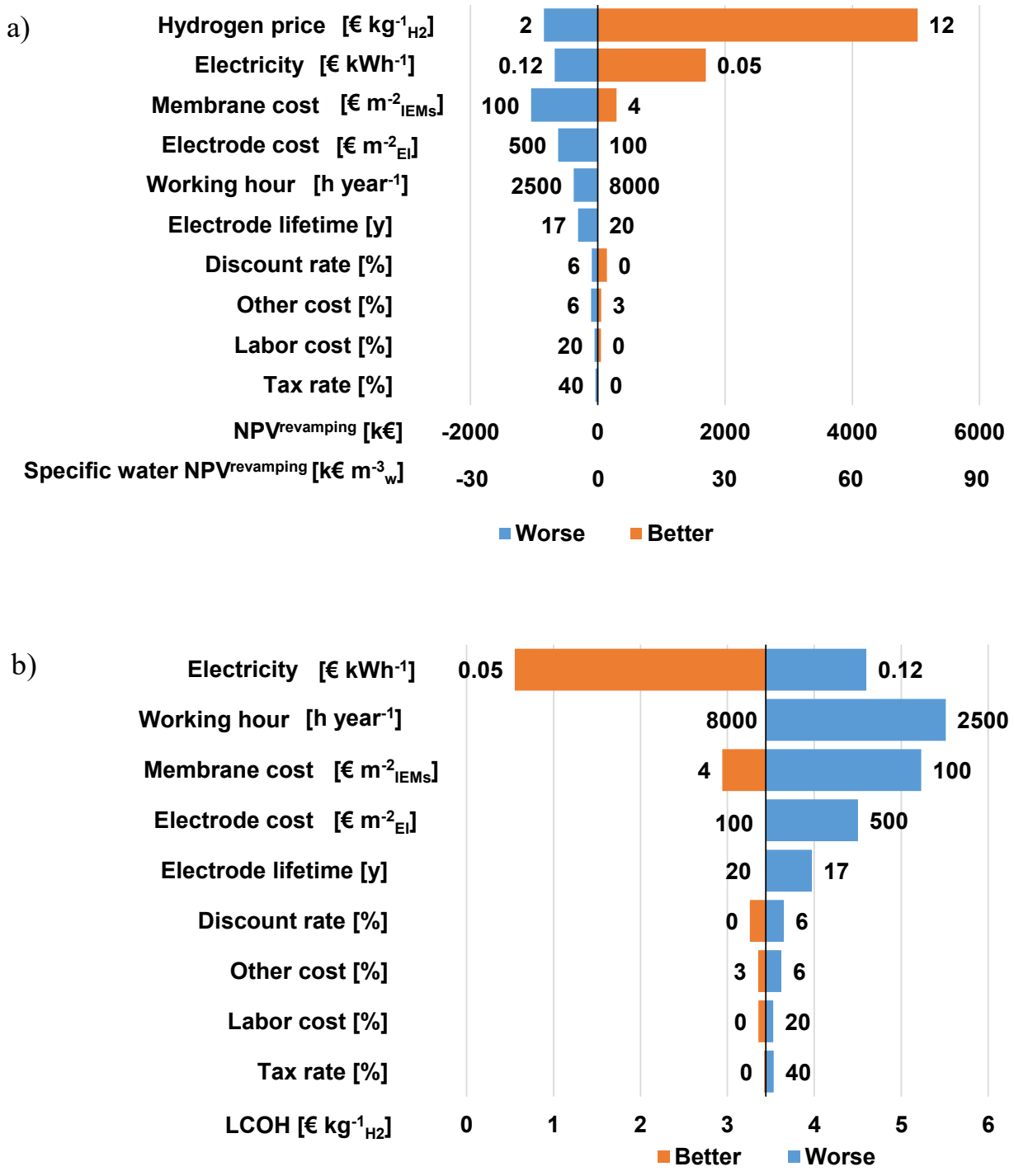

Fig. 26 Tornado diagrams for different economic data input: a) $NPV^{revamping}$ and Specific water $NPV^{revamping}$ and b) LCOH. The hydrogen selling price is set equal to 3.43 € kg^{-1}_{H2} for (a). In both figures the selling price of water is 0.14 € m^{-3}_{w}.

The membrane cost is another economic data that can importantly affect the $NPV^{revamping}$: a membrane cost of 100 € m^{-2}_{IEMs} which is high, yet still comparable with some current ones, may lead

to a negative $NPV^{revamping}$, or to a still acceptable increase of LCOH up to 5.23 € kg^{-1}_{H2}. The impact of the membranes on the costs are related to the additional end membranes which have to be added to the ED stack together with the additional electrodes. Working hours may also be an important parameter. In case one wants to supply the plant with RES without installing an electric energy storage system, the working hours per year might drop down to 2500 h per year (typical values for a PV working 7 hours per day, [119]). In such a scenario, LCOH would encounter a ~60% increase. Assuming a (i) fixed working hours and a (ii) constant power input for the RES is a simplification of this work. Further analyses should be needed in order to study more in depth the coupling between RES and HED technology. As an example, it would be beneficial to take into consideration a dynamic efficiency [121] that is able to account for both the daily discontinuity and the variation of the power output as well as the overload capacity due to the maximum peak of the RES.

All the other parameters variation investigated were found not to have a significant impact on the results. Importantly, in the worst scenario investigated, the corresponding LCOH was found equal to a still promising 5.51 € kg^{-1}_{H2}, thus suggesting that HED might have good chance to be a profitable idea.

4.4 Final remarks and future perspectives for HED

The results obtained from the analysis seem to be very promising and certainly leave room for further in-depth analysis. Under not conservative conditions, a LCOW of 0.14 € m^{-3}_{w} was identified for the case of water production with classical ED.

The (A-)RED and the ED do not require currents being particularly high (e.g. compared to conventional electrolysers) and consequently this strongly limits the productivity of hydrogen. In ED, the current is limited by (i) the desalination target and (ii) the geometry, defined by the design suggested in existing plants. To overcome this problem, the proposed strategy was to insert extra electrodes between the cell pairs of the unit, in order to increase the number of electrodes and therefore the productivity itself (as is customary for traditional electrolysers). This has actually greatly increased the productivity of hydrogen, for which the highest productivity was obtained when an electrode was inserted in every single cell pair. In this case, a productivity of 440 kg_{H2} $year^{-1}$ was achieved and when the production of desalinated water (which has not changed in the new configuration) is considered for selling, the system shows an increase in overall revenue. The point

of view of a desalinated water producer with ED, who also wants to produce hydrogen while maintaining the same cost of producing water, was therefore considered. In this new case (revamping) a LCOH of 3.44 € kg^{-1}_{H2} was identified. In addition, the analyses also showed that selling hydrogen at 8 € kg^{-1}_{H2} could accomplish an $NPV^{revamping}$ of almost 3 M€. The technology therefore concretely represents a valid opportunity for the production of hydrogen and water.

ED is normally used in the desalination of water with a low salt content, and since the amount of salt to be moved is defined and limited, the currents involved are also lower. As mentioned above, the productivity of hydrogen is directly proportional to the current of the system, so increasing this current could be further advantageous. For this reason, it was decided to carry out a second HED analysis for the case in which the feed to be desalinated is seawater so that, the currents involved can also be increased. The SWHED case is discussed in the following chapter.

5 *Hydrogen Electrodialysis HED: Sea water*

Electrodialysis is a process that is normally used for the desalination of BW to reduce its salinity and produce freshwater, but it is not commonly used in the desalination of seawater. This is mainly due to the high costs of the technology, since the entire desalination is proportional to the amount of electricity consumed. In literature, there are few studies dedicated to seawater desalination with ED (SWED), and most of them agree with a multi-stage configuration, to pursue the desalination target.

In the seawater desalination field, the inevitable comparison is with reverse osmosis. RO is currently the most widespread and industrially used technology for desalination, which accounts for up to 69% of the installed desalination capacity. A SWRO consumes in a variable range between 2.5- 4 kWh m^{-3} [122], depending on when the plant was built, the location, the salinity and the presence of pressure exchangers (PX) finalised to the recovery of the energy. Generous et al [53] reported a techno-economic analysis comparing ED and RO, identifying a map of costs as the concentration of feeds varies. The results of the analysis show that the costs of ED are almost always higher than RO, especially as feed concentration increases. According to their study, ED can cost up to 1.5 \$ m^{-3} for SW at 35 g L^{-1}, against the almost constant cost of RO which stands at 55 c\$ m^{-3} of water (and up to 85 c\$ m^{-3} in the case of RO without PX). The authors also estimate an ED SEC of more than 4.5 kWh m^{-3} for the desalination of water at 35 g L^{-1}. Results showed that ED becomes competitive compared to RO as the concentration decreases. The threshold is equal to 7 g L^{-1}, and below this value, there is a greater convenience of ED. This is also confirmed by the employment of ED in the industrial sector for the brackish water desalination.

Giacalone et al [103] reported an exergy study on ED for the BW and SW desalination case, for which the efficiency of the process is evaluated and the main sources of irreversibility are identified, such as the ohmic resistance of solutions and membranes and unwanted transport phenomena. The results showed that by improving the membranes, thus reducing their resistance, the efficiency of the process can increase as they are mainly responsible for the loss of the system exergy. The SWED case is also studied in two configurations, a single unit that performs the desalination entirely, or a multi-stage configuration with 2 units. The two-stage configuration in SWED, reduces the specific energy consumption, bringing it from 6 to about 4 kWh m^{-3}. What Giacalone et al. investigated also

proves previous technical and experimental investigations, which highlight the energy benefits (SEC reduction) of multistage configurations.

However, it should be kept in mind that there is a thermodynamic minimum that comes out by the integration of the free energy of mixing linked to the osmotic pressure. This value is equal to 1.06 kWh m^{-3} for the desalination of seawater (35 g L^{-1}), assuming a recovery of 50 %. A value that determines the minimum thermodynamic expense, net of all the irreversibility of the system [123]. Clearly, the real energy expenditure will also have to consider all the other equipment employed, such as the intake pump, the instrumentation of the plant and the pump efficiencies, further increasing the final energy consumption.

In an experimental investigation, Doornbusch et al [124] operated a pilot-scale system for 18 days with real seawater (388 mM, Wadden Sea), maintaining a dilute concentration stable at a value of 1.9 g L^{-1} and with a SEC of about 3 kWh m^{-3}. The test involved the use of 3 stacks of 22 x 22 cm^2 placed in series with a number of reducing cell pairs, for a consequent increase in channel velocities aimed at "delaying" the limit current. Although the SEC is promising, it must be considered that the starting concentration of the Wadden Sea has a salinity of around 22 g L^{-1} and, in the case of more concentrated waters, this value is destined to increase.

The literature shows that SWED is still far from a real industrial application, however, the opportunity to simultaneously produce hydrogen opens new horizons to the possibility of using technology for the desalination of water with a higher saline content.

In this chapter, the possibility of desalinating seawater and at the same time producing hydrogen at the cathode was studied. This was firstly carried out with an experimental investigation in laboratory to obtain data and verify the technical feasibility of the proposal. Later, since there is no technical-industrial correspondence, different plant schemes were considered, which were individually analysed. The proposal, for which a lower desalination cost was observed, was then studied with a view of producing hydrogen at the cathode, according to an analysis similar to that made for the BWED case.

5.1 Experimental

5.1.1 Experimental Set-up

The experiments were conducted using the same stack and methodology described in 3.1.1. Since the same unit can work both in ED and (A-)RED configurations. From an electrical point of view, the polarity of the electrodes changes in ED (see Appendix III) while the only structural difference adopted for the ED tests is related to the use of cationic fumasep® FKB-PK-130 and anionic fumasep® FAB-PK-130 as end-membranes to isolate the cathode and anode electrode compartments, respectively. This is because they are more selective than Fujifilm membranes and more resistant to acid and basic solutions. The system was used to carry out tests in open loop, keeping separated the inlet with the outlet, and in closed loop (Fig. 27), by setting the solutions in recirculation. Each test was repeated and the variability of the data is calculated as standard deviation.

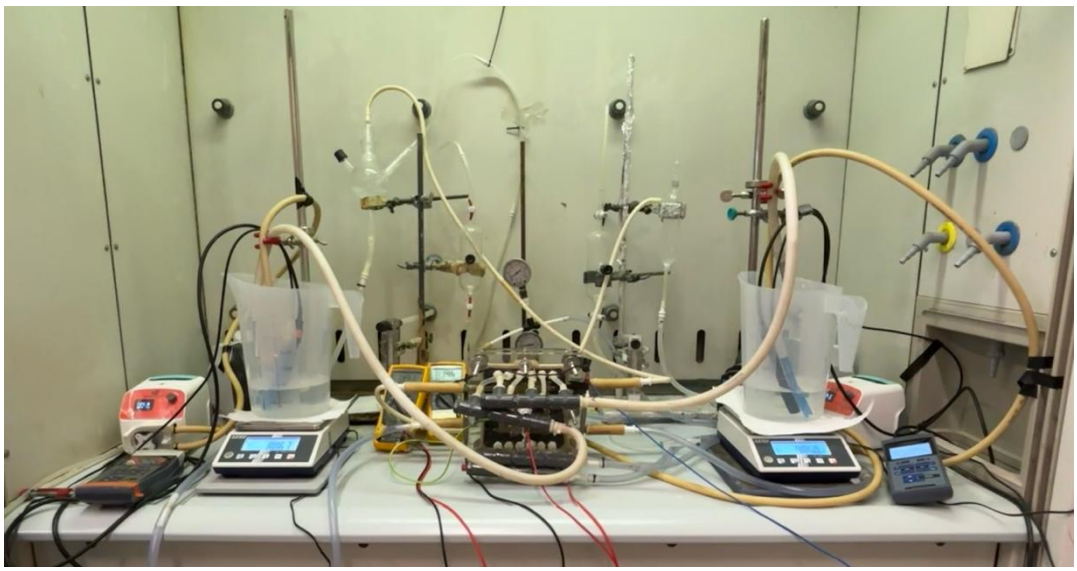

Fig. 27 Picture of the closed loop test.

Furthermore, a new configuration was also studied, corresponding to the case of the techno-economic analysis showed in the previous chapter (4). The new case experimented involves an alkaline NaOH 1M solution for both catholyte and anolyte. The system did not work with both acidic electrolyte solutions, as they promote the competitive reaction of chlorine gas Cl_2 at the anode (see 1.2.1). For the latter configuration, it was necessary to modify the system as follows:

1) Use a cationic fumasep® FKB-PK-130 end-membrane for both electrodes, so as to retain the OH^- ions in the electrode compartments and secure the salt bridge by allowing the Na^+ to pass through;

2) For technical and safety reasons, two separate electrode solutions such as anolyte and catholyte were used, identifying two separate recirculation loops.

Compared to the case of Acid/Base (A/B) solutions at the cathode and anode, there is a difference in the thermodynamic potential that goes from 0.401 to 1.229 V. In addition, the A/B mode system worked with one diluted compartment less. On the contrary, the addition of a cationic end membrane created a new feed channel in the Base/Base (B/B) case, and as a result, both diluted and concentrated have the same number of channels.

5.1.2 Multi-stage open loop test

The possibility of desalinating a feed at the same concentration as seawater with a single 10 x 10 cm^2 laboratory unit consisting of 20 cell pairs was investigated. Direct desalination is clearly not possible: this is why a multi-stage approach was used, i.e. the use of many ED modules placed in series for desalinating a solution with a concentration equal to that of seawater (35 g L^{-1}) to a lower concentration typical of brackish water (5-10 g L^{-1}).

Having only one stack available, the series configuration was implemented with an intrinsically discontinuous system, and in each test, the next stage received the diluted solution from the previous stage as feed. The solutions used are all artificial solutions consisting of NaCl only.

For each stage, polarization curves were carried out while monitoring the concentrations of diluted and concentrated solutions, the pH variations as well as the stack and the cell package (platinum wires) voltages. For each stage, the limit current was uniquely and consistently determined for each test by the Isaacson and Sonin method (see Appendix IV). The concentration of the solution used as the feed for the next stage was determined by the concentration corresponding to 85 % of the limit current value. This value should be regarded as conservative as it allows better control and protection of the equipment: in fact, close to the limit current, small variations in the current correspond to large variations in the applied potential, causing (i) voltages harmful to materials and instrumentation, and (ii) high consumption by the unit, which corresponds to higher operating and maintenance costs.

Fig. 28 shows a summary of the 6 tests carried out. The solution is desalinated in the first ED unit, and the same solution is sent as feed to the next unit. The concentrated solution, on the other hand, is stored in a separate bin.

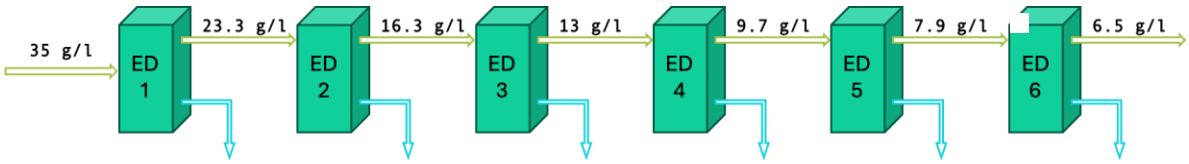

Fig. 28 Electrodialysis stages performed during the experimental campaign

For the sake of brevity, only the data of the 3rd ED stage are shown below, while the cumulative graphs of all the tests are shown in Fig. 30.

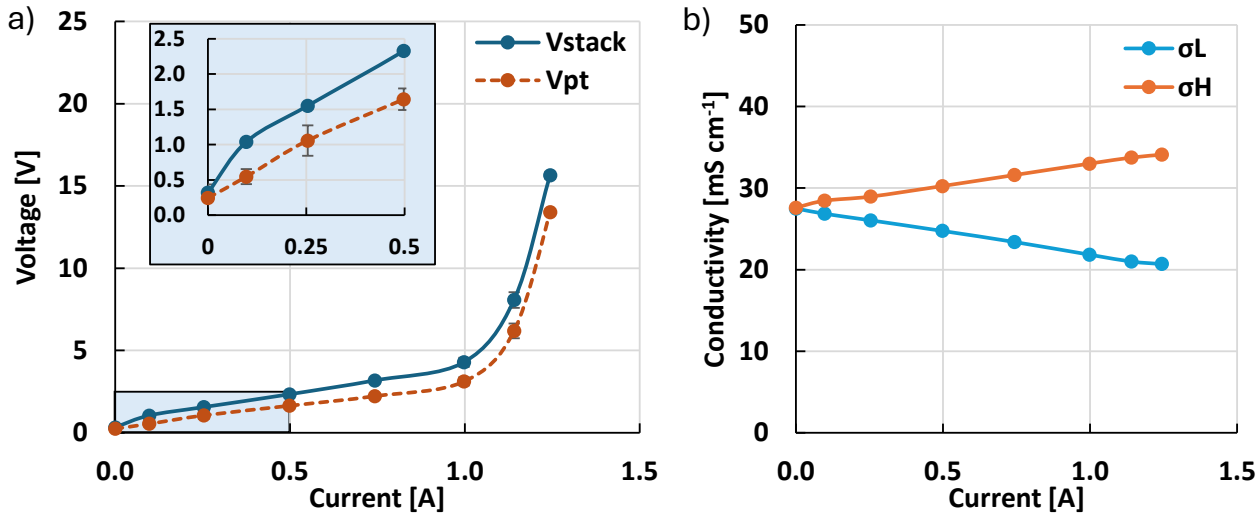

Fig. 29 Trend of (a) voltage across the stack (Vstack) and platinum wires (Vpt) and (b) conductivity of diluted and concentrate solutions versus the current. Plots refers to the 3rd stage corresponding to a feed concentration of almost 13 g L^{-1}.

Fig. 29a shows the trend of the voltage measured at the stack and at the platinum wires as a function of the applied current. The platinum wires measure represents the voltage across the cell package and allows the electrode contributions to be isolated. The difference between V_{stack} and V_{pt} represents this contribution that takes into account, in addition to the potential of the reactions, also the ohmic contributions related to the 2 end membranes and electrode solutions. The desalination contribution (V_{pt}) and the electrode compartments both create a drop in potential, and energy has to be provided to the system. The electric potential generated across the cell pair (eq. 28) assesses that, in the case where the system is fed by the same solution, the electromotive force is zero, as the ratio within the logarithm is unitary. However, as can be seen from the zoom in Fig. 29a, both V_{pt} and V_{stack} have a non-zero value, this is due to the use of electrode solutions different from the adjacent solution in the channels, which generate a Donnan potential across the membrane. Nevertheless, V_{pt} should still be equal to zero, but a greater potential is read due to the diffusion phenomena that occur between the end-membranes at time zero. However, as expected,

V_{pt} immediately grows linearly as desalination takes place, the stack potential instead (that includes the electrodes) grows first with a very high slope (due to activation overvoltage, η_{act}) and then grows linearly from about 0.1 A in the ohmic region of the system. In this region, the difference between V_{stack} and platinum is always greater than 0.401V.

Ohmic linear growth occurs in accordance with Ohm's law in the range 0.1 - 1 A. For higher current values, at about 1 A there is a clear variation in the slope, at which the limit current is reached. In this case, according to the Isaacson-Sonin method, the limit current is 1.1 A, and the condition for the next stage is for a current value of 0.93 A which corresponds to an output conductivity of the diluted of 21.9 mS cm^{-1} (about 13 g L^{-1}). The graph in Fig. 29b shows the conductivity trend of the two solutions coming out of the system. Clearly, the trend of diluted and concentrated concentrations, which tend to move away, is a direct consequence of the desalination that leads the ions (Na^+ and Cl^-) to move into the concentrated channels. For values slightly above 1 A, it can be seen how the conductivity vary less and less, reaching a plateaux, meanwhile a similar but opposite trend occurs for the concentrated solution.

The data of the 6 stages were collected in a single graph in Fig. 30. The stack voltage trends V_{stack} (solid line) and the platinum wires V_{pt} (dotted line) are shown in Fig. 30a for all the ED stages carried out, while the values of the conductivities of the diluted streams are shown in Fig. 30b. The curves are parameterized with the concentration of the feed, and show how the limit current value is anticipated as the concentration of the input feed decreases. Since the limit current drastically impacts the operating current of the system, this implies a lower degree of desalination achievable. Fig. 30b shows the trend of the conductivities (and concentrations) of the diluted solutions at the exit of the stages. As mentioned, each stage works at 85 % of the calculated limit current, which concentration represents the input concentration for the next stage, as indicated by the horizontal dotted lines. Despite the six stages used, under the same conditions of 85 % of the limit current found for the 6^{th} stage, the output concentration would be equal to 6.7 g L^{-1}, highlighting even more how the efficiency of desalination at low conductivities becomes progressively worse.

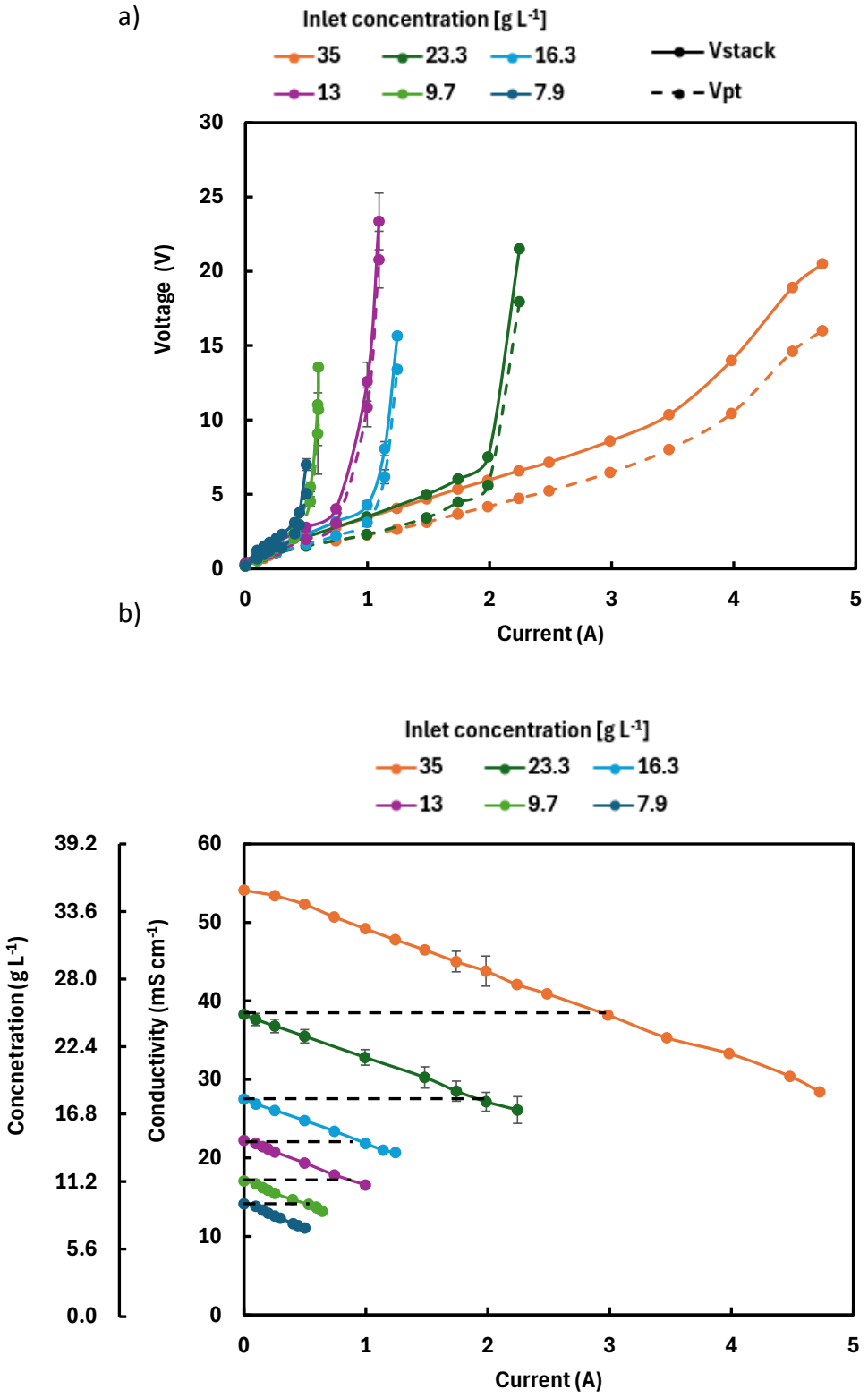

Fig. 30 Trend of (a) voltage at the stack and wires of Pt and (b) of the conductivities of the dilute solutions at the outlet of each stage as the current varies. The curves are parameterized as the concentration of the input feed at the ED stage varies. In (b) the dashed horizontal curves represent the calculated limit current point for each stage, identifying the input concentration of the next stage.

This is even more highlighted in Fig. 31, by an alternative representation of the graph in Fig. 30b. In fact, Fig. 31 shows the desalination trend stage by stage by diagramming, for each, the input and output concentrations. The latter is therefore the value of the inlet concentration to the next stage. From this further diagram it can be seen again how with the progress of the number of stages the desalination efficiency decreases (the slope of the line that characterizes the stage decreases) tending more and more to a horizontal curve, and requiring an increasing number of stages, to reach lower concentrations.

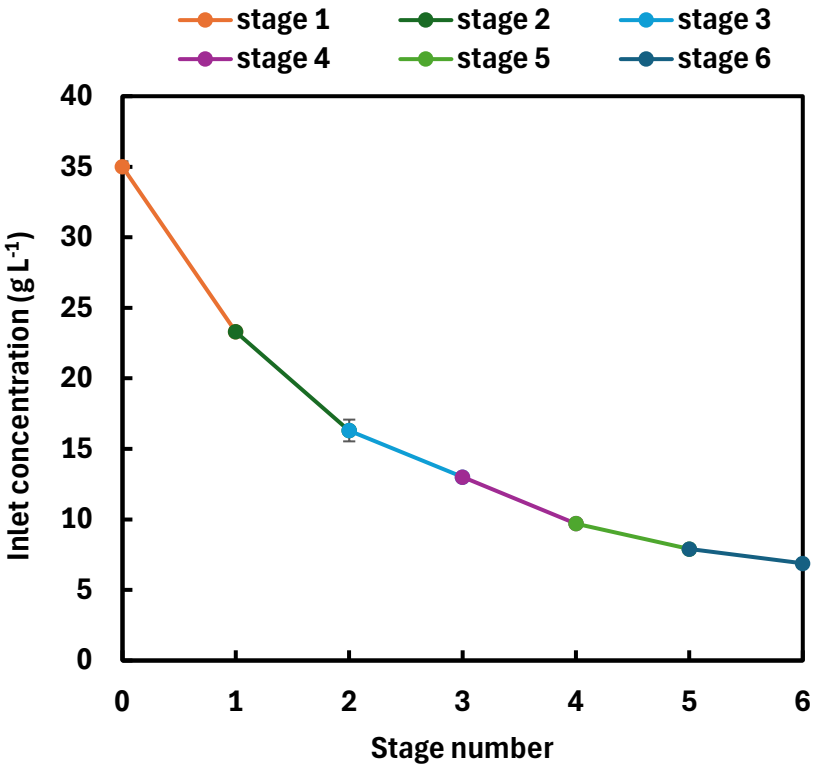

Fig. 31 Concentration trend for each desalination stage

Assuming that the system performs under the operating conditions identified for each stage, the power required by the 6 stages to desalinate from 35 to 6.9 g L^{-1}, thus obtaining a brackish water, would be 44.2 W. Considering that the system has always treated 151 mL min^{-1} (corresponding to a velocity of 0.5 cm s^{-1} in the channels), the entire desalination would require 4.88 kWh m^{-3}, of which 1.28 kWh m^{-3} are due to the electrode voltage drop (electrodes and end-membranes).

This system with only one cathode would produce a quantity of hydrogen equal to 260 mg h^{-1}. As expected, there would be a HSEC of 800 kWh kg^{-1}_{H2} due to (i) the limited production related to a single cathode, and also because it has to (ii) take charge of the desalination contribution of 20 cell

pairs. An absolute high HSEC, that would drop to 240 kWh kg^{-1}_{H2} if the maximum number of electrodes are inserted in the unit, as done in the previous chapter.

The tests conducted led to the achievement of the desired target, i.e. the desalination to brackish water. Clearly, as it can be seen from these figures, it is certainly possible to desalinate water with a high saline content through the use of multiple ED stages, although a decrease in the input concentration implies the need for an increasing number of ED units. However, it must be also considered that the following study was conducted on a small 10 x 10 cm^2 unit and that a much larger industrial unit would compact many of these stages in one single step. In addition, the proposed configuration is only one of the possibilities. In fact, different configurations of recirculation of currents could be imagined, both to increase the desalination capacity of the system and to reduce energy consumption.

5.1.3 Polarization curves A/B vs B/B

Having introduced the modification of the set-up to have the same electrode solution in both electrodes, the system was tested in both A/B and the B/B configuration in order to obtain a polarization curve corresponding to the feed of 35 g L^{-1} and to compare their performance.

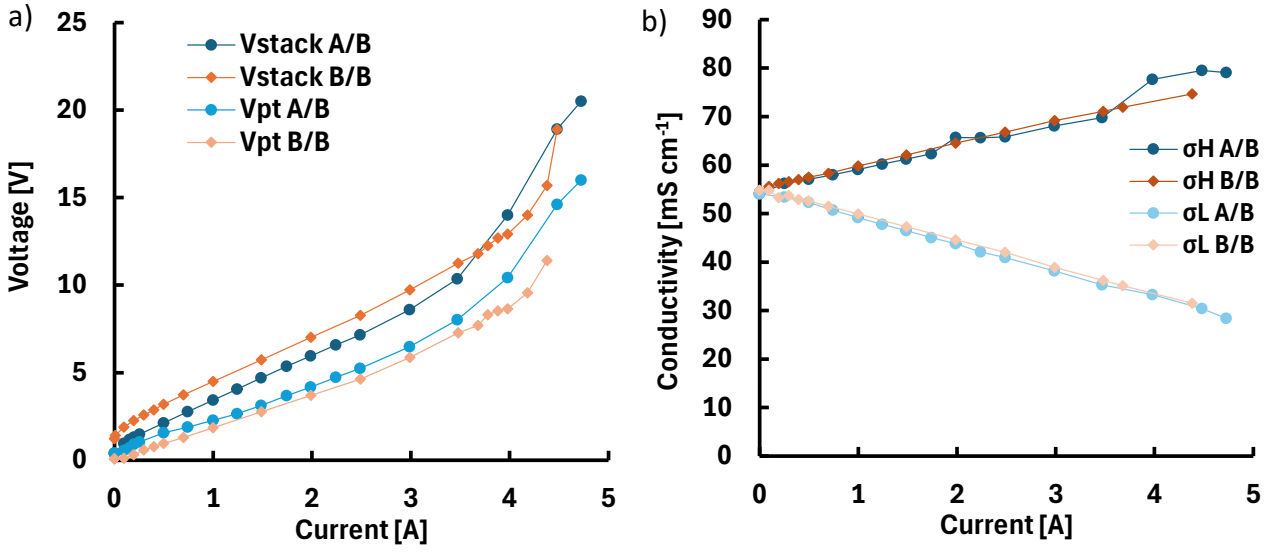

Fig. 32 Trend of (a) stack voltage and Pt wires and (b) conductivities of diluted and concentrated as a function of current for A/B and B/B tests.

The trend of the stack and platinum potential measures as a function of the applied current are shown in Fig. 32a. Unless there is a different slope for lower currents, according to the charge

transfer electrode overvoltage, both curves have an ohmic region with linear behaviour until the limit current regime is reached.

As expected, the B/B curve is higher than the A/B curve indicating that a higher thermodynamic voltage contribution of 0.83 V is required. Unless a different initial transient, due to different electrode reactions (η_{act}), the potential difference between the two systems is always 1.05 V, inducing higher energy consumption. From the point of view of desalination, however, the two processes work in the same way as shown in Fig. 32b, net of small variations in conductivity of less than 2.5 %. These variations are also observable in the potential difference of platinum, however it should be remembered that in the case of A/B there is one channel less, which means that the energy to be spent on desalination is slightly lower.

5.1.4 Closed-Loop tests

The other type of tests involved closed loop dilution tests. A total of 2 L of solution at 35 g L^{-1} was treated for desalination, of which 1 L was part of the diluted circuit and 1L was in the concentrated one. The test was conducted in voltage control of 4 V, leaving the current free to vary. This was necessary, as consequence of the results obtained in section 5.1.2. In fact, the tests had the goal of reaching at least 5 g L^{-1}, and as the desalination proceeds, the limit current could be reached earlier, drastically incrementing the differential voltage applied. Tests were conducted in both A/B and B/B configurations.

5.1.4.1 A/B closed loop test

Throughout the entire duration of the test, the feed solutions (concentrated and diluted), which at the beginning of the test have the same concentration, were recirculated in two different containers, whose weights were monitored over time. Excluding the dead volume of the tubes, it can be seen in Fig. 33 that, there is an increase in the weight of the concentrated solution, and at the same time, a decrease in that of the diluted one.

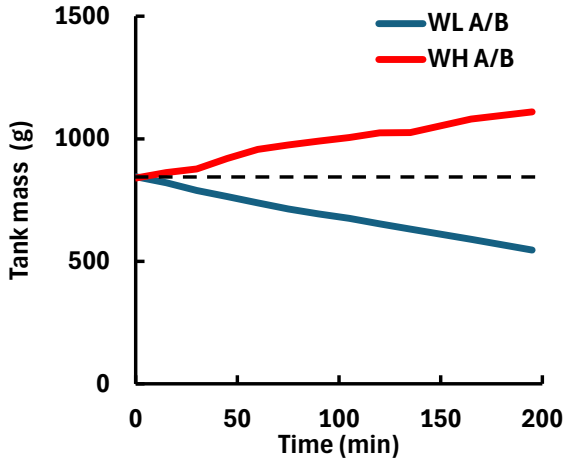

Fig. 33 Mass of diluted and concentrated solutions as a function of time for A/B closed loop tests.

At the start of the experiment, the weights of the jugs were recorded at approximately 850 g. Over the duration of the experiment, an increase in weight was observed, reaching 1109 g and 546 g for the concentrated and diluted solutions, respectively. It is noteworthy that the mass balance was not closed by more than 2%, which is the designated leak test threshold. The observed change in weight can be attributed to two factors: firstly, the migration of the salt from the diluted compartments, and secondly, the water dragged by osmotic and electro-osmotic phenomena.

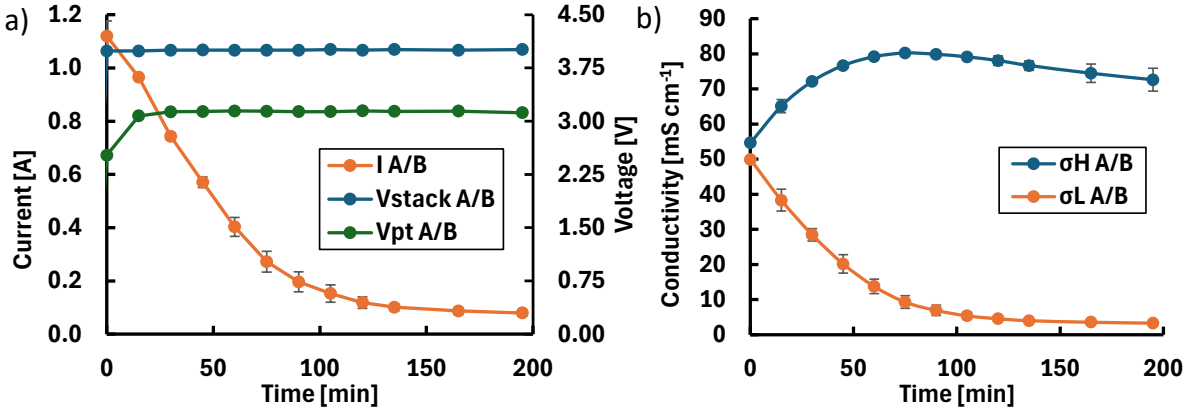

Fig. 34 Trend of (a) electrical variables of the system and (b) conductivity for closed loop tests in A/B

In Fig. 34 is shown how at the beginning of the process, when the solution is still at about 35 g L^{-1}, the resistance of the system is relatively low and there is the maximum current circulating in the stack. The more time passes, the more ions pass through the membranes and the greater the degree of desalination obtained. However, the dilute compartment reduces its concentration more and more, consequently increasing its ohmic resistance, and as shown by the graph, reducing its current (Fig. 34a). In the last part of the test, after about 120 minutes, a plateau is reached due to the very few ion charges left in the diluted and to a maximum resistance to transport reached. From this

moment on, the dilution rate becomes extremely low, and the system continues to consume energy without any real benefit (Fig. 34b). The test lasted for a total of 195 min, and the final concentration of the diluted was 1.76 g L^{-1}. The trend of the concentrated was curious, which has a maximum around 75 minutes and then decreases again. The most plausible explanation is that in the first part of the test, the salt is transported mainly by migration from the diluted to the concentrated. At 75 min, however, the current of the system begins to decrease consistently, passing from the initial value of 1.16 A, to the value of 0.25 A at the maximum point, until it decreases to 70 mA at the end of the test. At 0.25 A the current is relatively small, and part of the energy is no longer used to desalinate the diluted material, but on the contrary, to oppose to the spontaneous diffusive flow that would bring the salt from the concentrated to the diluted solution (as in RED). This explains why the concentration of the diluted material does not change any more (Fig. 34b). On the contrary, the osmotic flow that would normally occur from the diluted to the concentrated (as a water flux) is accentuated to restore the osmotic pressure. The concentrated is then diluted by this water flux, reducing its concentration. This also explains the reason for the asymmetrical trend of the masses (Fig. 33) that is pronounced in the final part of the test.

It is interesting to note that the voltage trend at the platinum wires is more or less constant at a value of 3 V for the entire duration of the test, meaning that the variation in the current is due only to the desalination aspect.

The trends in the concentrations of the electrode solutions (Fig. 35a) that are subject to decrease during the test, due to the consumption of H^+ and OH^- by the half-reactions, are also reported. It can be seen that the concentration of HCl decreases more than that of the base, due to the diffusion phenomena that occur at the end-membrane and the greater mobility of the H^+ ion compared to the OH^-.

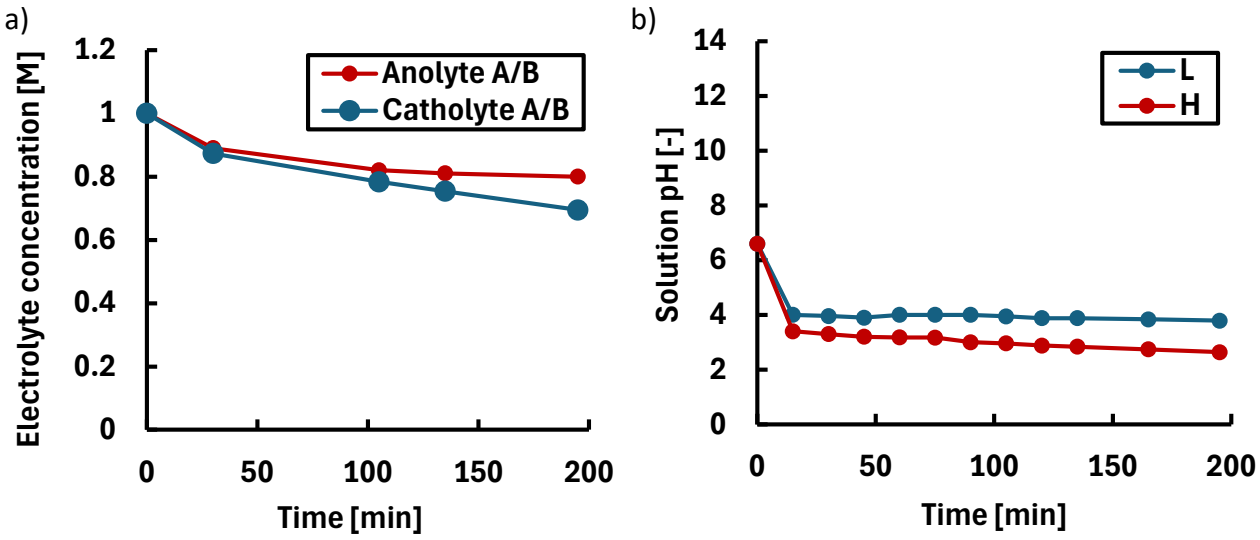

Fig. 35 Trend of (a) electrode solution concentrations and (b) pH of saline solutions for closed loop A/B tests

This effect is also confirmed by the pH trend of the diluted and concentrated solution (Fig. 35b) which tends to be acidified as a result of the phenomenon described, which is more found for the concentrated, given its presence adjacent to the acid electrode compartment.

5.1.4.2 Comparison closed loop tests: A/B vs B/B

For the sake of brevity, the results of the similar analysis made for the B/B system is omitted, however, in the following section these results will be deepened in comparison with the A/B test. The B/B test inherently required higher potentials, which meant that the duration of the test was different. Also in this case the test was interrupted as soon as the current became 70 mA, in total it lasted 240 min, and at the end of the test the concentration of 3.8 g L^{-1} was reached.

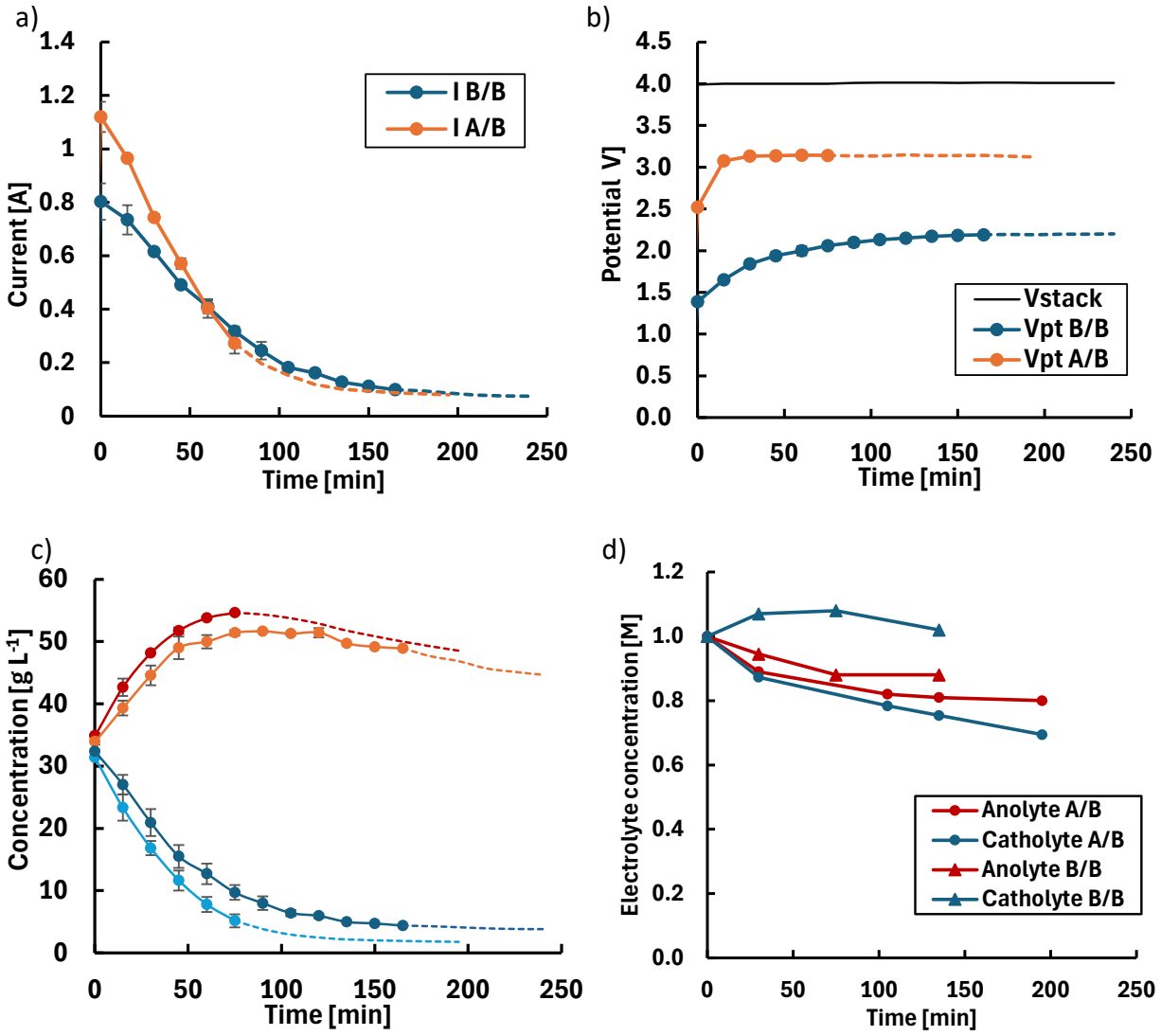

Fig. 36 Trend against time of (a) currents, (b) voltages, (c) concentrations of the output solutions and (d) concentrations of the electrolyte solutions for tests A/B and B/B. The tests are studied until they reach 5 g L- 1 of diluted. The dotted lines represent the entire test duration up to 70 mA. Note that due to an incident it was not possible to monitor electrolyte concentrations for the entire duration of the B/B (d) test.

To achieve a consistent comparison for the two different operating conditions, a concentration target of 5 g L^{-1} was chosen. Both system are fed with a solution of 35 g L^{-1} of NaCl and differ in the solutions adopted as electrolytes. The curves in Fig. 36a show the trend of the current as a function of time for the two tests. It can be seen that the current circulating in the system at the beginning of the test is lower in the case of the B/B system, and that also follows the trend seen for A/B for which the desalination rate asymptotically zero. The trend of the voltage at the platinum wires (Fig. 36b) is also lower in the case of the B/B test due to the higher consumption occurred at the electrodes, which depends mainly on the standard potential of the half-reaction, which, as previously explained, is greater in the case of reactions both carried out in a basic environment.

In Fig. 36c the desalination trend is also shown by evaluating the concentration of the two solutions as a function of time. The trend already described and observed in the previous section occurs also for the B/B test, in which beyond a certain current the diluted does not dilute further, but on the contrary, as a result of the preponderant osmotic flow, the concentration of the concentrated begins to decrease. For the two tests, two different times are necessary for achieving the same outlet concentration. In particular, the A/B case carries out desalination faster, requiring 75 minutes of operation compared to 165 of the B/B case. Concerning the electrolyte solutions and according to the reactions reported in Table 1, in A/B case the H^+ is directly consumed at the cathode while OH^- is consumed at the anode. On the contrary, in case B/B, consistently with what is expected, the concentration of anolyte decreases, but on the contrary, that of catholyte increases. If the two solutions were recirculated, after a good separation of the gases, the OH^- produced by the reduction of water at the cathode, would compensate for the demand of OH^- at the anode, keeping the concentration constant (clearly without considering possible water flows and decrease in volumes due to the electrochemical reaction). However, as the two circuits are kept separate, there will inevitably be an increase in the concentration of OH^- at the cathode and a decrease at the anode. After about 75 minutes, there is a decrease in concentration in case B/B, this is due to diffusion phenomena of OH^- towards adjacent channels. This statement is also justified by the progressive basification of the two solutions up to 10.7 pH.

During the tests, gas-samples were also taken and a faradic efficiency for hydrogen was found, as expected, always around 100%.

Specific Energy Consumption (SEC) were also calculated for the two cases. The SEC were calculated on the basis of the energy required by the system to bring the salinity of the diluted from 35 g L^{-1} to about 5 g L^{-1}. This concerned the first 75 and 165 minutes of closed loop tests, respectively for A/B and B/B test. The SEC of A/B case is 6.13 kWh m^{-3} while that of case B/B is 5.37 kWh m^{-3}. Both SECs refer to m^3 of diluted water produced, and although the B/B test took longer to desalinate, the largest SEC was found for the A/B case. This is mainly due to weight measurement, which lead to a lower volume in the A/B case, and consequently a higher SEC. Values just above, but still in line, with the 4.88 kWh m^{-3} estimated with multi-stage tests. However, if we compare only the energy spent, this would be 3.35 Wh for case A/B and 3.84 Wh for case B/B, indicating as expected, a lower energy expenditure due to the smaller redox potential required. However, there are two other aspects to be highlighted. The first is related to the fact that the technology has been also studied

with the purpose to make hydrogen, and the quantity produced between the two tests is different. In fact although the A/B configuration lasted less, it still used a higher current than the B/B case, and since hydrogen is directly proportional to the current, this is also greater. Indeed, 31.5 mg of H_2 were produced in the 75 min test of case A/B compared to 9.34 mg of H_2 in 165 min of case B/B.
The second aspect to consider is that, net of possible unseen and undesired losses of the A/B system, the most advantageous system still seems to be the B/B system because it was subjected of less irreversibility. On the other hand, in the hypothesis where there was indeed a leakage problem, the lowest energy is exactly for the A/B case. However, this difference is not as marked as might be expected, and possibly, only an economic analysis can define the most convenient configuration.

5.2 Technical model

5.2.1 Model equations

The technical model used is the same as in 4.2 with the only difference being the modelling of the electrodes. The potential drop that would occur at the electrodes is defined in equation 10, where it is given by the sum of the thermodynamic potential plus all the dissipations of the electrodes. The thermodynamic potential $E°$ is reduced to being the standard water reduction potential, since the simulated SWHED system works at room temperature and the electrode solutions are assumed at a constant concentration of 1M. Furthermore, assuming a B/B configuration, this potential is 1.229 V (and 0.401 V in A/B case). In the analysis of chapter 4, the term E_{el} was used to create a plausible value with an estimated potential for common electrolysers (of 1.7 V) that took into account both the reversible term and the activation overpotential, η_{act}. In this case, the term was estimated on the basis of an experimental investigation to obtain the parameters of the Tafel equation (see Appendix V). The ohmic term, as in equation 29, took into account the ohmic resistance of the end membrane and electrode solutions, while the term relating to mass transport was considered negligible due to the low characteristic currents of the system, i.e., ~100 A m^{-2}. Equation 10 is then rewritten here in 47:

$$E_{el} = E^{\circ} + \eta_{act} + \eta_{ohm} + \eta_{diff} = 1.23V + \eta_{act} + (r_{EM}i + r_{ERS}i) \qquad 47$$

This equation, together with equation 29, defines the new and different modelling of the electrode compartments.

5.2.2 Model validation

On the basis of the experiments conducted in the experimental section, and together with the parameters found by the analysis of the LSVs, the calibration and validation of the model was carried out. For the sake of brevity, two cases are reported at different concentrations and for different electrode configurations. Fig. 37 shows the trend of stack and platinum voltages and the trend of the output concentrations predicted by the model compared to the experimental values for the 35 g L^{-1} B/B case. As can be seen, the model is able to satisfactorily predict experimental trends, both according to electrical and physical variables, such as concentrations.

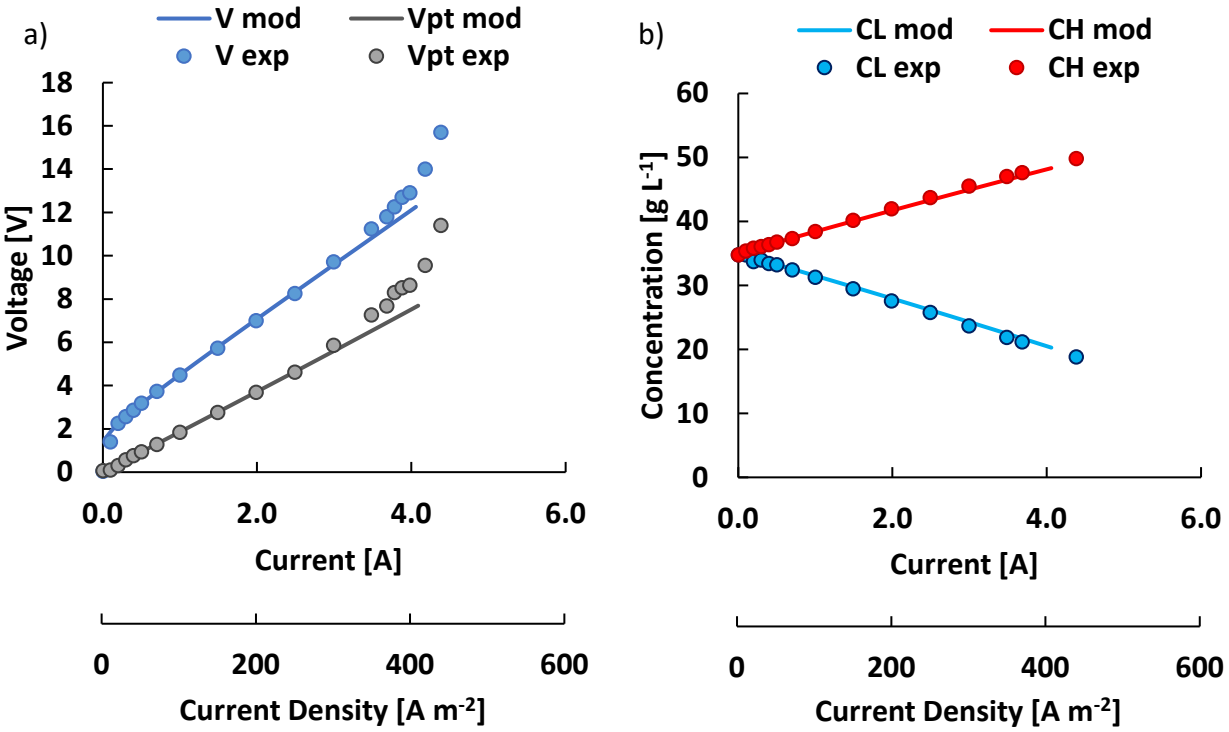

Fig. 37 Trend of (a) stack voltage and platinum wires and (b) output conductivities versus the current and the current density of the system. The experimental data and simulation refers to an SWHED unit that treats an inlet flow rate of 35 g L^{-1} with a velocity of 0.5 cm s^{-1}. The electrode configuration is B/B.

The introduction of BV also makes it possible to estimate the first part of the curvature of the curves, for which the potential increases relative to the overvoltage due to activation. Platinum wires, on the other hand, start from zero and grow almost entirely linearly. This linear trend also occurs when experimentally the system reaches the limit current condition, for which the voltage increases exponentially with respect to the current. This variation cannot be predicted well by the ED model and consequently, the higher the current, the greater the error that the model makes.

Another validated case reported, is the desalination at 7.9 gL^{-1}, for the A/B electrode configuration.

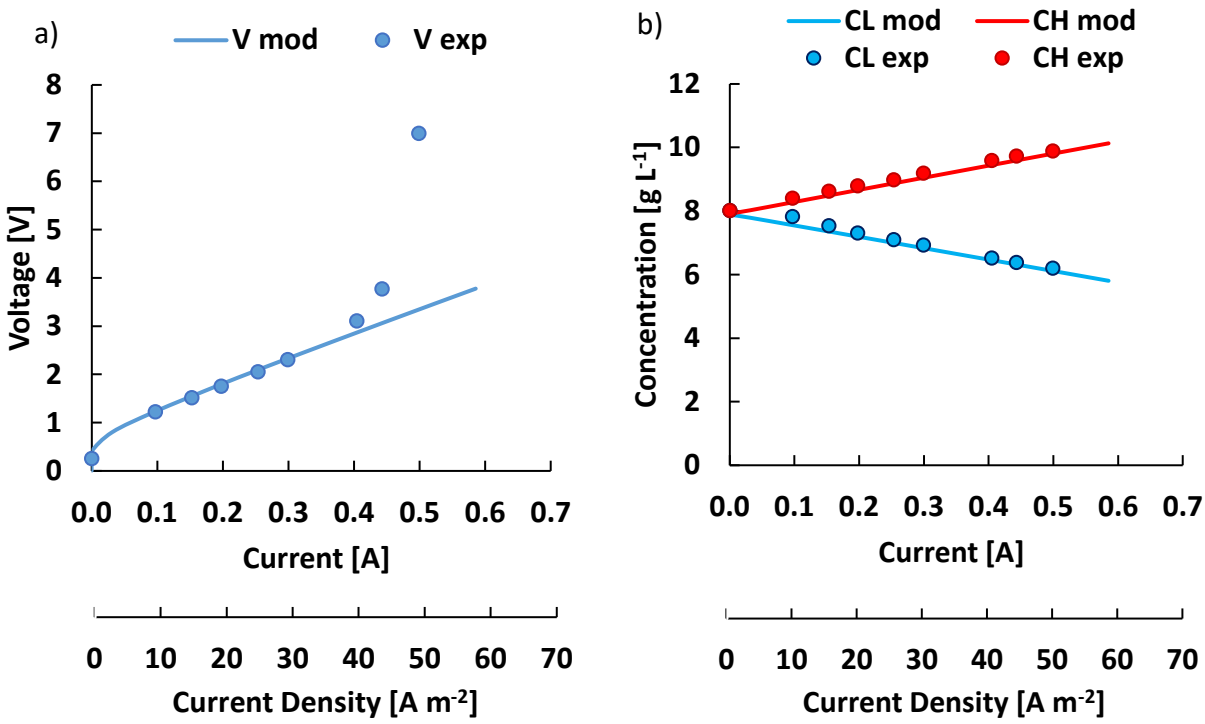

Fig. 38 Trend of (a) stack voltage and (b) output conductivities versus the current and the current density of the system. The experimental data and simulation refers to an HED unit that treats an inlet flow rate of 7.9 g L^{-1} with a velocity of 0.5 cm s^{-1} and refers to the A/B electrode configuration.

In this case, the characteristic curvature due to the overvoltage by charge transfer is even more evident. The model also predicts the output concentration of the two solutions quite well. But even in this case it fails to predict the limit current. More generally, it is good practice in ED systems to not desalinate more than half of feed inlet concentration, to avoid ending up in a limit current condition. According to the method of Sonin and Isaacson, the limit current of the 35 g L^{-1} B/B case is about 4 A which would correspond to a concentration of 20 g L^{-1} of dilute output. In the case of Fig. 38, on the other hand, the concentration of the output diluted in the limit current would be about 6 g L^{-1}, showing in both cases less than half concentration. However, it is true that the tests were conducted at velocity of 0.5 cm s^{-1} and that generally higher velocities are used (range 2- 5 cm s^{-1}) precisely to reduce the thickness of the boundary layer and consequently increase the threshold value of the limit current. This is why, in the case of application of the process to an industrial case, this last reference will be taken as a target in the scheme proposals in the following paragraph.

5.3 Economical aspects and future perspectives

5.3.1 Case studies

As mentioned, ED is not used industrially in the field of seawater desalination due to its high costs. As a result, there are no real references in the plant proposals. Some suggest multistage configurations [103,124], others provide configurations with recirculation, even if suggested for the BW case [125]. In this analysis, 5 possible configurations, shown in Fig. 39, were proposed and studied.

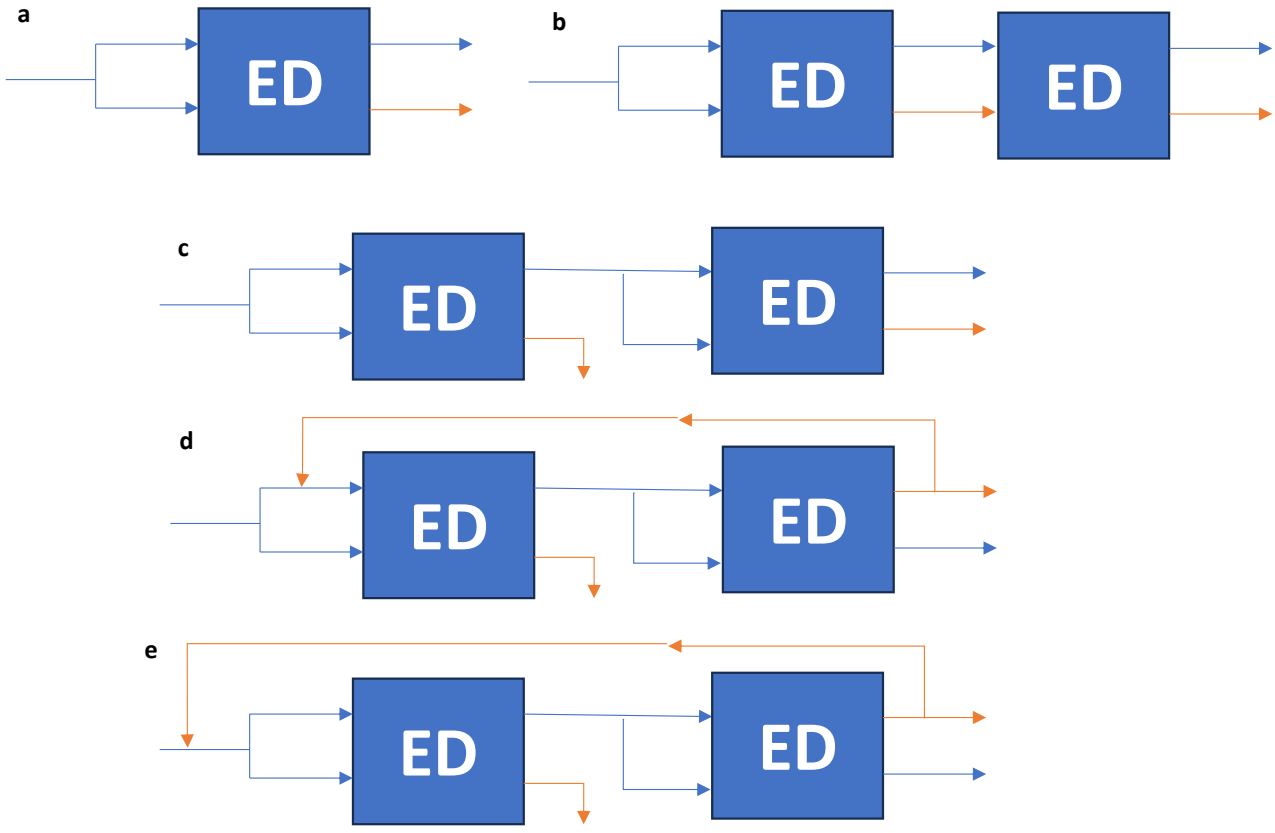

Fig. 39 Proposed plant diagrams for techno-economic analysis

In scheme (a), a single unit is used for promoting desalination in a single step. Although it was said that it is not a good practice to desalinate in a single step, this extreme scenario should be taken more as a standard than as a real application case. The multi-stage configuration, on the other hand, is proposed in all the other schemes (b-e). However, in scheme (b) the two stages can be imagined as a single longer stack that works with two separate electrodes, since the outputs of the first enter directly as feeds into the second. The latter can also be considered as a standard for a possible comparison. Indeed, in the second ED stage, the two solutions enter at a different concentration,

and they have to be powered with a potential higher than the OCV to desalinate them, moreover, a part of the current has to be used by the system only to overcome the spontaneous flow of salt that doughs it from the concentrated to the diluted. In configuration (c), in order to avoid the RED behaviour of the system, it is proposed to send only the diluted solution to the second stack. Clearly, in this case, the stack handles a flow rate equal to half the diluted stream (to avoid pressure differences between the channels), and works with higher residence time, with current limit anticipation. To avoid this issue, in cases (c-e), the second ED stacks always work with a number of cell pairs equal to half of the ED1. The concentrated stream of the first stack is directly discharged.
Schemes (d) and (e) are instead more concrete possibilities, for which, the concentrated solution leaving the second stage is partly recirculated (d) on the diluted or (e) on the feed stream of the first stage (Feed and Bleed F&B configuration). This would lead to a mutual benefit for desalination, as it (i) reduces the amount of water to be treated as incoming and (ii) partly desalinates the feed, reducing its concentration and therefore the energy to be spent. However, from the point of view of hydrogen production, the latter two cases would mean lower currents in the system and consequently less hydrogen production.
All systems have been studied assuming that each unit is a 0.5 x 1 m^2 stack consisting of 500 cell pairs. The channel velocity are assumed to be around 2 cm s^{-1} treating a feed flow rate of 15 m^3 h^{-1}. For the cases of multi-stage systems, the first unit desalinates up to 15 g L^{-1} and the second stage up to 1 g L^{-1}. The configuration adopted for the electrodes is B/B, therefore with an alkaline electrolyte of NaOH 1 M, for which the solution is recirculated after a gas separation stage, as already proposed in Fig. 15. All compartments have dimensions of 500 µm (including electrode solution channels), membrane resistances are assumed to be 1.2 Ω cm^2, except for the end-membranes which have resistance of 6 Ω cm^2. The Butler-Volmer parameters are the same calculated in the experimental analysis reported in Appendix V.

5.3.2 Techno-economic analysis

The first analysis was done exclusively on ED, as the technology is mainly intended for that purpose. The same Fig. 39 cases have also been investigated with regard to the simultaneous production of hydrogen, and therefore the HED configuration. Finally, a more in-deep analysis was made for the most convenient scheme.

Fig. 40 reported the histograms showing the WSEC and LCOW for the 5 proposed schemes in the ED cases. The 5 proposed cases have different advantages and benefits. The first two cases (a) and (b) are to be intended as borderline technologies for possible comparisons. The dotted lines represent precisely these two extremes, i.e. the possibility of carrying out the entire desalination with a single stack (a) and that of doing it with 2 stacks in series (b). These cases represent the scenario with the maximum water recovery (about 44 %) and the stacks are constituted by 500 cell pairs. On the contrary, the scenarios to be analysed as feasible proposals are those (c-e). These 3 schemes treat in the second stage half the flow rate of the diluted coming out of the first. Intrinsically, they produce a flow rate of water about half compared to cases (a) and (b), and this inevitably implies an increase in consumption and therefore in costs. On the contrary, the recirculated flow rate for cases (d) and (e) is equal to 75 % of the concentrated solution leaving the second stage, which means that the recovery of the system is greater (about 27 % of recovery) for cases (d) and (e) than scenario (c).

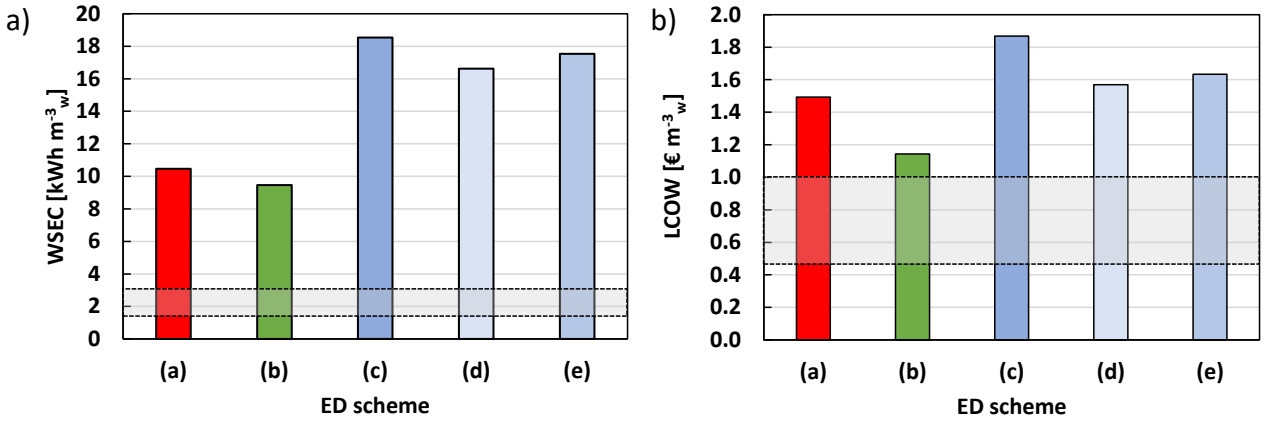

Fig. 40 (a) WSEC and (b) LCOW for the 5 plant diagrams in case ED. The greyed out region refers to the range of values typically associated with the consumption and cost of an SWRO.

This is well shown in Fig. 40a, where it can be seen that the relative consumption of cases (c-e) is always above (a) and (b) cases, as their capacity is double. However, if the only power supplied is compared, it is lower than 30 % for the case (c-e) respect the case (a). In the grey box, on the other hand, the range of consumption of typical SWROs is highlighted, which are still lower than SWED in any cases, justifying the non-use of this technology for the desalination of seawater. In Fig. 40b the LCOWs corresponding to the 5 cases are reported. As expected, cases (a) and (b) are the cheapest, as the flow rate produced, and therefore sold, is twice than the other cases. Among them, case (c) is the most expensive scenario, with a LCOW of about 1.87 € m^{-3}_{w}, while case (d) is the most convenient of the cases (c-e). The most convenient overall is case (b), although compared to case

(a) it has twice as much capital expenditure. The benefit, however, is due to the fact that the system requires less energy than (a). Indeed, it has been seen [126] that in ED the main of the process takes place in the first parts of the unit. Since as the degree of desalination increases, there is a sudden increase in the resistance of the diluted channel, which leads to an effect whereby the current is distributed more in the first portions of the stack length and less in the final parts. However, the costs are always higher than those of SWRO, for which it often refers to 0.46 – 1.21 € m^{-3}_{w} [127], but not so high as to directly exclude the technology from further analysis. In fact, the research question was: "can the possibility of producing hydrogen simultaneously reduce costs and make SWED technology more competitive for the market?".

As made for the brackish water case, the SeaWater Hydrogen-Electrodialysis (SWHED) technology is proposed both for desalination and hydrogen production, by the addition of shared electrodes between the cell pairs. In the following analysis, the configuration for which there is only one cell pair between each consecutive electrode was the only one analysed, being the most advantageous configuration for the BWHED case. Furthermore, since the number of cell pairs differs between the two stacks in cases (c-e), a different total number of electrodes is considered for these cases.

Fig. 41a shows the WSEC and HSEC of the SWHED technology. From the easy comparison that can be made with the previous Fig. 40, it is clear that switching to HED implies much higher energies, due not only to desalination, but also to the production of hydrogen itself. In this case, having also considered real electrodes, the voltage drops are about 2 V, therefore even higher than those estimated in the BWHED case of 1.7 V. However, the trends of the WSEC are similar, and all 3 cases (c-e) are disadvantageous compared to the limiting cases (a) and (b). Again, solution (d) turns out to be the most advantageous in term of energy consumption, and this is due to a higher water recovery compared to case (c) and to (d). In terms of HSEC, the three configurations are the least energy-intensive, but rather similar to each other and with case (b); on the contrary, the consumption for case (a) is about 8 kWh kg^{-1}_{H2} higher. This can be explained by the fact that the production of hydrogen is not twice as high as in the SWED case for water, but is directly proportional to electric current, which in this case is relatively similar.

As far as costs are concerned, in the comparison between the SWED and SWHED case of Fig. 41b, it is immediately seen that these are significantly higher. However, the LCOH of the SWHED case refers to a hydrogen sales price of 0 € kg^{-1}_{H2}, therefore without any remuneration from it. The histogram,

compared to the pure SWED case, makes each case decidedly disadvantageous, with lower costs for case (a) and (b). While among the case (c-e), the (d) is always the more economically advantageous

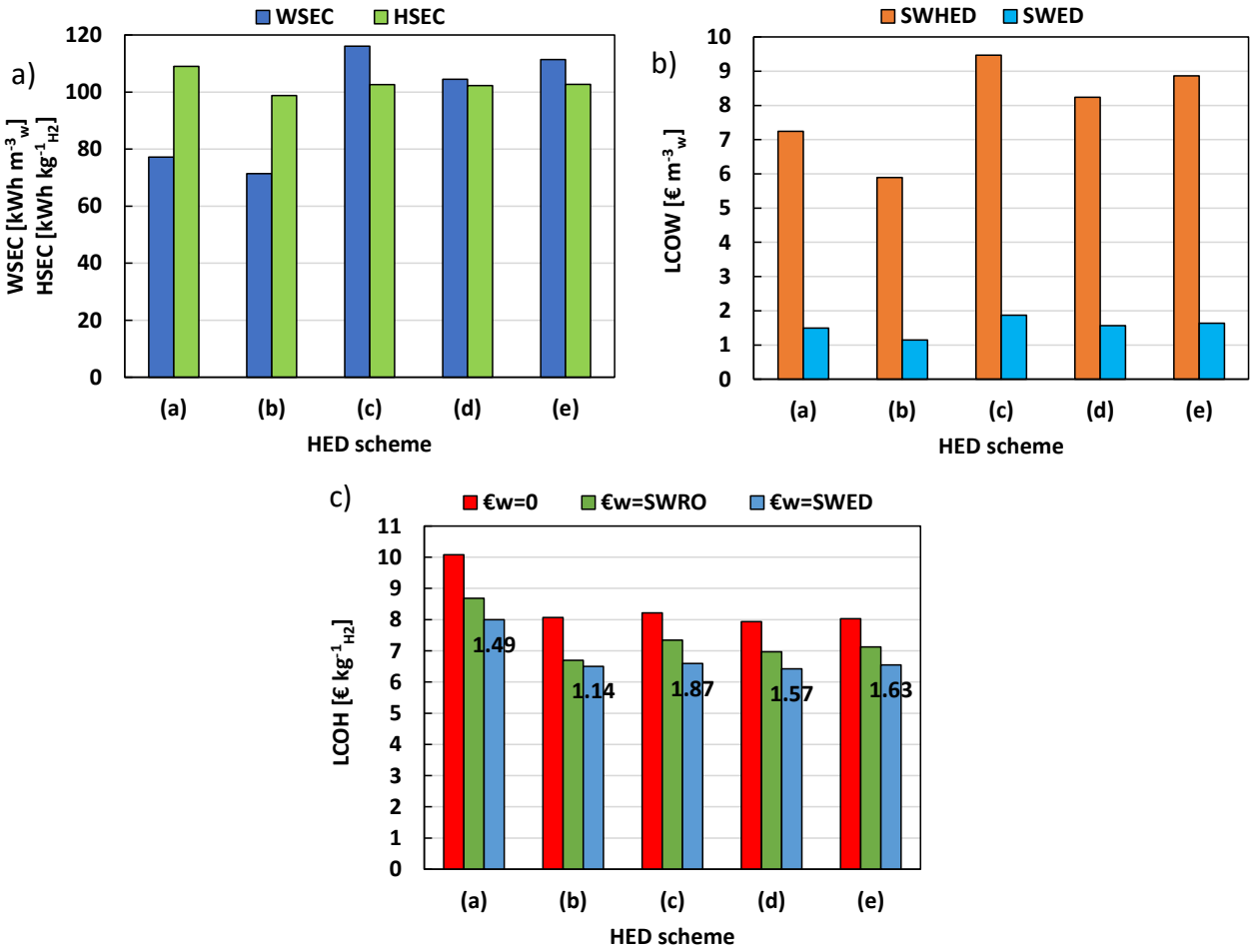

Fig. 41 Histograms of (a) specific consumption of water WSEC and hydrogen HSEC, (b) LCOW in the case H_2 is not sold and (c) LCOH for the 5 plant schemes. With regard to Figure (c), the LCOH is reported for three distinct water prices. The red histogram represents the scenario in which water is not sold, the green histogram shows the scenario in which water is sold at the price of SWRO (1 € m^{-3}_w), and the blue histogram represents the scenario in which water is sold at the same price as the LCOW identified in Fig. 40b. The values reported as label represent the price of the LCOW identified in Fig. 40b, also reported for easing of reading.

Fig. 41c shows the LCOH trends for the different schemes at three different water prices. If water were not sold (in red), the cost of hydrogen would be about similar for all cases (b-e) fluctuating on a value of about 8 € kg^{-1}_{H2}. On the other hand, if water were sold at the price of the water of a SWRO (in green), i.e. 1 € m^{-3}_w, there would be a lower cost for case (d), which would correspond to an LCOH of 7.12 € kg^{-1}_{H2}. The other case is when the water is sold at the price corresponding to the respective LCOH of the SWED (in blue, see also Fig. 40b), each for its own schemes, value that is also shown as label in the figure. The LCOHs vary with the same trend as the LCOWs of Fig. 41b and also

in this case the lowest cost is for case (d) with its 8.03 € kg^{-1}_{H2} if the water was not sold, and 6.42 € kg^{-1}_{H2} if it was sold at 1.57 € m^{-3}_{w}. Therefore, assuming (d) as the most advantageous case, a more in deep analysis was done.

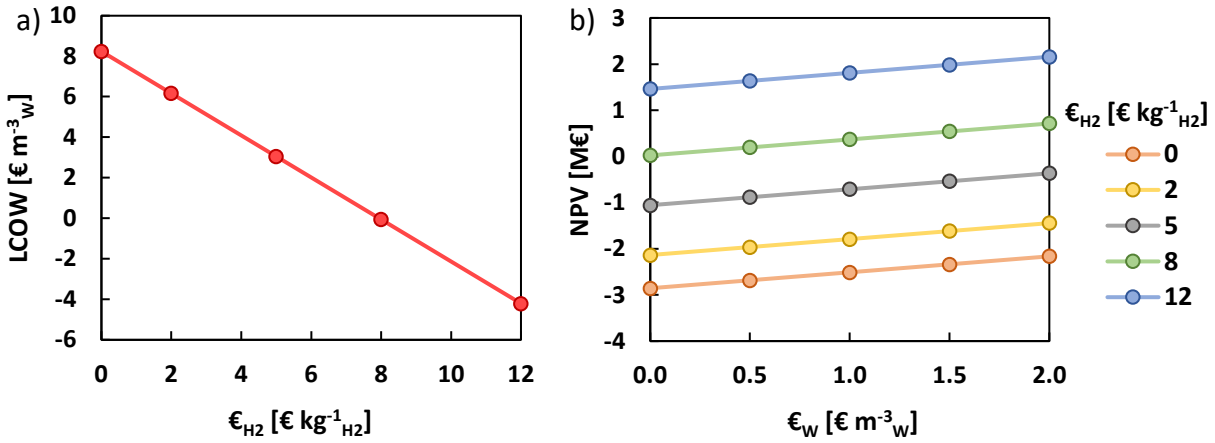

Fig. 42 Trend of (a) LCOW as the price of hydrogen changes and (b) NPV as the price of water parameterized to the price of hydrogen changes.

Fig. 42a shows the trend of the LCOW as the price of hydrogen changes, and as it can be seen, the LCOW is strongly influenced by the selling price of hydrogen. In fact, when this is not sold, the LCOW reaches prohibitive values of almost 8 € m^{-3}_{w}, but gradually decreases as the other product is sold. However, for a plausible hydrogen price of about 8 € kg^{-1}_{H2} the LCOW becomes zero, and therefore the full price of desalination is fully paying back, while for higher sales prices the LCOW becomes even negative. This clearly has no economic significance, except that the plant can only have a positive NPV, and therefore a greater profit. It should be noted that the production cost equal to that of SWRO, occurs when hydrogen is sold at 6.97 € kg^{-1}_{H2}, which is still in the range of the current LCOH of common electrolysers.

Conversely, the NPV trend is shown in Fig. 42b as the price of water changes and parameterized with that of hydrogen. This NPV refers to the case in which the higher the selling prices, the greater the earnings of the process. According to the above, if hydrogen is sold at 8 € kg^{-1}_{H2}, for any selling price of water there is a positive NPV, which can also be about 0.5 M€ if water is sold at 1.5 € m^{-3}_{w}. A sensitivity analysis was also performed for the (d) case. The volcano plots with the variation of NPV and LCOH are shown in Fig. 43a and Fig. 43b, respectively.

a)

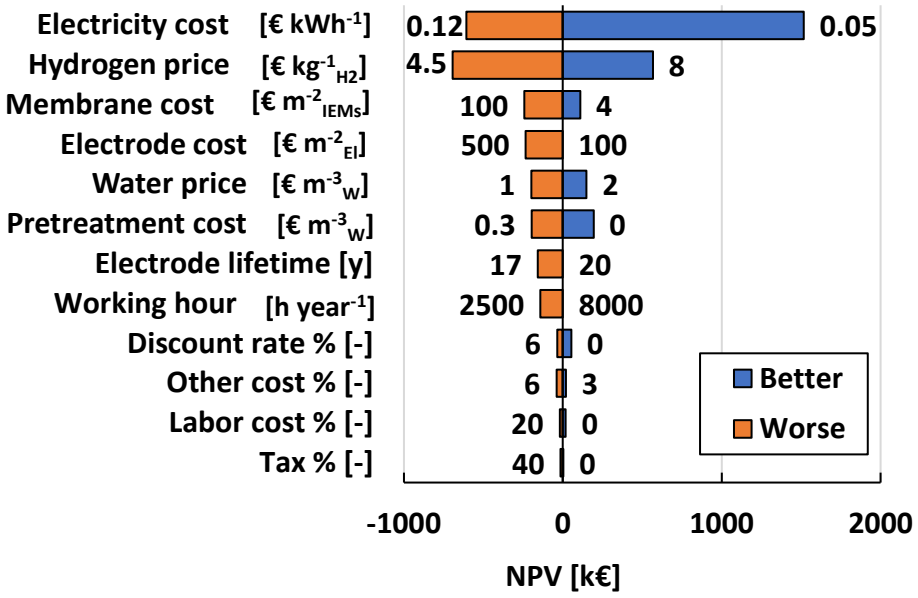

b)

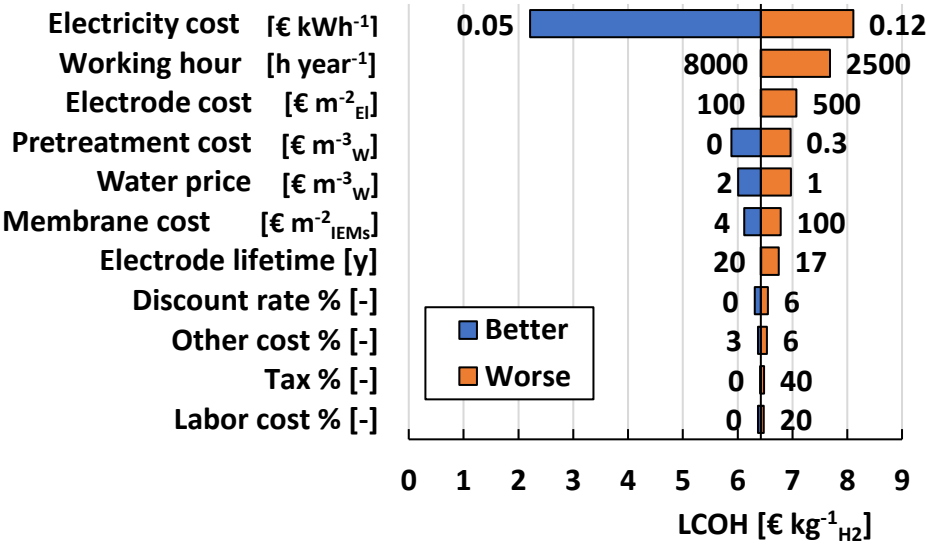

Fig. 43 Sensitivity analysis for the (d) scheme. In (a) the NPV of the plant and in (b) the LCOH.

In the case of revamping, the water is sold at its LCOW identified for the SWED case, i.e. 1.57 € m^{-3}_{w}. Consequently, all the extra expenses (for additional electrodes) are borne by hydrogen, for which the LCOH of 6.42 € kg^{-1}_{H2} is identified and clearly an NPV equal to zero. The variation of the economic parameters for the sensitivity analysis are reported in Table 11.

Table 11 Economical data input for the scenario analysis of the SWHED

Input Scenario			*Worse*	*Base case*	*Better*
Discount rate	**[%]**	[65,92,95]	6	3	0
Membrane cost	**[€ m_{IEMs}^{-2}]**	[65,95,98,105]	50	25	4
Electrode cost	**[€ m_{el}^{-2}]**	[12,89]	500	100	-
Electrode lifetime	**[y]**	[12]	17(60000 h)	20	20
H_2 selling price	**[€ kg_{H2}^{-1}]**	[13,117]	4.5	6.42	8
Water selling price	**[€ m_w^{-3}]**		1	1.57	2
Pretreatment cost	**[€ m_w^{-3}]**		0.3	0.15	0
Tax rate	**[%]**	[65]	40	10	0
Electricity cost	**[€ kWh^{-1}]**	[65,105]	0.12	0.10	0.05
Labour cost	**[%]**	[65,84,95,98]	20	10	0
Other costs	**[%]**	[89,95,98]	6	4	3
Working hours	**[$h\ y^{-1}$]**	[65,119]	2500	8000	-

The variation that has the most repercussions on the system is the one related to the cost of electricity, an increase of only 2 cents causes NPV to lose about €600k, or increases the LCOH by almost 1.7 € kg^{-1}_{H2}. On the contrary, a decrease to 50 € MWh^{-1} makes it incredibly earn more (up to 1.7 M€) or reduces the cost of hydrogen production to about 2.2 € kg^{-1}_{H2}, making it very attractive to the market. A negative variations of about 30 % on the cost of hydrogen cause significant losses to the plant (-700 k€). The same 30 % variation was made for the selling price of water, for which there is a smaller variation of about 200 k€. This defines how much the process is most strongly influenced by the cost of hydrogen. A fair increase in the price of water and hydrogen of 25 %, respectively, results in a gain of more than 150 k€ and 570 k€.

Other interesting variable are the number of working hours in a year, which impact the cost of hydrogen by up to 20 % in worsening case and the electrode and the pretreatment cost that influence the LCOH for a good 10 %.

On the contrary, NPV is more affected by the cost of membranes, pre-treatment and the cost/life of the electrodes, for which there are variations of more than 140k€. Threshold value, for which there is always an excess of operating costs compared to revenue, with a consequent certain bankruptcy of the plant. All the other variables imply more marginal variations, such as the discount rate, labour and other costs, and taxes for which there are variations contained in 2 % for LCOH and no more than 55 k€ for NPV.

5.3.3 A/B and B/B comparison

Having identified case (d) as the best case among those proposed in 5.3.1, and in accordance with the analysis made in the experimental section 5.1, a further analysis was conducted to investigate whether it was more convenient to use an A/B or B/B configuration for the system for multiple electrodes. The model was then promptly modified with the relative values of the LSVs to study case (d) in the A/B configuration.

However, the technical model remains the same for the latter case, with the only variation being the potential required by the electrodes, resulting in a reduction in overall energy expenditure. In fact, in case B/B the system overall required 283 kW against 194 kW in case A/B, for which a lower energy expense is required, with a WSEC of 58.9 kWh m^{-3}_{w} and an HSEC of 57.7 kWh kg^{-1}_{H2}. From an economic point of view, however, the model takes into account the expenses related to the reagents used. In case B/B, as the solution is recirculated, there is a reduction of water at the cathode with its consequent consumption. On the contrary, in the A/B case, the H^+ is reduced at the cathode and the OH^- at the anode, which are constantly supplied by HCl and NaOH solutions. The equations relating to reactants cost is added to the model as operative costs, for which costs of 0.1 € kg^{-1}_{HCl} and 0.2 € kg^{-1}_{NaOH} have been assumed.

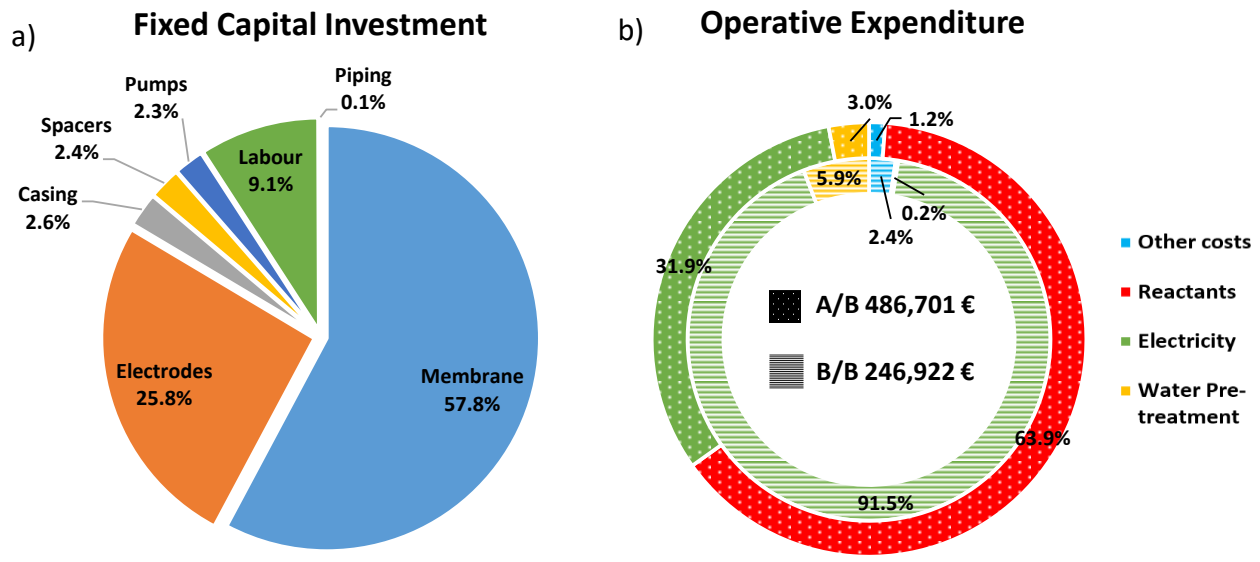

Fig. 44 Pie charts representing (a) the Fixed Capital Investment FCI, and (b) the Operative expenditure for the case (d) in the two configurations studied. The operating costs are different for A/B (outer ring) and B/B (inner ring) cases.

Fig. 44 shows the pie charts relating to capital and operating costs for case (d) studied. Capital costs (Fig. 44a), are common for both B/B and A/B cases, as the variation is exclusive to operating costs. As shown, membrane costs are the majority of stack costs. However, these take into account both the two membranes per cell, the end-membrane and the replacement membranes after 7 years. Electrodes, on the other hand, are the second largest cost, accounting for 25.8 % of the total capital expenditure, which amounts to 146 k€. The difference between case A/B and B/B is shown in Fig. 44b, where the operating costs of the plant are reported for the 4 categories of expenditure, i.e. all the expenses related to the plant including (i) maintenance costs (other costs), (ii) reagents, (iii)electricity and (iv) seawater pre-treatment. As can be immediately seen, in the A/B case (outer ring) the majority cost is due precisely to the expense of the reagents, which weigh a good 63.9 %. Electricity costs, on the other hand, are lower and weigh 31.9% of operating costs. On the contrary, these are almost totalitarian (91.5 %) in the B/B case. From this analysis, it is clear that having changed electrode reactions to electrodes has a significant impact on cost distribution. In addition, the A/B case greatly burdens the economy of the process, with operating costs that are almost double those of the same plant in alkaline conditions. As a consequence, the A/B configuration, despite the lower electricity consumption, does not lead to any benefit of the LCOH which is 7.32 € kg^{-1}_{H2} against 6.24 € kg^{-1}_{H2} in the B/B case. However, if the reagents did not impact the economy of the process, the LCOH would drop to a competitive value of 3.75 € kg^{-1}_{H2}, which is quite advantageous.

5.4 Final remarks and future perspectives for SWHED

The SWHED case was intended to better perform comparing to H(A-)RED and BWHED cases, due to the greater number of electrodes and the higher current densities of the equipment for the higher degree of desalination required.

The basic ED process for SW desalination, SWED, has limitations due to high energy costs for which the technology has not been successful so far. The concept of integrating the desalination of seawater with hydrogen arises from the desire to (i) reduce the costs and (ii) increase hydrogen production rates. The system has been studied both experimentally and then, through a techno-economic analysis. The experimental part had raised the problem of the limit current, for which it was not possible to carry out the entire desalination in a single stage. As a result, several cases were

examined in the technical analysis, such as the multi-stage configuration with the possibility of recirculating the concentrated solution to increase the capacity of the plant. Among the case studies, (d) scenario was among the most advantageous in terms of cost, for which the desalination of the water was 1.57 € m^{-3}_{w}. Not exorbitant price, but still about double the costs of desalinating seawater with RO. The addition of shared electrodes between cell pairs, for the production of hydrogen at the cathode, could have helped the technology by reducing the cost of water. However, it has been seen that hydrogen must be sold at least 8 € kg^{-1}_{H2} to obtain water for free and that assuming a water price of 1 € m^{-3}_{w} (as SWRO) the gains expressed as NPV remain limited (about 250 k€ per unit). Clearly, the analysis was carried out on a plant with a capacity of 4 m^3_w h^{-1} (or about 15 m^3_w h^{-1} of seawater), and the intrinsic modularity of the process would allow to gain 1 million only by quadrupling the capacity. If we take the case of one of the largest desalination plants in the world (137 million m^3 $year^{-1}$, Hadera Israel), and considering the case (d) of SWHED with the same working hours and the same water recovery, there would be a gain of about 288 million euros at the end of the 20 years of the plant.

The SWHED proposal has also been studied for the A/B configuration, i.e. the one in which two different electrode solutions are used at the cathode and at the anode, in order to reduce the thermodynamic potential of water electrolysis. From an electrical point of view the SECs are almost halved, however the operating costs related to the purchase of acid/alkaline solutions become highly prohibitive for the technology, forcing this possibility to be excluded.

Finally, the SWHED technology was certainly not more advantageous than the BWHED case and the limitation is mainly due to the high energy costs necessary for desalination. Furthermore, having estimated the electrode potential to be around 2 V based also on the LSV results, the system worked under slightly worse conditions than in the BWHED case. In fact, if a fixed potential of 1.7 V had been used, the new LCOH would have been 5.6 € kg^{-1}_{H2}. Instead, a more interesting NPV of 660 k€ would have been reached while selling hydrogen at 8 € kg^{-1}_{H2} and water at 1 € m^{-3}_{w}.

To a lesser extent, the increase in capital costs has also influenced the economics of the process. The increase in capital costs is related to the multi-stage configuration, which is necessary to avoid the case of limit current. This is mainly due to a matter transport problem, whereby the concentration at the interface becomes zero, as well as the fact that the diluted solution, continuously deconcentrated, significantly increases its ohmic resistance. Electrodialysis, more generally, could be used not only with a view to desalination, but also, where necessary, to

concentrate brines. In this case, the problem of the limit current would be more marginal and this would therefore allow for a smaller number of devices and even higher currents. Which could be an advantageous configuration for HED technologies in general, and for hydrogen production.

6 Hydrogen Electrodialysis with bipolar membrane HEDBM

The strategies adopted for increasing hydrogen production, i.e. increasing the electrode surface area, have certainly shown a greater convenience of HED processes compared to the H(A-)RED case. The increase in salinity in the case of seawater desalination could undoubtedly have increased the electrical current of the system with a consequent increase in the hydrogen yield. However, the results showed how electricity cost heavily contained the economics of the process, leading to limited results.

HEDBM is proposed as a technology that can overcome the above mentioned limits. Currents are typically higher compared to RED/ED, reaching even one order more of magnitude. The technology, as done for HED, can be assembled with multiple shared electrodes to increase the active electrode area, and the production of chemicals can further benefit the convenience of the process. In addition, the use of bipolar membranes as end-membranes favours the production of H^+ at the cathode and OH^- at the anode necessary for water electrolysis, reducing electrode consumption and eliminating the expense related to HCl and NaOH solutions, which had strongly blocked the choice of the A/B configuration in the previous analysis. In this chapter, therefore, HEDBM technology is proposed for the production of chemicals and hydrogen. To this aim, an already-existent multi-scale model, capable of comprehensively simulating the EDBM process, was purposely modified to account for the behaviour of electrodes and validated with experimental data. In addition, appropriate economic equations were introduced to estimate the operative and capital costs of EDBM, as well as to identify the plant profitability and the production costs.

The following chapter contain some experimental results published in [128]. An examination of these findings is provided in the next paragraphs.

6.1 Experimental

4.2.2 Experimental Set-up

During the experimental campaign, a crossflow EDBM unit (FT-ED-100, Fumatech BWT Gmbh, Germany) with an active area of 10 x 10 cm^2 was used, which was assembled with 5 triplets, composed of commercial ion exchange membranes (IEMs) and Woven PVC/ECTFE spacers 480 µm

thick. The IEMs used are: (i) cationic, fumasep® FKB-PK-130; (ii) anionic, fumasep® FAB-PK-130; and (iii) bipolar, fumasep® FBM. Two platinum wires were inserted into the most external compartments and the end-membranes to measure the triplets voltage. Concerning the electrode compartments, Ti mesh grid substrate with Pt/Ir ox (MMO - Mixed Metal Oxide) was used for both cathode and anode for the HER and OER (Lasia, 2010; Suen et al., 2017b; Trasatti, 1972), while 1 M HCl and NaOH were used as catholyte and anolyte, respectively.

The catholyte, the anolyte, and the feed solutions (acid, base, and salt) for the EDBM were prepared using demineralized water including HCl (37% Merck), NaOH (98-100% Honeywell Fluka) and NaCl (99.7% ChemSolute). The conductivity was measured for all solutions, while the pH was measured only for the salt solution, for which a WTW conductivity and pH meter (WTW™ ProfiLine™ pH/Cond 3320 Universal Multi-parameter Portable) were used, respectively. Two Cole-Parmer Masterflex I/P pumps (77601-00, Illinois, USA) were used to feed catholyte and anolyte to the system, with a flow rate of approximately 525 mL min^{-1}, while three Leadfluid YT15 pumps (BT601S, Lead Fluid Technology, CO LTD, China) were used to feed the EDBM, providing a flow rate of 150 mL min^{-1}. In particular, the electrodic solution flow rate was higher mainly to ensure a sufficient mixing in the electrodes and to facilitate the bubbles detachment and outflows. To ensure the reproducibility, each test was repeated twice. Inlet and outlet samples were taken from the EDBM solutions to analyse, by acid-base titration, the increase in concentration as the current density changed.

The part relating to (i) the instruments used to supply energy and measure electrical variables, (ii) the hydraulic gas circuit and (iii) the measurement of gas concentrations is extensively described in Section 3.1.1, to which reference is made for further details.

The schematic representation of the unit is reported in Fig. 45. At the electrodes, the electrolysis of water is promoted. Also in this case, an A/B configuration has been selected, and the IEMs at both ends of the cell pack allows to close the saline bridge of the galvanic cell.

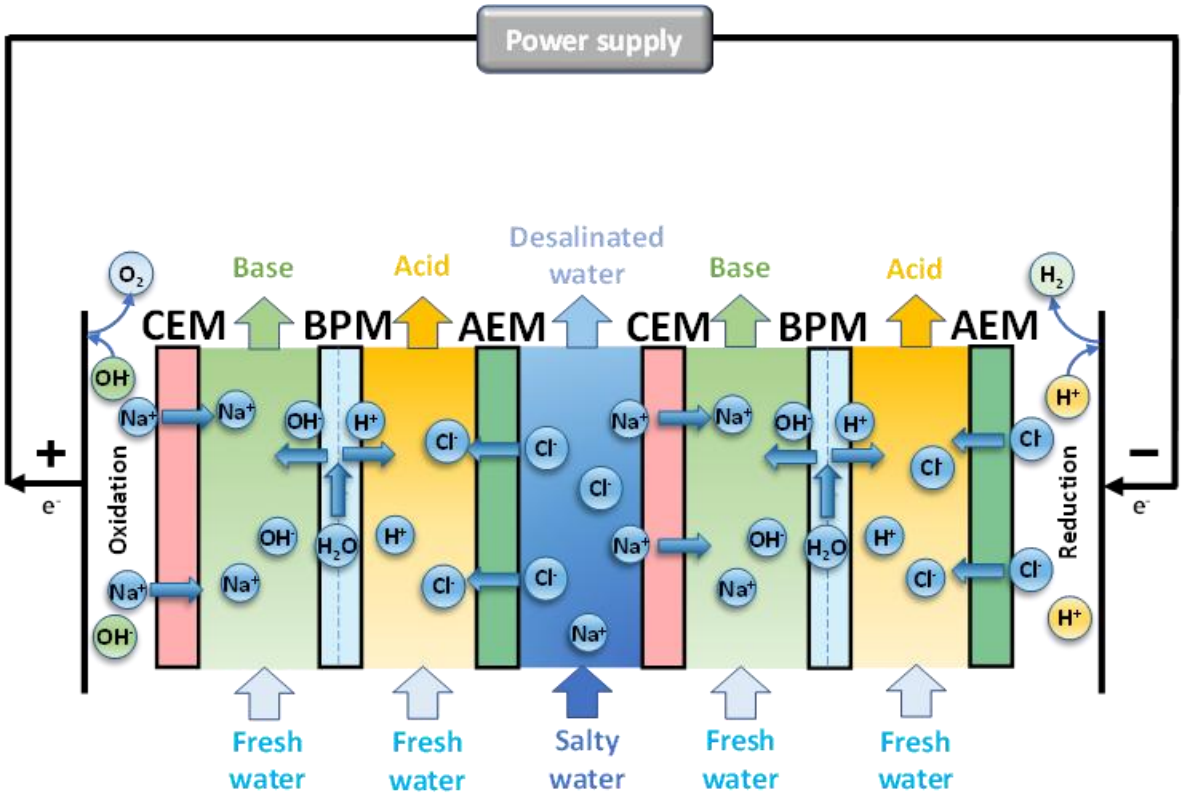

Fig. 45 Schematic representation of the HEDBM with IEMs as end-membrane.

4.2.3 Results

Polarization curves for three distinct acid and base concentrations—chosen for their representativeness and intermediate relation to desired targets—are shown in Fig. 46. As the concentration of the solution increased, the curves slope decreased significantly, as an effect of the relevant weight of the ohmic resistance of the acid and base compartments at low chemical concentrations. Indeed, according to Ohm's second law (eq. 19), the conductivity decreased by ranging from 1 to 0.2 M with a subsequent rise of the resistance of the channel, leading to a different slope in the plot. From the slopes, it is easy to calculate the resistances of the system, which were approximately 26, 29 and 35 Ω cm^2 N_{tr}^{-1} at 1, 0.6 and 0.2 M, respectively.

The low base and acid concentration values (0.2 and 0.6 M) would hardly be achieved in a real application of the technology, however these trends are indicative of how resistances vary within the system during a normal HEDBM test in closed loop mode, or would be representative of a part of the cell (along the main flow direction) for an open loop configuration. At the same time, it is interesting to note that in the first part of the curve a typical logarithmic variation of the potential

can be observed, related to the very first activation phase of the electrolysis reaction, and then a linear increase is shown in the ohmic region.

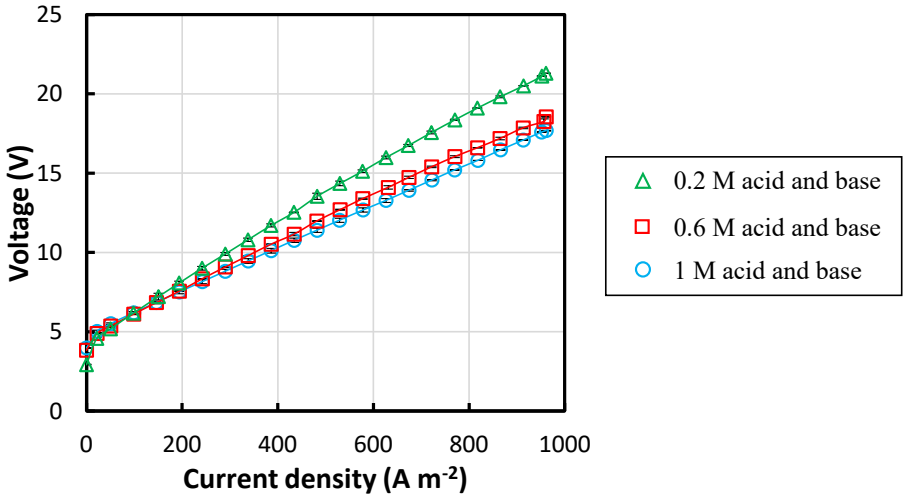

Fig. 46 Polarization curve of the HEDBM unit for 3 different concentrations of acid and base.

Moreover, for the case of 1M concentration, the electrolysis of water in the electrodic compartment was also studied in terms of productivity of hydrogen and oxygen and the relative faradaic efficiencies, as shown in Fig. 47. Electrolysis was performed at different current densities of 250, 500, and 1000 A m^{-2}. Hydrogen was always produced with Faradic efficiencies of almost 98 % for all the investigated current densities, as shown in Fig. 47a. The expected efficiency is 100 % and the variation observed of -2 % is mainly due to measurement errors of the instruments (e.g., the gas flow meter measure). In terms of productivity, on the other hand, the system obviously presents a linear trend with the current density, reaching a maximum value of 18.4 mol h^{-1} m^{-2} at 1000 A m^{-2}. This value is one order of magnitude higher than that found for the H(A-)RED system, which was about 1.72 mol h^{-1} m^{-2}. This results show how the HEDBM technology is more appropriate for hydrogen production, mainly due to the capability of working at higher currents compared to the technologies analysed so far.

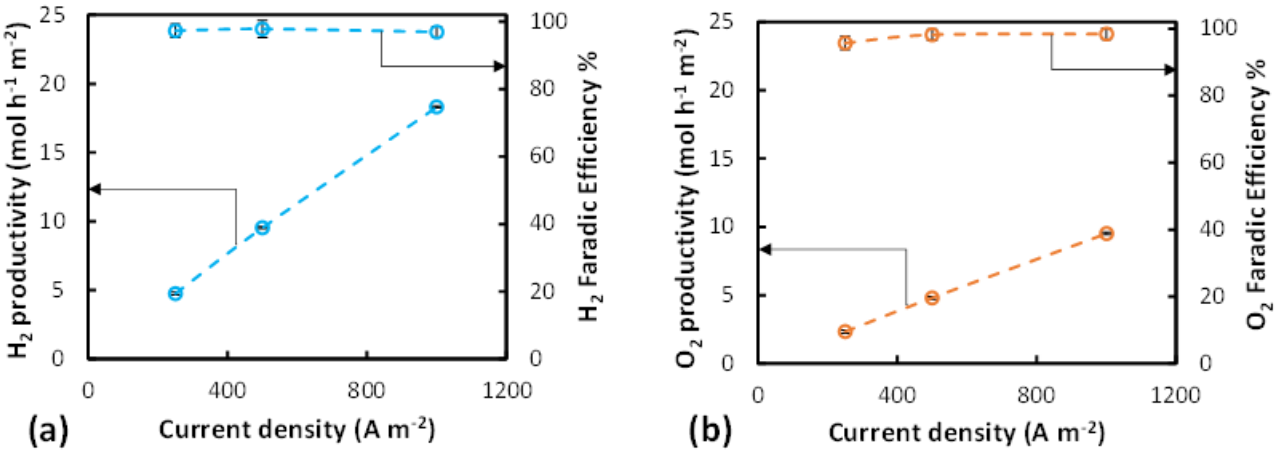

Fig. 47 (a) Hydrogen and (b) oxygen productivities and Faradic Efficiencies, as a function of current density (i.e., 250, 500 and 1000 A m-2).

The same trends were also found for the anode compartment (Fig. 47b), where a faradic efficiency of about 98 % was recorded with a ±2 % uncertainty. Clearly, since stoichiometry of the reaction does not lead to an equimolar formation of the products, the productivity of oxygen is about half that of hydrogen. The maximum oxygen productivity obtained from these tests was 9.3 mol h^{-1} m^{-2} at 1000 A m^{-2}. Contrary to what was observed for the RED/ARED system, an oxygen faradic efficiency of almost 100 % (net of instrument errors) suggests that there are no competitive reactions, related to Cl^- oxidation into hypochlorite, due to the Cl^- diffusion from the adjacent solutions to the anode. This is doubly beneficial, because all the energy supplied to the system is used to generate oxygen (increasing its production), and because there is no formation of the hypochlorite, which leads to a reduced potential of the system as well as preserves the membranes from degradation phenomena. This was possible thanks to the configuration of the system. In fact, by interposing acid and base channels between the electrode compartments and the first channels of the saline solution, it was possible to lengthen the path that the Cl^- ion must travel to reach the anode, thus reducing its diffusion. In addition, the end-membranes used (the same for the SWHED study), are reinforced membranes capable of working into acidic or basic environments and have greater permselectivity, minimizing the diffusive flux of salt in adjacent compartments.

6.2 Techno-economic HEDBM model

The EDBM model used in this study is described in the work of Virruso et al. [129] and here adopted for the H-EDBM process simulation. The model is characterised by a multi-scale structure with

distributed parameters along the main flow direction, thus the axial one. Six different sub models, properly collected, describe the entire behaviour of the process from the membrane/channel scale (lowest level) to the more external hydraulic circuit level (highest scale). The model also takes into account non-ideal phenomena such as diffusive fluxes, concentration polarization, and parasitic currents. The software gPROMS ModelBuilder® was adopted to implement the model and solve the set of equations. The model has also been readjusted to account for electrolysis reactions in the electrodes, adopting the same approach described in 5.2.1.

6.2.1 Model validation

The model, already available within the research group, after the necessary modifications relating to the prediction of potential drops at the electrodes, was validated with the experimental data. Among the various laboratory tests carried out with the unit described in 4.2.2, closed-loop tests (i.e., recirculating solutions within the stack) were also carried out. For more details and results, the reader is referred to the article of Pellegrino et al. [128]. In this paper, the HEDBM system has been studied for different configurations, which mainly concern the type of end-membrane used. The most advantageous case, following a very preliminary economic investigation, was the configuration in which 2 BPMs are used as end-membrane, with the consequent formation of H^+ and OH^- directly at the electrodes. A schematic representation of this technology is depicted in Fig. 48. This configuration was used for the following validation of the model and for the entire techno-economic analysis reported in this chapter.

All closed-loop tests were carried out using as feeds: 1 M NaCl salt solution with a volume of 1.2 L, simulating the brine concentration from a RO plant [130] and 0.05 M HCl and NaOH solutions, each with a 0.6 L volume. The choice of having an initial concentration of 0.05 M for the acidic and alkaline solution is to prevent the system from reaching high solutions resistances in the early stage of the test. Conversely, a 2:1 volume ratio was applied to counteract the desalination of the salty stream and limit the progressive increase in resistance, especially in the final stages of the test. This strategy is often employed in literature [77] to reduce SEC and achieve higher acid/base concentrations. The 1 M target concentration of acid and base determined the end of the tests, which were carried out galvanostatically at 250, 500, and 1000 A m^{-2}.

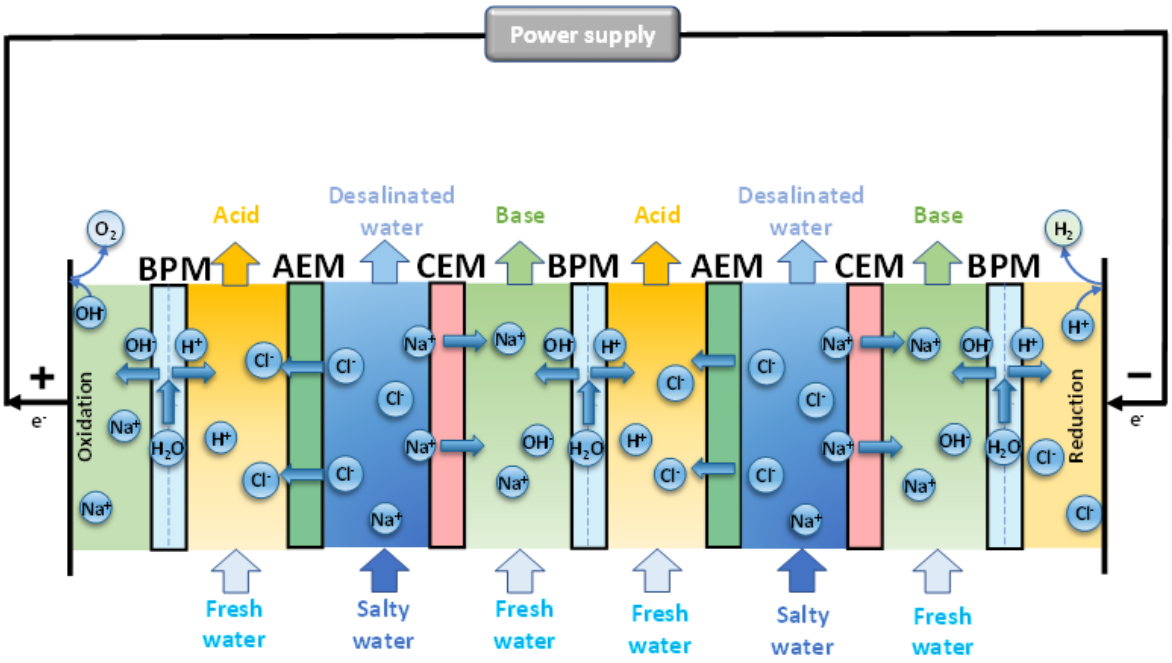

Fig. 48 Schematic representation of a HEDBM unit with BPMs as end-membranes

The validation graphs are shown in Fig. 49, and for the sake of brevity, only the results obtained for the 500 A m^{-2} test were reported.

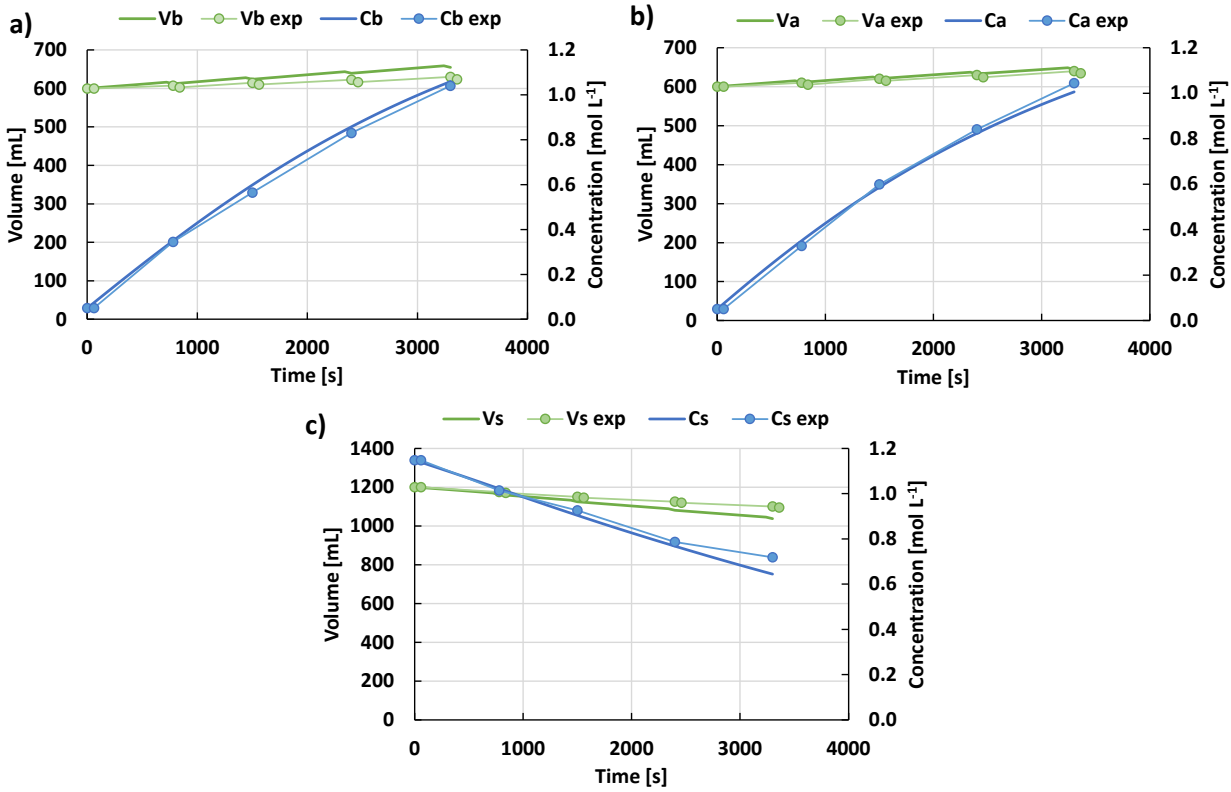

Fig. 49 Volume and concentration trends for closed-loop testing of the HEDBM system. In (a) the trends relating to the basic solution, in (b) those of the acid solution and in (c) those of the saline solution.

As expected, the concentrations of acid and base increase over time, while the concentration of salt decreases. This is due to the release of Na^+ and Cl^- ions, as a result of the formation of caustic soda and hydrochloric acid solutions, respectively. The volumes are also subject to variations, due to the transport of the salt for osmotic and electro-osmotic phenomena, leading to a volume increase for the acid and the base and a decrease for the saline solution. The sawtooth pattern of concentrations and volumes is related to the 5 mL samples that were collected for the analysis of the solutions. As can be seen immediately, the model is able to correctly estimate the trends of the process both in terms of volumes and concentrations, for which an error lower than 5.1% on volumes and 1.8% on concentrations are reached . Regarding the error on volumes, this is related to a failure in closing the mass balances of the experimental data, which precisely generate a difference of 30 mL compared to the model data.

However, the EDBM model had already been widely validated previously, and more attention was paid to the main modification of the model, related to the resolution of the equivalent electrical circuit. Fig. 50 shows the experimental data versus the model prediction, i.e. the parity plot, for the electrical variables of the unit. This experimental data are relative to the average values of the electrodes, triplets (platinum wires) and stack voltages for the three closed loop tests carried out at 250, 500 and 1000 A m^{-2}

As shown, the model is able to predict the experimental data quite well, keeping within an error of ± 11 %. In any case, the main error is measured in relation to the modelling of the triplets, while the electrodes (squares in yellow) are perfectly able to repeat the experimental data.

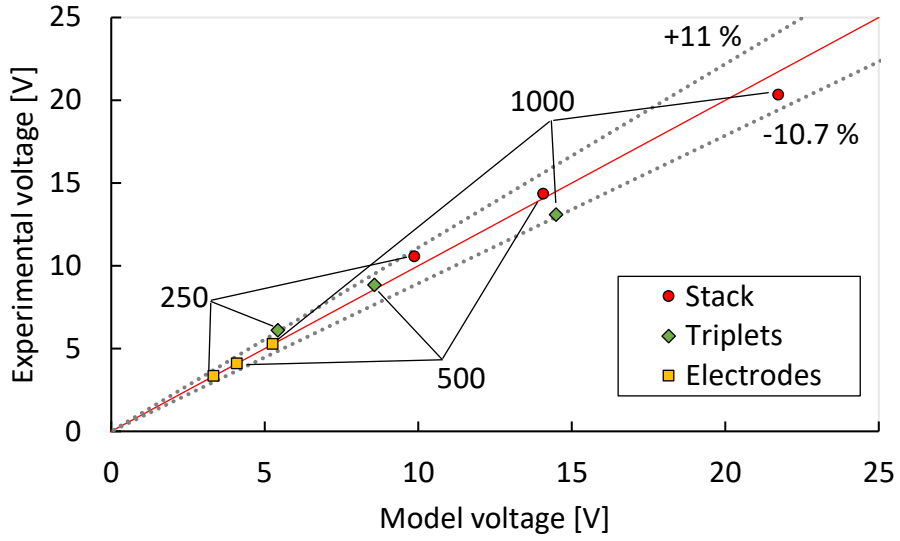

Fig. 50 Parity plot of the electrical variables of the HEDBM unit

The error in the triplet is mainly due to the resistance of the membranes. These were assumed to be a constant value, which is not fully representative of the variations in membranes found at different concentrations at the interface. Variations become even more evident with the variation of the current. The central point at 500 A m^{-2} (with the assumed resistance values) suits very well with the model. While the same resistance values lead to an overestimation of the experimental data for the case at 1000 A m^{-2}, and to an underestimation for the case at 250 A m^{-2}. In any case, the proposed model is satisfactorily able to predict the experimental data and it is considered validated.

6.2.2 Economic model

The technical model was coupled with an economic model which computes capital and operative costs in accordance with the correlations used by [129]. The capital cost for the HEDBM system takes into account the stack, the electrodes and the peripherals costs. Furthermore, in the capital expenditure the replacement of some of the components are also considered, as expressed in the following equation:

$$\mathrm{FCI} = \mathrm{N_s} C_{Stack} + \mathrm{N}_{el} C_{electrodes} + C_{peripheral} + \sum_{p}^{\mathrm{n}} C_{replacement} \qquad 48$$

where $\mathrm{N_s}$ is the total number of stacks, $\mathrm{N_{el}}$ is the number of electrodes and n is the number of useful years of the plant. The costs of the $\mathrm{N_s}$ stacks, electrodes and peripheral are all considered at year 0. The replacement costs take into account the substitution of the entire cell package and of all the electrodes every t_m and t_{el} years, respectively. Concerning $C_{electrodes}$, an electrode cost of 300 € m^{-2} was considered among the capital costs, due to the requirement of specific electrodes for hydrogen production; this cost is calculated assuming half the cost of an electrolyser (270 € kW^{-1}, [12]). The peripheral cost takes into account all the other components of the plant (e.g., pumps, power supply and monitoring and control devices) and this is calculated as a percentage of the cost of the stack (C_{Stack}). Since the peripherals do not grow linearly with the number of units, they have been calculated according to the following equation:

$$C_{peripheral} = \%_{peripheral} C_{stack} [1 + 0.3(N_s - 1)] \qquad 49$$

Electrode costs, on the other hand, are associated with a cost per m^2 of electrode and the costs of a single stack have been estimated as follows:

$$C_{stack} = C_{cells} + C_{casing} = (N_{tr}C_{tr} + C_{EM}) + \%_{casing}C_{cells} \quad (50)$$

where the cost of the cell package C_{cells} is the product of the N_{tr} triplets of the stack multiplied by the cost of a single triplet C_{tr} (calculated as the sum of the cost of the 2 IEMs, the BPM and the 3 spacers), plus an additional end-membrane, C_{EM}, which in this case is a BPM. C_{casing} is estimated as a percentage of the cost of the cell package.

The annual operating costs, on the other hand, are calculated as follows:

$$\text{Opex} = \tilde{C}_{maintanace} + \tilde{C}_{electricity} + \tilde{C}_{water} + d^{SL} \quad (51)$$

where maintenance costs are assumed to be a percentage of the initial FCI, the cost of electricity takes into account both the costs of the energy supplied per HEDBM and the costs of pumping the feed. Furthermore, water costs were also taken into account, both for (i) freshwater (needed to produce the chemicals) and for (ii) the stoichiometrically reacted water to make the hydrogen. Moreover, as done in the analysis in 4.2.3, depreciation was considered within the operating costs, and calculated according to the straight line method [112].

The system revenue is determined by 4 products, i.e. base and hydrogen as high-value products as well as oxygen and acid solution, as follows:

$$\mathcal{R} = \mathcal{R}_B + \mathcal{R}_{H_2} + \mathcal{R}_{HCl} + \mathcal{R}_{O_2} = \bar{\text{C}}_{NaOH}\dot{\text{Q}}_{NaOH} + \bar{\text{C}}_{\text{H2}}\dot{\text{Q}}_{\text{H2}} + \bar{\text{C}}_{HCl}\dot{\text{Q}}_{HCl} + \bar{\text{C}}_{\text{O2}}\dot{\text{Q}}_{\text{O2}} \quad (52)$$

where $\bar{\text{C}}$ is the specific product price in € kg^{-1} and $\dot{\text{Q}}$ is the mass flow rate in kg y^{-1}.

The sum of the capital investment and the operative costs with the revenues defines the Net Present Value (NPV), which represents the cumulative cash flow value at the end of the plant lifetime (i.e., year n):

$$NPV = \sum_{p=1}^{n} \frac{\left[\mathcal{R}_p - FCI_p - Opex_p - Tax_p + d_p^{SL}\right]}{(1+i)^p} \quad (53)$$

A special case of the NPV is obtained when it assumes a value equal to zero, which corresponds to the condition in which all revenues equal all expenses at the end of the n years of the plant lifetime. In the case of NPV=0, by rearranging eq. 53, it is easy to isolate the Levelized Cost of Base (LCOB) and of Hydrogen (LCOH), defined by eqs. 54 and 55, respectively. This condition corresponds to the minimum price that must be given to a product to cover all production costs, or, in other words, it corresponds to the production cost for that product. Clearly, it will be necessary to price the other products (HCl, O_2 and H_2 in the case of LCOB or vice versa) to calculate the respective levelized cost, since multiple products are involved.

$$\mathrm{LCOB} = \frac{\sum_{p=1}^{n}\left(\frac{FCI_p + Opex_p + Tax_p - d_p^{SL} - \mathcal{R}_{H_2} - \mathcal{R}_{HCl} - \mathcal{R}_{O_2}}{(1+d)^p}\right)}{\sum_{\mathrm{p=0}}^{\mathrm{n}} \frac{\dot{\mathrm{Q}}_{\mathrm{NaOH}}}{(1+\mathrm{r})^p}} \quad 54$$

$$\mathrm{LCOH} = \frac{\sum_{p=1}^{n}\left(\frac{FCI_p + Opex_p + Tax_p - d_p^{SL} - \mathcal{R}_{B} - \mathcal{R}_{HCl} - \mathcal{R}_{O_2}}{(1+d)^p}\right)}{\sum_{\mathrm{p=0}}^{\mathrm{n}} \frac{\dot{\mathrm{Q}}_{\mathrm{H2}}}{(1+\mathrm{r})^p}} \quad 55$$

Also in this case, Tax are calculated as percentage of the net profit ($\mathcal{R} - Opex$). All the economic parameters and prices assumed in the techno-economic analysis are collected in Table 12.

6.3 Techno-economic analysis

6.3.1 Case study

For the simulation, a commercial EDBM unit, FT-ED-1600-3 from FuMA-Tech GmbH (Germany) was investigated. The unit is characterised by an active membrane area of 34.5 x 45.4 cm^2, and a spacer thickness of 350 µm. An open-loop configuration was adopted since it enables the continuous production of base and acid stream, keeping high performance. The salty feed has a concentration of 1 M while the base and acid solutions are initialized at very low concentrations (0.05 M).

Generally, an EDBM unit consists of a limited number of triplets installed between the electrodes, and this number does not exceed 50/100 triplets due to process performance decreases, mainly related to shunt currents. For this reason, the analysis considered a stack with no more than 20 installed triplets in each cell pack, which has shown a promising performance [78]. To increase the process capacity, several stack units were considered in parallel to reach a total number of triplets in the plant equal to 100 in all the investigated configurations.

Table 12 Table of costs and economic parameters employed for the techno-economic analysis of the HEDBM unit

Parameter	***Value***	***[-]***	***Parameter***	***Value***	***[-]***
BPM	580	€ m^{-2}_{BPMs}	Water	1	€ m^{-3}_{w}
IEMs	114	€ m^{-2}_{IEMs}	Electricity	0.075	€ kWh^{-1}
Spacer	25	€ m^{-2}_{IEMs}	HCl price	0.01	€ kg^{-1}_{HCl}
Electrode	300	€ m^{-2}_{IEMs}	O2 price	0.1	€ kg^{-1}_{O2}
Casing $\%_{Cells}$	50	-	Plant lifetime	20	y
Peripheral $\%_{STACK}$	120	-	Membrane lifetime	7	y
Maintenance $\%_{FCI}$	10	-	Electrode lifetime	60000	h
Salvage value $\%_{FCI}$	10	-	Discount rate %	3	-
Load factor	0.91	-	Tax %	10	-

The EDBM can be operated at a current density, one order of magnitude larger compared to other electro-membrane processes, thus allowing a higher hydrogen production, as the latter is strictly proportional to the current. For this reason, the simulations were done for different current densities, ranging from 250 and 1000 A m^{-2}. A faradic efficiency of 100 % was assumed (according to experimental data), and overall the plant capacity is always equal to 21 kg_{NaOH} h^{-1} of soda. Thus, to ensure the same amount of soda (same system capacity), more stacks will be required, and since the geometry of the system is fixed, each unit must work at different velocities depending on the current densities.

Also in this case, to increase the process productivity, an increase of the electrode active area would be beneficial, however, the EDBM geometry is defined by the manufacturers due to technical limitations. Consequently, the insertion of additional shared electrodes between the triplets is proposed as a strategy to increase hydrogen productivity, while keeping a constant chemicals production. In this way, it is possible to imagine an EDBM stack constituted overall by 100 triplets arranged in 5 units of 20 triplets each with 6 electrodes, or 26 shared electrodes stack with 4 triplets each; up to the limiting case of 100 stacks whose the 101 electrodes are spaced by a single triplet. Clearly, a bipolar end-membrane is inserted in each cell package between two electrodes to ensure the proper functioning of the unit.

6.3.2 Technical analysis

The specific energy consumption for the production of hydrogen (HSEC) and for NaOH (BSEC) versus the number of triplets (N_{tr}) assembled per stack is shown in Fig. 51. The squares refer to the two extreme cases: (i) alkaline electrolyser (in orange) and (ii) EDBM stack with 20 triplets (in blue). The alkaline electrolyser is assumed to work under the same operating conditions of the EDBM unit, thus, the same geometries and the same current density. In Fig. 51, (a) shows the trend for the 250 A m^{-2} current density case, (b) refers to 500 A m^{-2} and (c) is related to the 1000 A m^{-2} case.
For such an electrolyser, an $HSEC|_{el}$ of 59.7 kWh kg^{-1}_{H2} is calculated (assuming an overall potential drop of 2.23 V per cell, in which 1.23 V is due to the thermodynamic potential, 0.93 V is due to the electrodes overvoltage and 0.07 V due to the ohmic losses). The linear trend of the HSEC is shown on a logarithmic axis for ease of reading. As it can be seen, the HSEC increases as the number of triplets rises, in accordance with the reduction of the quantity of H_2 produced (Fig. 52). The difference between the one-triplet HSEC and the electrolyser case (N_{tr}=0) is due to the chemical production expenditure of the EDBM process. HSEC ranges from 90.7 to 103.7 kWh kg^{-1}_{H2} when the current rises from 250 to 1000 A m^{-2}.
Fig. 52 shows the flow rate trends as the triplets vary, both for hydrogen and for the NaOH. When 20 triplets are considered, the lowest hydrogen productivity is obtained, equal to 0.029 kg_{H2} h^{-1}, which causes the HSEC to increase dramatically. Conversely, as mentioned above, the base production remains unchanged as the number of electrodes assembled changes, maintaining an average production of 23.5 kg_{NaOH} h^{-1}. The no-perfectly horizontal trend of the NaOH mass flow rate is explained by the fact that the current efficiency of the EDBM process decreases as the number of triplets increases, due to the increase in dissipation due to parasitic currents, falling from 98 % to 96.6 %.
BSEC increases as the number of triplets decreases. When 20 triplets are assembled, the case with the lowest energy consumption is the one at 250 A m^{-2}, as it decreases the power expended and increases (albeit slightly) the current efficiency. The highest consumption, on the other hand, is obtained for the case at 1000 A m^{-2}. When the number of triplets decreases, the BSECs increase, reaching values which are approximately twice the value at 20 triplets. For N_{tr}=1, the BSEC is about 2.20 kWh m^{-3}_{NaOH} at 250 A m^{-2} , while it rises to 3.99 kWh m^{-3}_{NaOH} at 1000 A m^{-2} .

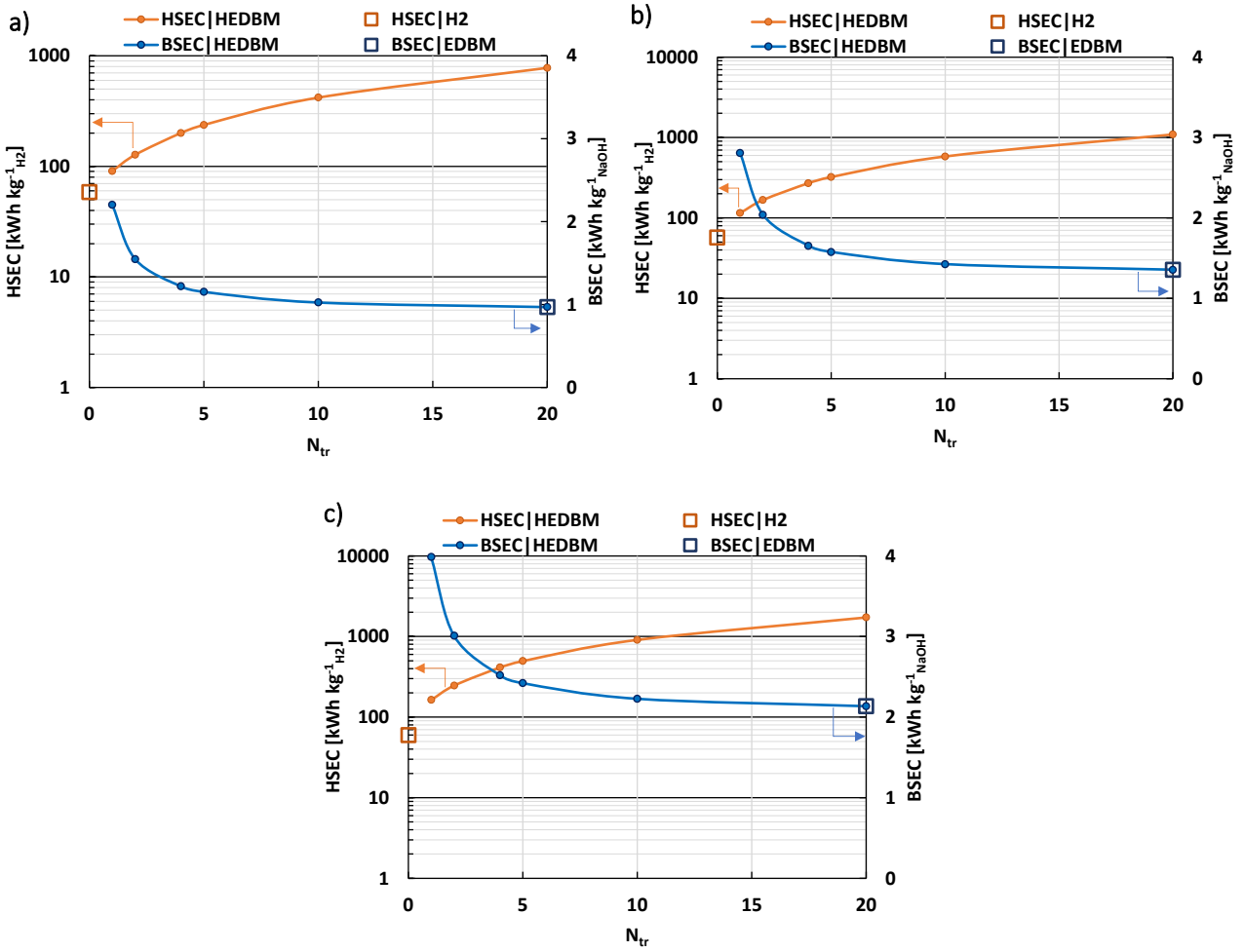

Fig. 51 Trend of the specific energy consumption for the production of hydrogen (HSEC) and NaOH (BSEC); versus the number of triplets N_{tr} assembled between two consecutive electrodes. The empty squares represent the two-limit cases of an alkaline electrolyser (orange) and the EDBM stack assembled with 20 triplets (blue). The order of the figures refers to 250, 500 and 1000 A m^{-2}.

In Fig. 51, BSEC decreases with the number of triplets, as the energy expended is mainly due to the migration of ions for the production of chemicals, meanwhile, the electrodic voltage losses cannot be considered negligible for low N_{tr}. These voltage drops at the electrodes are about 3 V, which take into account (i) the thermodynamic potential of 0.4 V (since the unit works with an acidic solution at cathodes and an alkaline one at the anodes), (ii) the electrodes overvoltage of 0.73 V and (iii) the ohmic losses that weight for 1.92 V, due to the ohmic resistances and to the water dissociation energy attributable to the end-membrane (i.e., the BM).

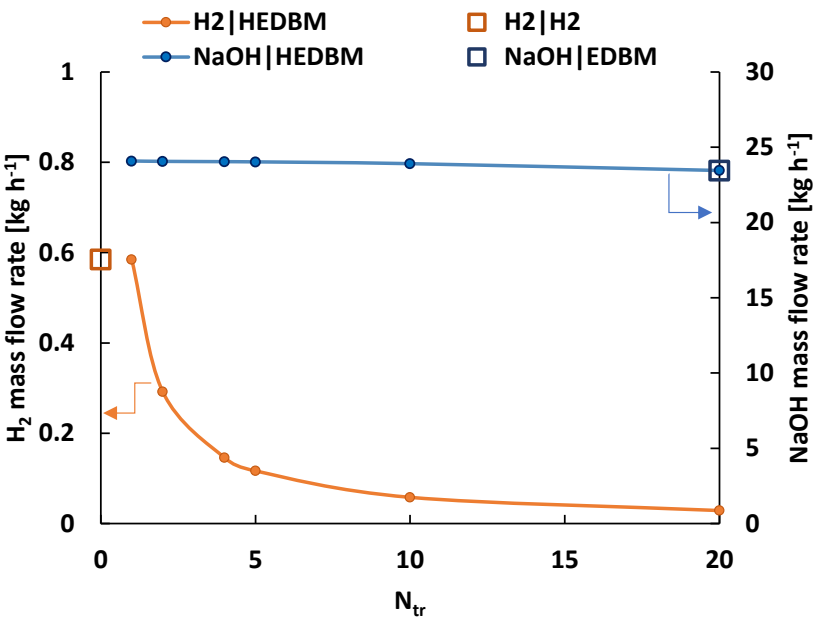

Fig. 52 Trends of the mass flow rate of hydrogen and soda NaOH. The empty squares represent the two-limit cases of an alkaline electrolyser (orange) and the EDBM stack assembled with 20 triplets (blue). The order of the figures refer to 250, 500 and 1000 A m^{-2}.

6.3.3 Economic analysis

Fig. 53 shows the LCOB and LCOH trends as the current density varies for an EDBM consisting of 20 triplets and for an electrolyser working in its same condition. For the electrolyser, a capital cost of 600 € m^{-2} was assumed (270 € kW^{-1}, [12]).

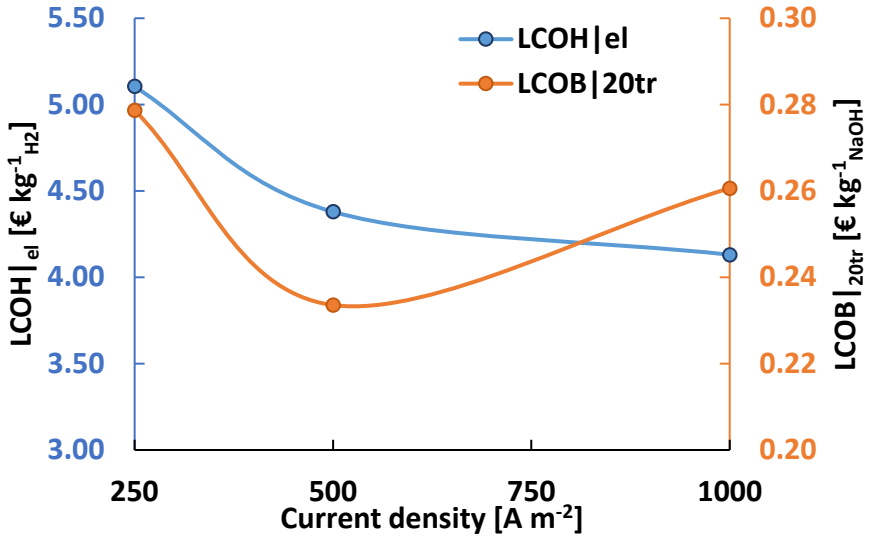

Fig. 53 LCOH for an electrolyser and LCOB for a 20 triplets EDBM unit versus the current density.

As expected, the cost of hydrogen decreases with the increase in electricity, as the quantity of hydrogen produced is greater while the capital cost is fixed. This leads to LCOH which goes from

5.11 to 4.13 € kg^{-1}_{H2}. Conversely, the challenging conditions of 1000 A m^{-2} are not the most cost-effective for the EDBM system. For lower current densities, the costs increase again, because for the same capacity of the system, the capital costs increase considerably, while the operating costs, on the other hand, decrease. The compromise between the two conditions leads to a minimum cost of the base of about 0.23 € kg^{-1}_{NaOH}, in correspondence of 500 A m^{-2}.

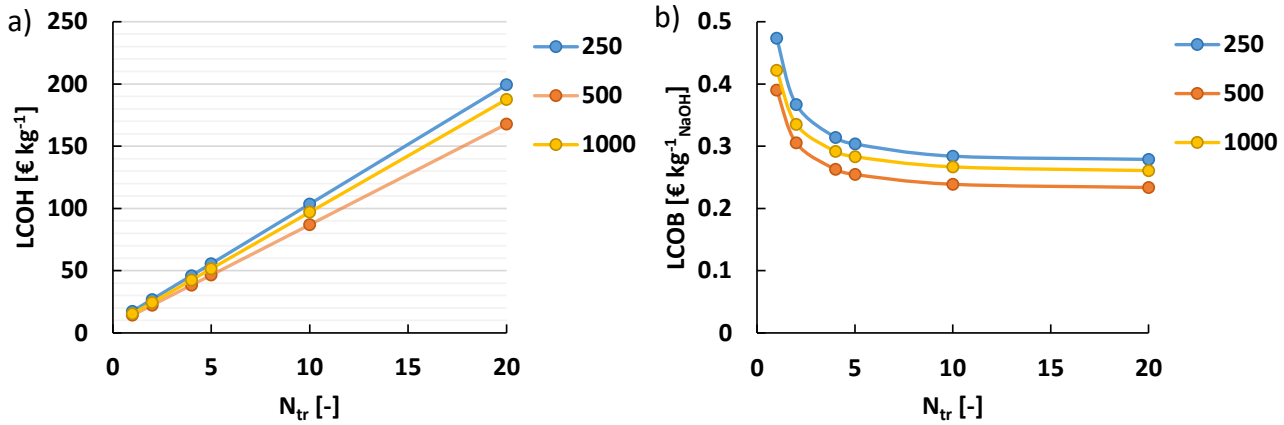

Fig. 54 Trend of the LCOH and LCOB versus the number of triplets N_{tr}. The other main product (NaOH for the hydrogen, and hydrogen for the NaOH) is not sold. The curves are parameterized as a function of the current density.

In Fig. 54a, the trends of LCOH and LCOB are reported as the number of triplets varies, parameterized with the current density. The lowest LCOH is always observed when there is just 1 triplet per stack and for all the current densities (about 14.2-17.4 € kg^{-1}_{H2}). By increasing the number of installed triplet, the LCOH rises significantly, reaching a value up to 200 € kg^{-1}_{H2} for the 250 A m^{-2} at 20 triplets. This can be explained by considering that, as N_{tr} increases, the production of hydrogen decreases and its production cost becomes dramatically higher. Furthermore, the plot was obtained by assuming a zero selling price of the other main product, therefore the LCOH also takes into account the costs related to the production of the other chemicals.

The LCOB, when hydrogen is not sold, is shown in Fig. 54b. It is less affected by the number of triplets, indeed it goes from 0.28 to 0.47 € kg^{-1}_{NaOH}, with a 68 % increase compared to its reference cost for the worst case of 250 A m^{-2}. Furthermore, the lowest LCOB are shown the 500 A m^{-2} case, that is confirmed to be the most convenient configuration both in term of hydrogen and NaOH production. What should be noted is that, even if the cost of hydrogen is at least one order of magnitude higher compared to the base cost, the production (mass flow rate) of the alkaline stream is 2 orders of magnitude higher than hydrogen. This evidence strengthens the need of using a high

number of electrodes to increase the production of hydrogen, similar to a large hydrogen production industry, for which up to 1000 cells can be used for a single electrolyser. However, the LCOH and LCOB shown in Fig. 54 are the costs when the other product is not sold, and consequently, this implies higher costs for the individual products.

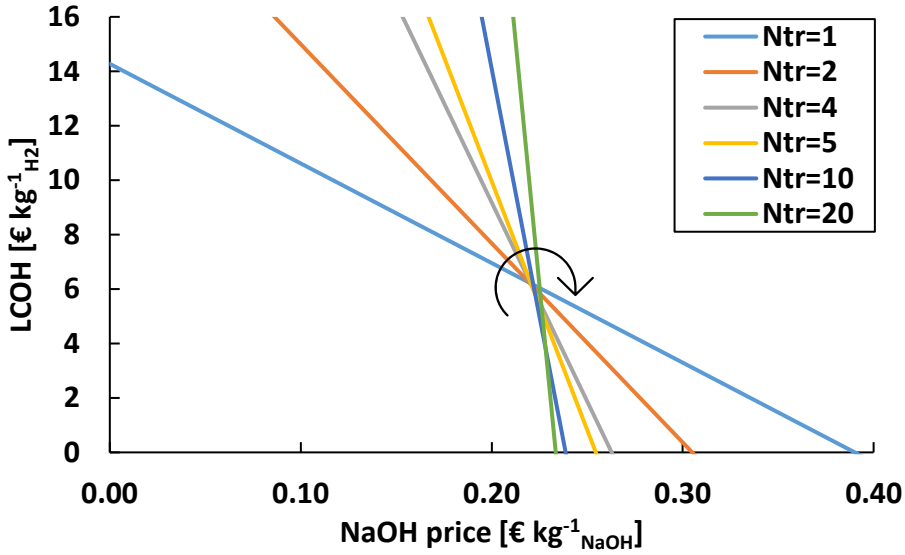

Fig. 55 LCOH at varying of the price of soda. The curves are parameterized respect the number of triplets and the LCOH increases clockwise direction. The plot refers to the 500 A m^{-2} case.

In Fig. 55, the locus of point of the LCOH is reported as the price of the NaOH varies, parameterized with the number of triplets, and it refers to the 500 A m^{-2} case. Clearly, for the definitions given, each point in the line represents a condition for which the NPV is zero, and therefore, at the end of the useful years of the plant, the expenses have equalled the revenues. The curves tend to intersect at a point, which corresponds to the coordinates 0.23 € kg^{-1}_{NaOH} for the base and 5.73 € kg^{-1}_{H2} for hydrogen. More generally, for prices lower than the latter, the plant will always be in economic loss, while for higher prices the plant will be profitable. The case at N_{tr}=1 is the one with the lower slope, identifying lower LCOHs for soda prices less than 0.23 € kg^{-1}_{NaOH}, or conversely, requiring a greater increase to reduce the cost of hydrogen. As mentioned, having a higher number of triplets implies fewer electrodes and consequently less hydrogen. Indeed, for a higher number of triplets, the slopes of the curves increase consistently, identifying a lower economic weight of hydrogen in the process economy.

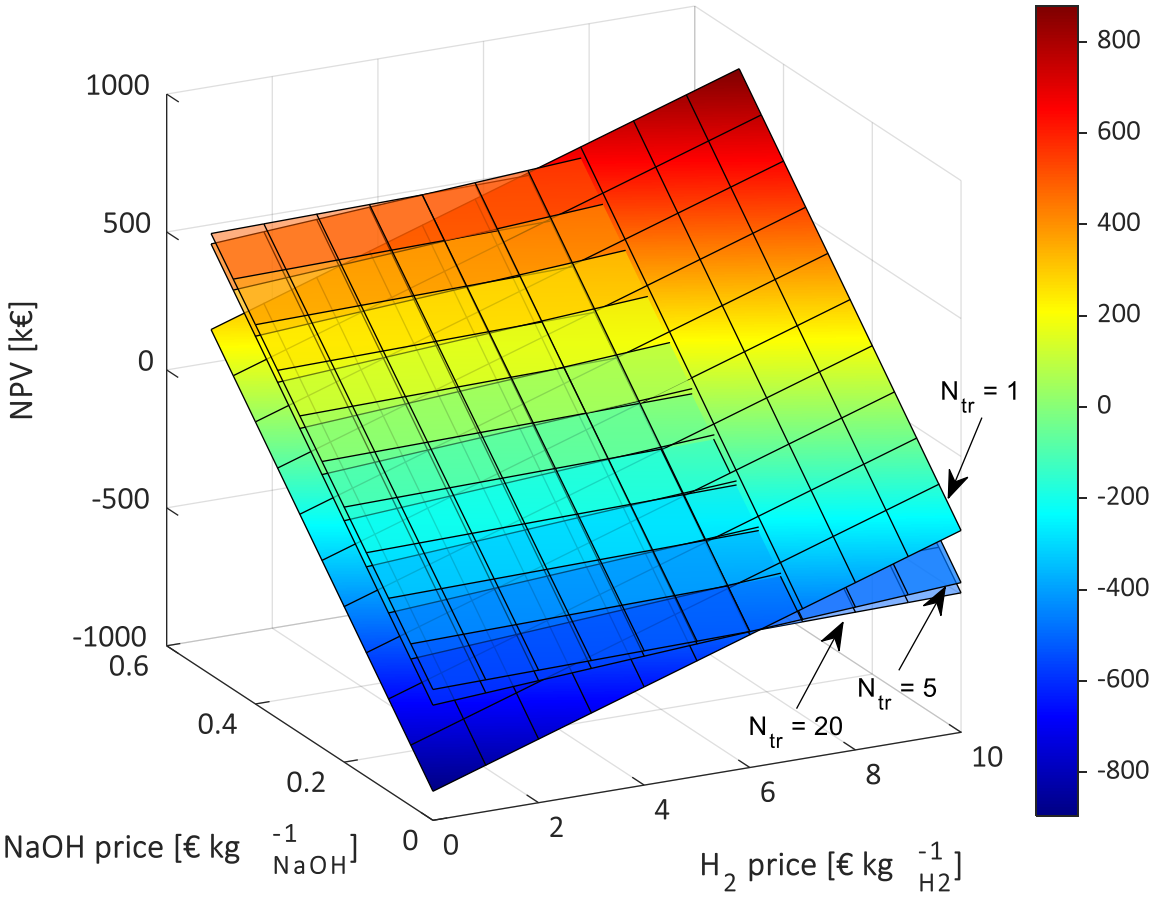

Fig. 56 NPV trend versus the soda and hydrogen price at varying of the number of triplets. For the sake of readability, only the 1, 5 and 20 triplets surfaces have been represented.

In addition to the previous figure, a 3D map of the NPV as the costs of soda and hydrogen vary is shown in Fig. 56. As expected, NPV increases as the selling prices of both products increase. At high numbers of triplets, a quasi-independence of the curves from the variation in the price of hydrogen is observed, showing that the NPV is exclusively dependent to NaOH. For the case of 20 triplets, the NPV ranges from -525 k€ (if the base is not sold) to almost 600 k€ when it is sold at 0.6 € kg^{-1}_{NaOH} corresponding to an increase of 220 %; while it rises to 630 k€ if hydrogen is also sold at 10 € kg^{-1}_{H2} for which the profit has an imperceptible variation. This trend is totally overturned when there is only 1 triplet, in this case the sale of hydrogen has its weight in the economy of the entire plant and can raise the NPV up to 880 k€, if a base price of 0.6 € kg^{-1}_{NaOH} and a hydrogen price of 10 € kg^{-1}_{H2} are assumed.

The NPV trend for different hydrogen prices (in the range 0-10 € kg^{-1}_{H2}) when the base is sold at a plausible price of 0.4 € kg^{-1}_{NaOH} [131] for the 3 current densities studied is shown in Fig. 57, furthermore, the surface are parameterized with the number of triplets.

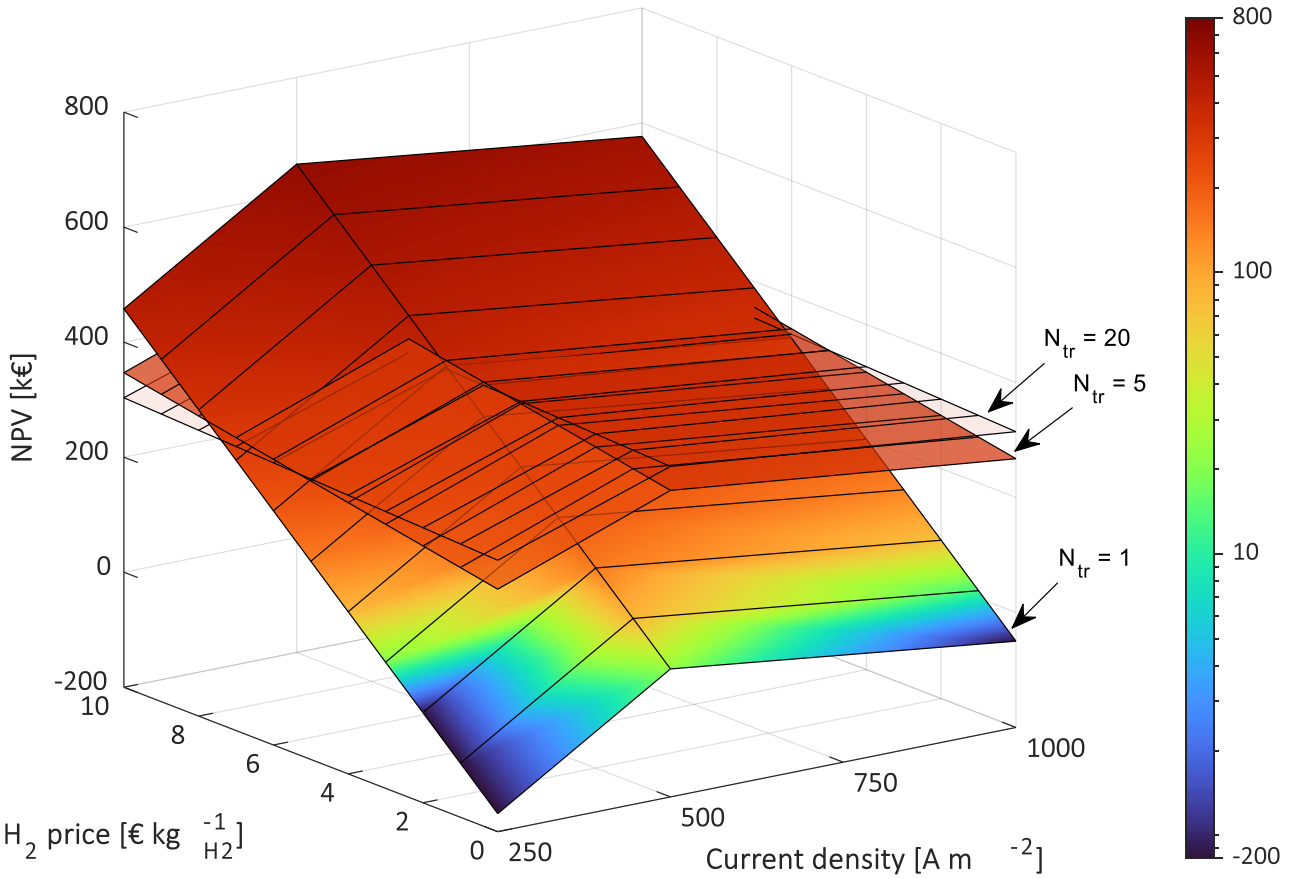

Fig. 57 NPV surfaces at varying of hydrogen price and current density, parameterized with the N_{tr}. The NaOH is sold at a fixed price of 0.4 € kg^{-1}_{NaOH}. For the sake of readability, only the 1, 5 and 20 triplets surfaces have been represented.

In the case of 20 triplets, considered as a reference for a common EDBM unit, and assuming that the hydrogen is not sold, the scenario leads to NPV values of about 350 k€ for high current densities. The NPV value decreases down to 272 k€ for 250 A m^{-2}, which turns out to be the worst possible configuration. Even considering a price of 6 € kg^{-1}_{H2}, there is not improvement in profit, due to the almost constant trend. The same sort occurs even if the number of triplets drops to 5.

The decrease in the number of triplets leads to a reduction in the NPV when hydrogen is not sold, low down to -38 k€ at 1000 A m^{-2} and precipitate to -168 k€ for 250 A m^{-2} also for 1 triplet, due to the high voltage drop that occurs at the electrodes. But in this case, when hydrogen is sold, the higher the selling price, the larger the obtained profit. Thanks to the addition of a relevant number of electrodes, the benefit of selling the hydrogen can be seen for a low number of triplets. For N_{tr}=1, in the case of 1000 A m^{-2}, an NPV of 520 k€ can be achieved if the hydrogen is sold at 8 € kg^{-1}_{H2}. As a counterproof of what has also been seen in the previous figures, the best profit (following a decrease in production costs) is for the case at 500 A m^{-2}, for which if the base is sold at

0.4 € kg^{-1}_{NaOH} and hydrogen at 8 € kg^{-1}_{H2} there would be an NPV of 530 k€, about 50 % more than the case without hydrogen with 20 triplets.

The obtained NPV is relatively small, but it should be considered that the EDBM units, just like electrolysers, are modular, hence, it is possible to increase the size by adding units in parallel. As a consequence, the Levelized Costs would remain more or less constant, but the NPV would result larger. For example, in this work, a system that produces a flow rate of 21 kg h^{-1} of NaOH (about 0.5 m^3 h^{-1}) was considered, which is a pilot size. Therefore, if a flow rate of 50 m^3 h^{-1} is used, the corresponding NPV would become about 53 million euros in the case of 1 triplet per stack and a hydrogen price of 8 € kg^{-1}_{H2}. Furthermore, it must also be considered that the system would be affected by a beneficial scale effect, reducing the specific capital costs, which positively influences the economics of the entire process.

In addition, a scenario analysis was also performed in order to establish the profitability of the process and the LCOH when some of the economic parameters are changed. Table 13 shows the economic parameters used to study the worst and the best cases for the HEDBM system. Fig. 58a shows the tornado diagram for NPV, while Fig. 58b shows the variation relative to LCOH. Both graphs refer to the standard case, also defined in Table 13, for which the NaOH is sold to a prices of 0.23 € kg^{-1}_{NaOH} and the hydrogen at 5.73 € kg^{-1}_{H2}, which represent the LCOB of the classic EDBM system assembled with a stack of 20 triplets and the LCOH obtained at this NaOH price, respectively. It is important to note that these values are the ones that correspond to the point of intersection of the line shown in Fig. 55. The scenario analysis was carried out for the case at 500 A m^{-2}, which was identified as the operating condition for which there are the lowest costs, and with an N_{tr} equal to 1, for which there are the best profits in terms of producing both hydrogen and the base.

As shown in the two figures, there are variables that are of greater significance from the point of view of the system's balance and variables that are partially influential. For instance, all the parameters from the discount rate downwards, up to the % of peripherals shown variations contained in the range of 10 % of the LCOH and among the ±51 k€ as regards the NPV. However, negative variations of more than 60 k€ define a sure bankrupt of the plant. Clearly, to remedy this situation, it is necessary to increase the selling prices of products. The other variables, on the other hand, are more incisive, but still with limited variations in both the NPV balance and the LCOH value.

Table 13 Economic parameters changed for the scenario analysis for the HEDBM unit

Input Scenario			*Worse*	*Standard case*	*Better*
Discount rate	**[%]**	[65,92,95]	6	3	0
IEMs cost	**[€ m_{IEMs}^{-2}]**		250	114	25
IEMs lifetime	**[y]**		4	7	10
Spacer cost	**[€ m_{IEMs}^{-2}]**		10	25	50
BPMs cost	**[€ m_{BPMs}^{-2}]**		1114	580	100
Electrode cost	**[€ m_{el}^{-2}]**	[12,89]	500	300	100
Electrode lifetime	**[h]**	[12]	32000	60000	>80000
Casing	**[%]**		25	50	75
H_2 selling price	**[€ kg_{H2}^{-1}]**	[13,117]	3	5.73	8
Water cost	**[€ m_{w}^{-3}]**		1.2	1	0.8
NaOH selling price	**[€ m_{NaOH}^{-3}]**		0.1	0.23	0.4
Electricity cost	**[€ kWh^{-1}]**	[65,105]	0.12	0.075	0.05
Peripheral	**[%]**		130	120	110
Other costs	**[%]**		15	5	10
Working hours	**[$h\ y^{-1}$]**	[65,119]	2500	8000	-

The parameters that strongly influence the economy of the system are the cost of bipolar membranes and electricity, the number of annual working hours and the price of soda (and hydrogen in the case of Fig. 58a). With regard to NPV, the biggest variation is with the price of soda, for which the NPV was analysed at a minimum sales value of 0.1 € kg^{-1}_{NaOH}. and a maximum value of 0.4 € kg^{-1}_{NaOH}. For this situation, the NPV fluctuates between a dramatic -306 and a substantial +382 k€. The effect of the price of the soda has less impact on the LCOH than the number of working hours, although it should be noted that if the soda were sold at 0.4 € kg^{-1}_{NaOH}, an even negative LCOH is obtained, always highlighting that the main product of the plant remains the soda. This also has an effect in LCOH and in the order of the tornado diagram, for which a change in the number of annual production hours makes hydrogen jump to a cost of about 16.6 € kg^{-1}_{H2}. Another variable that also affects the profitability of the plant is electricity, which consistently influences the plant with a variation of 7.2 k€ of NPV for each variation of 1 € MWh^{-1}. For the same variations, there would be an increase in LCOH up to about 11 € kg^{-1}_{H2} if energy were sold at 120 € MWh^{-1} or a decrease to 2.8 € kg^{-1}_{H2} if it were sold at 50 € MWh^{-1}.

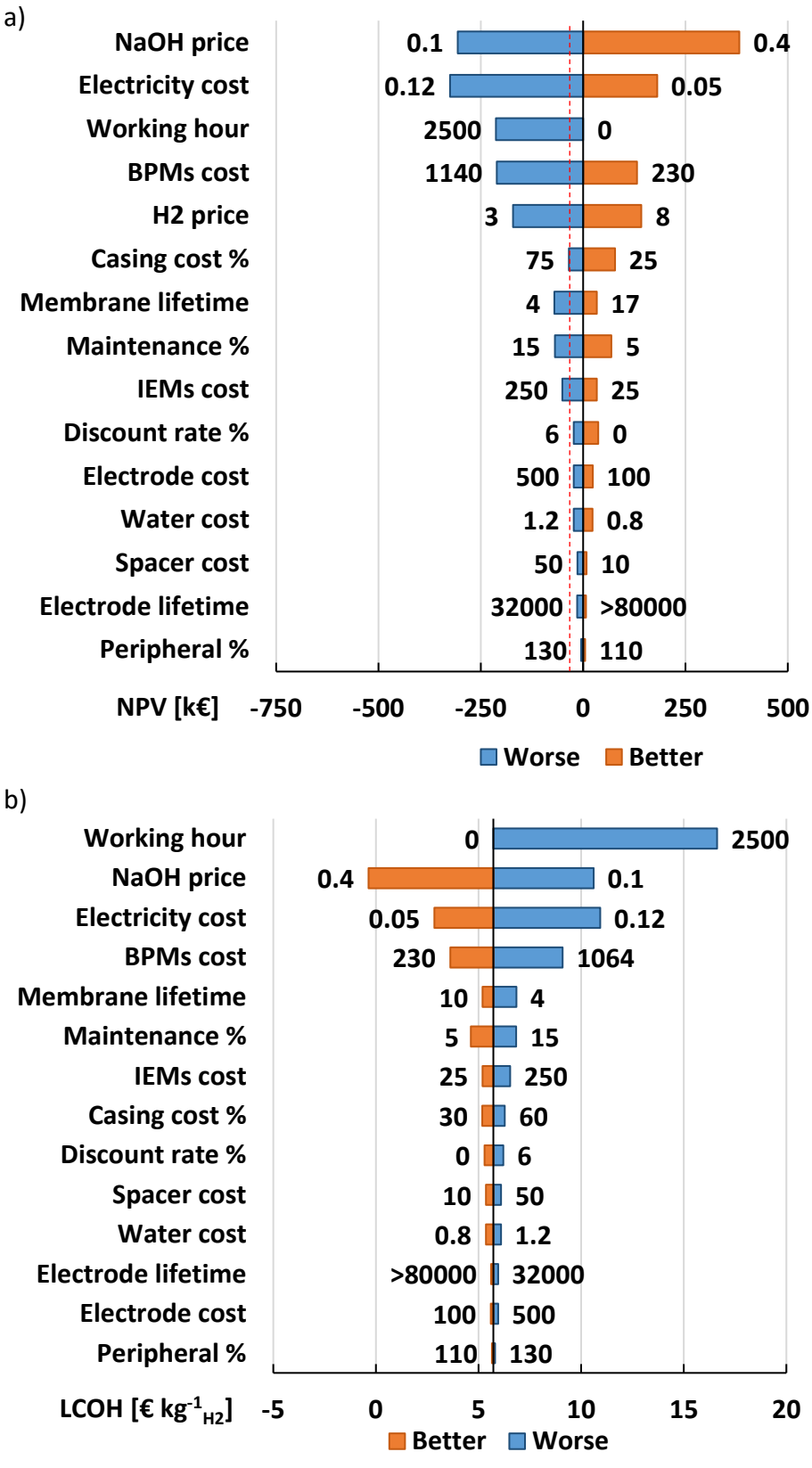

Fig. 58 Tornado diagram of (a) NPV and (b) LCOH at varying the economic parameters according to Table 13. The vertical red dashed line represents the limiting negative NPV for which, values below, cause an irreversible bankruptcy of the system.

Finally, BPM are the capital costs that most influence the system. The price used for all the simulations is the one found by the authors in various quotes nowadays, while the maximum cost is equal to the one proposed a couple of years ago by Culcasi et al [73], and the minimum cost has been chosen as double the cost of the IEMs membranes (i.e., 2x 114 € m^{-2}_{IEMs}). Bipolar membranes represent the key cost of the technology, so if their cost will decrease in the near future, it can certainly reduce the costs of EDBM first and then of the HEDBM technology.

6.4 Final remarks and future perspectives for HEDBM

This section investigated the use of an EDBM unit for the co-production of hydrogen at the cathode. First, an experimental analysis was carried out on a 10 x 10 cm^2 laboratory unit with 5 triplets, and then the results of this analysis were used to validate and calibrate a mathematical model capable of predicting the main results of the unit.

Once validated, the technical model was coupled with an economic model to provide a preliminary estimate of the unit cost and the main economic indicators of the process, such as Levelized Costs and Net Present Values. An EDBM unit capable of operating at different current densities (250, 500 and 1000 A m^{-2}) was considered. For such a system, an increase in current would reduce the capital cost of the EDBM as fewer units would be required to produce the same amount of NaOH solution. However, as shown in the techno-economic analysis, this would correspond to an increase in operating costs, which would lead to an increase in the LCOB. Conversely, operating at lower currents would reduce operating costs at the expense of capital costs, which would increase costs again. Hence, a minimum cost for the NaOH was identified at a current density of 500 A m^{-2}. The hydrogen production cost for an equivalent electrolyser operating under the same conditions as the EDBM unit (i.e. current density, geometry and number of cells) was also considered. As would be expected, the cost of hydrogen production decreases with increasing current density, as more hydrogen is produced and therefore more revenue is generated. The EDBM unit allows additional electrodes to be inserted between the triplets, which means that hydrogen productivity can also potentially be increased. For this reason, a similar analysis as in the previous chapters has been carried out for the EDBM. The addition of extra electrodes will undoubtedly increase the hydrogen yield, but will also lead to an increase in capital cost due to (i) the additional electrodes and to the (ii) extra bipolar end membranes. Furthermore, also the operative cost increases due to the

repeated potential drops that would occur at the electrodes. However, the benefit to be gained from increased hydrogen production could be significant.

The HEDBM system was therefore investigated at different current densities and with different numbers of electrodes. The results showed, as predicted by the single EDBM analysis, that as the current density varies, the best operating condition is found at 500 A m^{-2}. Furthermore, the condition for which the hydrogen production cost is lowest is for the maximum number of electrodes assembled in the system, i.e. in the configuration where there is only one triplet between the electrodes. In EDBM a LCOB of 0.23 € kg^{-1}_{NaOH} was found and looking to the revamping of such a plant, a LCOH of 5.67 € kg^{-1}_{H2} was also identified (at 500 A m^{-2}). These costs may seem less advantageous than in the cases studied previously, but it should be remembered that the economic conditions in which the analyses were carried out are much more conservative. Just think of the cost of the bipolar membranes (580 € m^{-2}) which strongly influences the process economy. In fact, the sensitivity analysis showed how a reduction in these costs can only improve the economics of the process, leading to much more competitive hydrogen values. Furthermore, the unit used for the economic analysis is a pilot unit, selected among the commercially available. This puts a heavy burden on the technology due to the limited electrode area (for hydrogen) and the need for several units to produce NaOH.

However, even under these ultra-conservative conditions, the technology is still in the range of costs, showing a good profit margin (530 k€) for the pilot unit considered, and up to an excellent 53 M€ for a capacity of 50 kg h^{-1}. These results making the HEDBM an emerging technology on the market with a potential window of opportunity for the hydrogen production.

7 On the modelling of PEM water electrolysers

PEMWEs are proposed, today, as the most promising large-scale electrolysers, due to the higher purity of hydrogen, lower volumes involved and risk issues, and the possibility of working at higher current densities (i.e., higher productivity). Current density can reach values up to 10 A cm^{-2}, which represents the highest current achievable by common electrolysers, even if at this current density the electrodes degradation phenomena are faster.

The PEMWE unit consists of a repetition of cells made up of different components (e.g., channels, porous transport layer PTL, etc.). A cell single-straight-channel was studied by a CFD model purposely developed in Ansys Fluent®. The model, after a preliminary calibration, was able to predict, within a certain margin of error, the data available in literature, showing some of the phenomena that occur within the electrochemical cell

The activities illustrated in this chapter were carried out during the period abroad spent at the Dutch research centre TNO.

7.1 PEMWE system description

Hydrogen production with PEM electrolysers can be considered on several levels. The highest level (system) concerns the entire production plant, i.e. the electrolyser, the renewable energy grid and all other plant equipment, often referred to as the BoP (Balance of Plant), which takes into account pumps, storage, cooling and separation systems. Specifically, the single electrolyser (stack level), as mentioned several times throughout this work, is made up of a very large number of electrochemical cells hydraulically connected in parallel, which can operate with different electrical configurations (monopolar or bipolar) [132]. The individual cell (cell level) of the stack is made up of several components, each with different functionalities. A schematic representation of the entire flow field of a PEMWE is shown in Fig. 59a. A normal electrolyser is made up of several individual cells that share the bipolar plate (BP), a solid component made of highly conductive material that has the specific function of separating the anode (positive) of the cell from the cathode (negative) of the immediately adjacent cell, reason for the name. A schematic representation of a single repetitive unite is shown in Fig. 59b. Inside the bipolar plates are channels (CH) through which the

water required for the electrolysis reaction and the gases produced by the reaction will pass. The core of the cell is the Proton Exchange Membrane (PEM), on which a very thin catalytic layer (Catalyst Layer, CL) is applied using a special coating process. This is the place where the reactions take place and it is often referred, together with the membrane, as MEA (Membrane Electrode Assembly). The catalyst is particularly sensitive to mechanical and pressure stresses, which can be caused both by bubble formation and, above all, by the passage of water. For this reason, highly conductive Porous Transport Layers (PTLs) are used to protect the MEA. In addition, special chemical-physically enhanced O-rings are used to seal the unit to prevent cells and external leakage. A schematic representation of the components of the cell is reported in Fig. 59c. Note that only a portion of a single channel is considered for the CFD analysis. Furthermore, the cell considered is a portion of the channel satisfactorily away from the manifolds, so as not to be influenced by them.

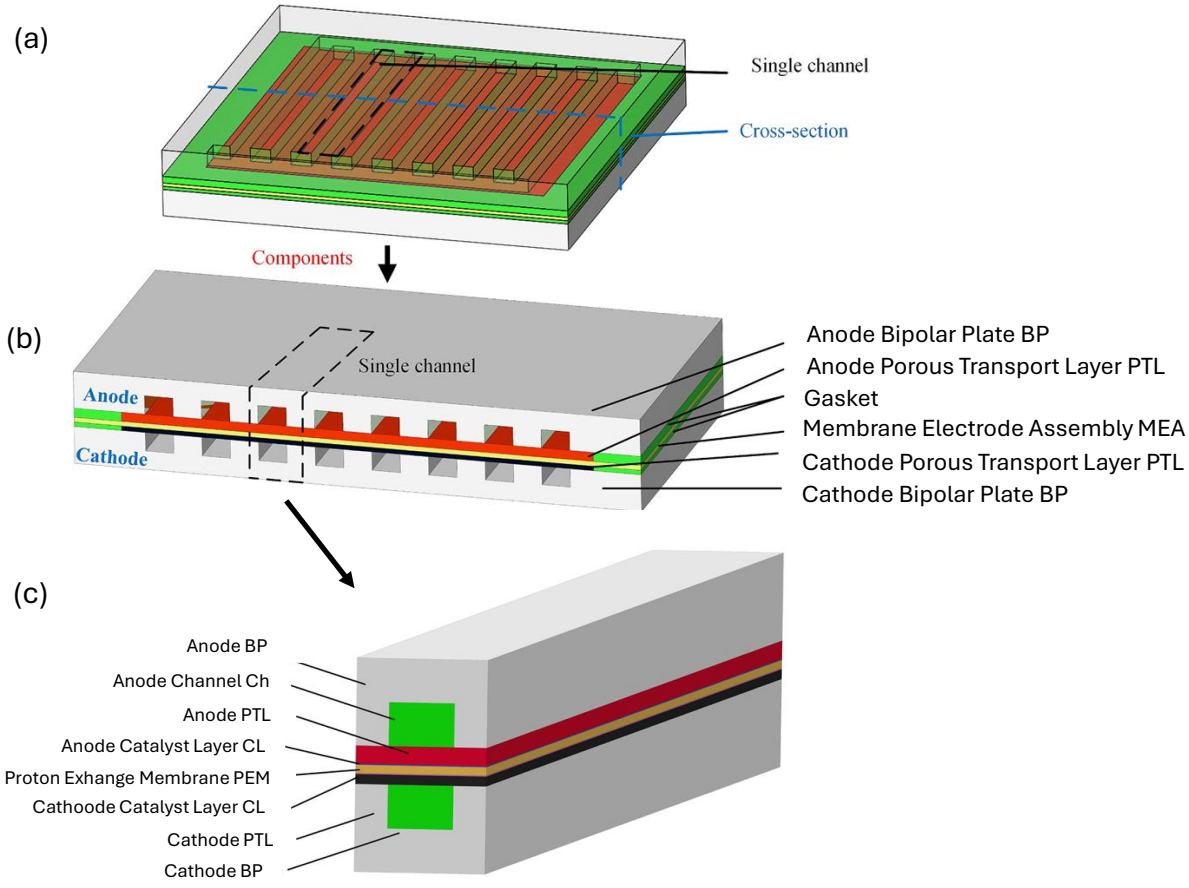

Fig. 59 Schematic representation [133] of the (a) flow field of a PEM electrolyser and of (b) the elements of a single repetitive unit. In (c) a schematisation of a single cell and its components.

PTLs are also referred to as GDLs (Gas Diffusion Layers), especially on the cathode side, as a dry cathode configuration is often used, i.e. without supplying water to the cathode. This makes it possible to produce an entirely hydrogen gas stream at the cathode with a low moisture content, which would facilitate the subsequent stream separation and purification steps. On the other hand, the reaction takes place at the anode, where the reduction occurs with the consequent formation of O_2, electrons and H^+, according to the Table 1 reactions in an acidic media. Then, the proton crosses the cation exchange membrane and produces H_2 at the cathodic CL. From an electrical point of view, the numerous cells of the unit are surrounded by 2 outermost current collectors (CC) where the stack potential is applied, which is the sum potential of each individual cell. This is because systems such as PEMWEs (and AEMWEs) use bipolar electrical configurations, where the high potential applied polarises the system and allows current to flow, resulting into hydrogen production. In this case, each cell operates at the same current. In contrast, AWEs prefer a monopolar configuration where the cathodes are all equipotential (as the anodes) and the system current is given by the sum of the currents of each cell. This configuration is preferred in AWEs to avoid problems with shunt currents in the manifolds. Temperature is typically a factor that improves the kinetics of electrochemical reactions, so operating conditions are typically between 60 and 80 °C. An increase in temperature could reduce the energy required for the reaction (due to the decrease in potentials). However, it would also lead to degradation of the polymer membrane and an increase in the moisture content of the gases produced, which would increase the cost of separation. The water used must be strictly ultrapure due to problems of electrode corrosion and competitive reactions due to the presence of chlorides, as well as the possibility of scaling phenomena. From a strictly stoichiometric perspective, the requirement for hydrogen is approximately 9 L of water per kg of hydrogen, even if 11-13 L of water are usually considered for inefficiencies and losses (such as drag and evaporation). However, these litres must first be produced, which is why the amount of untreated water required is significantly higher. In general, the greater the water quality requirements, the more complex the desalination plant design and the lower the water recovery rate. Water treatment costs are often negligible in relation to the economics of hydrogen production and its levelized cost. However, economic analyses do not consider the environmental and social impact of producing large quantities of water for the construction of large-scale hydrogen production facilities, such as mega or giga farms. The main

resources required, i.e. water and green electricity, must be available, and it must also be ensured that the basic needs of local communities are not compromised.

PEMs also have the advantage over alkaline (AWE) of pressurising the cathode, which reduces compression costs. However, this creates an increased flow of H_2 towards O_2, driven by a pressure gradient, which would lead to crossover problems with the possible formation of explosive mixtures and contamination of the oxygen stream. Oxygen would potentially be a very profitable gas [134,135], especially in the hospital sector, as long as its purity is not greatly compromised. However, its value is usually neglected in economic analyses, or in any case considered very low. Indeed, the oxygen market is quite limited because air is usually used and treated directly where possible. Currently, oxygen is produced using Pressure Swing Adsorption (PSA), cryogenic processes, membrane technologies or produced as by-product [136]. Each air separation technology produces oxygen at different pressures, purities, and flow rates, and its price fluctuates around 0.05 € kg^{-1}_{O2} [115]. Due to its low market value relative to the high cost of hydrogen, oxygen is often neglected in market analyses and, in some cases, entirely excluded from the economic assessment of the process.

7.2 Technical model

The equations governing the system are collected in Table 14. In fact, each component, on the basis of its features and functions, must be studied and modelled with different assumptions. In addition, the presence of both solid components and liquid and gaseous phases further complicates the modelling of the system, as this is a multiphase problem.

For each component, 6 equations are solved, namely the classical continuity, momentum and energy equation, the equation on the volume fraction of the liquid phase and the N-1 equations for each gas that potentially constitutes the gas phase (H_2, O_2 and H_2O). Depending on the component, some equations are not solved (e.g. being the BP a solid no porous component, no continuity and momentum equations are considered). Furthermore, the equations that take into account the potential and the electrochemical reaction must also be considered. Given the complexity of the problem, a numerical CFD software (ANSYS Fluent 2024R2) was used to solve the equations of the system.

The resolution of the Navier-Stokes equations occurs only in the channels, in the PTLs and in the CLs, as the BPs are solid and are not in motion, while in the membrane the assumption of absence of motion is made by which the species pass exclusively by diffusion. In addition, PTLs and CLs are porous materials, which is why the equations are further modified (compared to CH) to take into account the porosity and capillarity of the materials. Further details of the model employed can be found in [137].

The complexity of the model is related to (i) the multiphase, for which it is necessary to solve the equation of the volumetric fraction of the liquid and (ii) the electrochemical reaction.

As far as the multiphase is concerned, the system is modelled through a mixture model, which takes into account the properties mediated between the gas and liquid phases, for the characterization of the single volume-element in which the equations are solved. For instance, the density of the element is a mixture density, calculated as the weighted average of the volumetric fractions of the phases $\rho_m = \sum_{k=1}^{n} \alpha_k \rho_k$ with α_k volumetric fraction of phase k. Since the system is biphasic, k will be equal to 2. The mixture model approach is also relative to all the other quantities of the system (e.g., velocity, enthalpies, viscosity, etc.).

The electrochemical model is described by the potential Laplacian, defined as the product between the conductivity of the material and the gradient of the electric field $\sigma_s \nabla \phi_s$. There are 2 types of potential expressed in the model: ϕ_s and ϕ_m. In fact, this is a purely mathematical artifice to describe a phenomenology described by the same equation, but linked to different modalities. In fact, the system consists of the anodic and the cathodic BPs. The highest potential is applied to the anodic side, while there would be a zero potential to the cathode, thus, the potential decreases due to ohmic drops and to the electrolysis reaction.

Starting from the anode, a series of ohmic drops are observed due to the resistance opposed by the materials, i.e. BP, PTL and CL. In the channels, there is no charge transport as the solution is ultra-pure water. On the CL, the electrochemical reaction takes place and the cell potential reduces due to (i) the thermodynamic potential of almost 1.217 V (for the higher temperature) and to (ii) the activation overvoltage estimated by the Butler-Volmer equation. In the anodic CL, H^+ protons are generated and, after crossing the membrane, they produce hydrogen in the cathodic CL. In this context, ions are the charge carriers.

Table 14 Main CFD model equations for PEMWE, collected by cell component

Material		*Equation*	*Boundary Condition*
BP	*Potential (56)*	$\nabla \cdot (\sigma_s \nabla \phi_s) = i_s$	$\mathrm{i}_m = 0$ $\phi_m = 0$
	Energy (57)	$\frac{\partial(\rho_s c_p T)}{\partial t} + \nabla \cdot (\rho_m \bar{v}_m c_p T) = \nabla \cdot (\nabla k_{eff} T) - \nabla \cdot \sum_{k=1}^{n} \sum_{i=1}^{p} \mathrm{h}_{ik} J_{ik} + \nabla \cdot [\overline{\overline{\tau}_{ij}} \bar{v}_m] + \frac{\partial p}{\partial t} + S_{\mathrm{h}}$	
CH	*Potential (58)*	$\nabla \cdot (\sigma_s \nabla \phi_s) = 0$	$\mathrm{i}_m = 0$ $\phi_m = 0$ $\bar{v}_{dr,k} = 0$
	Continuity (59)	$\frac{\partial \rho_m}{\partial t} + \nabla \cdot (\rho_m \bar{v}_m) = 0$	
	Momentum (60)	$\frac{\partial(\rho_m \bar{v}_m)}{\partial t} + \nabla \cdot (\rho_m \bar{v}_m \bar{v}_m) = -\nabla p + \nabla \cdot [\mu_m (\nabla \bar{v}_m + \nabla \bar{v}_m{}^T)] + \rho_m \bar{g} - \nabla \cdot (\sum_{k=1}^{n} \alpha_k \rho_k \bar{v}_{dr,k} \bar{v}_{dr,k})$	
	Energy (61)	$\frac{\partial(\alpha_l \varepsilon \rho_l)}{\partial t} + \nabla \cdot (\alpha_l \varepsilon \rho_l \bar{v}_m) + \nabla \cdot \left(\bar{\imath}_m \frac{n_d}{F} M_w\right) = \nabla \cdot \left(-\frac{\rho_l K K_r}{\mu_l} \frac{dp_c}{d\alpha_l} \nabla \alpha_l\right) + S + S_{gl}$	
	Volume fraction of liquid (62)	$\frac{\partial(\rho_m c_p T)}{\partial t} + \nabla \cdot (\rho_m \bar{v}_m c_p T) = \nabla \cdot (\nabla k_{eff} T) - \nabla \cdot \sum_{k=1}^{n} \mathrm{h}_k J_k + \nabla \cdot [\bar{\bar{\tau}}_{ij} \bar{v}_m] + \frac{\partial p}{\partial t}$	
	Gas phases species (63)	$\frac{\partial(\alpha_g \rho_g Y_{ig})}{\partial t} + \nabla \cdot (\alpha_g \rho_g \bar{v}_m Y_{ig}) = \nabla \cdot (\alpha_g \rho_g D_{eff} \nabla Y_{ig}) + S$	
PTL	*Potential (64)*	$\nabla \cdot (\sigma_s \nabla \phi_s) = 0$	$\mathrm{i}_m = 0$ $\phi_m = 0$ $\bar{v}_{dr,k} = 0$
	Continuity (65)	$\frac{\partial \rho_m}{\partial t} + \nabla \cdot (\rho_m \bar{v}_m) = 0$	
	Momentum (66)	$\frac{\partial(\rho_m \bar{v}_m)}{\partial t} + \nabla \cdot (\rho_m \bar{v}_m \bar{v}_m) = -\nabla p + \nabla \cdot [\mu_m (\nabla \bar{v}_m + \nabla \bar{v}_m{}^T)] + \rho_m \bar{g} - \nabla \cdot (\sum_{k=1}^{n} \alpha_k \rho_k \bar{v}_{dr,k} \bar{v}_{dr,k})$	
	Energy (67)	$\frac{\partial(\rho_m c_p T)}{\partial t} + \nabla \cdot (\rho_m \bar{v}_m c_p T) = \nabla \cdot (\nabla k_{eff} T) - \nabla \cdot \sum_{k=1}^{n} \mathrm{h}_k J_k + \nabla \cdot [\bar{\bar{\tau}}_{ij} \bar{v}_m] + \frac{\partial p}{\partial t}$	
	Volume fraction of liquid (68)	$\frac{\partial(\alpha_l \varepsilon \rho_l)}{\partial t} + \nabla \cdot (\alpha_l \varepsilon \rho_l \bar{v}_m) + \nabla \cdot \left(\bar{\imath}_m \frac{n_d}{F} M_w\right) = \nabla \cdot \left(-\frac{\rho_l K K_r}{\mu_l} \frac{dp_c}{d\alpha_l} \nabla \alpha_l\right) + S$	
	Gas phases species (69)	$\frac{\partial(\alpha_g \rho_g Y_{ig})}{\partial t} + \nabla \cdot (\alpha_g \rho_g \bar{v}_m Y_{ig}) = \nabla \cdot (\alpha_g \rho_g D_{eff} \nabla Y_{ig}) + S$	
CL	*Potential (70)*	$\nabla \cdot (\sigma_s \nabla \phi_s) + \mathrm{R}_{\mathrm{s}} = 0$ $\nabla \cdot (\sigma_m \nabla \phi_m) + \mathrm{R}_{\mathrm{m}} = 0$	$\mathrm{i}_m = 0$ $\phi_m = 0$ $\bar{v}_{dr,k} = 0$
	Continuity (71)	$\frac{\partial \rho_m}{\partial t} + \nabla \cdot (\rho_m \bar{v}_m) = 0$	
	Momentum (72)	$\frac{\partial(\rho_m \bar{v}_m)}{\partial t} + \nabla \cdot (\rho_m \bar{v}_m \bar{v}_m) = -\nabla p + \nabla \cdot [\mu_m (\nabla \bar{v}_m + \nabla \bar{v}_m{}^T)] + \rho_m \bar{g} - \nabla \cdot (\sum_{k=1}^{n} \alpha_k \rho_k \bar{v}_{dr,k} \bar{v}_{dr,k})$	
	Energy (73)	$\frac{\partial(\rho_m c_p T)}{\partial t} + \nabla \cdot (\rho_m \bar{v}_m c_p T) = \nabla \cdot (\nabla k_{eff} T) - \nabla \cdot \sum_{k=1}^{n} \mathrm{h}_k J_k + \nabla \cdot [\bar{\bar{\tau}}_{ij} \bar{v}_m] + \frac{\partial p}{\partial t}$	
	Volume fraction of liquid (74)	$\frac{\partial(\alpha_l \varepsilon \rho_l)}{\partial t} + \nabla \cdot (\alpha_l \varepsilon \rho_l \bar{v}_m) + \nabla \cdot \left(\bar{\imath}_m \frac{n_d}{F} M_w\right) = \nabla \cdot \left(-\frac{\rho_l K K_r}{\mu_l} \frac{dp_c}{d\alpha_l} \nabla \alpha_l\right) + S$	
	Gas phases species (75)	$\frac{\partial(\alpha_g \rho_g Y_{ig})}{\partial t} + \nabla \cdot (\alpha_g \rho_g \bar{v}_m Y_{ig}) = \nabla \cdot (\alpha_g \rho_g D_{eff} \nabla Y_{ig}) + S$	
PEM	*Potential (76)*	$\nabla \cdot (\sigma_m \nabla \phi_m) = 0$	$\bar{v}_m = 0$
	Volume fraction of liquid (77)	$\frac{\partial(\alpha_l \varepsilon \rho_l)}{\partial t} + \nabla \cdot (\alpha_l \varepsilon \rho_l \bar{v}_m) + \nabla \cdot \left(\bar{\imath}_m \frac{n_d}{F} M_w\right) = \nabla \cdot \left(-\frac{\rho_l K K_r}{\mu_l} \frac{dp_c}{d\alpha_l} \nabla \alpha_l\right) + S$	
	Gas phases species (78)	$\frac{\partial(\alpha_g \rho_g Y_{ig})}{\partial t} + \nabla \cdot (\alpha_g \rho_g \bar{v}_m Y_{ig}) = \nabla \cdot (\alpha_g \rho_g D_{eff} \nabla Y_{ig}) + S$	

There is therefore a need to separate the two charge contributions related to the electrons (electric potential) in the solid phase ϕ_s and to the protons (electrolyte potential) in the liquid phase ϕ_m.

According to the above description, the electrolyte potential ϕ_m is modelled and defined only in the CLs and in the membrane. More generally, the equations of potentials can be written as:

$$\nabla \cdot (\sigma_s \nabla \phi_s) + R_s = 0 \quad 70$$

$$\nabla \cdot (\sigma_m \nabla \phi_m) + R_m = 0 \quad 79$$

where σ_i is the conductivity of the material, ϕ_i is the potential, while R_i is the source term for the electrochemical reaction, for which the following relationships exist:

$$R_s = -R_m = \begin{cases} -R_{an} \\ R_{cat} \end{cases} \quad 80$$

R_{an} and R_{cat} are the volumetric current densities, described by Butler-Volmer equation:

$$R_{an} = \zeta_{an} j_{an}(T) \left[e^{\frac{\alpha_{an} F \eta_{an}}{RT}} - e^{-\frac{\alpha_{cat} F \eta_{an}}{RT}} \right] \quad 81$$

$$R_{cat} = \zeta_{cat} j_{cat}(T) \left[-e^{\frac{\alpha_{an} F \eta_{cat}}{RT}} + e^{-\frac{\alpha_{cat} F \eta_{cat}}{RT}} \right] \quad 82$$

where ζ_i is the specific active surface area of electrode (m^2 m^{-3}), j_i is the exchange current density described by an Arrhenius law $j_i(T) = j_i^{ref} \exp\left(-E_a / RT(1 - \frac{T}{T_i^{ref}}) \right)$ and takes into account the reference exchange current density j_i^{ref} and the activation energy E_a, while α_i and η_i are the transfer coefficient and the activation overpotential, respectively. Note that α embed the number of electrones n, therefore its value can range between 0 and 2. The source terms R exist only where the reaction occurs, and therefore in the catalytic layer CL, in all other components it is zero and the potential varies linearly with the height (Y-direction).

The set of equations is closed by the definition of the cell potential, taking into account the reversible thermodynamic potential of the electrolysis reaction E_{th}:

$$\eta_{an} = \phi_s - \phi_s - E_{th} \quad 83$$

$$\eta_{cat} = \phi_s - \phi_s \quad 84$$

The current is related to the potential according to ohm's first law $i_s = -\sigma_s \nabla \phi_s$ and $i_m = -\sigma_m \nabla \phi_m$ and overall the law of conservation of the charge must always be valid $\nabla \cdot i = 0$.

Since the reaction leads to the production of hydrogen and oxygen and to the decrease of water amount, in the equation of the volume fraction of liquid phase and of gas phases species the terms S represent the massive source term, related to the volumetric current density, and to the respective molecular weights, according to the expression 86.

$$S = \begin{cases} S_{H_2O} = -\dfrac{M_{w,H_2O}}{2F} R_{an} \\ S_{H_2} = \dfrac{M_{w,H_2}}{2F} R_{cat} \\ S_{O_2} = \dfrac{M_{w,O_2}}{4F} R_{an} \end{cases} \quad 85$$

7.3 Simulated scenario

The case analysed for CFD analysis is the one reported by Jiang et al. [138]. The system is like the one described in section 7.1, for which the quantities shown in Table 15 are identified.

Table 15 Size of the PEMWE cell components. [138] geometry.

	Anode		**Cathode**	
Component	Height [µm]	Width [µm]	Height [µm]	Width [µm]
BP	1500	3000	2500	3000
CH	1000	1500	2000	1500
PTL	500	3000	500	3000
CL	20	3000	20	3000
PEM*	183	3000		

***Nafion™ N117**

The cell is asymmetrical, having a greater height on the cathode side, and is 50 mm long. A simplified representation of it is shown in b. After a preliminary grid dependence analysis, the system resulted to be more subject to the influence of height, i.e. the same direction in which the current flows (Y- direction). In addition, a representation of the mesh is shown in a 6 core desktop (Intel® Core™ i7-10750H CPU @ 2.60 GHz) with 16 GB RAM. The computational time is about 6 hours due to the high number of elements.

The extension of the channels (10 mm) was deliberate, so that at the entrance and exit of the PEMWE there was an already fully developed motion regime. In addition, the dry cathode configuration means that there is only one output channel for hydrogen.

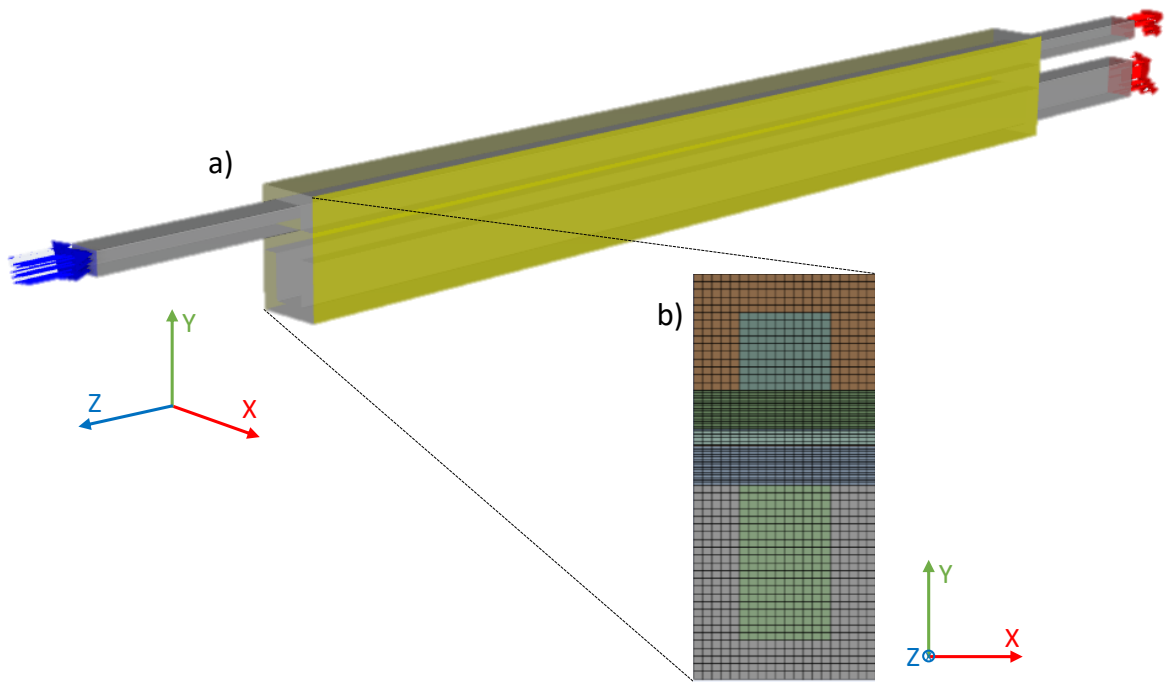

Fig. 60 Representation (a) of the cell (lateral view) and (b) of the mesh (front view). With reference to figure (b) at the top is the anode and at the bottom is the cathode.

The potential is applied at the top of the PEM cell, while at the bottom a zero potential is defined. The side walls are constrained to symmetry, because, if placed far enough from the external walls, the individual channels of an entire flow field are equally conditioned by each other. The velocity of the incoming water is 0.12 m s^{-1}, the system operates at a temperature of 340 K and at atmospheric pressure. All materials have a porosity of 0.6 and the capillarity pressure is estimated as Leverett function.

7.4 Polarization curves and results

The system described has been analysed for different potentials applied in the range 1.23 – 2 V. Fig. 61 shows the polarization curve obtained by Jiang et al. [138] in orange, while in blue is shown the polarization curve of this work. The difference in the potential, within 5 % error, is mainly due to two different models employed, indeed, the Jiang model was entirely built as UDFs (Users Defined Functions), while the one of this work used the Potential/Electrochemistry model, built-in by ANSYS Fluent.

The model seems to predict satisfactorily the literature data, moreover it is perfectly in line with the range of polarization curves reported by Carmo et al. [139] for single-cell PEM electrolysers.

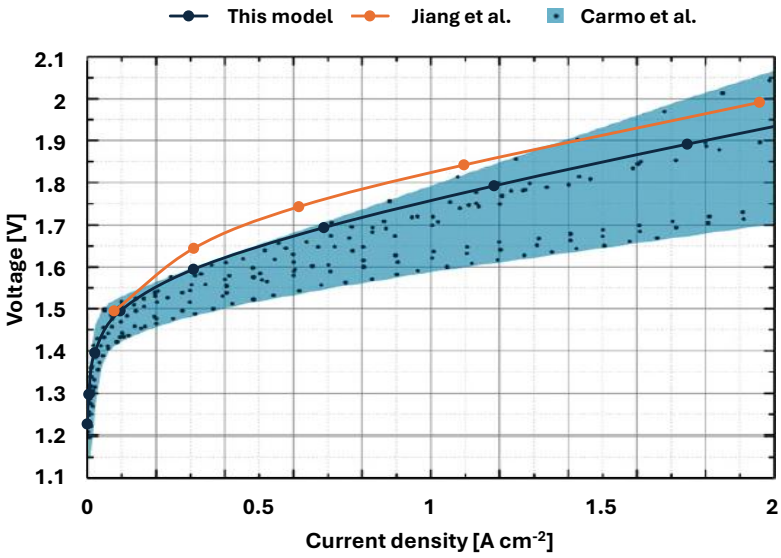

Fig. 61 Polarization curves of model compared to (i) the Jiang model [138] and (ii) the cloud of experimental data reported by Carmo [139].

As also shown by the figure, the current densities in electrolysers are one order of magnitude higher than those seen for electro-membrane processes. In addition, PEMs have nominal operating conditions between 1.5 and 2.0 A cm^{-2}, making the PEMWE much better even than other electrolysers, whose normally do not exceed 1 A cm^{-2} as nominal operating condition.

Since 1.8 V is a typical operating potential for the units, Fig. 62 shows the distribution of the current density magnitude with respect to the frontal view of the cell at 1.8 V. The absence of any visible current distribution with respect to the channels is related to the ultrapure water feed devoid of dissolved ions, a condition that effectively precludes the possibility of charge transport. The current density, as indicated by the thicker harpoons of the vector plot, is more concentrated close to the edges. The symmetry boundary condition applied to the lateral faces maintains the primary vertical direction of the current, precluding anomalous phenomena that could influence its behaviour.

According to the potential model, the membrane does not facilitate the passage of current, which is attributable to the fact that the charge is not transported by electrons (to which this current refers) but rather by H^+ ions.

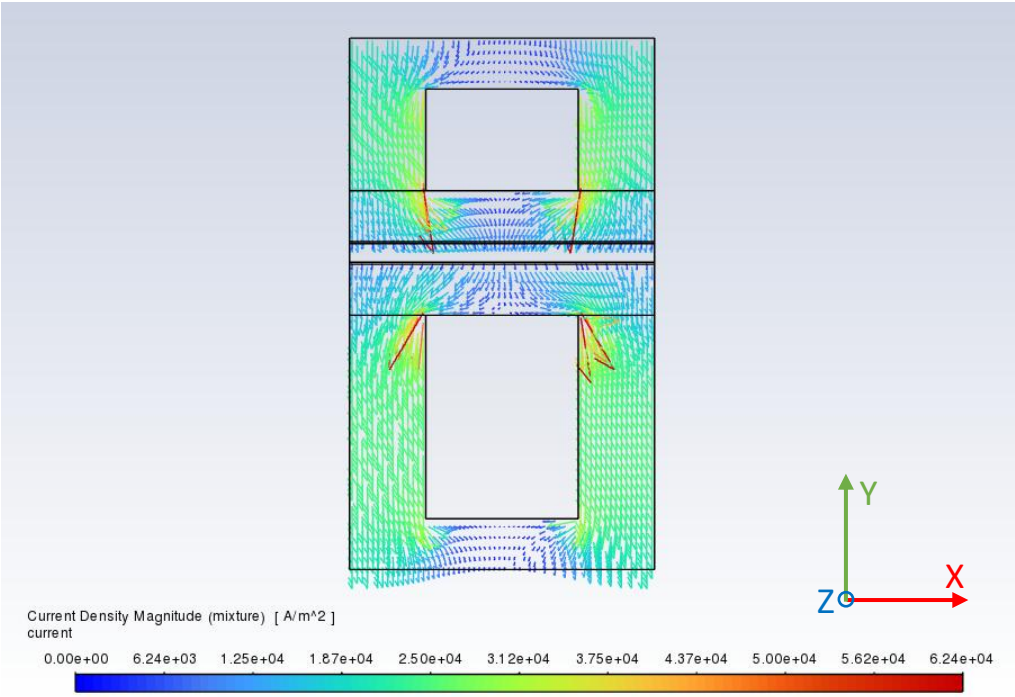

Fig. 62 Vector plot of the current distribution (frontal view) of the cell. The iso-surface is taken in the middle of the Z-length (Z=25 mm). The simulation referred to a potential of 1.8 V.

Conversely, the electric and electrolyte potentials ϕ_s and ϕ_m are reported respectively in Fig. 63a and Fig. 63b. According to what has been said, the cell potential is applied to the anodic upper face, while the bottom is associated with a potential of 0 V. Although the colours of the map fail to highlight the potential gradient that occurs due to the ohmic drops in BPs and PTLs, in reality these decrease by approximately 18 mV. This electric potential drop is very limited, as specially highly conductive materials are chosen (10^4 – 10^7 S m^{-1}), in order to minimize the potential drops associated with them. The majority of the potential drop is attributable to the electrochemical reaction, which is in turn associated with the MEA. It is imperative to incorporate two factors into the thermodynamic potential: (i) the overvoltage resulting from electrode activation, and (ii) the potential drop of the membrane. The overvoltage observed align closely with the data reported in the literature, where the model estimated 0.315 V and -0.004 V for the anode and cathode, respectively. Conversely, the electrolyte potential (Fig. 63b) is estimated to be approximately 0.224 V. As illustrated in the figure, this potential is determined exclusively within the region where there is an ionic transport of charge, commencing from the anodic CL, traversing the PEM membrane, and culminating at the cathode CL.

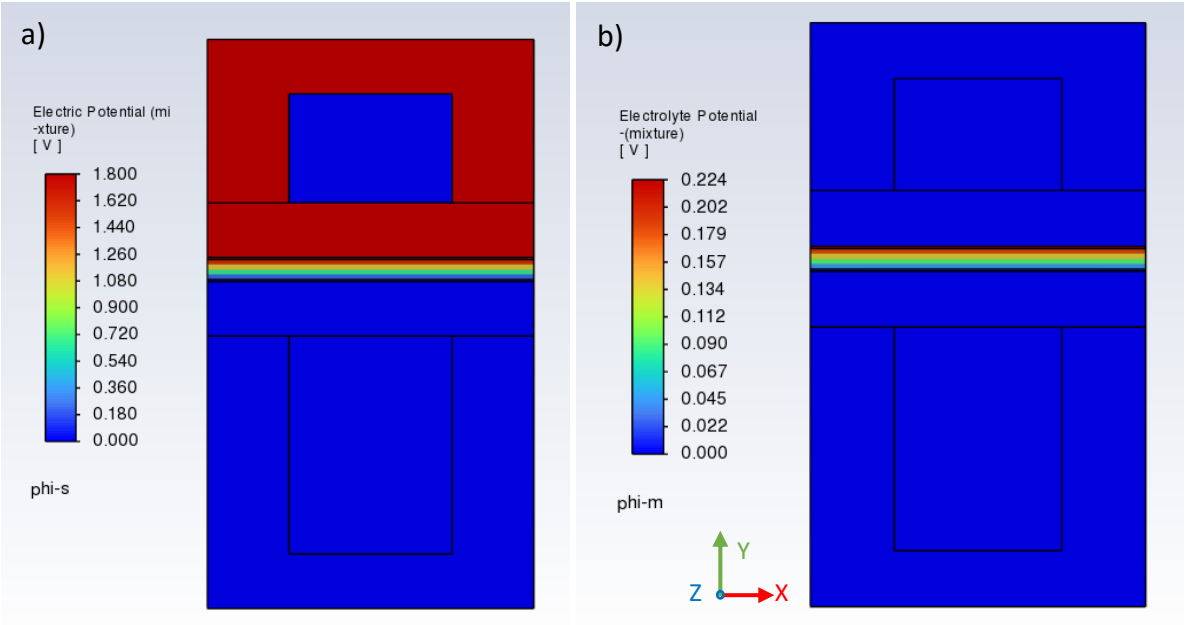

Fig. 63 Contour plot of the (a) electric and (b) electrolyte potential. The simulation referred to a potential of 1.8 V.

The flow regime (velocity) and the volumetric fractions of the gas and liquid phase are reported in Fig. 64. The velocity is illustrated in Fig. 64a, where it is evident that in the anode-side inlet channel, the velocity in the boundary layer is homogeneous and equivalent to 0.12 cm s^{-1}. The 10 mm channel extension facilitates the establishment of a fully formed velocity profile at the cell inlet. As the solution progresses within the cell, an increase in its velocity is observed, a phenomenon that is also attributed to the formation of the gas phase. The gas phase (volumetric fraction) is illustrated in Fig. 64b, where it is evident that this increases along the channel, in accordance with the advance of the reaction. Additionally, the force of gravity exerts an influence along the Y-direction, thereby giving rise to a colour variation extending up to the first 10 mm of the channel's length. According to the force of gravity, the less dense gas phase tends to be located at the top of the channel. Additionally, a slight gas accumulation can be identified in the proximity of the anodic CL, which contributes to an increase up to 0.6 in the volumetric fraction. This phenomenon is likely associated with the continuous reduction in water levels during electrolysis, as evidenced by the volumetric fraction of the liquid phase depicted in Fig. 64c. Conversely, at the cathode, in the absence of oxygen and water fluxes towards the cathode, the volumetric fraction of the unit gaseous phase is indicative of hydrogen presence, according to the dry cathode conditions. Furthermore, given that the cathode inlet is closed, a flow rate is established as the gas accumulates towards the only open outlet, for which there are velocities of about 0.2 cm s^{-1}.

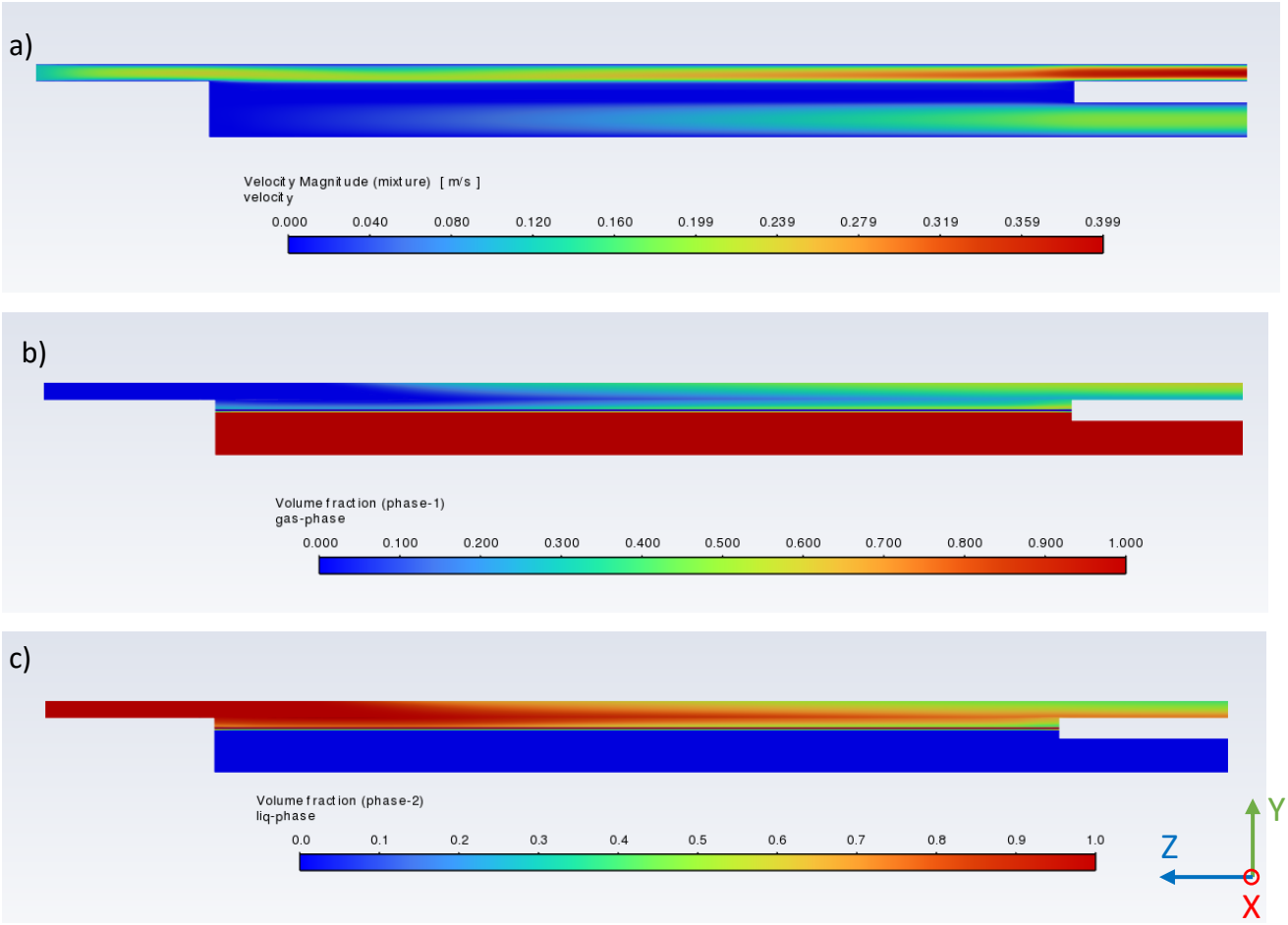

Fig. 64 Contour plot of (a) velocity, (b) gas phase volumetric fraction and (c) liquid phase volumetric fraction. The simulation referred to a potential of 1.8 V. Lateral view of the cell.

7.5 Final remarks

The model used to describe the behaviour of a single cell of a PEM electrolyser was satisfactorily accurate in describing the case analysed, remaining within a 5 % error on the potential estimated by the literature reference. Utilising this model, preliminary analyses were conducted to evaluate the characteristic quantities involved. These comprised (i) electrical quantities, such as current and potentials, and (ii) fluid dynamic quantities, including velocity and volumetric fractions of the multiphase system.

The investigation reported in this chapter is truly preliminary, however, the development of an effective model is the basis of a possible more detailed simulation campaign. Porosity, permeability and capillary pressure on the PTLs are just some of the variables that should be studied more.

Preliminary analysis indicated a moderate influence of these parameters on the overall performance of the electrolytic cell. The identification of the optimal chemical-physical features of the material could serve as starting point for potential manufacturers or researchers seeking to enhance the performance of the unit, both in terms of consumption (and associated potential drops) and in terms of component preservation, showing that there is still room for further investigation.

Moreover, the results that can be obtained from such an analysis are not only of great importance for the improvement of PEM water electrolyser, but also create new possibilities for modelling the electrodic compartments in general, including electro-membrane processes.

8 Conclusion and Final remarks

Hydrogen has been identified as the main alternative to the use of fossil fuels, for a green revolution and a decarbonised society. And for this reason today there is a great deal of attention on its production, both for (i) the improvement of existing technologies and in (ii) the search for new ways for its production.

Electro-membrane processes are defined as those in which a large repetition of ionic exchange membranes are enclosed by two electrodes. The movement of ions within the system (whether forced or spontaneous) leads to an electronic movement towards the electrodes, and since their design, the potential for hydrogen production through them has been investigated. The modus operandi that characterised the entire investigation entailed the (i) preliminary verification of the technical feasibility of the process on laboratory units, and the (ii) subsequent implementation (or readaptation) of technical models capable of describing the unit behaviour. The calibrated and validated models were then associated with equations of an economic nature, allowing a more in-depth estimate of the process costs, identifying production costs and plant profitability.

The first technology studied was (A-)RED. This process involves the exploitation of the mixing energy associated with two solutions of differing salinity, with the aim of converting it into electrical energy. This energy could be entirely transferred to the electrodes to produce hydrogen (RED_{SC}) or reduce the external potential required by the unit in the Assisted case (A-RED). The results of the experimental investigation confirmed the possibility of producing hydrogen at the cathode with a productivity of 0.39 mol h^{-1} m^{-2} in RED_{SC} and with 100 % faradic efficiency, as there are no competitive reactions at the cathode. Furthermore, since the electrodes are far from each other (separate from the cell package), there is also no possibility of crossover phenomena between oxygen and hydrogen, and thus maximum purity of hydrogen.

The results obtained from the associated economic analysis were surprisingly positive, for which a minimum LCOH of 3.2 € kg^{-1}_{H2} was identified for a system operating in short-circuit with a concentrated solution of 300 g L^{-1}. The analysis was performed by considering the values obtained experimentally, and could be further improved by a system optimization, leaving room for possible other investigations. However, LCOH was obtained under particularly favourable economic conditions, such as the low membrane cost (4 m^{-2}_{IEMs}) for which the overall LCOH was greatly

reduced. In addition, the process is particularly affected by low productivity due to the low currents of the unit (10 – 100 A m^{-2}). In RED, one way to increase the current could be to increase the number of repeating units (cell pairs), as the potential generated is directly proportional to them. However, it should be remembered that as the number of cell pairs increases, there is also an increase in dissipations, reducing the performance of the technology. In addition, hydrogen develops exclusively at the cathode, and the limited active surface area further reduces its productivity.

In electrodialysis, on the other hand, it is possible to transfer energy to the system to desalinate the water and in the case of HED, there is also the intention to produce hydrogen at the cathode. Electrodialysis enables currents of a magnitude slightly greater than that of the RED to be used, thereby enhancing hydrogen production. Moreover, the insertion of additional electrodes shared between the cell pairs of the unit is a viable option without compromising the freshwater yield and allowing for a significant increase in hydrogen productivity.

The HED system has been studied both for the desalination of a brackish water BW and for the desalination of seawater SW. For the BWHED system, a 1 x 1 m^2 stack consisting of 1000 cell pairs (ED references) was considered, to which electrodes shared between the cell pairs were added. The analysis showed that the case, for which there is the highest production and the lowest cost of hydrogen, coincides with the scenario for which there is the maximum number of electrodes and only one cell pair between each of them. Assuming that water is always produced at the same cost (identified as 0.14 € m^{-3}_{w} for the ED reference case) a LCOH of 3.43 € kg^{-1}_{H2} was obtained from the analysis. On the other hand, if water production cost did not change, but hydrogen was sold at a plausible price of 8 € kg^{-1}_{H2}, an NPV of 2.7 M€ could be obtained at the end of the lifetime of the unit. A value that could increase significantly if the modularity of the technology is taken into account.

Worldwide, there are several industrial applications of BW desalination with ED (e.g. EDR plant of Ebrera, Spain). However, SWED is not used industrially due to the high energy costs and high costs of ion exchange membranes, which make the technology much less advantageous than RO. The absence of an industrial case consequently also makes it very difficult to choose a water desalination chain, for which the desalination cannot be carried out with a single stage due to the limit current. For this reason, a multi-stage configuration was adopted with the possibility of implementing a recirculation of the solution (Feed&Bleed). Initially, the most economical plant proposal for desalination was evaluated, and subsequently, the same analysis was applied as for the BWHED

case, with the maximum number of electrodes being inserted. The analysis showed that desalination cost for the SWED is 1.57 € m^{-3}_{w}, a very high value compared to that of RO. However, the possibility of simultaneously producing hydrogen could reduce the costs of desalination in SWHED. In fact, it has been seen that if hydrogen were sold at 8 € kg^{-1}_{H2}, the cost of water would be totally repaid by hydrogen. Whereas, for a desalination cost equal to that of RO (1 € m^{-3}_{w}), hydrogen must be sold at 6.97 € kg^{-1}_{H2}. These values are higher than those of the BWHED case, yet still acceptable, leaving much room for further investigation. In addition, the costs obtained are also related to the choice of plant design and since not a fully optimization has been carried out in this regard, there is a whole range of possible configurations that can be examined to further reduce costs.

In general, coupling ED with hydrogen production is not particularly innovative, as this normally occurs in standard ED units, although the amount of hydrogen produced is negligible. The idea of emulating traditional electrolysers by adding electrodes between the cell packages means that hydrogen production can be increased up to a level that is cost-effective.

Among electro-membrane processes, an emerging technology is EDBM, for which it is possible to produce chemicals (acid and base solutions) and reduce the salinity of a salty solution. The EDBM can also have higher current densities than the ED, reaching up to 1000 A m^{-2}. With a view to producing hydrogen, it is evident that the unit is well-suited to this purpose, thanks to the higher current density and the additional possibility of adding electrodes.

The EDBM unit used in the economical investigation was a commercially available pilot scale unit of 34.5 x 45.4 cm^2 for which 100 triplets collected in blocks of 20 were considered to limit the effect of eddy currents. The unit was analysed for different current densities, showing a minimum in the LCOB of 0.23 € kg^{-1}_{NaOH} at 500 A m^{-2}. The addition of electrodes between the triplets greatly increases the production of hydrogen and also in this case the lower cost of the HEDBM unit is associated with the greater number of electrodes inserted. Furthermore, the lowest costs of hydrogen occur when working at a current density of 500 A m^{-2}, as for the LCOB. A cost of 5.73 € kg^{-1}_{H2} has been identified for this system. While for the single unit an NPV of half a million of euros was found if the NaOH is sold at 0.4 € kg^{-1}_{NaOH} and hydrogen at 8 € kg^{-1}_{H2}. These values were obtained under very conservative economic conditions, based mainly on the current costs of the technology, but in a futuristic perspective, a reduction of the capital expenditure would significantly reduce the costs and further increase the profitability of the technology.

The analysis carried out in this thesis work was aimed at investigating different membrane technologies for the production of hydrogen. The results that emerged from the analysis are promising. First of all, it is possible to produce hydrogen with these technologies in a satisfactory way, maintaining high faradic efficiencies and excellent purities of the products in the gas phase. Models of the technologies were enriched with electrode modelling equations so that the electrolysis reaction of water could be taken into account. The models were validated and showed error always below 10 % compared to the experimental data. In addition, techno-economic analyses revealed the need to increase the active area of the electrode and the process currents. Adding electrodes or employing processes that notoriously work at higher current densities certainly leads to a benefit both in terms of hydrogen production and cost, keeping the productions that would normally be in the unit unchanged. These technology can therefore be used for the simultaneous production of hydrogen and chemicals/freshwater with the possibility of a further gain of the process. The significance of these results may be a breakthrough in the desalination field for the ED, which still has limitations for its large-scale use and for the EDBM as emerging membrane technology.

To make it easier to compare the units studied in this work, Table 16 summarises and compares the main technical and economic information about the processes. The information for AWE electrolysers is also included to allow for comparison with the reference industrial electrolyser. Each technology has its pros and cons compared to the others. In technical terms, only HEDBM can match the nominal current density of AWEs, while H(A-)RED and HED involve current densities being even one order of magnitude smaller. Voltages, both when assumed and when calculated using experimental data, are perfectly within the range of a single cell of an electrolyser. The voltage behaviour in the H(A-)RED case differs due to the specific electrode solutions used, which lower the thermodynamic potential from 1.23 V to 0.6 V. The technologies studied, which are made up of IEMs, do not allow for very high temperatures. These have been studied assuming a temperature of 25 °C. However, temperatures of up to 55 – 60 °C can be used to help diffusion and reaction at the electrodes. Note that further higher temperatures can damage the membranes. On the contrary, AWE have no membranes assembled (they use porous diaphragms), so they do not suffer from any temperature issues and can operate at temperatures of up to 90 °C, although higher temperatures lead more water to evaporate. All technologies operate at atmospheric pressure and it is not recommended to operate under pressure due to the mechanical membranes resistance. AWEs can

also operate under pressure up to 30 bar, but this can cause crossover phenomena, which can reduce the purity of the gases.

Table 16 Comparison of the technologies studied in this work and the alkaline water electrolyser AWE

	AWE **[12]**	H(A-)RED	BW HED	SW HED	HEDBM
Nominal current density [A m^{-2}]	200 - 800	20 - 150	~150	~200	250 - 1000
Voltage [V]	1.3 - 3	0.6	1.7	2	2.23
Operating temperature [°C]	70 - 90	25 (less than 60)	25 (less than 60)	25 (less than 60)	25 (less than 60)
Cell pressure [bar]	< 30	1	1	1	1
HSEC [kWh Kg^{-1}_{H2}]	47 - 66	0 - 94	~57	~103	~115
Stack unit size [kW]	1000	0 – 0.5	~310	~344	~67
Electrode/active membrane area [m^2]	1 – 3	1	1	1	0.16
Cell repetition	Up to 1000	1	1000	500	200
Number of cell pair/triplets	-	20	1000	500	200
Capital cost [€ kW^{-1}]	270	2156	1250	424	739
Membrane cost [€ m^{-2}_{IEMs}]	-	4	25	25	114 (580 € m^{-2}_{BPM})
LCOH [€ kg^{-1}_{H2}]	4-8	3.2 - 13	3.43	6.42	5.73
Co-product	Oxygen	Oxygen Energy (if RED)	Oxygen Water	Oxygen Water	Oxygen Acid (HCl) Base (NaOH) Water

The typical HSEC of an electrolyser is between 47 and 66 kWh kg^{-1}_{H2}, depending on how efficiently it works. Concerning the electro-membrane processes, the HSEC increases moving towards the right

of the row, as the HSEC takes into account the energy needed for *other* processes, such as desalination or acid and base production (see Fig. 65). The exception is the H(A-)RED, which depends on the operation mode (short-circuit or assisted): H(A-)RED can have zero or significantly higher HSECs. In the short-circuit operation mode HREDsc, the energy is entirely provided by the salinity gradient, on the other case (i.e. assisted operation mode, HARED) the energy is partially provided by an external supplier. A noticeable detail is the stack unit size of 0.5 kW, which reflects its design as a single unit comprising a single cathode. In contrast, significantly higher power outputs, and consequently greater hydrogen production, are achieved in the HED and HEDBM configurations, where multiple electrodes are assembled.

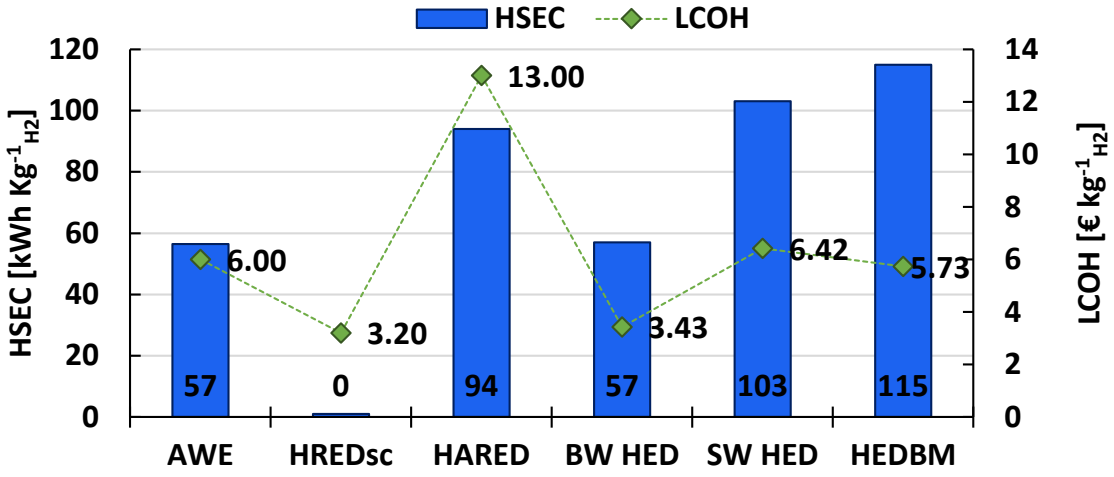

Fig. 65 Histogram of the HSEC and LCOW for all the technologies analysed.

Capital costs are clearly affected by the addition of ion exchange membranes. For the H(A-)RED system, the cost is 2156 € kW^{-1}, and for the BW HED system, the cost is 1250 € kW^{-1}. Lower costs have been found for the other technologies due to the technical choices adopted (lower number of cell pairs or active membrane area). These costs result certainly higher than those for AWE, due to the cost of membranes, spacers and auxiliaries. Lastly, the LCOH obtained (Fig. 65) from the economic analyses are perfectly in line with those of common electrolysers, which promotes, albeit preliminarily, the proposed technologies. In addition, it should be noted that the production of co-products can help the economics of the process and represent another source of income for the plant.

This thesis aimed to study these technologies from technical and economic perspectives, evaluating their potential as alternatives for simultaneously producing hydrogen in the relevant sector. The results obtained are quite promising and suggest that adopting these technologies in a

plant is feasible. However, if the ultimate goal is to produce hydrogen exclusively, much more efficient technologies have been designed specifically for this purpose. Nevertheless, when it comes to revamping existing plants, the proposed technologies have been identified as valid alternatives. It should be noted that the experiments were conducted on a setup that was not optimised for hydrogen production. Consequently, the technical models did not simulate the best possible conditions. For instance, no CFD study was conducted on the fluid dynamics of the electrode compartments; consequently, the spacers and other design components were not optimised to effectively remove bubbles from the system. Therefore, there is considerable room for improvement in the observed technologies, which could further enhance the economic efficiency of the process.

The analyses performed in this study are preliminary and there is large room for further specification and improvement. However, the encouraging profitability results are promising. They justify additional scientific efforts being devoted to more detailed analyses of the coupling of electro-membrane processes with hydrogen production, suggesting these technologies as promising methods of simultaneously producing freshwater or chemicals and green hydrogen.

Appendix

Appendix I: Model equations

Model equations which were not reported in the main text for the sake of brevity are included in the following table:

Table 17 Model equations

CFD correlations			
Sherwood correlation (Gurreri et al., 2014; la Cerva et al., 2017)	$Sh_{sol}(k) = (-1.48x10^{-7}Re^5 + 3.74x10^{-5}Re^4 - 3.25x10^{-3}Re^3 + 0.112Re^2 + 0.135Re + 6.95)(Sc/568)$	-	(A.1)
Reynold correlation	$Re(k) = \frac{\rho_{sol}\, u_{sol}\, (2\delta_{sp,sol})}{\mu_{sol}}$	-	(A.2)
Void velocity	$u_{sol} = \frac{v_{sol}}{(1 - f_{sp})}$	m·s^{-1}	(A.3)
	where f_{sp} is the relative spacer volume assumed 0.18		
Schimdt correlation	$Sc(k) = \frac{\mu_{sol}}{\rho_{sol} D_{sol}}$	-	(A.4)
Polarization factor[1] of concentrated sol.	$\theta_H(k) = \frac{c_H^{int}}{C_H^b} = \left[1 - \frac{J_{salt}\,(2\delta_{sp,sol})}{Sh_H D_H c_H^b}\right]^{sgn(J_{salt})}$	-	(A.5)
Polarization factor[1] of diluted sol.	$\theta_L(k) = \frac{c_L^b}{c_L^{int}} = \left[1 + \frac{J_{salt}\,(2\delta_{sp,sol})}{Sh_L D_L c_L^b}\right]^{sgn(J_{salt})}$	-	(A.6)
Pressure Drop	$\Delta p_{sol}(k) = \frac{1}{2} f_{fr,\ sol} \frac{\rho_{sol} u_{sol}^2 \Delta x}{2\delta_{sp,sol}}$	Pa	(A.7)
Friction factor (Gurreri et al., 2014; la Cerva et al., 2017)	$f_{fr,\ sol} = (5.71x10^{-5}\, Re^2 + 2.64x10^{-2}\, Re + 6.6)\ 96/Re$	-	(A.8)
Permselectivity	$\alpha_{IEM} = \frac{t_{IEM}^{counter} - t_{SOL}^{counter}}{t_{SOL}^{co}}$	-	(A.9)
		Transport Phenomena	
Total salt flux	$J_{salt}(k) = J_{mig}(k) + J_{dif}(k)$	$mol \cdot m^{-2} \cdot s^{-1}$	(A.10)
Migrative salt flux [2]	$J_{mig}(k) = [t_{CEM} - (1 - t_{AEM})] \frac{i(k)}{F}$	$mol \cdot m^{-2} \cdot s^{-1}$	(A.11)
Diffusive salt flux	$J_{dif}(k) = \frac{2\, D_{NaCl}}{\delta_m} \left[c_H^{int}(k) - c_L^{int}(k)\right]$	$mol \cdot m^{-2} \cdot s^{-1}$	(A.12)

Interface concentration	$c_{sol}^{int}(k) = \theta_{sol}(k)\, c_{sol}^{b}$	$mol \cdot m^{-3}$	(A.13)
Water total flux	$J'_w(k) = J_{osm}(k) - J_{e-osm}(k)$	$m^3 \cdot m^{-2} \cdot s^{-1}$	(A.14)
Osmotic water flux	$J'_{osm}(k) = 2L_p(\Pi_H - \Pi_L)$ where the water permeability $L_p = 6.24$	$m^3 \cdot m^{-2} \cdot s^{-1}$ $mL\ (bar \cdot h \cdot m^2)^{-1}$	(A.15)
Electro-osmotic water flux	$J'_{e-osm}(k) = n_h\, J_{tot}(k) \frac{PM_w}{\rho_w}$ where the number of hydration of salt $n_h = 7$	$m^3 \cdot m^{-2} \cdot s^{-1}$	(A.16)
Osmotic pressure	$\Pi_{sol} = 2R_g T c_{sol}^{int} \varphi_{sol}$	Pa	(A.17)

[1]the transport number of the ion in the IEMs can be linked with the permselectivity of the membrane using the A.9 where the terms $t^{counter}$ and t^{co} represents the transport number of the counter-ion and co-ion in solution.

Appendix II: Solution properties

Salt diffusivity D :

The diffusivity is based on Vitignano and Lyons equation (Vitignano & Lyons, 1955):

For $c < 0.4$ $\quad \mathrm{D} = 1.47\mathrm{x}10^{-9} + 1.3\mathrm{x}10^{-10}\exp(-c/70)$ (A.24)

For $c > 0.4$ $\quad \mathrm{D} = -2.87262\mathrm{x}10^{-21}c^3 + 2.0321\mathrm{x}10^{-17}c^2 - 8.44113\mathrm{x}10^{-15} + 1.4705\mathrm{x}10^{-9}$ (A.25)

where c is the concentration of the salt solution expressed in mol·m^{-3}. Diffusivity has m^2·s^{-1} dimension.

Conductivity σ:

The conductivity correlation used in the Islam modified equation (Islam et al., 1991):

$$\sigma = \left[\Lambda_0 - \frac{B_1\sqrt{c\prime}}{1+Ba_0\sqrt{c\prime}}\right]\left[1 - \frac{B_2 F\sqrt{c\prime}}{1+Ba_0\sqrt{c\prime}}\right]\cdot c' \quad (A.26)$$

where for a single-charged ion (as NaCl) is: $B = 50.29x10^8/\varepsilon_0 T^{0.5}$, $B_1 = 92.5/\mu_0\sqrt{\varepsilon_0 T}$, $B_2 = 8.204x10^5/\sqrt[2]{(\varepsilon_0 T)^3}$, $F = (\exp(0.2929B\sqrt{a_0}) - 1)/0.2929Ba_0\sqrt{c}$. Λ_0 is the equivalent conductance of the aqueous NaCl solution (equal to 115 S·cm^2 at 25°C), μ_0 and ε_0 are the viscosity and the dielectric constant of water, T is the temperature and c' is the molar concentration of salt in mol·dm^{-3}. The conductivity so calculated has dimension of mS·cm^{-1}. The equation is referred to a NaCl aqueous solution and the advantages of using this correlation is the predictive ability to describe a wide range of salt concentrations.

Activity γ and osmotic ϕ coefficients:

For a binary system of singly charged ions, according to the Pitzer virial equation (Partanen, 2012) the osmotic coefficients became:

$$\varphi - 1 = -A_1 \frac{\sqrt{m}}{1+ b'\sqrt{m}} + m\, B^{\varphi} + m^2\, C^{\varphi} \quad \text{(A.27)}$$

$$B^{\varphi} = \beta^{(0)} + \beta^{(1)} e^{-\alpha\sqrt{m}} \quad \text{(A.28)}$$

where m is the molality, A_1 is the modified Debye-Huckel constant (equal to 0.3915 at 25°C), α and b' are fixed constant equal respectively to 2 and 1.2 (kg·mol^{-1})$^{0.5}$ meanwhile $\beta^{(0)}$, $\beta^{(1)}$ and C^{φ} are functions of the electrolyte and for a NaCl aqueous solution are equal to 0.06743 , 0.3301 and 0.00263 respectively.

The activity coefficient can be obtained as:

$$\ln \gamma_{\pm} = -A_1 |z_+ z_-| \left[\frac{\sqrt{m}}{1+ b'\sqrt{m}} + \frac{2}{b'} \ln\left(1 + b'\sqrt{m}\right) \right] + m\, B^{\gamma} + m^2\, C^{\gamma} \quad \text{(A.29)}$$

where $|z_+ z_-|$ is the product between the valence of cations and anions, respectively. It is equal to 1 for NaCl. Meanwhile B^{γ}, C^{γ} are adjustable parameters and can be calculated as follow:

$$B^{\gamma} = 2\beta^{(0)} + 2\beta^{(1)} \left[1 - \left(1 + \alpha\sqrt{m} - \frac{\alpha^2}{2} m\right) e^{-\alpha\sqrt{m}}\right] \frac{1}{\alpha^2 m} \quad \text{(A.30)}$$

$$C^{\gamma} = \frac{3}{2} C^{\varphi} \quad \text{(A.31)}$$

Appendix III: Electrodes polarization

Between the two configurations ED and (A-)RED, the only change that occurs is the polarity of the electrodes, for which the cathode is polarized negative in the case of ED and positively in the case of (A-)RED. In RED, the cathode polarizes positively as a result of the movement of ions in the system, and this basically depends on which solution (diluted or concentrated) is placed as the first compartment of the first cell (i.e. the one immediately adjacent to the electrodes). In fact, it is the direction of the positive charges, in accordance with the spontaneous migration of these by gradient, that defines an accumulation of charge in the electrode compartments, which will lead to a positive polarization of one electrode (cathode) and to the negative polarization of the other (anode). In a generic unit in which reversible redox pairs are used, in order to produce energy, it does not matter who is the anode and who is the cathode. But in our system, however, in which there are two distinct electrode solutions (HCl and NaOH) specifically designed to reduce the redox potentials of the electrolysis reaction, it is essential to know a priori who is the cathode and vice versa who is the anode. Furthermore, with reference to the Pourbaix diagram of chlorine Fig. 2b, if the electrode immersed in the HCl solution became the anode, the production of gaseous Cl_2 would

be favoured, a gas that is particularly corrosive to the materials of the system and dangerous to human health, in addition to the fact that this would be competitive with oxygen, compromising its quality. For this reason, in order to define the cathode as the electrode immersed in HCl solution, the dilute solution is the one immediately adjacent to it. In A-RED, in order to maintain the same directions of the flows, and therefore to improve the transport of salts from the concentrate to the diluted, the power supply (PS) must be connected in series to the stack (which in fact, also acts as a current generator). For this reason, the negative of the PS must be linked to the positive of the stack, i.e. the cathode.

In ED the situation becomes complicated. The simplest case (and also the traditional one) is that the system is fed with the same feed. In this case there is no polarization of the electrodes, and therefore the negative of the PS negatively charges the cathode and the desalination occurs. In the extreme case of solutions that instead have different salinity, their order determines the ED or A- RED mode, therefore, assuming that the diluted is the solution adjacent to the electrodes (as in the suggested case RED), it is already known who is the cathode and vice versa. Therefore, having to reverse the polarity, the positive of the PS must be connected to the cathode and according to Fig. 6, only when the applied potential is greater than the electromotive force of the system, i.e., at the OCV, can there be a reversal of the polarities, thus the unit work in ED. It is also interesting to note that in the case of solutions with different salinity, part of the initial energy must be given to guarantee a migrative flux greater than the diffusive one. Indeed, for low potential, there is no real desalination of the diluted stream, but an attempt will be made to counter-balance the spontaneous diffusive flux that would lead the salt to go from the concentrated to the diluted. At the equality of the 2 fluxes (neglecting all the other dissipative fluxes), although energy is transferred to the system, the two output concentrations will be equal. The greater the potential, the greater the migratory flux compared to the diffusive one, and desalination can finally take place.

Appendix IV: Limit current estimation methods

The limit current for electrodialysis is defined as the current for which there is a problem of mass transport close to the membrane interface. Indeed, the migrative flux acts as an agent that consumes ions concentration at the interface, reducing it compared to the bulk of the solution. The higher the current, the higher the rate of consumption, and consequently, when the current for which the concentration at the interface becomes zero is reached, the limit current has been gotten.

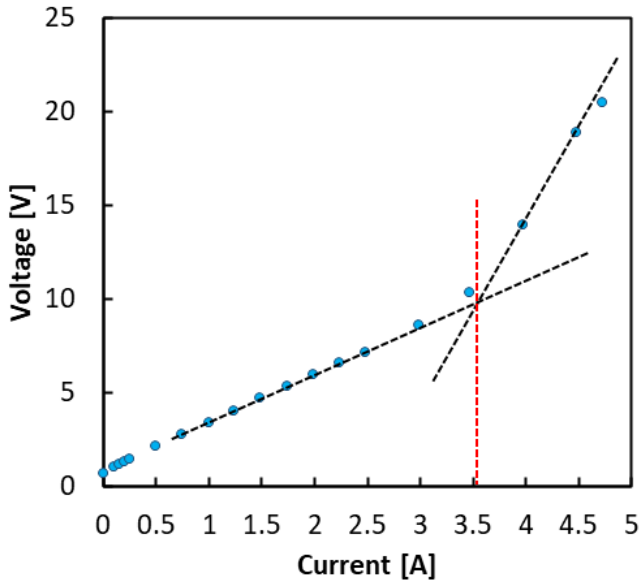

Fig. 66 Isaacson and Sonin graphic method for the determination of the current limit of an ED unit.

Several in the literature have tried to give a mathematical definition of the limit current [140,141] or to identify it through semi-empirical correlations [142–144]. In any case, its prediction is still complicated, and ad-hoc experiments are the best and fast approach to evaluate it. The polarization curve of the system is a very powerful tool, and from it, the limit current can be identify. Among the different methods for the identification of the limit current, the Isaacson and Sonin method [145] was used in the experimental treatment in 5.1.2.

The graphical method consists in diagramming the trend of the voltage as a function of the current, and tracing two tangents that approximate the trend of the experimental points when occurs the exponential behaviour. By the reading on the abscissa, the limit current value can be calculated at the intersection of these two lines. An example of Isaacson and Sonin's method is shown in Fig. 67. From the analysis in the figure, a limit current of about 3.53 A emerges. As industrial custom and for safety reason, the 85% of the limit current is chosen as the maximum current to be processed, and therefore a current of 3 A would be employed in the experiment.

Appendix V: Linear sweep voltammetry

Experimental set-up:

Linear voltammetry (LSV) tests are performed to study the electrochemical behaviour of the electrodes and obtain kinetic parameters such as η overvoltage, the i_0 exchange current density and

the standard potentials of the reactions. These tests are made inside a glass cell into which the electrodes are immersed in the electrodic solution.

The measurement system consists of three electrodes: (i) Working electrode, where the reaction of interest takes place, a Ti mesh substrate with Pt/Ir oxides (MMO – Mixed Metal Oxide) of 0.184 cm^2, (ii) Platinum electrode, used as a counter electrode to close the electrical circuit and (iii) Calomel electrode, used as a reference.

The measurements are carried out using a potentiostat, which allows a potential to be applied to the working electrode; the circulating current is then recorded in the system corresponding to the applied voltage. The entire setup is positioned inside a metal Faraday cage to shield the system from external electromagnetic interference and thus ensure greater accuracy of the measurement made.

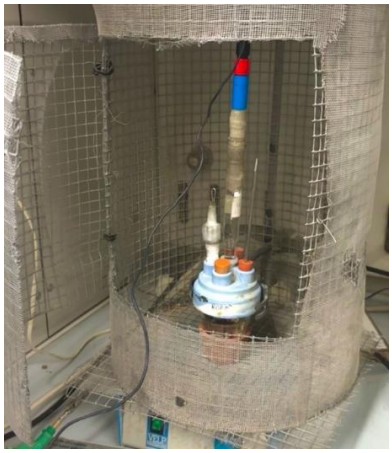

Fig. 67 Set-up for the LSV test

The tests were performed for each of the operating conditions in which the electrodes operate: both the anode and the cathode were tested in basic conditions (1M of NaOH), while only the cathode was analysed in an acid media (1M of HCl). Since the acid media at the anode must be avoided due to the possible formation of chlorine gas due to the environment rich in chlorides.

During the tests, a cell with a perforated cap was used in order to allocate the electrodes. The electrode solution inside the cell is kept in constant agitation by a magnetic stirrer, which favours the outgoing of the gas bubbles developed in the cell. The system is enclosed within a Faraday cage to isolate the system from any electromagnetic disturbances. Each electrode is connected to an AUTOLAB potentiostat - Metrohm (PGSTAT1, Utrecht, The Netherlands), and the voltage range analysed was up to 2.15 V vs SCE with a scan rate of 3 mV s^{-1} , which allowed LSVs to be performed. A figure of the set-up is shown in Fig. 67. Each test was carried out 3 times for the reproducibility and validity of the data obtained

Data analysis:

From the study of LSVs it is possible to obtain the parameters of the Tafel line (eq. 11) following a reprocessing of the data. The potentiostat applies gradually higher voltage to the system and records the corresponding values of current circulating in the system. The voltage is then measured at the reference electrode, i.e., the Calomel electrode. The values in Fig. 68a are SCE voltage values (Standard Calomelan Electrode). Adding to these potential, the calomel potential with respect to hydrogen (0.242 V SHE), all values are reported to the hydrogen reference. By making the logarithm of the current density, it is possible to obtain the graph in Fig. 68b, representing the polarization curve of the electrode. However, this value takes into account all the terms of equation 10, therefore, neglecting the ohmic component (very conductive solution and small distance between working and counter electrode) and subtracting the corresponding thermodynamic potential, the remaining overvoltage can be plotted against the Log(i) as shown in Fig. 68c. By placing at low fields, i.e., in a portion sufficiently distant from the change in slope indicative of mass transport, and making a linear regression of these points (line in red) it is possible to obtain the corresponding Tafel equation.

Several useful information can be obtained from the coefficients of the Tafel line. For example, its slope, generally expressed as mV dec^{-1} represents how many mV of potential drop would occur for a base ten (decade) increase in the current, or again from the intercept it is possible to calculate the value of i_0, the exchange current density of the reaction, which is indicative of how fast a redox reaction is. In addition, it is possible to calculate the value of α, the Butler-Volmer barrier coefficient. On the latter, several sources [146,147] indicate that the number of electrons that is representative of the BV is relative to the actual reaction that takes place in the charge transfer step and is not necessarily equal to the number of electrons of the global reaction. This means that the α parameter (which can only be estimated by the knowledge of n), is not a certain parameter. In this study, it is assumed that the number of electrons involved for the estimation of α is, indeed, that of the global reaction (n=2).

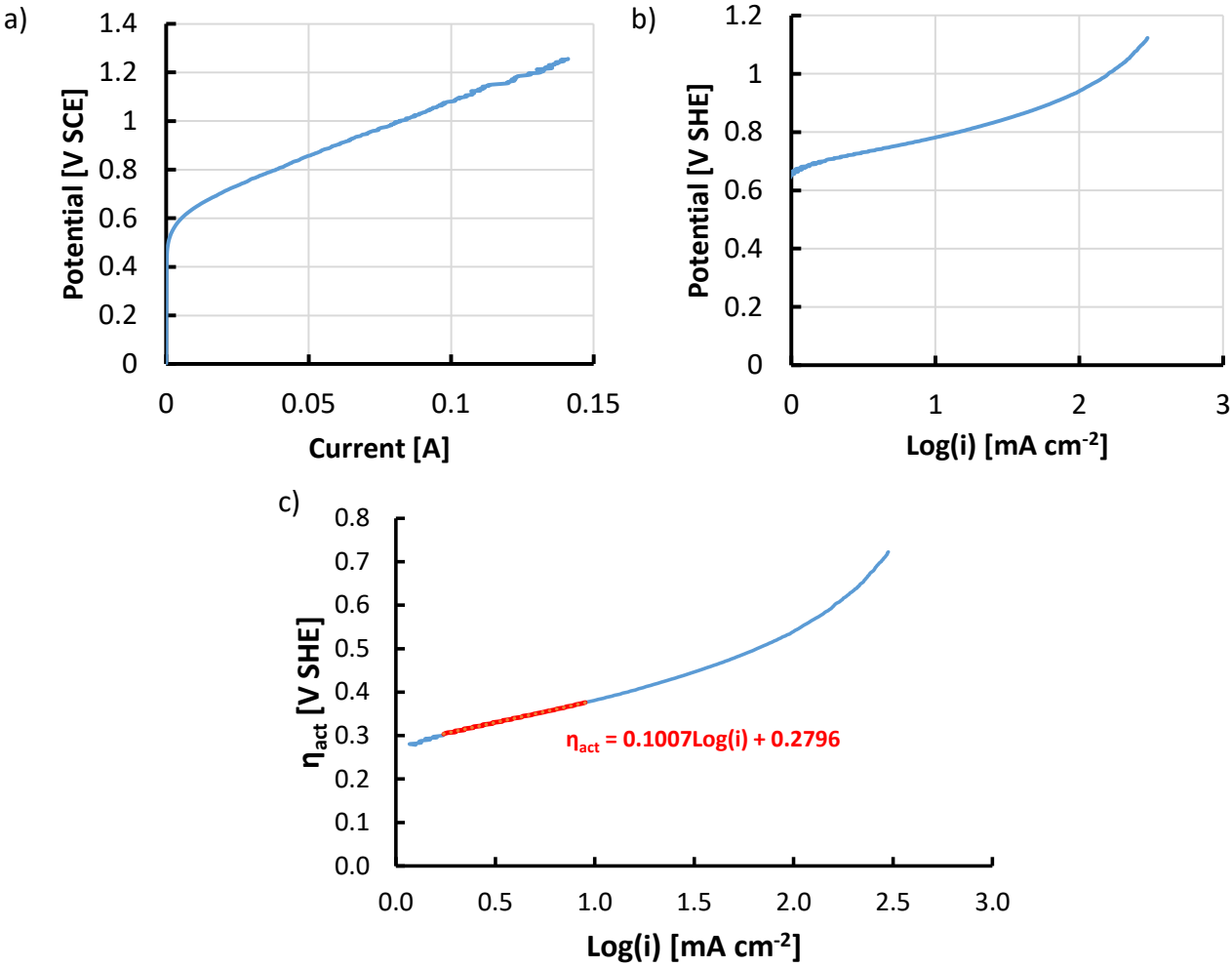

Fig. 68 (a) voltage vs current density, (b) voltage vs Log(i), (c) overvoltage vs Log(i)

Table 18 shows the parameters relating to the three operating conditions studied.

Table 18 Kinetic parameters derived from LSV tests

	a=-b*Log(i₀)	***b [V dec⁻¹]***	***b [V dec⁻¹]***	***i₀ [A cm⁻²]***	***α***
ANODE NaOH	**0.2796**	0.1007	100.7	1.67E-06	0.696495
CATHODE HCl	**-0.0724**	-0.0802	-80.2	-8.02E-02	0.7364105
CATHODE NaOH	**-0.22895**	-0.11273	-112.725	9.31E-06	0.524317

List of ISI publications

Pellegrino A., Campisi G., Proietto F., Tamburini A., Cipollina A., Galia A., Scialdone O., Micale G., «Hydrogen-Electrodialysis with Bipolar Membrane (H-EDBM): First experiments and preliminary economic evaluation» Desalination, (Dec 2024), DOI: 10.1016/j.desal.2024.118169

Campisi G., Pellegrino A., Tamburini A. and Micale G., «Techno-economic modelling of a hydrogen-electrodialysis (HED) unit for the simultaneous production of freshwater and hydrogen». Desalination 587, Jul 2024, 117920. DOI: 10.1016/j.desal.2024.117920

Campisi G., Cosenza A., Randazzo S., Tamburini A., and Micale G., «An Innovative Plant for the Desalination and Treatment of Produced Waters». In: Mannina, G., Ng, H.Y. (eds) Frontiers in Membrane Technology. IWA-RMTC 2024. Lecture Notes in Civil Engineering, vol 525. Springer, Cham. DOI:10.1007/978-3-031-63357-7_34

Campisi G., Pellegrino A., Cipollina A., Tamburini A., Micale G., «Producing Hydrogen and Fresh Water from Brackish Water Desalination via Electrodialysis», Chemical Engineering Transactions, 105, 103-108 DOI:10.3303/CET23105018

Pellegrino A., Campisi G., Proietto F., Tamburini A., Cipollina A., Galia A., Micale G., and Scialdone A., «Green hydrogen production via reverse electrodialysis and assisted reverse electrodialysis electrolyser: Experimental analysis and preliminary economic assessment». Int. J. of Hydrogen Energy 76, Jan 2024, 1-15, DOI: 10.1016/j.ijhydene.2023.12.273

Campisi G., Cosenza A., Randazzo S., Tamburini A., and Micale G., «Economic Analysis of an Innovative Scheme for the Treatment of Produced Waters». Chemical Engineering Transactions, 105, 367-372 DOI:10.3303/CET23105062

Pellegrino A., Campisi G., Proietto F., Tamburini A., Scialdone A., and Micale G., «Electro-Membrane Processes for the Green Hydrogen Production». Chemical Engineering Transactions, 105, 85-90 DOI:10.3303/CET23105015

Campisi G., Cosenza A., Giacalone F., Randazzo S., Tamburini A., and Micale G.. «Desalination of Oilfield Produced Waters via Reverse Electrodialysis: A Techno-Economical Assessment». Desalination 548, Feb 2023, 116289. DOI:10.1016/j.desal.2022.116289

Campisi G., Cosenza A., Randazzo S., Tamburini A., Micale G., «Salinity Reduction of Real Produced Waters via Assisted Reverse Electrodialysis», Chemical Engineering Transactions 99, May 2023, 445-450, DOI:10.3303/CET2399075

Cosenza A., Campisi G., Giacalone F., Randazzo S., Cipollina A., Tamburini A., and Micale G. «Power Production from Produced Waters via Reverse Electrodialysis: A Preliminary Assessment». Energies 15, Jun 2022, 4177. DOI:10.3390/en15114177

Abstracts at international conferences

Campisi G., Sorrenti A., Bosco Mofatto P.M., Cosenza A., Randazzo S., Corsino S.F., Capodici M., Torregrossa M., Tamburini A., and Micale G., "Desalination and treatment of oilfield produced waters", ICHEAP17 (2025)

Cosenza A., Campisi G., Ilardo G., Randazzo S., Lo Brutto R., Tamburini A., Cataldo S., Muratore N., Pettignano A., and Micale G., "Assisted reverse electrodialysis for salinity reduction of produced waters", E2DT2025 (2025)

Campisi G., Virruso G., Pellegrino A., Tamburini A., Cipollina A., Micale G., "Techno-economic assessment of electrodialysis with bipolar membranes for hydrogen production", E2DT2025 (2025)

Campisi G., Sorrenti A., Cosenza A., Randazzo S., Corsino S. F., Tamburini A., Micale G., «A chain for the treatment of oilfield produced waters: case study and experimental analysis», SIDISA, 1-4 Oct 2024, Palermo, Italy

Pellegrino A., Campisi G., Proietto F., Tamburini A., Cipollina A., Galia A., Micale G., and Scialdone A., « Experimental investigation and preliminary economic assessment on the green hydrogen production through (Assisted-)Reverse Electrodialysis». EUROMEMBRANE 2024, 8-12 Sep Prague, Czech Republic

Pellegrino A., Campisi G., Proietto F., Tamburini A., Cipollina A., Galia A., Micale G., and Scialdone A., «Hydrogen-Electrodialysis with Bipolar Membrane: the first experimental campaign and preliminary economic assessment». EUROMEMBRANE 2024, 8-12 Sep, Prague, Czech Republic

Campisi G., Pellegrino A., Tamburini A., Cipollina A. and Micale G., «A preliminary Techno-economic Assessment on the Simultaneous Production of Freshwater and Hydrogen through Electrodialysis». EUROMEMBRANE 2024, 8-12 Sep, Prague, Czech Republic

Campisi G., Cosenza A., Randazzo S., Tamburini A., and Micale G., «An Innovative Plant for the Desalination and Treatment of Produced Waters». In: Mannina, G., Ng, H.Y. (eds) Frontiers in Membrane Technology. IWA-RMTC 2024, 18-21 Jun 2024, Palermo, Italy

Campisi G., Pellegrino A., Proietto F., Cipollina A., Galia A., Tamburini A., Scialdone A., and Micale G., «An improved Electrodialysis System for the Simultaneous Production of Fresh Water and Hydrogen: A Preliminary Assessment». EUROMED 2024, 6-9 May 2024, Sharm El Sheikh, Egypt

Pellegrino A., Campisi G., Proietto F., Cipollina A., Galia A., Tamburini A., Micale G., and Scialdone A., «Electro-membrane processes for green hydrogen production». Green Hydrogen Generation and its Application as a Fuel, 1st HyGen Workshop, 8-10 Apr 2024.

Campisi G., Tamburini A., Micale G., Tedesco M. and Dussi S., «Proton Exchange Membrane Water Electrolysers (PEMWEs): a 3D Computation Fluid Dynamics Analysis», Green Hydrogen Generation and its Application as a Fuel, 1st HyGen Workshop, 8-10 Apr 2024.

Campisi G., Pellegrino A., Cipollina A., Tamburini A., and Micale G., «Producing Hydrogen and Fresh Water from Brackish Water Desalination via Electrodialysis». E2DT, 22-25 Oct 2023, Palermo, Italy

Campisi G., Cosenza A., Randazzo S., Tamburini A., and Micale G., «Economic Analysis of an Innovative Scheme for the Treatment of Produced Waters». E2DT, 22-25 Oct 2023, Palermo, Italy

Pellegrino A., Campisi G., Proietto F., Tamburini A., Scialdone A., and Micale G., «Electro-Membrane Processes for the Green Hydrogen Production». E2DT, 22-25 Oct 2023, Palermo, Italy

Campisi G., Pellegrino A., Proietto F., Tamburini A., Micale G., and Scialdone A., «Coupling desalination electrodialysis technology with green hydrogen production». GEI 2023, 17-21 Sep 2023, Cefalù, Italy

Pellegrino A., Campisi G., Proietto F., Tamburini A., Scialdone A., and Micale G., «Electro-Membrane Processes for the Green Hydrogen Production». GEI 2023, 17-21 Sep 2023, Cefalù, Italy

Campisi G., Cosenza A., Randazzo S., Tamburini A., Micale G., «Salinity Reduction of Real Produced Waters via Assisted Reverse Electrodialysis», ICHEAP16, 21-24 May, Napoli, Italy

Campisi G., Cosenza A., Tamburini A., Micale G., «An application of Reverse ElectroDialysis: energy production from produced water», DOI:10.3303/BOA2201, GRICU 2023, 3-6 Jul 2023, Ischia, Italy

Cosenza A., Campisi G., Giacalone F., Randazzo S., Cipollina A., Tamburini A., and Micale G. «Reverse electrodialysis for power production from oilfield wastewaters». MELPRO 2022, 18-21 Sep 2022

Submitted abstract for oral presentations

Campisi G., Sorrenti A., Cosenza A., Randazzo S., Corsino S. F., Tamburini A., Micale G., «A chain for the treatment of oilfield produced waters: case study and experimental analysis», SIDISA, 1-4 Oct 2024, Palermo, Italy

Campisi G., Pellegrino A., Proietto F., Cipollina A., Galia A., Tamburini A., Scialdone A., and Micale G., «An improved Electrodialysis System for the Simultaneous Production of Fresh Water and Hydrogen: A Preliminary Assessment». EUROMED 2024, 6-9 May 2024, Sharm El Sheikh, Egypt

Campisi G., Tamburini A., Micale G., Tedesco M. and Dussi S., «Proton Exchange Membrane Water Electrolysers (PEMWEs): a 3D Computation Fluid Dynamics Analysis», Green Hydrogen Generation and its Application as a Fuel, 1st HyGen Workshop, 8-10 April 2024.

Campisi G., Pellegrino A., Cipollina A., Tamburini A., and Micale G., «Producing Hydrogen and Fresh Water from Brackish Water Desalination via Electrodialysis». E2DT, 22-25 Oct 2023, Palermo, Italy

Campisi G., Pellegrino A., Proietto F., Tamburini A., Micale G., and Scialdone A., «Coupling desalination electrodialysis technology with green hydrogen production». GEI 2023, 17-21 Sep 2023, Cefalù, Italy

Bibliography

[1] COMMUNICATION FROM THE COMMISSION TO THE EUROPEAN PARLIAMENT, THE EUROPEAN COUNCIL, THE COUNCIL, THE EUROPEAN ECONOMIC AND SOCIAL COMMITTEE AND THE COMMITTEE OF THE REGIONS The European Green Deal, (n.d.). https://eur-lex.europa.eu/legal-content/EN/TXT/?uri=COM%3A2019%3A640%3AFIN.

[2] European Commission, Directorate-General for Energy, B. Breitschopf, L. Zheng, M. Plaisir, J. Bard, R. Schröer, D. Kawale, J. Koornneef, Y. Melese, M. Schaaphok, J. Gorenstein Dedecca, C. Bene, O. Cerny, F. Gérard, The role of renewable H_2 import & storage to scale up the EU deployment of renewable H_2 : report, Publications Office of the European Union, 2022. https://doi.org/10.2833/727785.

[3] Renewable energy and jobs annual review 2021, International Renewable Energy Agency International Labour Organization, Abu Dhabi, Geneva, 2021.

[4] Y. Naimi, A. Antar, Hydrogen Generation by Water Electrolysis, in: M. Eyvaz (Ed.), Advances In Hydrogen Generation Technologies, InTech, 2018. https://doi.org/10.5772/intechopen.76814.

[5] J. Incer-Valverde, A. Korayem, G. Tsatsaronis, T. Morosuk, "Colors" of hydrogen: Definitions and carbon intensity, Energy Conversion and Management 291 (2023) 117294. https://doi.org/10.1016/j.enconman.2023.117294.

[6] H. Mehmood, H. Akbar, P. Nilsalab, S.H. Gheewala, Exploring the spectrum: an environmental examination of hydrogen's diverse colors, Energy Adv. 4 (2025) 224–238. https://doi.org/10.1039/D4YA00570H.

[7] J.M.M. Arcos, D.M.F. Santos, The Hydrogen Color Spectrum: Techno-Economic Analysis of the Available Technologies for Hydrogen Production, Gases 3 (2023) 25–46. https://doi.org/10.3390/gases3010002.

[8] S.M. Alizadeh, Y. Khalili, M. Ahmadi, Comprehensive Review of Carbon Capture and Storage Integration in Hydrogen Production: Opportunities, Challenges, and Future Perspectives, Energies 17 (2024) 5330. https://doi.org/10.3390/en17215330.

[9] Md. Ariful Islam, A. Chowdhury, I. Jahan, O. Farrok, Mitigation of environmental impacts and challenges during hydrogen production, Bioresource Technology 415 (2025) 131666. https://doi.org/10.1016/j.biortech.2024.131666.

[10] A. Ajanovic, M. Sayer, R. Haas, The economics and the environmental benignity of different colors of hydrogen, International Journal of Hydrogen Energy 47 (2022) 24136–24154. https://doi.org/10.1016/j.ijhydene.2022.02.094.

[11] M. Newborough, G. Cooley, Developments in the global hydrogen market: The spectrum of hydrogen colours, Fuel Cells Bulletin 2020 (2020) 16–22. https://doi.org/10.1016/S1464-2859(20)30546-0.

[12] Green hydrogen cost reduction: Scaling up electrolysers to meet the 1.5C climate goal, (n.d.).

[13] International Energy Agency, Global Hydrogen Review 2022, IEA, 2022. www.iea.org.

[14] M. Yue, H. Lambert, E. Pahon, R. Roche, S. Jemei, D. Hissel, Hydrogen energy systems: A critical review of technologies, applications, trends and challenges, Renewable and Sustainable Energy Reviews 146 (2021) 111180. https://doi.org/10.1016/j.rser.2021.111180.

[15] M. Chatenet, B.G. Pollet, D.R. Dekel, F. Dionigi, J. Deseure, P. Millet, R.D. Braatz, M.Z. Bazant, M. Eikerling, I. Staffell, P. Balcombe, Y. Shao-Horn, H. Schäfer, Water electrolysis: from textbook knowledge to the latest scientific strategies and industrial developments, Chem. Soc. Rev. 51 (2022) 4583–4762. https://doi.org/10.1039/D0CS01079K.

[16] M. David, C. Ocampo-Martínez, R. Sánchez-Peña, Advances in alkaline water electrolyzers: A review, Journal of Energy Storage 23 (2019) 392–403. https://doi.org/10.1016/j.est.2019.03.001.

[17] S.W. Sharshir, A. Joseph, M.M. Elsayad, A.A. Tareemi, A.W. Kandeal, M.R. Elkadeem, A review of recent advances in alkaline electrolyzer for green hydrogen production: Performance improvement and applications, International Journal of Hydrogen Energy (2023) S0360319923040879. https://doi.org/10.1016/j.ijhydene.2023.08.107.

[18] Y. Chen, C. Liu, J. Xu, C. Xia, P. Wang, B.Y. Xia, Y. Yan, X. Wang, Key Components and Design Strategy for a Proton Exchange Membrane Water Electrolyzer, Small Structures 4 (2023) 2200130. https://doi.org/10.1002/sstr.202200130.

[19] S. Shiva Kumar, V. Himabindu, Hydrogen production by PEM water electrolysis – A review, Materials Science for Energy Technologies 2 (2019) 442–454. https://doi.org/10.1016/j.mset.2019.03.002.

[20] Dhiyanesh Ravichandran, (n.d.). https://etn.news/buzz/lhyfe-occitanie-green-hydrogen-facility-construction-france-details (accessed December 12, 2023).

[21] K. Monroe, (n.d.). https://www.ir.plugpower.com/press-releases/news-details/2023/Plug-Preferred-Supplier-Of-550-MW-PEM-Electrolyzers-To-Fortescue-For-Proposed-Gibson-Island-Project/default.aspx (accessed December 12, 2023).

[22] D. Ellis, (n.d.). https://www.h2-view.com/story/galp-reaches-fid-on-green-hydrogen-hvo-and-saf-projects/2099527.article/ (accessed December 12, 2023).

[23] G. Liu, Y. Xu, T. Yang, L. Jiang, Recent advances in electrocatalysts for seawater splitting, Nano Materials Science 5 (2023) 101–116. https://doi.org/10.1016/j.nanoms.2020.12.003.

[24] L.A. Melnik, D.A. Krysenko, Ultrapure Water: Properties, Production, and Use, J. Water Chem. Technol. 41 (2019) 143–150. https://doi.org/10.3103/S1063455X19030020.

[25] ASTM.org, Standard Guide for Ultra-Pure Water Used in the Electronics and Semiconductor Industries, (2013). https://store.astm.org/d5127-13.html.

[26] H. Becker, J. Murawski, D.V. Shinde, I.E.L. Stephens, G. Hinds, G. Smith, Impact of impurities on water electrolysis: a review, Sustainable Energy Fuels 7 (2023) 1565–1603. https://doi.org/10.1039/D2SE01517J.

[27] H. Lee, Y. Jin, S. Hong, Recent transitions in ultrapure water (UPW) technology: Rising role of reverse osmosis (RO), Desalination 399 (2016) 185–197. https://doi.org/10.1016/j.desal.2016.09.003.
[28] X. Zhang, Y. Yang, H.H. Ngo, W. Guo, H. Wen, X. Wang, J. Zhang, T. Long, A critical review on challenges and trend of ultrapure water production process, Science of The Total Environment 785 (2021) 147254. https://doi.org/10.1016/j.scitotenv.2021.147254.
[29] P. Zhao, Y. Bai, B. Liu, H. Chang, Y. Cao, J. Fang, Process optimization for producing ultrapure water with high resistivity and low total organic carbon, Process Safety and Environmental Protection 126 (2019) 232–241. https://doi.org/10.1016/j.psep.2019.04.017.
[30] M.M. Zubair, H. Saleem, S.J. Zaidi, Recent progress in reverse osmosis modeling: An overview, Desalination 564 (2023) 116705. https://doi.org/10.1016/j.desal.2023.116705.
[31] I. Nurjanah, T.-T. Chang, S.-J. You, C.-Y. Huang, W.-Y. Sean, Reverse osmosis integrated with renewable energy as sustainable technology: A review, Desalination 581 (2024) 117590. https://doi.org/10.1016/j.desal.2024.117590.
[32] Z.U. Khan, M. Moronshing, M. Shestakova, A. Al-Othman, M. Sillanpää, Z. Zhan, B. Song, Y. Lei, Electro-deionization (EDI) technology for enhanced water treatment and desalination: A review, Desalination 548 (2023) 116254. https://doi.org/10.1016/j.desal.2022.116254.
[33] P. Palenzuela, D.-C. Alarcón-Padilla, G. Zaragoza, Concentrating Solar Power and Desalination Plants: Engineering and Economics of Coupling Multi-Effect Distillation and Solar Plants, Springer International Publishing, Cham, 2015. https://doi.org/10.1007/978-3-319-20535-9.
[34] A. Campione, L. Gurreri, M. Ciofalo, G. Micale, A. Tamburini, A. Cipollina, Electrodialysis for water desalination: A critical assessment of recent developments on process fundamentals, models and applications, Desalination 434 (2018) 121–160. https://doi.org/10.1016/j.desal.2017.12.044.
[35] S. Al-Amshawee, M.Y.B.M. Yunus, A.A.M. Azoddein, D.G. Hassell, I.H. Dakhil, H.A. Hasan, Electrodialysis desalination for water and wastewater: A review, Chemical Engineering Journal 380 (2020) 122231. https://doi.org/10.1016/j.cej.2019.122231.
[36] M. Sedighi, M.M. Behvand Usefi, A.F. Ismail, M. Ghasemi, Environmental sustainability and ions removal through electrodialysis desalination: Operating conditions and process parameters, Desalination 549 (2023) 116319. https://doi.org/10.1016/j.desal.2022.116319.
[37] M. Ayaz, M.A. Namazi, M.A.U. Din, M.I.M. Ershath, A. Mansour, el-H.M. Aggoune, Sustainable seawater desalination: Current status, environmental implications and future expectations, Desalination 540 (2022) 116022. https://doi.org/10.1016/j.desal.2022.116022.
[38] Z.M. Ghazi, S.W.F. Rizvi, W.M. Shahid, A.M. Abdulhameed, H. Saleem, S.J. Zaidi, An overview of water desalination systems integrated with renewable energy sources, Desalination 542 (2022) 116063. https://doi.org/10.1016/j.desal.2022.116063.
[39] S. M.S., T. Elmakki, K. Schipper, S. Ihm, Y. Yoo, B. Park, H. Park, H.K. Shon, D.S. Han, Integrated seawater hub: A nexus of sustainable water, energy, and resource generation, Desalination 571 (2024) 117065. https://doi.org/10.1016/j.desal.2023.117065.
[40] H. Kariman, A. Shafieian, M. Khiadani, Small scale desalination technologies: A comprehensive review, Desalination 567 (2023) 116985. https://doi.org/10.1016/j.desal.2023.116985.
[41] A. Hauch, S.H. Jensen, S. Ramousse, M. Mogensen, Performance and Durability of Solid Oxide Electrolysis Cells, J. Electrochem. Soc. 153 (2006) A1741. https://doi.org/10.1149/1.2216562.
[42] J.P. Stempien, Q. Sun, S.H. Chan, Solid Oxide Electrolyzer Cell Modeling: A Review, (2013).
[43] N. Du, C. Roy, R. Peach, M. Turnbull, S. Thiele, C. Bock, Anion-Exchange Membrane Water Electrolyzers, Chem. Rev. 122 (2022) 11830–11895. https://doi.org/10.1021/acs.chemrev.1c00854.
[44] C. Santoro, A. Lavacchi, P. Mustarelli, V. Di Noto, L. Elbaz, D.R. Dekel, F. Jaouen, What is Next in Anion-Exchange Membrane Water Electrolyzers Bottlenecks Benefits and.pdf, 15 (2022). https://doi.org/10.1002/cssc.202200027.
[45] J. Mohammed-Ibrahim, H. Moussab, Recent advances on hydrogen production through seawater electrolysis, Materials Science for Energy Technologies 3 (2020) 780–807. https://doi.org/10.1016/j.mset.2020.09.005.
[46] E. Katz, Electrochemical contributions: Julius Tafel (1862–1918), Electrochemical Science Adv 2 (2022) e2260002. https://doi.org/10.1002/elsa.202260002.
[47] A.J. Bard, L.R. Faulkner, Electrochemical methods: fundamentals and applications, 2nd ed, Wiley, New York, 2001.
[48] E.J.F. Dickinson, A.J. Wain, The Butler-Volmer equation in electrochemical theory: Origins, value, and practical application, Journal of Electroanalytical Chemistry 872 (2020) 114145. https://doi.org/10.1016/j.jelechem.2020.114145.
[49] A. Lasia, Mechanism and kinetics of the hydrogen evolution reaction, International Journal of Hydrogen Energy 44 (2019) 19484–19518. https://doi.org/10.1016/j.ijhydene.2019.05.183.
[50] N.-T. Suen, S.-F. Hung, Q. Quan, N. Zhang, Y.-J. Xu, H.M. Chen, Electrocatalysis for the oxygen evolution reaction: recent development and future perspectives, Chem. Soc. Rev. 46 (2017) 337–365. https://doi.org/10.1039/C6CS00328A.
[51] F. Marangio, M. Santarelli, M. Cali, Theoretical model and experimental analysis of a high pressure PEM water electrolyser for hydrogen production, International Journal of Hydrogen Energy 34 (2009) 1143–1158. https://doi.org/10.1016/j.ijhydene.2008.11.083.
[52] P. Quaino, F. Juarez, E. Santos, W. Schmickler, Volcano plots in hydrogen electrocatalysis – uses and abuses, Beilstein J. Nanotechnol. 5 (2014) 846–854. https://doi.org/10.3762/bjnano.5.96.

[53] M.M. Generous, N.A.A. Qasem, U.A. Akbar, S.M. Zubair, Techno-economic assessment of electrodialysis and reverse osmosis desalination plants, Separation and Purification Technology 272 (2021) 118875. https://doi.org/10.1016/j.seppur.2021.118875.
[54] M. Fidaleo, M. Moresi, Electrodialysis Applications in The Food Industry, in: Advances in Food and Nutrition Research, Elsevier, 2006: pp. 265–360. https://doi.org/10.1016/S1043-4526(06)51005-8.
[55] H. Strathmann, Electrodialysis, a mature technology with a multitude of new applications, Desalination 264 (2010) 268–288. https://doi.org/10.1016/j.desal.2010.04.069.
[56] M.A. Acheampong, R.J.W. Meulepas, P.N.L. Lens, Removal of heavy metals and cyanide from gold mine wastewater, J. Chem. Technol. Biotechnol. 85 (2010) 590–613. https://doi.org/10.1002/jctb.2358.
[57] C.R. Gally, T. Benvenuti, C.D.M. Da Trindade, M.A.S. Rodrigues, J. Zoppas-Ferreira, V. Pérez-Herranz, A.M. Bernardes, Electrodialysis for the tertiary treatment of municipal wastewater: Efficiency of ion removal and ageing of ion exchange membranes, Journal of Environmental Chemical Engineering 6 (2018) 5855–5869. https://doi.org/10.1016/j.jece.2018.07.052.
[58] L. Gurreri, M. La Cerva, J. Moreno, B. Goossens, A. Trunz, A. Tamburini, Coupling of electromembrane processes with reverse osmosis for seawater desalination: Pilot plant demonstration and testing, Desalination 526 (2022) 115541. https://doi.org/10.1016/j.desal.2021.115541.
[59] J.-Y. Nam, K.-S. Hwang, H.-C. Kim, H. Jeong, H. Kim, E. Jwa, S. Yang, J. Choi, C.-S. Kim, J.-H. Han, N. Jeong, Assessing the behavior of the feed-water constituents of a pilot-scale 1000-cell-pair reverse electrodialysis with seawater and municipal wastewater effluent, Water Research 148 (2019) 261–271. https://doi.org/10.1016/j.watres.2018.10.054.
[60] J. Veerman, M. Saakes, S.J. Metz, G.J. Harmsen, Reverse electrodialysis: Performance of a stack with 50 cells on the mixing of sea and river water, Journal of Membrane Science 327 (2009) 136–144. https://doi.org/10.1016/j.memsci.2008.11.015.
[61] J. Veerman, M. Saakes, S.J. Metz, G.J. Harmsen, Electrical Power from Sea and River Water by Reverse Electrodialysis: A First Step from the Laboratory to a Real Power Plant, Environ. Sci. Technol. 44 (2010) 9207–9212. https://doi.org/10.1021/es1009345.
[62] F. Volpin, Y.C. Woo, H. Kim, S. Freguia, N. Jeong, J.-S. Choi, J. Cho, S. Phuntsho, H.K. Shon, Energy recovery through reverse electrodialysis: Harnessing the salinity gradient from the flushing of human urine, Water Research 186 (2020) 116320. https://doi.org/10.1016/j.watres.2020.116320.
[63] M. Bevacqua, A. Carubia, A. Cipollina, A. Tamburini, M. Tedesco, G. Micale, Performance of a RED system with ammonium hydrogen carbonate solutions, Desalination and Water Treatment 57 (2016) 23007–23018. https://doi.org/10.1080/19443994.2015.1126410.
[64] F. Giacalone, F. Vassallo, F. Scargiali, A. Tamburini, A. Cipollina, G. Micale, The first operating thermolytic reverse electrodialysis heat engine, Journal of Membrane Science 595 (2020) 117522. https://doi.org/10.1016/j.memsci.2019.117522.
[65] G. Campisi, A. Cosenza, F. Giacalone, S. Randazzo, A. Tamburini, G. Micale, Desalination of oilfield produced waters via reverse electrodialysis: A techno-economical assessment, Desalination 548 (2023) 116289. https://doi.org/10.1016/j.desal.2022.116289.
[66] A. Cosenza, G. Campisi, F. Giacalone, S. Randazzo, A. Cipollina, A. Tamburini, G. Micale, Power Production from Produced Waters via Reverse Electrodialysis: A Preliminary Assessment, Energies 15 (2022) 4177. https://doi.org/10.3390/en15114177.
[67] Campisi, Cosenza, Alessandro, Randazzo, Serena, Tamburini, Alessandro, Micale, Giorgio, Salinity Reduction of Real Produced Waters via Assisted Reverse Electrodialysis, Chemical Engineering Transactions 99 (2023b) 445–450. https://doi.org/10.3303/CET2399075.
[68] P. Ma, X. Hao, F. Proietto, A. Galia, O. Scialdone, Assisted reverse electrodialysis for CO2 electrochemical conversion and treatment of wastewater: A new approach towards more eco-friendly processes using salinity gradients, Electrochimica Acta 354 (2020) 136733. https://doi.org/10.1016/j.electacta.2020.136733.
[69] M. Vanoppen, E. Criel, G. Walpot, D.A. Vermaas, A. Verliefde, Assisted reverse electrodialysis—principles, mechanisms, and potential, Npj Clean Water 1 (2018) 9. https://doi.org/10.1038/s41545-018-0010-1.
[70] M. La Cerva, L. Gurreri, A. Cipollina, A. Tamburini, M. Ciofalo, G. Micale, Modelling and cost analysis of hybrid systems for seawater desalination: Electromembrane pre-treatments for Reverse Osmosis, Desalination 467 (2019) 175–195. https://doi.org/10.1016/j.desal.2019.06.010.
[71] W. Li, W.B. Krantz, E.R. Cornelissen, J.W. Post, A.R.D. Verliefde, C.Y. Tang, A novel hybrid process of reverse electrodialysis and reverse osmosis for low energy seawater desalination and brine management, Applied Energy 104 (2013) 592–602. https://doi.org/10.1016/j.apenergy.2012.11.064.
[72] Q. Wang, X. Gao, Y. Zhang, Z. He, Z. Ji, X. Wang, C. Gao, Hybrid RED/ED system: Simultaneous osmotic energy recovery and desalination of high-salinity wastewater, Desalination 405 (2017) 59–67. https://doi.org/10.1016/j.desal.2016.12.005.
[73] A. Culcasi, L. Gurreri, A. Cipollina, A. Tamburini, G. Micale, A comprehensive multi-scale model for bipolar membrane electrodialysis (BMED), Chemical Engineering Journal 437 (2022) 135317. https://doi.org/10.1016/j.cej.2022.135317.
[74] M. Reig, S. Casas, O. Gibert, C. Valderrama, J.L. Cortina, Integration of nanofiltration and bipolar electrodialysis for valorization of seawater desalination brines: Production of drinking and waste water treatment chemicals, Desalination 382 (2016) 13–20. https://doi.org/10.1016/j.desal.2015.12.013.
[75] H. Ma, S. Yue, H. Li, Q. Wang, M. Tu, fermentation stillage: Feasibility and effects of substrates, Separation and Purification Technology (2019).

[76] J. Bi, Bipolar membrane electrodialysis integrated with in-situ CO2 absorption for simulated seawater concentrate utilization, carbon storage and production of sodium carbonate, Journal of Environmental Sciences (2024).
[77] A. Filingeri, In-depth insights on multi-ionic transport in Electrodialysis with bipolar membrane systems, Chemical Engineering Journal (2023).
[78] C. Cassaro, G. Virruso, A. Culcasi, A. Cipollina, A. Tamburini, G. Micale, Electrodialysis with Bipolar Membranes for the Sustainable Production of Chemicals from Seawater Brines at Pilot Plant Scale, ACS Sustainable Chem. Eng. 11 (2023) 2989–3000. https://doi.org/10.1021/acssuschemeng.2c06636.
[79] J.-H. Han, H. Kim, K.-S. Hwang, N. Jeong, C.-S. Kim, Hydrogen Production from Water Electrolysis Driven by High Membrane Voltage of Reverse Electrodialysis, J. Electrochem. Sci. Technol 10 (2019) 302–312. https://doi.org/10.33961/jecst.2019.03160.
[80] X. Zhu, M.C. Hatzell, B.E. Logan, Microbial Reverse-Electrodialysis Electrolysis and Chemical-Production Cell for H_2 Production and CO_2 Sequestration, Environ. Sci. Technol. Lett. 1 (2014) 231–235. https://doi.org/10.1021/ez500073q.
[81] V.J. Watson, M. Hatzell, B.E. Logan, Hydrogen production from continuous flow, microbial reverse-electrodialysis electrolysis cells treating fermentation wastewater, Bioresource Technology 195 (2015) 51–56. https://doi.org/10.1016/j.biortech.2015.05.088.
[82] M.C. Hatzell, X. Zhu, B.E. Logan, Simultaneous Hydrogen Generation and Waste Acid Neutralization in a Reverse Electrodialysis System, ACS Sustainable Chem. Eng. 2 (2014) 2211–2216. https://doi.org/10.1021/sc5004133.
[83] M. Nazemi, J. Zhang, M.C. Hatzell, Harvesting Natural Salinity Gradient Energy for Hydrogen Production Through Reverse Electrodialysis Power Generation, Journal of Electrochemical Energy Conversion and Storage 14 (2017) 020702. https://doi.org/10.1115/1.4035835.
[84] Y.D. Raka, H. Karoliussen, K.M. Lien, O.S. Burheim, Opportunities and challenges for thermally driven hydrogen production using reverse electrodialysis system, International Journal of Hydrogen Energy 45 (2020) 1212–1225. https://doi.org/10.1016/j.ijhydene.2019.05.126.
[85] X. Chen, C. Jiang, Y. Zhang, Y. Wang, T. Xu, Storable hydrogen production by Reverse Electro-Electrodialysis (REED), Journal of Membrane Science 544 (2017) 397–405. https://doi.org/10.1016/j.memsci.2017.09.006.
[86] X. Chen, C. Jiang, M.A. Shehzad, Y. Wang, H. Feng, Z. Yang, T. Xu, Water-Dissociation-Assisted Electrolysis for Hydrogen Production in a Salinity Power Cell, ACS Sustainable Chem. Eng. 7 (2019) 13023–13030. https://doi.org/10.1021/acssuschemeng.9b02131.
[87] R.A. Tufa, J. Hnát, M. Němeček, R. Kodým, E. Curcio, K. Bouzek, Hydrogen production from industrial wastewaters: An integrated reverse electrodialysis - Water electrolysis energy system, Journal of Cleaner Production 203 (2018) 418–426. https://doi.org/10.1016/j.jclepro.2018.08.269.
[88] M. Higa, T. Watanabe, M. Yasukawa, N. Endo, Y. Kakihana, H. Futamura, K. Inoue, H. Miyake, J. Usui, A. Hayashi, M. Matsuhashi, Sustainable hydrogen production from seawater and sewage treated water using reverse electrodialysis technology, Water Practice and Technology 14 (2019) 645–651. https://doi.org/10.2166/wpt.2019.048.
[89] A. Pellegrino, G. Campisi, F. Proietto, A. Tamburini, A. Cipollina, A. Galia, G. Micale, O. Scialdone, Green hydrogen production via reverse electrodialysis and assisted reverse electrodialysis electrolyser: Experimental analysis and preliminary economic assessment, International Journal of Hydrogen Energy (2024) S0360319923065734. https://doi.org/10.1016/j.ijhydene.2023.12.273.
[90] J. Hu, H. Zhang, W. Xu, Z. Yuan, X. Li, Mechanism and transfer behavior of ions in Nafion membranes under alkaline media, Journal of Membrane Science 566 (2018) 8–14. https://doi.org/10.1016/j.memsci.2018.08.057.
[91] A. Zlotorowicz, R.V. Strand, O.S. Burheim, Ø. Wilhelmsen, S. Kjelstrup, The permselectivity and water transference number of ion exchange membranes in reverse electrodialysis, Journal of Membrane Science 523 (2017) 402–408. https://doi.org/10.1016/j.memsci.2016.10.003.
[92] F. Giacalone, M. Papapetrou, G. Kosmadakis, A. Tamburini, G. Micale, A. Cipollina, Application of reverse electrodialysis to site-specific types of saline solutions: A techno-economic assessment, Energy 181 (2019) 532–547. https://doi.org/10.1016/j.energy.2019.05.161.
[93] M. Tedesco, A. Cipollina, A. Tamburini, I.D.L. Bogle, G. Micale, A simulation tool for analysis and design of reverse electrodialysis using concentrated brines, Chemical Engineering Research and Design 93 (2015) 441–456. https://doi.org/10.1016/j.cherd.2014.05.009.
[94] A. Cipollina, Sustainable Energy from Salinity Gradients, Andrea Cipollina, Giorgio Micale, 2016. https://doi.org/10.1016/C2014-0-03709-4.
[95] A. Daniilidis, R. Herber, D.A. Vermaas, Upscale potential and financial feasibility of a reverse electrodialysis power plant, Applied Energy 119 (2014) 257–265. https://doi.org/10.1016/j.apenergy.2013.12.066.
[96] F. Giacalone, M. Papapetrou, G. Kosmadakis, A. Tamburini, G. Micale, A. Cipollina, Application of reverse electrodialysis to site-specific types of saline solutions: A techno-economic assessment, Energy 181 (2019) 532–547. https://doi.org/10.1016/j.energy.2019.05.161.
[97] M. Ciucci, Renewable energy, (2025).
[98] A. Ranade, K. Singh, A. Tamburini, G. Micale, D.A. Vermaas, Feasibility of Producing Electricity, Hydrogen, and Chlorine via Reverse Electrodialysis, Environ. Sci. Technol. 56 (2022) 16062–16072. https://doi.org/10.1021/acs.est.2c03407.
[99] R.F. Alshebli, B. Yuzer, Y. Bicer, Experimental investigation of simultaneous hydrogen production and desalination via electrodialysis process, International Journal of Hydrogen Energy (2023) S0360319922058207. https://doi.org/10.1016/j.ijhydene.2022.12.104.

[100] M.J.D.C. Fonseca, F.V.D. Fonseca, C.P. Borges, Electrodialysis feasibility for simultaneous generation of desalinated water and hydrogen as by-product, International Journal of Hydrogen Energy 53 (2024) 1396–1403. https://doi.org/10.1016/j.ijhydene.2023.12.058.
[101] G. Campisi, A. Pellegrino, A. Tamburini, G. Micale, Techno-economic modelling of a hydrogen-electrodialysis (HED) unit for the simultaneous production of freshwater and hydrogen, Desalination 587 (2024) 117920. https://doi.org/10.1016/j.desal.2024.117920.
[102] A. Campione, A. Cipollina, I.D.L. Bogle, L. Gurreri, A. Tamburini, M. Tedesco, G. Micale, A hierarchical model for novel schemes of electrodialysis desalination, Desalination 465 (2019) 79–93. https://doi.org/10.1016/j.desal.2019.04.020.
[103] F. Giacalone, P. Catrini, L. Gurreri, A. Tamburini, A. Cipollina, G. Micale, A. Piacentino, Exergy analysis of electrodialysis for water desalination: Influence of irreversibility sources, Energy Conversion and Management 258 (2022) 115314. https://doi.org/10.1016/j.enconman.2022.115314.
[104] L. Gurreri, A. Tamburini, G. Micale, Electromembrane Processes: Experiments and Modelling, Membranes 11 (2021) 149. https://doi.org/10.3390/membranes11020149.
[105] F. Giacalone, A. Filingeri, A. Tamburini, A. Cipollina, G. Micale, Electrodialysis for sustainable management of seawater-brine: Increasing water recovery via production of hypersaline solution for brine-mining processes, Desalination 575 (2024) 117294. https://doi.org/10.1016/j.desal.2024.117294.
[106] S.S. Islam, R.L. Gupta, K. Ismall', Extension of the Falkenhagen-Leist-Kelbg Equation to the Electrical Conductance of Concentrated Aqueous Electrolytes, (1991).
[107] Making the breakthrough: Green hydrogen policies and technology costs, IRENA, Abu Dhabi, 2021.
[108] M. La Cerva, M. Di Liberto, L. Gurreri, A. Tamburini, A. Cipollina, G. Micale, M. Ciofalo, Coupling CFD with a one-dimensional model to predict the performance of reverse electrodialysis stacks, Journal of Membrane Science 541 (2017) 595–610. https://doi.org/10.1016/j.memsci.2017.07.030.
[109] F. Giacalone, P. Catrini, A. Tamburini, A. Cipollina, A. Piacentino, G. Micale, Exergy analysis of reverse electrodialysis, Energy Conversion and Management 164 (2018) 588–602. https://doi.org/10.1016/j.enconman.2018.03.014.
[110] K.W. Harrison, R. Remick, G.D. Martin, Hydrogen Production: Fundamentals and Case Study Summaries; Preprint, (n.d.).
[111] S. Quoilin, S. Declaye, B.F. Tchanche, V. Lemort, Thermo-economic optimization of waste heat recovery Organic Rankine Cycles, Applied Thermal Engineering 31 (2011) 2885–2893. https://doi.org/10.1016/j.applthermaleng.2011.05.014.
[112] R. Turton, ed., Analysis, synthesis, and design of chemical processes, 4th ed, Prentice Hall, Upper Saddle River, NJ, 2012.
[113] S. Chae, H. Kim, J. Gi Hong, J. Jang, M. Higa, M. Pishnamazi, J.-Y. Choi, R. Chandula Walgama, C. Bae, I.S. Kim, J.-S. Park, Clean power generation from salinity gradient using reverse electrodialysis technologies: Recent advances, bottlenecks, and future direction, Chemical Engineering Journal 452 (2023) 139482. https://doi.org/10.1016/j.cej.2022.139482.
[114] T.R. Lucas, A.F. Ferreira, R.B. Santos Pereira, M. Alves, Hydrogen production from the WindFloat Atlantic offshore wind farm: A techno-economic analysis, Applied Energy 310 (2022) 118481. https://doi.org/10.1016/j.apenergy.2021.118481.
[115] J.R. Serrano, F.J. Arnau, L.M. García-Cuevas, F.A. Gutiérrez, Thermo-economic analysis of an oxygen production plant powered by an innovative energy recovery system, Energy 255 (2022) 124419. https://doi.org/10.1016/j.energy.2022.124419.
[116] S.K. Patel, M. Qin, W.S. Walker, M. Elimelech, Energy Efficiency of Electro-Driven Brackish Water Desalination: Electrodialysis Significantly Outperforms Membrane Capacitive Deionization, Environ. Sci. Technol. 54 (2020) 3663–3677. https://doi.org/10.1021/acs.est.9b07482.
[117] Y. Zhou, S. Searle, COST OF RENEWABLE HYDROGEN PRODUCED ONSITE AT HYDROGEN REFUELING STATIONS IN EUROPE, (2022).
[118] Ionics EDR handles surface water variability and trihalomethane precursors for Barcelona Electrodialysis reversal (EDR) proves to be a superior solution for local drinking water, (2021). https://www.watertechnologies.com/sites/default/files/documents/CS1298EN.pdf.
[119] A. Maraj, X. Kërtusha, A. Lushnjari, Energy performance evaluation for a floating photovoltaic system located on the reservoir of a hydro power plant under the mediterranean climate conditions during a sunny day and a cloudy-one, Energy Conversion and Management: X 16 (2022) 100275. https://doi.org/10.1016/j.ecmx.2022.100275.
[120] International Renewable Energy Agency IRENA, Renewable Power Generation Costs in 2021 - Executive Summary, (2021).
[121] M. Rezaei, A. Akimov, E.MacA. Gray, Economics of renewable hydrogen production using wind and solar energy: A case study for Queensland, Australia, Journal of Cleaner Production 435 (2024) 140476. https://doi.org/10.1016/j.jclepro.2023.140476.
[122] Y. Kim, J. Byun, K. Park, Y.-G. Park, Comprehensive analysis of energy saving and high-quality permeate production strategies for a large-scale seawater reverse osmosis desalination plant with diverse process configurations and external resource utilization, Desalination 596 (2025) 118292. https://doi.org/10.1016/j.desal.2024.118292.
[123] M. Elimelech, W.A. Phillip, The Future of Seawater Desalination: Energy, Technology, and the Environment, Science 333 (2011) 712–717. https://doi.org/10.1126/science.1200488.
[124] G. Doornbusch, M. Van Der Wal, M. Tedesco, J. Post, K. Nijmeijer, Z. Borneman, Multistage electrodialysis for desalination of natural seawater, Desalination 505 (2021) 114973. https://doi.org/10.1016/j.desal.2021.114973.
[125] R.W. Baker, Membrane technology and applications, McGraw-Hill, New York, 2000.
[126] A. Filingeri, L. Gurreri, M. Ciofalo, A. Cipollina, A. Tamburini, G. Micale, Current distribution along electrodialysis stacks and its influence on the current-voltage curve: behaviour from near-zero current to limiting plateau, Desalination 556 (2023) 116541. https://doi.org/10.1016/j.desal.2023.116541.

[127] E.R. Cornelissen, D.J.H. Harmsen, B. Blankert, L.P. Wessels, W.G.J. Van Der Meer, Effect of minimal pre-treatment on reverse osmosis using surface water as a source, Desalination 509 (2021) 115056. https://doi.org/10.1016/j.desal.2021.115056.
[128] A. Pellegrino, G. Campisi, F. Proietto, A. Tamburini, A. Cipollina, A. Galia, O. Scialdone, G. Micale, Hydrogen-Electrodialysis with Bipolar Membrane (H-EDBM): First experiments and preliminary economic evaluation, Desalination 592 (2024) 118169. https://doi.org/10.1016/j.desal.2024.118169.
[129] G. Virruso, C. Cassaro, A. Culcasi, A. Cipollina, A. Tamburini, I.D.L. Bogle, G.D.M. Micale, Multi-scale modelling of an electrodialysis with bipolar membranes pilot plant and economic evaluation of its potential, Desalination 583 (2024) 117724. https://doi.org/10.1016/j.desal.2024.117724.
[130] A. Nada, M.G. Ibrahim, M. Elshemy, M. Fujii, M. Sharaan, Integrated water quality and performance assessment of seawater desalination plants along two coasts in Egypt, Desalination 586 (2024) 117844. https://doi.org/10.1016/j.desal.2024.117844.
[131] W. Zhang, M. Miao, J. Pan, A. Sotto, J. Shen, C. Gao, B. Van Der Bruggen, Process Economic Evaluation of Resource Valorization of Seawater Concentrate by Membrane Technology, ACS Sustainable Chem. Eng. 5 (2017) 5820–5830. https://doi.org/10.1021/acssuschemeng.7b00555.
[132] D.M.F. Santos, C.A.C. Sequeira, J.L. Figueiredo, Hydrogen production by alkaline water electrolysis, Quím. Nova 36 (2013) 1176–1193. https://doi.org/10.1590/S0100-40422013000800017.
[133] J.L. Fu, Z.G. Qu, J.F. Zhang, G.B. Zhang, Performance analysis of PEMEC with non-uniform deformation based on a comprehensive numerical framework coupling image recognition and CFD, Applied Energy 350 (2023) 121772. https://doi.org/10.1016/j.apenergy.2023.121772.
[134] G. Maggio, G. Squadrito, A. Nicita, Hydrogen and medical oxygen by renewable energy based electrolysis: A green and economically viable route, Applied Energy 306 (2022) 117993. https://doi.org/10.1016/j.apenergy.2021.117993.
[135] G. Squadrito, A. Nicita, G. Maggio, A size-dependent financial evaluation of green hydrogen-oxygen co-production, Renewable Energy 163 (2021) 2165–2177. https://doi.org/10.1016/j.renene.2020.10.115.
[136] P. Rao, M. Muller, Industrial Oxygen: Its Generation and Use, (2007).
[137] S. Wallin, A. Johansson, Fluent Theory Guide, (2024).
[138] Y. Jiang, Y. Li, Y. Ding, S. Hu, J. Dang, F. Yang, M. Ouyang, Simulation and experiment study on two-phase flow characteristics of proton exchange membrane electrolysis cell, Journal of Power Sources 553 (2023) 232303. https://doi.org/10.1016/j.jpowsour.2022.232303.
[139] M. Carmo, D.L. Fritz, J. Mergel, D. Stolten, A comprehensive review on PEM water electrolysis, International Journal of Hydrogen Energy 38 (2013) 4901–4934. https://doi.org/10.1016/j.ijhydene.2013.01.151.
[140] T.L. Hill, G. Scatchard, B.A. Pethica, Ing.J. Straub, R. SchlöGl, G. Manecke, R. SchlöGl, M. Nagasawa, I. Kagawa, P. Meares, K. Sollner, F.L. Tye, A. Despiá, G.J. Hills, F. Helfferich, R.J.P. Williams, A.M. Peers, F. Bergsma, A.J. Staverman, N. Krishnaswamy, F. Runge, F. Wolf, E. Glueckauf, D. Reichenberg, R. Neihof, R.D. Keynes, A.R. Ubbelohde, R.M. Barrer, General discussion, Discuss. Faraday Soc. 21 (1956) 117–140. https://doi.org/10.1039/DF9562100117.
[141] A. Nakayama, Y. Sano, X. Bai, K. Tado, A boundary layer analysis for determination of the limiting current density in an electrodialysis desalination, Desalination 404 (2017) 41–49. https://doi.org/10.1016/j.desal.2016.10.013.
[142] V. Geraldes, M.D. Afonso, Limiting current density in the electrodialysis of multi-ionic solutions, Journal of Membrane Science 360 (2010) 499–508. https://doi.org/10.1016/j.memsci.2010.05.054.
[143] H.-J. Lee, H. Strathmann, S.-H. Moon, Determination of the limiting current density in electrodialysis desalination as an empirical function of linear velocity, Desalination 190 (2006) 43–50. https://doi.org/10.1016/j.desal.2005.08.004.
[144] Y. Tanaka, Limiting current density of an ion-exchange membrane and of an electrodialyzer, Journal of Membrane Science 266 (2005) 6–17. https://doi.org/10.1016/j.memsci.2005.05.005.
[145] M.S. Isaacson, A.A. Sonin, Sherwood Number and Friction Factor Correlations for Electrodialysis Systems, with Application to Process Optimization, Ind. Eng. Chem. Proc. Des. Dev. 15 (1976) 313–321. https://doi.org/10.1021/i260058a017.
[146] R. Guidelli, R.G. Compton, J.M. Feliu, E. Gileadi, J. Lipkowski, W. Schmickler, S. Trasatti, Defining the transfer coefficient in electrochemistry: An assessment (IUPAC Technical Report), Pure and Applied Chemistry 86 (2014) 245–258. https://doi.org/10.1515/pac-2014-5026.
[147] P. Khadke, T. Tichter, T. Boettcher, F. Muench, W. Ensinger, C. Roth, A simple and effective method for the accurate extraction of kinetic parameters using differential Tafel plots, Sci Rep 11 (2021) 8974. https://doi.org/10.1038/s41598-021-87951-z.